Graduate Theses and Dissertations   Graduate School

June 2017

Enhanced Visible Light Photocatalytic Remediation of Organics in Water Using Zinc Oxide and Titanium Oxide Nanostructures

Srikanth Gunti
University of South Florida, srikanth2@mail.usf.edu

Enhanced Visible Light Photocatalytic Remediation of Organics in Water Using Zinc Oxide

and Titanium Oxide Nanostructures

by

Srikanth Gunti

A dissertation submitted in partial fulfillment
of the requirements for the degree of
Doctor of Philosophy
Department of Mechanical Engineering
College of Engineering
University of South Florida

Co-Major Professor: Manoj K. Ram, Ph.D.
Co-Major Professor: Ashok Kumar, Ph.D.
Rajiv Dubey, Ph.D.
Andrew Hoff, Ph.D.
Sylvia Thomas, Ph.D.
Sagar Pandit, Ph.D.

Date of Approval:
June 14, 2017

Keywords: nanoparticle vs nanowire, doping, surfactant, binder, photoelectrochemical catalysis

DEDICATION

I dedicate my work to my mother & father – Veeramani & Rajalingam Gunti for their love, endless support and encouragement.

ACKNOWLEDGMENTS

I am thankful to Dr. Ashok Kumar for his kind support and guidance in my Ph.D. research. I sincerely thank my co-major advisor Dr. Manoj K. Ram for his invaluable support. His personal and professional guidance throughout my research helped me to become a better researcher. Also, a special word of gratitude to the committee members, Dr. Rajiv Dubey, Dr. Andrew Hoff, Dr Sylvia Thomas and Dr. Sagar Pandit, for their helpful suggestions. Further, extending my thanks to Dr. Arash Takshi for being the chairperson for my Ph.D. defense and his support to finish my dissertation. I convey my sincere thanks to the chair of Mechanical Engineering, Dr. Rajiv Dubey, and Graduate Advisor, Dr. Rasim Guldiken, for their advice and support in completing my graduate studies at the University of South Florida. I would like to express my gratitude to the Department of Mechanical Engineering for giving me an opportunity to work as a graduate teaching assistant which helped me to learn and experience the fun in teaching. I would like to thank Nanotechnology Research and Education Center (NREC) at University of South Florida for their kind support to provide the facilities for various measurements. Part of this dissertation is supported by NSF grant #1066649.

I thank my fellow Ph.D. student Michael McCrory for his helpful and intellectual research discussions and kind friendship. Also, I want to thank all of my lab mates in Nanomaterial Research Laboratory for their company during these years. Finally, I would like to acknowledge my beloved wife, Shruthi whose love and understanding helped me to get through the most difficult times.

TABLE OF CONTENTS

LIST OF TABLES

LIST OF FIGURES

vi

viii

ix

ABSTRACT

The techniques mostly used to decontaminate air as well as water pollutants have drawbacks in terms of higher costs, require secondary treatment, and some methods are very slow. So, emphasis has been given to water though the use of photocatalysts, which break organic pollutants to water and carbon dioxide and leave no trace of by-products at the end. Photocatalytic remediation aligns with the waste and wastewater industries' zero waste schemes with lower cost, eco-friendly and sustainable treatment technology. The commonly used photocatalysts such as titanium oxide (TiO_2), zinc oxide (ZnO), tungsten oxide (WO_3) have band gap of nearly 3.2 eV. The lower energy band-gap of a semiconductor makes it a better photocatalyst. The major drawbacks of photocatalysts are its inefficiency to work under visible light and high photocorrosion which limits its uses. These limitations can be mitigated through dopants and the formation of varying morphologies like nanowires, nanoparticles, nanotubes etc. Several organic pollutants are insoluble in water, which inhibits the pollutant (insoluble) to come in contact with photocatalytic material thus hindering remediation characteristic of a photocatalyst. Binder material used to immobilize the photocatalytic material tends to decompose due to oxidative and reduction reactions around the photocatalyst which causes the loss of photocatalytic material.

This investigation displays the advantage of organic remediation in visible radiation using graphene (G) doped TiO_2 nanoparticles and nanowires. The nanostructured G-TiO_2 nanoparticles and G-TiO_2 nanowires were synthesized using sol-gel and hydrothermal methods.

The nanostructured materials were characterized using scanning electron microscopy (SEM), Transmission electron microscopy (TEM), X-ray diffraction (XRD), UV-visible spectroscopy (UV-vis), Fourier transform infrared spectroscopy (FTIR) and particle analyser procedures. The remediation of organic compounds (methyl orange) in water was achieved under visible radiation using graphene doped nanostructured photocatalytic materials. The sol-gel synthesized G-TiO$_2$ nanoparticles has shown complete remediation of methyl orange (MO) in less than four hours, thus displaying enhanced photocatalytic activity achieved through graphene doping on TiO$_2$ nanostructures

The dopant and structure introduced in zinc oxide (ZnO) nanomaterials bring foundation for enhanced photocatalytic activity due to lowering of the band gap, and decreasing of photocorrosion through delaying of electron-hole recombination. The challenge to synthesize both nanowire and nanoparticle structures of ZnO doped with graphene (G) are carried out by simple and cost effective hydrothermal as well as super saturation precipitation techniques, respectively. Various nanostructures of ZnO have been synthesized using precipitation and hydrothermal methods are ZnO nanoparticles, G doped ZnO nanoparticles, ZnO nanowires, G doped ZnO nanowires, TiO$_2$ seeded ZnO nanowires and G doped TiO$_2$ seeded ZnO nanowires The synthesized ZnO based nanostructures were characterized using SEM, TEM, XRD, UV-vis, FTIR and particle analyser methods respectively. The standard organic pollutant methyl orange (MO) dye was employed in the water to understand the effective remediation using ZnO nanostructured materials under visible light radiation. The G-ZnO NW structure has shown effective remediation of MO in water in three hours compared to other synthesized nanostructured ZnO materials.

The petroleum compounds were photocatalytically remediated from water using G- TiO$_2$ nanoparticles material in visible light radiation. The G-TiO$_2$ nanoparticle was synthesized using sol-gel technique and used on various petroleum-based chemicals (toluene, naphthalene and diesel) were remediated, and samples were analysed using optical and gas chromatography (GC) techniques. The importance of pollutant to come in contact with photocatalyst have been demonstrated by employing surfactant along with G-TiO$_2$ nanoparticles to remediate naphthalene.

Earlier studies in this investigation have shown that graphene (G) doping in both titanium oxide (TiO$_2$) and zinc oxide (ZnO), has brought about a reduction in photocorrosion, and an increase in the photocatalytic efficiency for remediation of organics under visible light ($\lambda >$ 400nm). However, the graphene doped photocatalysts have proven to be hard to coat on a surface, due to the strong hydrophobic nature of graphene. So, attempts have been made to use polyaniline (PANI), a conducting polymer, as a binder material by insitu polymerization of aniline over G-TiO$_2$ nanoparticles (G-TiO$_2$ NP) and G-ZnO nanowires (G-ZnO NW) & characterized using SEM, XRD, UV-vis and FTIR techniques. The photocatalytic, as well as photoelectrochemical catalytic performance of PANI:G-TiO$_2$ NP and PANI:G-ZnO NW, were investigated. The standard MO in water was used for both PANI:G-TiO$_2$ NP and PANI:G-ZnO NW electrodes on conducting substrates. 1:1 PANI:G-TiO$_2$ NP shows an increase of 31% in the remediation of MO in water at potential of +1000 mV, and with the ease in coating PANI:G-TiO$_2$ NP and PANI:G-ZnO NW on various substrates, on top of the visible light remediation allows for the use of these materials and process to be used for practical applications of remediation of organics from water.

CHAPTER 1: INTRODUCTION

1.1 Problem Description and Motivation

Photocatalysts have been studied extensively in recent times resulting more than thousands of publications in the last decade. The titanium oxide (TiO_2) is the most common photocatalyst which is named as "Honda-Fujishima effect after its discovery in 1970[1, 2]. The TiO_2 was used for water splitting application in 1980's and photocatalytic applications in 1990's. Since 1990's, photocatalysts have been used for air purifiers, air-condensers, household equipment's, and water purification for household applications. The photocatalyst has been initially commercialized in Japan then in United States followed by China.

TiO_2 and zinc oxide (ZnO) are very decent photocatalytic materials, but function most effectively in the ultraviolet spectrum of light radiation for the remediation of pollutants from both air and water. However, the low sensitivities in visible light radiation inhibited those high performing photocatalysts for wide range of commercial applications. Extensive research has been done in the scientific community for the development of photocatalysts that can work effectively in the visible light spectrum, so that they can be used under solar radiation (which has nearly 50% of visible light spectrum). In an effort to increase the efficiency of the photocatalysts, metal dopants have been employed by modifying the bandgap. One of the major difficulties has been the loss of photocatalytic activity due to recycling of photocurrent. The photocatalytic activity of doped photocatalysts under visible light is dependent on the method of synthesis process and the type of dopant. In some cases, photocatalytic material with doping have shown

1

zero or low activity under visible light and low activity under UV light when compared to undoped photocatalyst due to the high carrier combination rate caused by the metal dopant.

Photocatalysts faces a major challenge due to faster electron-hole recombination time, which makes it difficult in organic remediation applications where there is insoluble organic compounds. But current research solves this issue by changing the interfacial charge though a doping process, and modification of surface properties/morphologies such as nanowires/nanotubes/nanoparticles. The reusability of a photocatalyst for both small scale and large-scale applications has not been addressed by scientists and researchers. The advancement of photocatalysts has led small-scale applications like home drinking water purification and home wastewater cleaning, but fundamental research is still needed for larger commercial scale applications. It is known that photocatalyst destroys any organic matrix which encounters, so the binder material should not react with photocatalyst and currently research is needed for the development of new kinds of binder materials, thereby limiting the current photocatalyst applications. There is no established standard for photocatalytic remediation, as photocatalysts are still under development and long-term research is desired to establish stringent methods of standardization can be applied to both private and public facilities. Toxicology and reusability effects of these photocatalysts on the environment are being investigated.

The objectives of this dissertation are:

- To enhance/increase the photoactivity of photocatalytic materials under visible spectrum of light, thus enabling it to use natural available energy (solar light) saving huge amount of resources.

- Enabling the use of surfactants along with new photocatalyst to further increase the rate of decontamination of organic pollutant.

2

- To overcome the issues of binder material by introducing conducting polymer into the photocatalyst thus further enabling the material to be used not only for just photocatalytic activity combined visible light based photocatalytic and electrochemical processes which is named 'photoelectrochemical catalytic' applications in visible spectrum of light.

1.2 Organization of the Dissertation

The structure of this dissertation can be summarized as follows.

Chapter 1 describes the problem and motivation to study the nanostructured photocatalytic materials and graphene doped photocatalytic materials and the main objectives of carrying out this dissertation work followed by the organization of the dissertation.

Chapter 2 is focused on the literature review on advantages and disadvantages of various technologies for the remediation of organic pollutants from air and water including physical, chemical and biological techniques. The later part of chapter two is devoted to the understanding of photocatalyst materials performance followed by several synthesis techniques and discussion on their advantages and technological limitations for the remediation of organic pollutants in visible light spectrum (wavelength $\lambda > 400$nm).

Chapter 3 describes the synthesis techniques used for the nanoparticles and nanowires structures of titanium oxide (TiO_2). A comparative photocatalytic activity study for remediation of organic pollutant for several dopants in TiO_2 nanowire with conclusion of graphene as chosen material, followed by comparative study of nanowires and nanoparticles structure of TiO_2 with respect to photocatalytic activity.

Chapter 4 describes the synthesis techniques used for nanoparticles and nanowires structures of zinc oxide (ZnO) with and without graphene as a dopant. A comparative photocatalytic activity study is presented for nanowires and nanoparticles of zinc oxide for

3

remediation of organic pollutants. Later part of chapter deals with the synthesis of tungsten oxide (WO$_3$) and alpha-hematite (α-Fe$_2$O$_3$) and their photocatalytic activities for remediation of organic pollutant.

Chapter 5 focusses on the importance of pollutant to remain in contact with photocatalyst for complete remediation and uses of surfactant for enabling the contact of photocatalyst with the pollutant. Later part of chapter presents naphthalene remediation data by a photocatalytic material with and without the use of surfactant. Finally, this chapter shows experimental data for photocatalytic remediation of toluene and diesel from water.

Chapter 6 describes a novel method for overcoming the peeling issues for graphene doped photocatalytic material from the substrate under wet condition. A conductive polymer (PANI) with photocatalytic material have been synthesized, and studied for photocatalytic remediation of organic pollutant under visible light radiation. These novel material enables the synthesized PANI based photocatalyst to be applied for photoelectrochemical catalytic application there by eliminating the organic pollutant at a faster rate by photoelectrochemical catalytic technique.

Chapter 7 concludes the dissertation with major findings of an increased photocatalytic activity achieved by employing graphene as dopant onto photocatalytic material. The chapter also focusses on findings obtained by introducing PANI with photocatalytic material which enabled it for photoelectrochemical catalytic application. The chapter has also focussed on the future recommendation research for the development of graphene based photocatalytic materials with conductive polymer for both photocatalytic and photoelectrochemical catalytic applications.

CHAPTER 2: LITERATURE REVIEW[1]

2.1 Introduction

On any given day, enormous amounts of waste materials are being released into the environment as pollutants. Among all the waste materials which are entering into the environment, organic pollutants take the biggest share [3]. These organic contaminants are generated from industrial, domestic and farming applications; enter into the air and water streams, thus creating irreversible damage to environment [4-16]. The organics, in gaseous phase, get released into the air, travel thousands of miles and are then absorbed into water, soil and vegetation through condensation at low temperatures [11]. Such pollutants come in contact with humans through inhalation as well ingestion of food and drinks, causing havoc in respiratory, digestive, urinary, nervous and cardiovascular systems [17-22]. A lot of research has been focused in removal of organics from environment by employing various approaches; i.e. chemical, physical and biological methods.

Organic compounds are also found near wastewater treatment facilities, as well as chemical and oil industries, which then mix into the air and water streams through known or unknown leakage. Standards for organic compound emissions in air and water have been established by the U.S Environmental Protection Agency (EPA), National Emission Standards for Hazardous organic pollutants and World Health Organization (WHO) [23]. Some organics

---

[1] Portions of these results have been communicated with 'International Materials Reviews'/Taylor & Francis Group publishers, with title "Nanostructured photocatalysis in the visible spectrum for the decontamination of air and water" with manuscript number - IMR490 and is currently under review.
Appendix A for copyright information.

can cause sick building syndrome (SBS), which includes symptoms of headache, mucous membrane irritation and fatigue [24-30]. Other organics are known to be carcinogenic [31], or cause liver and other organ failure [23]. Currently, poor indoor air quality and water contamination has increased health issues and wasted billions of dollars in the process of cleaning [32]. Research has been focused to improve air quality through chemical, physical and biological techniques.

Table 2.1 Advantages and disadvantages of techniques employed for air purification.

Technique	Advantage	Disadvantage
Thermal Oxidation [33, 34]	Recover up to 85% of energy	Halogenated & other organic compounds require special equipment, additional safety measures, and produce byproducts from combustion.
Catalytic Oxidation [35, 36]	Recover up to 70% of energy	Operating conditions can change efficiency, requires additional control equipment, some chemicals can deteriorate the catalyst performance and byproducts from combustion with additional safety measures.
Bio-filtration [37, 38]	Lower initial investment, as well as less hazardous waste	Slower process and decomposition of selective organics needs employed culture with no recovery material and some organics can be poisonous to microbes.
Condensation [34]	Product recovery can offset cost	High maintenance, can only be used for organics with boiling point less than $33^{\circ}C$, leaves behind condensation of organic compounds.
Absorption [39]	Product recovery can offset cost	High maintenance and some cases require pretreatments of organics with complicated systems.
Adsorption [40, 41]	Product recovery can offset cost	Moisture and some organics compounds could cause clogging of pores thereby decreasing efficiency and additional desorption process needed.
Membrane separation [42, 43]	No further treatment, product recovery may offset cost	Membrane is rare and extremely costly.

6

Table 2.2 Advantages and disadvantages of techniques employed for water purification.

Techniques	Advantages	Disadvantages
Reverse Osmosis [44, 45]	Removes salts, heavy metals & microorganisms	Trace amounts of oils and greases will cause fouling of membrane, doesn't remove organics.
Centrifuge [46, 47]	Removes small oil molecules and suspended solids materials, low retention time	High energy required, maintenance cost is high, solid slurry as waste, dissolved & hazardous pollutants will not be removed.
UV-based filtration [48, 49]	Removes microorganisms, high filtration capacity	Very low efficiency for organic pollutants with higher costs.
Adsorption [50, 51]	Cheaper, efficient and compact bed modules	Very high retention time and efficiency is lower at higher feed rates.
Precipitation [46]	No mechanical moving parts with greater efficiency, durability and ease in operation	Formation of huge quantity of air with higher retention time for the separation and skim volume.
Chemical Precipitation [52]	Cheaper & accessible	Post treatment is necessary, needs additional chemicals.
Ozone [53, 54]	Ease in operation, efficient in primary treatment for soluble constituents	Solids precipitate in slurry form, efficient only in the primary treatment, requirement for the on-site supply of oxidizer.
Micro and Ultra filtration [55-57]	Showing high rates in fresh water recovery, removal of organics	Requirement for the high-energy, membrane fouling.
Biological treatment [58-60]	Cheaper, clean & simple technology	Oxygen requirements, very large dimensions of filter and very slow process.

Organic compounds, in both air and water, at higher concentrations can easily be detected through smell (odour), but at lower concentrations it needs sophisticated techniques and instrumentation such as gas chromatography, atomic absorption spectroscopy and optical (UV visible, fluorescence and FTIR) techniques. Table 2.1 and Table 2.2 show current technologies with their advantages and disadvantages for both air and water purification methods. It can be

7

realized that most techniques have drawbacks in terms of higher cost, requirement of secondary treatment and some techniques are very slow. So, emphasis has been given to clean air and water though the use of photocatalysts, which break the organic pollutants to water and carbon dioxide without leaving a trace of by-products at the end.

Photocatalyst means alteration of the rate of chemical reaction by light radiation. Plants produce oxygen-utilizing energy from sunlight, similar to a photocatalysts. Fujishima and Honda used semiconducting titanium oxide (TiO_2) material as a photocatalyst in the early 1970's [2]. A photocatalyst absorbs photon energy from light radiation because of the unique electronic structure in the valance band (VB) and conduction band (CB), thus generating a hole and electron pair. The hole and electron pair reacts with surrounding molecules (water and pollutant), there by breaking down the pollutant through a chain of oxidation and reduction reactions. The energy levels between VB and CB, or band gap, determines the oxidizing and reducing capabilities of photo generated holes and electrons [61]. Figure 2.1 [62] shows the mechanism of a photocatalytic semiconductor. The band gap energy of the material generates electron hole pair when light of equal to or greater wavelength of the band energy falls on the material, which allows the reactions to proceed as given below:

$$Photocatalyst + h\nu \rightarrow e^- + h^+$$

$$H_2O \rightarrow H^+ + OH^-$$

$$e^- + O_2 \rightarrow O_2^-$$

$$h^+ + OH^- \rightarrow OH^\cdot$$

$$OH^\cdot + R \text{ (pollutant)} \rightarrow OH^- + R^* \text{ (oxidized)}$$

$$O_2^- + R \rightarrow O_2 + R^{**} \text{ (reduced)}$$

$$R^* \text{ (oxidized) or } R^{**} \text{ (reduced)} \rightarrow \text{ (final products)} \rightarrow CO_2 + H_2O$$

8
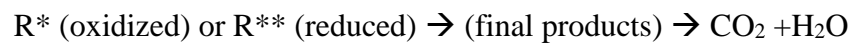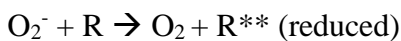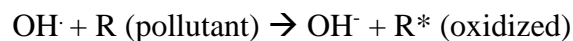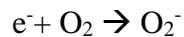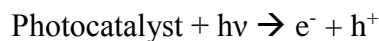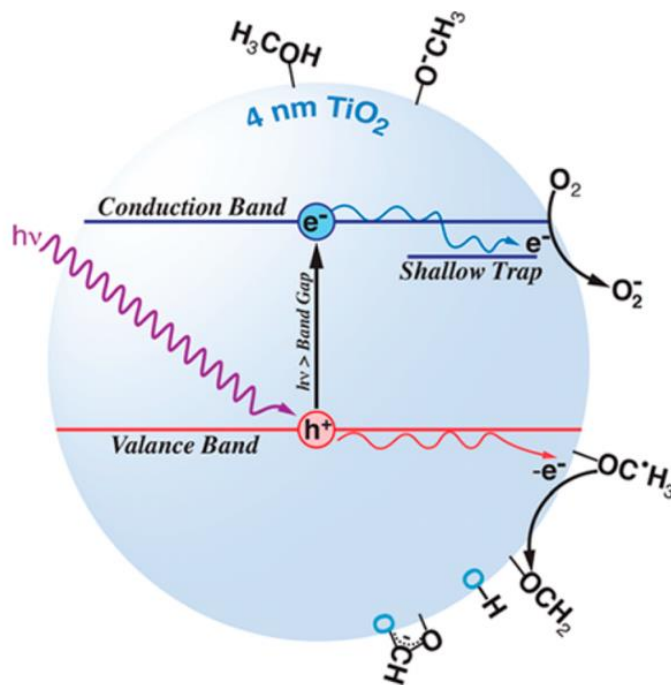
Figure 2.1 Photocatalytic mechanism of a TiO$_2$ semiconductor. Reprinted with permission from "Understanding TiO$_2$ Photocatalysis: Mechanisms and Materials" [62] by Schneider et al. © (2014) American Chemical Society.

In general, photocatalysts have significant advantages to perform catalytic activation from ultraviolet (UV) and visible spectrum of light depending upon the electronic structure and band gap of the material. Due to their different excited states, depending on the wavelength of irradiation, photocatalysts gives a tuning effect between the different reaction pathways of the pollutants [63]. The photocatalyst technique does not require any secondary disposal method and also leaves no trace of pollutants [64]. Photocatalytic remediation generally aligns with the zero waste plan for the waste & wastewater industry due to lower cost, environmental friendliness and sustainable treatment technology [65]. However, current photocatalytic materials show faster recombination time for electron and hole pair and poor absorption in visible light radiation [63].

The commonly used photocatalysts such as titanium oxide (TiO$_2$), zinc oxide (ZnO), tungsten oxide (WO$_3$) have band gap of nearly 3.2 eV as shown in Figure 2.2 [66]. The lower band gap energy of a semiconductor makes it a better photocatalyst. The cost, ease in

9

manufacturing, photostability, human & environment friendliness and effectiveness in solar light to catalyse the reaction are important factors in the selection of any photocatalyst [61, 67]. TiO_2, ZnO, WO_3, iron oxide (Fe_2O_3), and cadmium sulfide (CdS) are few important studied photocatalysts found in state-of-the-art literature [68]. The photocatalysts have a wide variety of applications like anti-fogging [69], anti-microbial [70], self-cleaning [71], air and water purification [65, 72], destruction of warfare agents [73], solar energy and hydrogen production through water splitting [74].
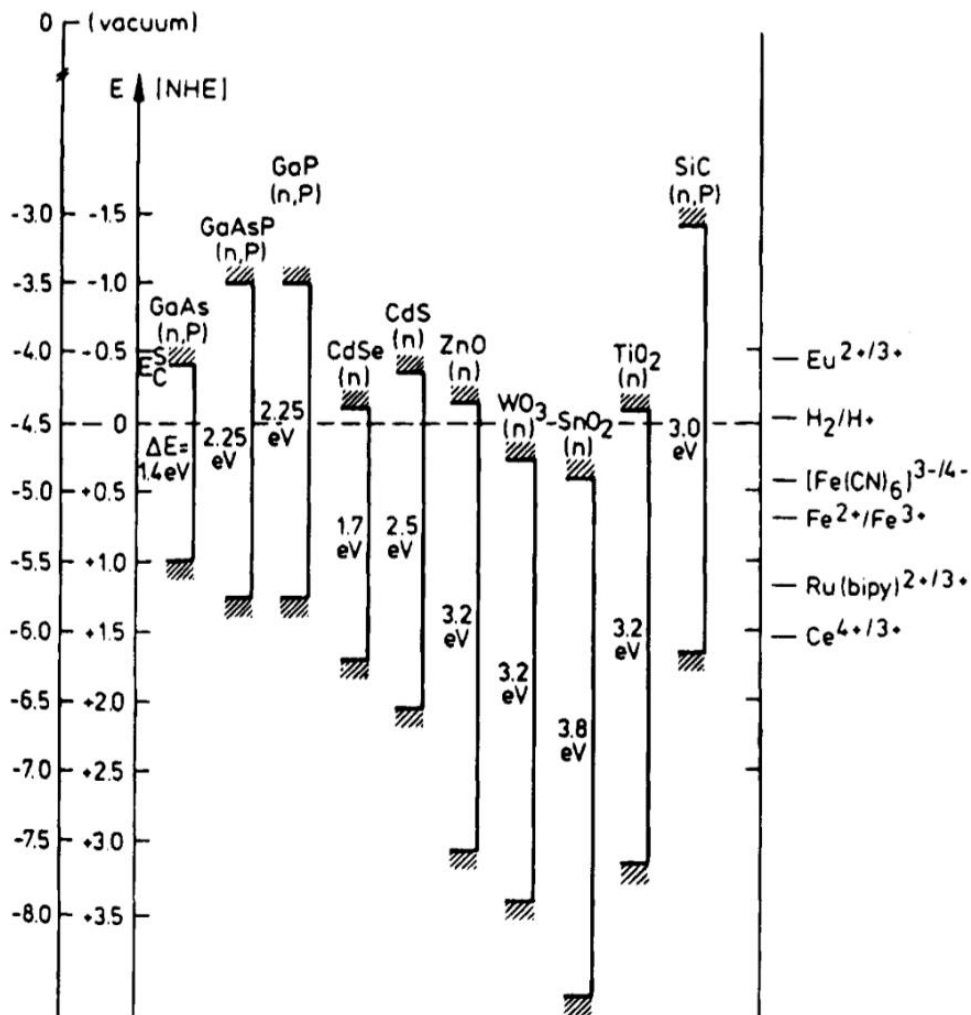
Figure 2.2 Band positions of various semiconductors at a pH of 1 (aqueous electrolyte). Reprinted with permission from "Light Induced Redox Reactions in Nanocrystalline Systems" [66] by Hagfeldt et al. © (1995) American Chemical Society.

10

2.2 Categories of Photocatalyst

2.2.1 Titanium Oxide (TiO_2)

TiO_2 is a semiconductor with a band gap of $3.0 - 3.2$ eV for rutile & anatase phases, respectively [75]. Electron (e^-) and hole (h^+) pair is created due to electron movement from VB to CB within femtoseconds due to the incident radiation photon energy of greater than or to ($\geq$) to band gap of TiO_2. In absence of pollutants, the electron and hole pair recombines and generates heat due to the faster recombination time of TiO_2 [76-79]. Serpone et al. found that more than 90% of photogenerated electrons had undergone recombination within 10 nanoseconds [80]. TiO_2 has been the most studied photocatalyst due to strong photocatalytic activity, high stability, low cost and non-toxicity [81, 82]. The work of Kato et al. has shown the decomposition of tetralin in a TiO_2 suspension [83], with further research done to oxidize ethylene and propylene [84]. Until the early 1970's, Fujishima and Honda described the photocatalytic prowess of TiO_2 as the "Honda-Fujishima effect" [1].

Extensive research was conducted to enhance the photocatalytic properties of TiO_2 for water and air decontamination of pollutants like ethanol, acetaldehyde, pentachlorophenol, methanol, acetic acid, propanol etc. [85-96]. Photo-application of TiO_2 has been used in dye synthesized solar cells [97-100], sensors [101-104], water splitting for hydrogen generation [105, 106], photocatalytic reduction of CO_2 [107, 108] and for remediation of various biological species [5, 109-114]. Apart from being explored as a photocatalyst, its major applications are also found in food products [115], pigments in paint [116], coatings [117], plastics [118], sunscreen/UV blocking pigments [119, 120], medicines [121] and most tooth pastes [122]. Currently, efforts are made to enhance the band gap for increasing the photocatalytic activity of TiO_2 by altering shape (nanowires, nanoparticles, etc.), size and doping (nitrogen, metal, and

11

carbon) [67, 123-136]. Figure 2.3(a) [137] shows the band diagram of undoped and N-doped TiO$_2$, while Figure 2.3(b) [137] reveals the reaction mechanism under visible light of N-doped TiO$_2$.
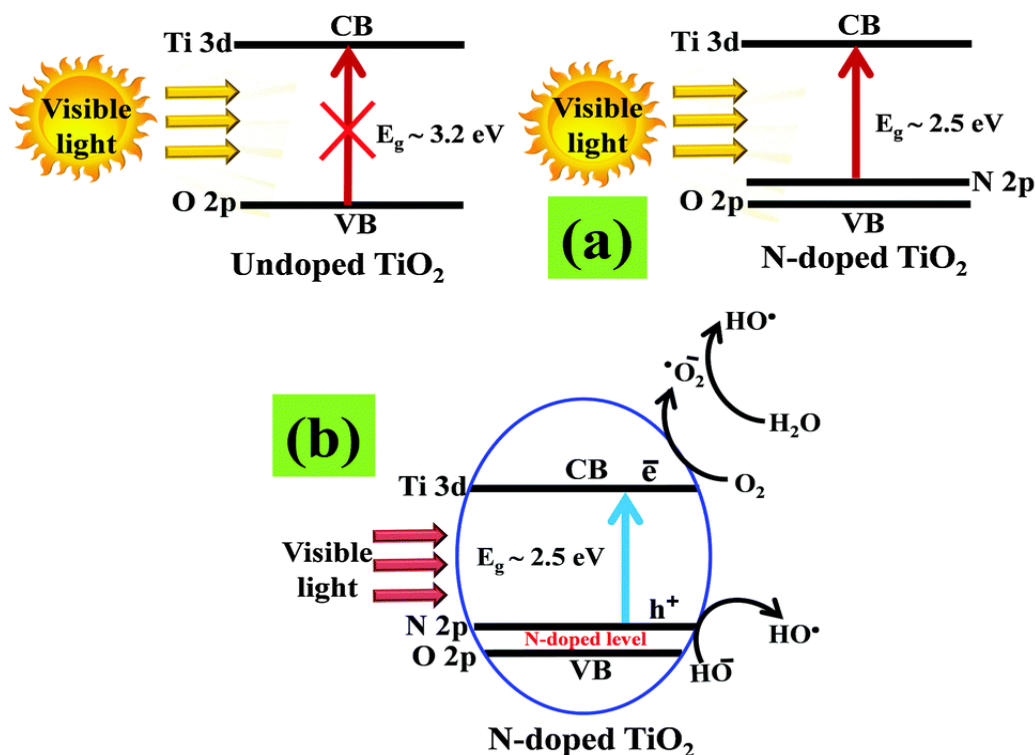
Figure 2.3 (a) TiO$_2$ –Energy level diagrams for undoped & N-doped (b) N-doped TiO$_2$ schematic for reaction mechanism under visible light irradiation. Reprinted with permission from "Nitrogen-doped titanium dioxide (N-doped TiO$_2$) for visible light Photocatalysis" [137] by Ansari et al. © (2016) Royal Society of Chemistry.

2.2.2 Zinc Oxide (ZnO)

ZnO has received attention due to complete photocatalytic remediation of environmental contaminants [138-154], having a band gap between 3.2-3.37 eV [155], and having properties similar to TiO$_2$ photocatalyst [75] [145, 156, 157]. ZnO has higher photocatalytic activity than TiO$_2$ due to point defects induced from oxygen vacancies generating higher hydroxyl ions and a faster reaction rate [158-163]. However, photo-corrosion of ZnO in the UV light spectrum results in decreased activity in an aqueous solutions [156, 164], but does not affect the gas phase

12

applications [165]. Figure 2.4 shows a silver ion grafted tip of ZnO has been used for the photo-reduction reaction of organic compounds [166, 167]. Photo-applications include dye-synthesized solar cells [168-170], sensors, water splitting [171-173] and biological applications. Apart from photo-applications, ZnO has been excessively used in the rubber industry [174, 175], ceramic industry [176, 177], medicines [178, 179], cigarette filters [180], food additives [181], pigments [182], UV absorbers [183], corrosion prevention [184], and piezoelectricity [185] among other uses. ZnO, similar to TiO_2, has a faster recombination time for the electron and hole pair, therefore various techniques have been employed to modify the crystalline size, morphologies, surface area and doping to alter the band gap of ZnO [79, 142, 186-194].
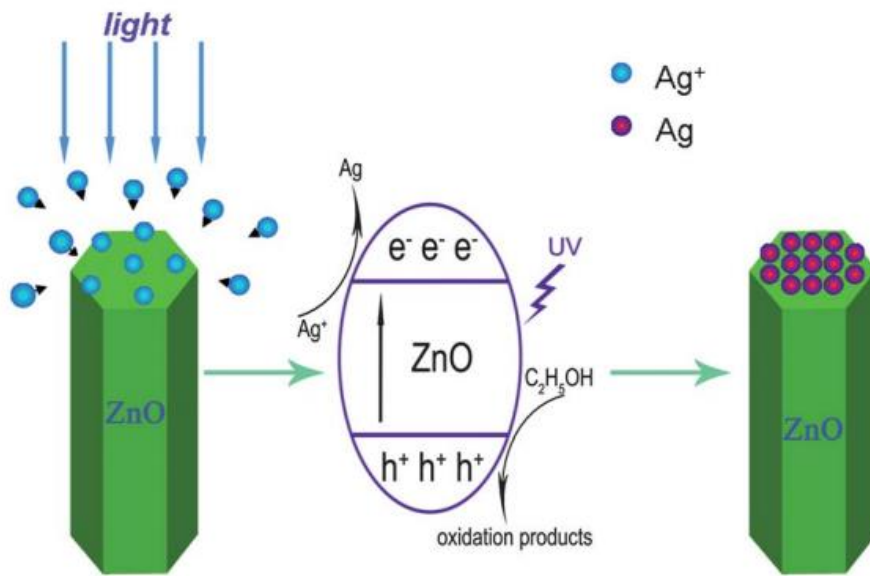
Figure 2.4 Photochemical reaction mechanisms for the formation of a Ag tip ZnO nanowire array. Reprinted with permission from "Vertically aligned ZnO nanowire arrays tip-grafted with silver nanoparticles for photoelectrochemical applications" [166] by Wang et al. ©(2013) Royal Society of Chemistry.

2.2.3 Tungsten Oxide (WO_3)

WO_3 is a transition metal oxide with metallic lustre in $LiWO_3$ shown by Wohler. Since the 1960's, tungsten oxides (WO_x) have been investigated with great interest for their chemical

13

and physical properties in electrochromic applications [195-207]. However, WO_x has an indirect band gap of 2.4 and 2.8 eV which is quite suitable for visible light photocatalysis as compared to TiO_2 and ZnO [196, 208, 209]. WO_x is an ideal candidate for efficiently using UV and visible light radiation for photocatalysis applications. WO_x nanoparticles have gained importance mainly due to the higher surface area to volume ratio, altered surface energies and quantum confinement effects [210]. Applications of WO_x consist of smart windows based on electrochromic devices [196, 197, 202, 205], solar cells [211-214], photocatalysis [215], optical recording devices [216, 217], sensors[218-225] and field emission applications [226-229] among other applications.

WO₃ is capable of working in the visible light spectrum, but its positive CB makes it thermodynamically unfavourable to split water into hydrogen. However, this limitation has been mitigated by applying an external potential to introduce photo-generated electrons [196]. By mixing the tungsten oxide particles with other metal oxides as a passive (secondary) photocatalyst, the CB has been shifted towards a negative potential there by promoting the photocatalyst performance [230]. WO₃ has been used in conjunction with TiO_2 to form a TiO_2/WO₃ photocatalyst which promotes photocatalytic activity [231]. Doping with non-metals like magnesium (Mg), cobalt (Co), nickel (Ni), copper (Cu), zinc (Zn), silver (Ag) and gold (Au) has shown enhanced photocatalytic performance compared to un-doped WO₃ [232-235]. Figure 2.5 shows the electron transfer in the CB of TiO_2 to WO₃ and similarly the hole transfer between the VB of WO₃ to TiO_2 [231]. The combined photocatalytic material shows the recycling of electrons, which enhances the lifetime of the electron–hole pair and helps stimulate the photocatalytic activity of WO₃. WO₃ has been effectively used as passive/assisted photocatalyst rather than employing as primary photocatalyst.

14
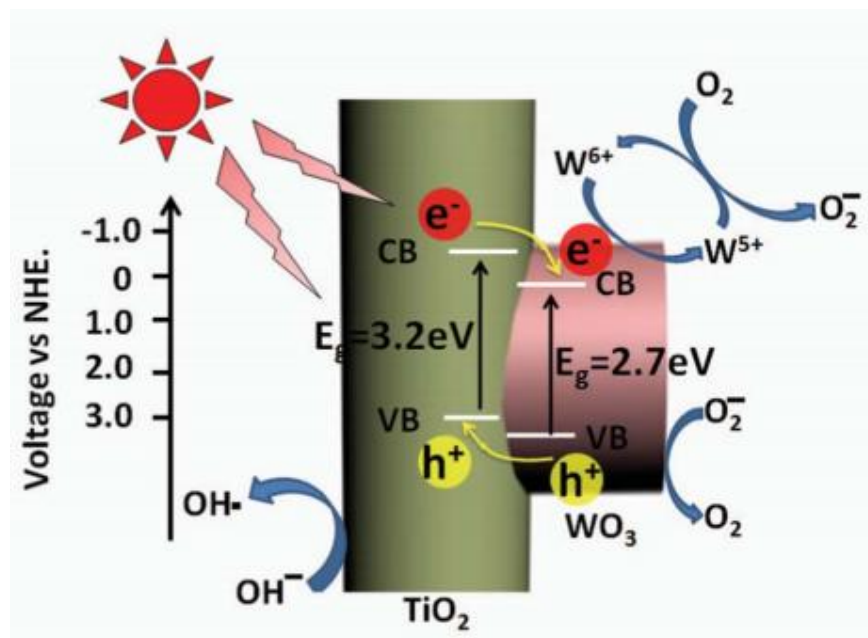
Figure 2.5 Energy band diagram of TiO$_2$/WO$_3$ nanofibers with the electron–hole pair separation. Reprinted with permission from "Hierarchical nanostructure of WO$_3$ nanorods on TiO$_2$ nanofibers and the enhanced visible light photocatalytic activity for degradation of organic pollutants" [231] by Zhang et al. © (2013) Royal Society of Chemistry.

2.2.4 Hematite (α-Fe$_2$O$_3$)

Iron oxide has three most common forms: Magnetite (Fe$_3$O$_4$), maghemite (γ-Fe$_2$O$_3$), and hematite (α-Fe$_2$O$_3$). Hematite is the most stable form of iron oxide and is an n-type semiconductor. It's applications include antiferromagnetic properties [236, 237], contrast material [238], therapeutic material for cancer treatment [239], gas sensors, lithium ion batteries [240-244] and as a water splitting photocatalyst for hydrogen production [241, 245-248].

2.2.5 Tin Oxide (SnO$_2$)

SnO$_2$-stannic oxide is a n-type semiconductor, having a bandgap of 3.6 eV at room temperature [249]. It has a very high electrical conductivity and optical transparency making it an important primary component for optoelectronic applications. SnO$_2$ applications extend from transparent conductors [250-252], catalysis [253-255], gas sensors [256-259], photocatalyst

15

applications [260, 261] including hydrogen production by water splitting [262, 263] , but mainly used as an assisted photocatalyst with TiO_2 and ZnO [262, 264-267].

2.3 Synthesis and Characterization of Photocatalyst Nanostructures

TiO_2 nanostructured photocatalysts have been synthesized through various techniques. The most commonly used synthesis techniques are sol-gel [268-275], sol [276-281], hydrothermal [282-288] and solvothermal [289-295]. Sol-gel and hydrothermal methods are used in an aqueous media, whereas sol and solvothermal employ a non-aqueous media for the reaction. Highly defined nanoparticle structures with chemical homogeneity is obtained through the sol-gel process [296-298]. In a typical process, titanium alkoxide is the precursor, which is then acidified for catalysing the process for preparation of the sol. The sol results in TiO_2, which is washed in deionized (DI) water and dried subsequently. Different shapes and sizes of TiO_2 nanoparticles have been synthesized by tweaking the process parameters.
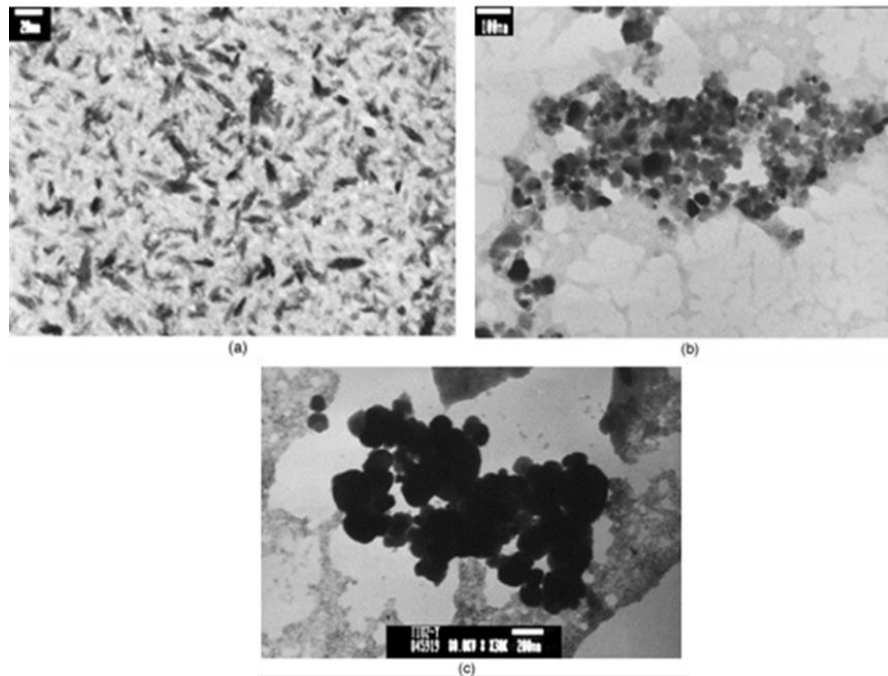
Figure 2.6 TEM image of (a) TiO_2 hydrosol, (b) dried TiO_2, (c) TiO_2 calcinated at 400 °C for 2 h. Reprinted with permission from "Sol–gel preparation and photocatalysis of titanium dioxide" [298] by Su et al. © (2004) Elsevier.

16

Figure 2.6 [298] shows TEM images of TiO_2 nanoparticles with diameters ranging from 20 to 40 nm. TiO_2 can be synthesized by heating the sol in air for longer time yielding single-phase anatase TiO_2 nanoparticles with varying size of particles in between 7 to 50 nm through sol-gel process [299-301]. Figure 2.7 shows XRD pattern of sol-gel synthesized TiO_2 dried at different temperatures from 400 to 700 °C. Samples of TiO_2 heated at 400 °C have crystalline structure with anatase phase, whereas heating of TiO_2 over 500 °C resulted in larger percentage of rutile phase of the TiO_2, which can be seen in Figure 2.7 [298]. This shows that controlled thermal treatment of TiO_2 will yield anatase or rutile phase.
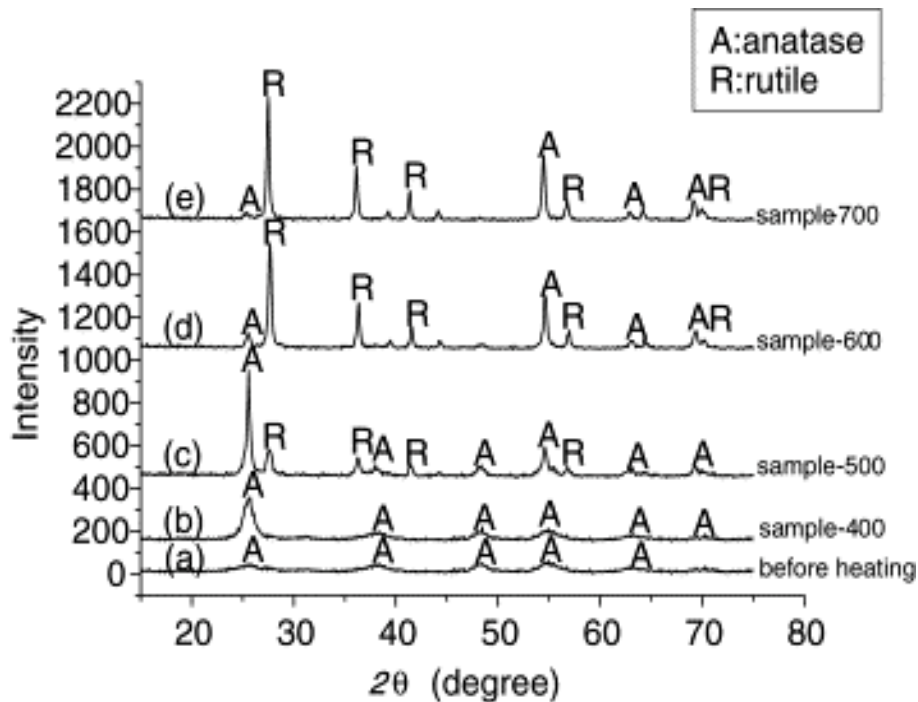
Figure 2.7 XRD pattern of sol-gel synthesized TiO_2 before heating and after heating to 400, 500, 600 and 700 °C for 2 h. Reprinted with permission from "Sol–gel preparation and photocatalysis of titanium dioxide" [298] by Su et al. © (2004) Elsevier.

Nanowire structures of TiO_2 can be obtained by employing a hydrothermal synthesis method. It employs a stainless steel pressure vessel with a Teflon liner to have controlled pressures and temperatures in an aqueous medium. Different nanostructures can be obtained

17

when TiO_2 nanoparticles are hydrothermally treated in the Teflon lined pressure vessel with NaOH/KOH with molarity ranging between 4-20 M and at temperatures ranging from 100–250°C. By varying the temperature between 100 -250 °C, the process can produce nanotubes, nanofibers and nanoribbons of TiO_2 [283].Figure 2.8 [283] shows the nanotube structure of TiO_2 synthesized through the hydrothermal technique in NaOH solution. It is shown that the outer diameter is within 8 to 10 nm, the inner diameter ranges from 5 to 6 nm, and the length ranges from 10 to 100 nm. Figure 2.9 [283] shows XRD pattern of TiO_2 synthesized at different temperatures. A small yield of 30% nanotube structure is observed for annealing at 100°C. However, an increase in temperature shows broadening in diffraction peaks due to increase in the size of the nanotubes [283].
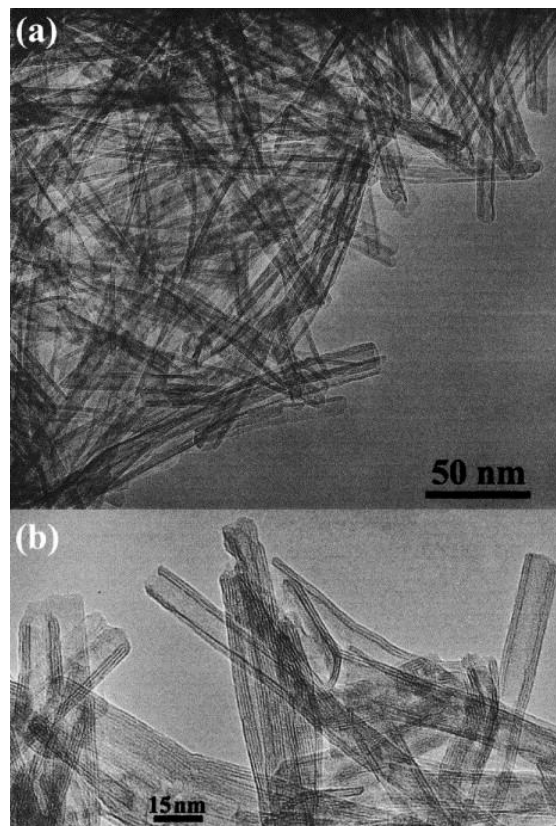
Figure 2.8 HRTEM image TiO_2 nanotubes (a) overall view (b) detailed view. Reprinted with permission from "Titanium oxide nanotubes, nanofibers and nanowires" [283] by Yuan et al. © (2004) Elsevier.

18
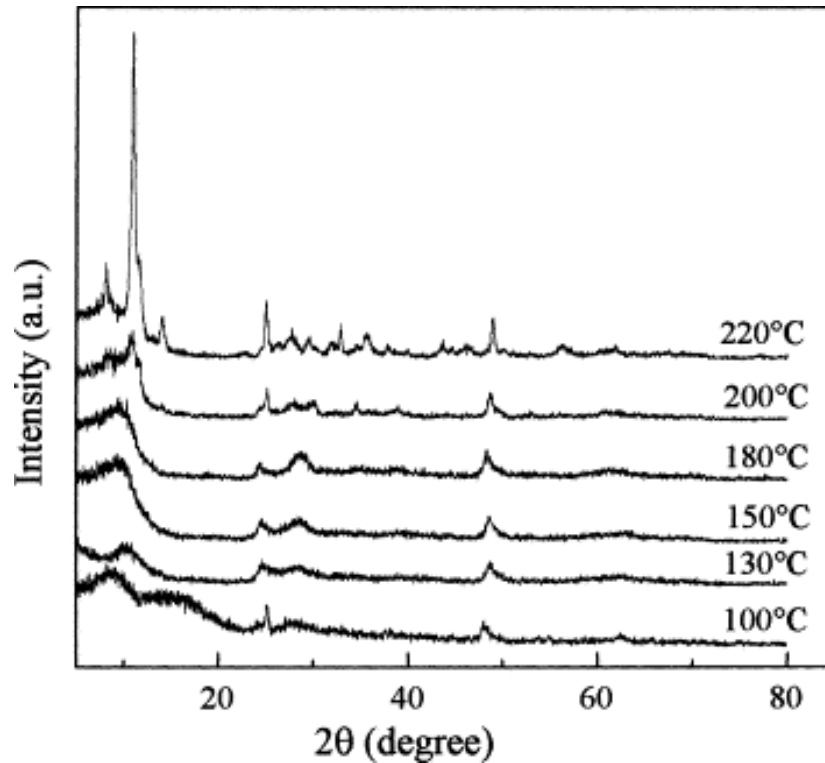
Figure 2.9 XRD pattern of TiO_2 (NaOH as precursor) at various temperatures. Reprinted with permission from "Titanium oxide nanotubes, nanofibers and nanowires" [283] by Yuan et al. © (2004) Elsevier.

ZnO is synthesized in various nanostructures such as nanoparticles, nanowires, nanofibers, nanoribbons etc. by employing general sol-gel [302-309], hydrothermal [142, 310-314] and vapour deposition techniques [315]. Typically ZnO nanostructures are obtained by mixing zinc salt with alcohol/water as solvent in NaOH/KOH, washing the precipitate in DI water and then drying at various temperatures [316]. Figure 2.10 [316] shows TEM images of ZnO nanoparticles where the diameters range between 12 to 38 nm. Figure 2.10a shows nanoparticles synthesized by employing aqueous media whereas Figure 2.10b shows non-aqueous media as solvent. It clearly shows that particle sizes are much smaller when non-aqueous media is employed which can be correlated to increase in BET surface area. Figure 2.11 [316] displays XRD patterns of ZnO nanoparticles synthesized through aqueous (Figure 2.11a)

19

and non-aqueous (Figure 2.11b) media. It is observed that Figure 2.11b has broader peaks, which

correlates to the smaller sized particles synthesized in non-aqueous media.
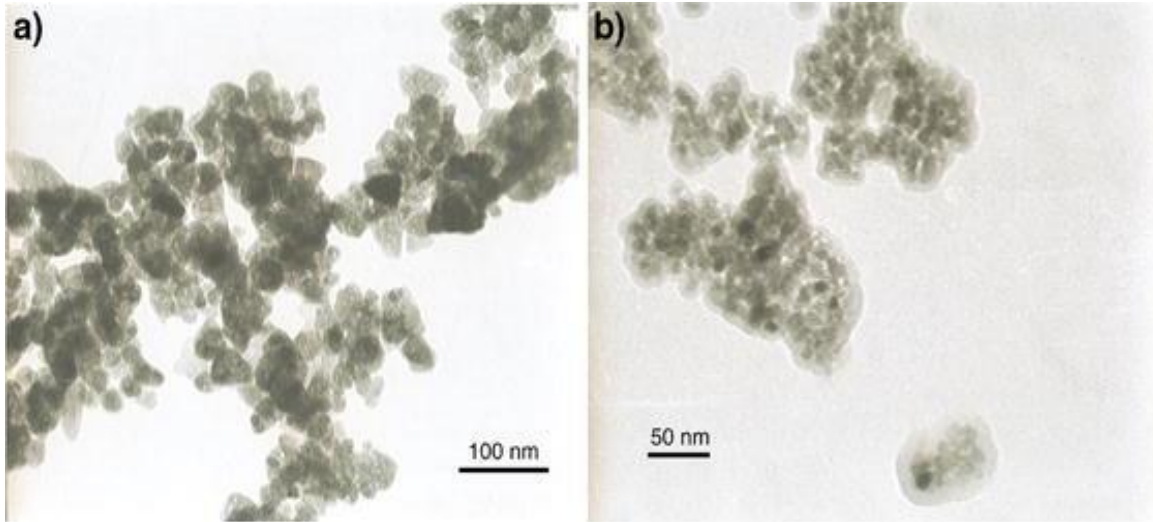
Figure 2.10 TEM images of ZnO nanoparticles synthesized in (a) aqueous media (b) non-aqueous media. Reprinted with permission from "Synthesis and characterization of zinc oxide nanoparticles: application to textiles as UV absorbers" [316] by Becheri et al. © (2007) Springer.
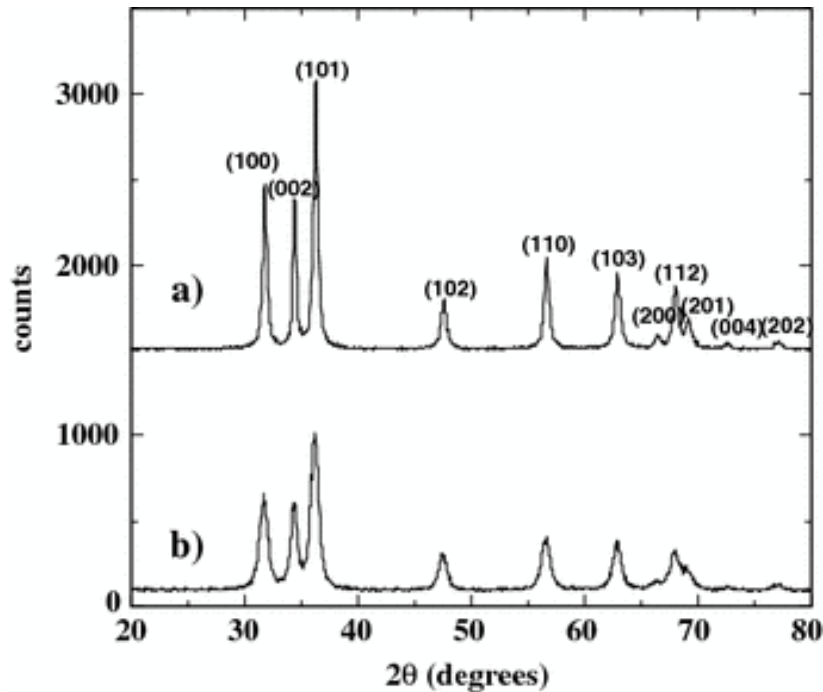
Figure 2.11 XRD patterns of ZnO nanoparticles synthesized in (a) aqueous media (b) non-aqueous media. Reprinted with permission from "Synthesis and characterization of zinc oxide nanoparticles: application to textiles as UV absorbers" [316] by Becheri et al. © (2007) Springer.

20

ZnO nanowires are synthesized using a hydrothermal technique, with zinc nitrate and hexamine as the precursors and zinc oxide nanoparticles acting as a seeding layer. Such techniques are used to vertically grow nanowires onto a substrate [317]. Figure 2.12 [318] shows the nanowire structures obtained through the hydrothermal process grown on thin film deposited on silicon substrate. Figure 2.13 [318] displays the XRD pattern of the ZnO nanowires. It is observed that peaks obtained from the XRD show the crystallographic planes of hexagonal ZnO. This method of hydrothermal synthesis of ZnO nanowires can you be used to grow nanowires onto a substrate as well as growing in colloidal form. The synthesis of aster like ZnO nanowires has been shown by Ladanov.et.al. using simple hydrothermal method with nanowires of uniform sizes were obtained [319].
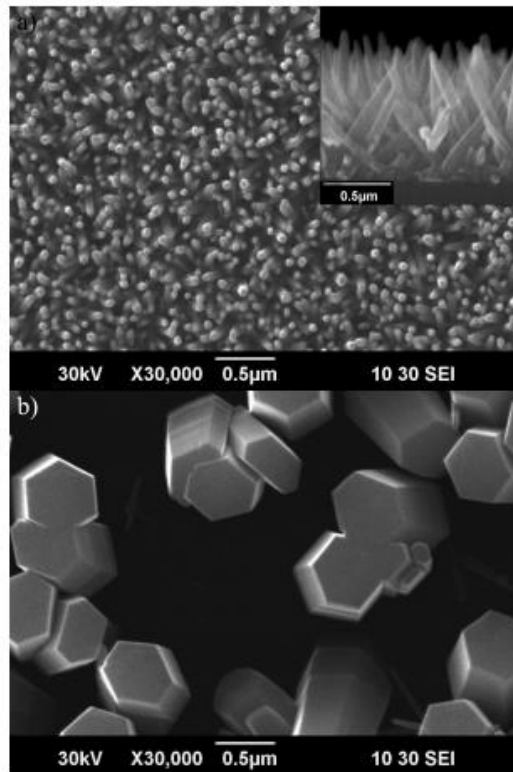
Figure 2.12 (a, b) SEM image for nanowire ZnO with varying magnifications. Reprinted with permission from "Structure and Opto-electrochemical Properties of ZnO Nanowires Grown on n-Si Substrate" by Ladanov et al. [318] © (2011) American Chemical Society.

21
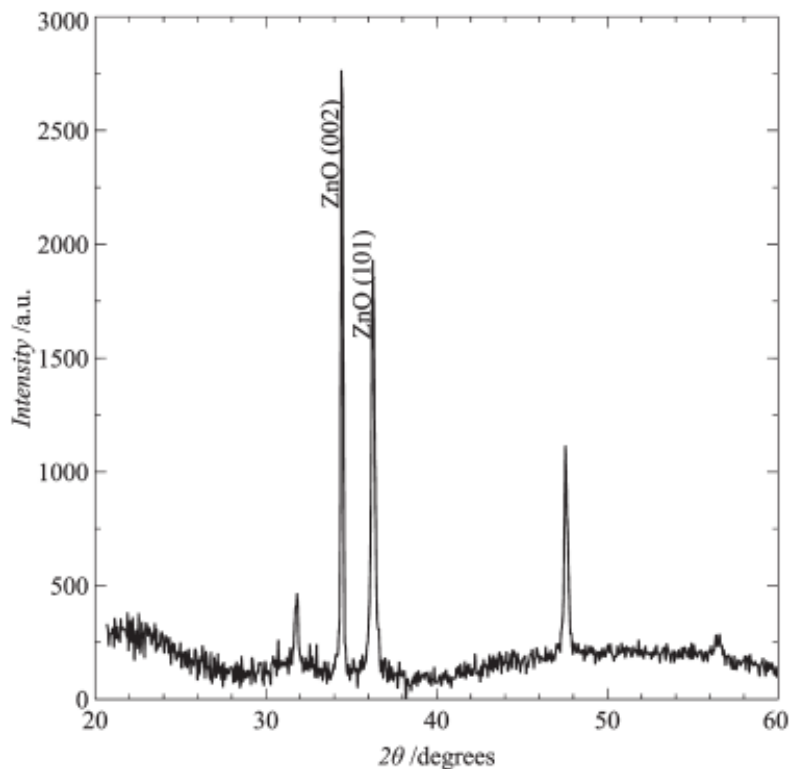
Figure 2.13 XRD pattern of nanowire ZnO grown on silicon substrate. Reprinted with permission from "Structure and Opto-electrochemical Properties of ZnO Nanowires Grown on n-Si Substrate" by Ladanov et al. [318] © (2011) American Chemical Society.

The nanoparticle structures of WO_3 have been synthesized through vapour phase [205, 320-324] and liquid phase like sol-gel [325-329], hydrothermal [293, 330-332] and anodization [333-335] techniques. The sol-gel method is employed to synthesize nanoparticles of WO_3 using tungstate salt (ammonium tungstate) and nitric acid, subsequent precipitation of sol followed by washing and drying to obtain WO_3 nanostructures [336]. Figure 2.14(a) [336] shows an SEM image, with EDS spectrum, of the WO_3 nanoparticles synthesized by the sol-gel method and Figure 2.14(b) shows the TEM image of the WO_3 where primary particle size is around 30 nm. Figure 2.15 [336] illustrates the XRD pattern of the WO_3 nanoparticles dried at different temperatures. The XRD pattern shows sharper peaks and an increase in degree of crystallinity of the WO_3 nanoparticles with an increase in temperature.

22
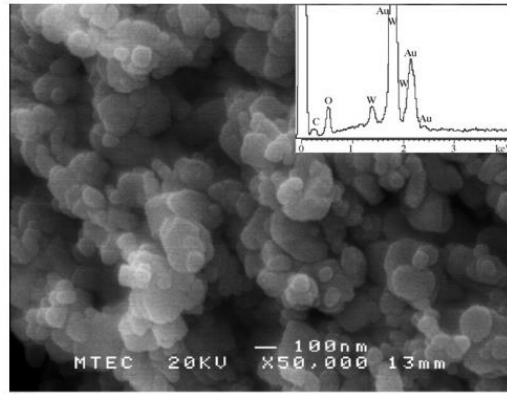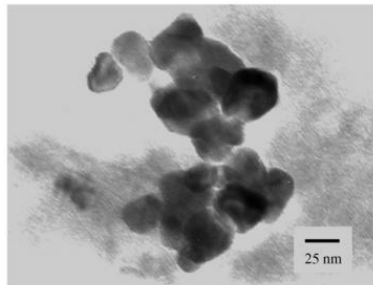
Figure 2.14 (a) SEM image of WO₃ calcinated at 400°C for 6 h. Inset is the EDS spectrum; (b) TEM image of the same sample. Reprinted with permission from "Synthesis of tungsten oxide nanoparticles by acid precipitation Method"[336] by Supothina et al. © (2007) Elsevier.
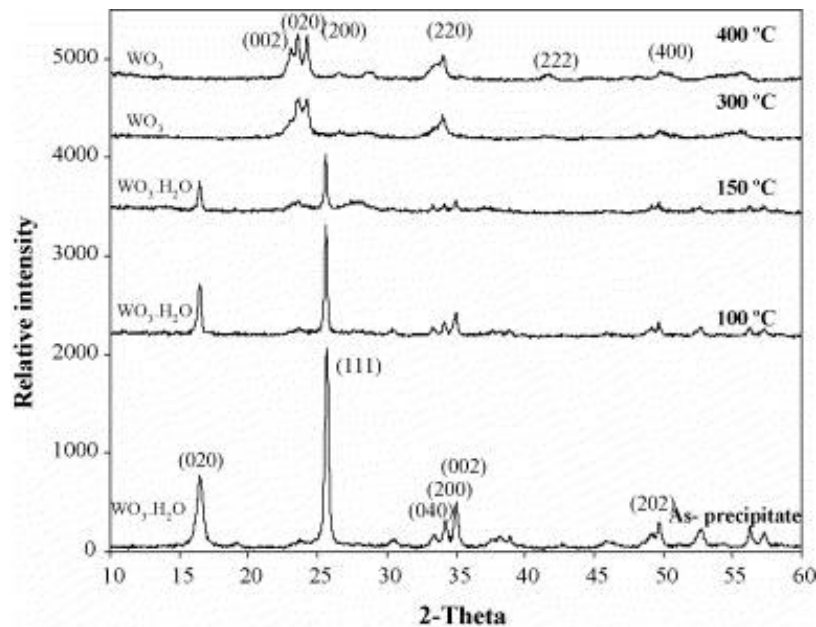
Figure 2.15 XRD pattern of WO₃ dried at various temperatures (100 to 400 °C). Reprinted with permission from "Synthesis of tungsten oxide nanoparticles by acid precipitation Method" [336] by Supothina et al. © (2007) Elsevier.

23
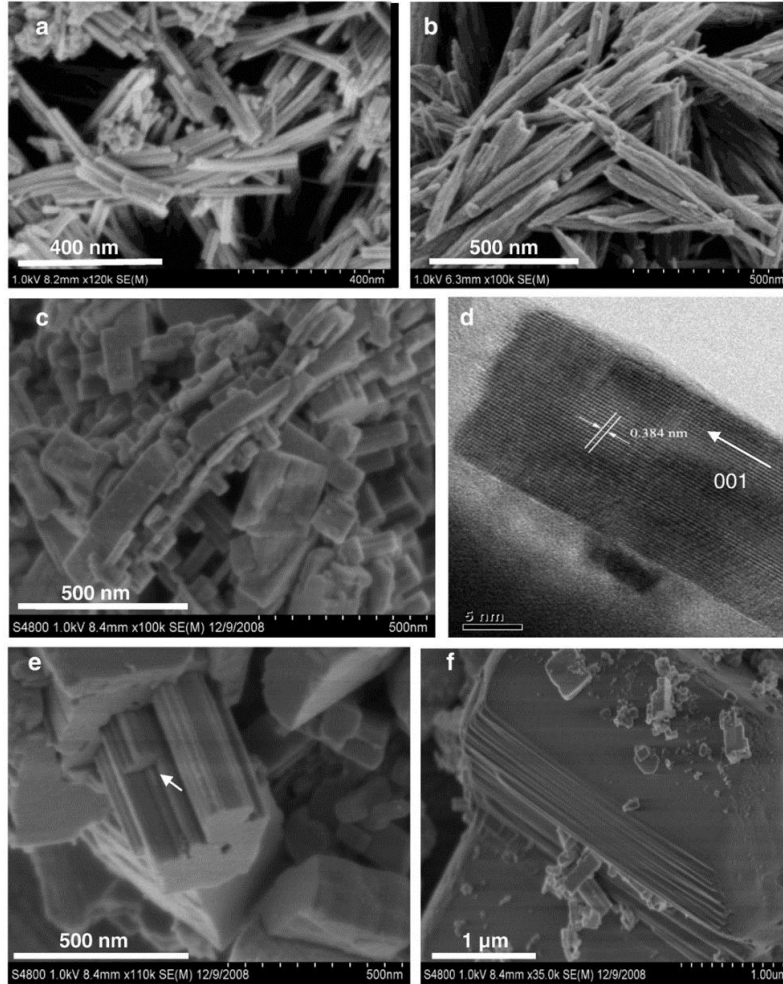
Figure 2.16 SEM images of WO_3 using (a) Na_2SO_4, (b) Li_2SO_4, (c) $FeSO_4$, (d) TEM image of cubic samples, (e, f) SEM images of cubic samples collected after 12 h & 72 h. Reprinted with permission from "Preparation of platinum loaded cubic tungsten oxide: A highly efficient visible light driven photocatalyst"[337] by Xu et al. © (2011) Elsevier.

Nanowires of WO_3 have been synthesized by a hydrothermal technique. In a typical synthesis process WO_3 sol materials have been prepared by dissolving sodium tungstate in DI water, followed by adding of HCl and oxalic acid. The precipitated WO_3 is transferred into a Teflon lined pressure vessel with the addition of sodium sulphate (Na_2SO_4)/ lithium sulphate (Li_2SO_4)/ iron sulphate($FeSO_4$). While keeping evertyhing else the same, the addition of these sulphates of sodium, lithium and iron cause WO_3 to form nanorods, toothpicks and cubic shapes respectively Figure 2.16 [337] shows the SEM images of WO_3 nanostructures formed at different

24

temperatures. It shows cubic, toothpick and nanorod stuctures of WO_3 obtained by varying the type of sulfate employed during synthesis. Figure 2.17 [337] shows the XRD patterns of the WO_3 nanorods, toothpicks, cubes and Pt doped nanorod structures. The peaks are narrow and strong for Figure 2.17 (a & b) which suggest perfect crystallinity of the hexagonal WO_3 in the nanorods and toothpicks, where as in Figure 2.17(c), the cubic samples show worse crystallinity compared to the nanorods and toothpicks.
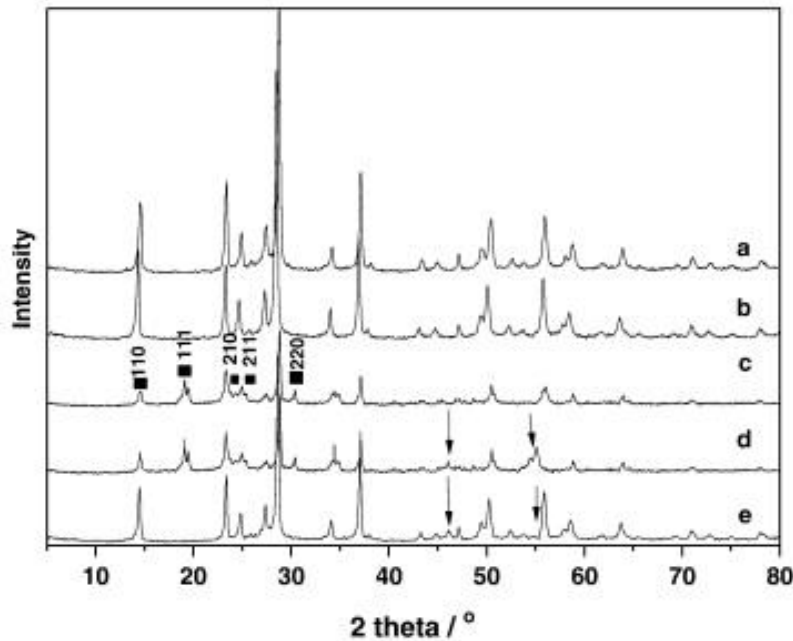
Figure 2.17 XRD patterns of (a) WO_3 nanorod, (b) WO_3 toothpick, (c) cubic WO_3, (d) Pt-WO_3 nanorod, (e) Pt-loaded cubic WO_3. Reprinted with permission from "Preparation of platinum loaded cubic tungsten oxide: A highly efficient visible light driven photocatalyst"[337] by Xu et al. © (2011) Elsevier.

2.4 Photocatalytic Activity

Commercial TiO_2 nanoparticles (P25 Degussa) are the most widely used material for photocatalytic remediation applications. Figure 2.18 [338] shows the UV-visible absorbance spectrum of TiO_2 (P25) and TiO_2 (P25) annealed at 150 °C for 10 h and 72 h. It is observed that the TiO_2 (P25) tends to absorb the UV light spectrum (<400nm), while thermal annealing of

25

TiO$_2$ (P25) enhances the absorbance of light radiation. The blue shifts into visible light radiation (wavelength >400nm) showed an increase in photocatalytic activity by heat treatment as shown by Yu et al. [339]. The major drawback of TiO$_2$ is being unable to function effectively in visible light radiation due to its faster recombination of electron-hole pair. Techniques like heat treatment, doping, and the use of different morphologies are employed to overcome these drawbacks. Table 2.3 shows the TiO$_2$ nanostructured materials, both with and without doping, for enhancement of photocatalytic properties under the visible light spectrum (wavelength > 400nm).
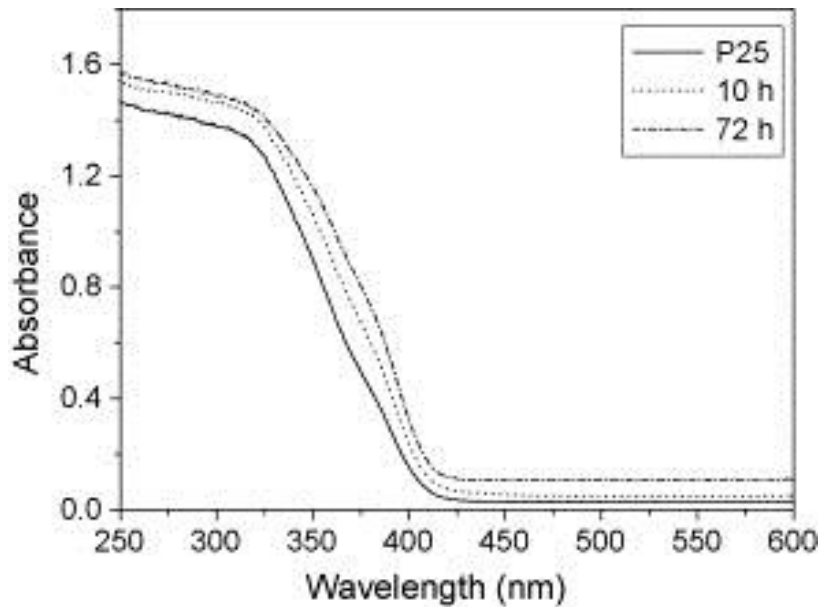
Figure 2.18 UV-Visible absorbance spectrum for TiO$_2$ (P25). Reprinted with permission from "Enhanced photocatalytic activity of TiO$_2$ powder (P25) by hydrothermal treatment" [338] by Yu et al. © (2006) Elsevier.

Table 2.3 reveals that doping TiO$_2$ with metal and non-metal ions enhances the photocatalytic behaviour under visible light radiation for remediating various organic contaminations in both air and aqueous media. Under identical conditions of light intensity and pollutant, the doped nanowires and nanotube structures have presented enhanced photocatalytic performance compared to the doped nanoparticle structures [340].

26

Table 2.3 TiO$_2$ nanostructured materials, with and without doping, for visible light photocatalytic remediation.

Material/Synthesis method	Properties of materials	Pollutant/light source	Results
P25 – commercial titania [340]	Average size 21 nm	Methylene blue (2 ppm)/solar light	100 min for complete remediation
TiO$_2$ nanowires /hydrothermal [340]	Width of 20-200 nm, length several μm		75% remediation in 100 min
Nitrogen - TiO$_2$ nanoparticle/ Solvothermal [341]	Average particle size of 9.6 nm	Methyl orange (10 ppm) & methyl blue (10 ppm) /visible	3 h for 100% remediation of MO & 60 min for 92 % degradation of MB
N-TiO$_2$ nanobelt/ hydrothermal [342]	50-400 nm wide and 10 μm long	Methyl orange (20 ppm)/ visible	50 % remediated after 6 h
Nitrogen -TiO$_2$ nanotubes/electrochemical anodization [343]	Average diameter of 80 nm, wall thickness of 15 nm	Methyl orange (20 ppm) pH 3 /visible	80% after 60 min.
Iodine -TiO$_2$ nanoparticle/ hydrolysis [344, 345]	Average diameter of 5 nm	Methyl orange (10 ppm)/visible	69.8% remediation after 180 min
Iodine-TiO$_2$ nanospheres/hydrothermal [344, 345]	Average diameter of 300-500 nm		92.8% remediation after 180 min
Iodine-TiO$_2$ nanotubes/ hydrothermal [346]	10 & 7nm outer & inner diameter respectively, length of 20-80 nm	Phenol (20 ppm)/ visible	Complete remediation after 240 min
Zirconium –iodine- TiO$_2$ nanoparticle /hydrolysis [347]	Grain size of 7.5 nm	Methyl orange (0.03 mM)/ visible	98% remediation after 180 min
Lanthanum-iodine- TiO$_2$/hydrolysis [348]	Crystalline size of 3.57 nm.	Oxalic acid/ visible	~ 95% removal after 180 min
Lanthanum- TiO$_2$ /hydrolysis [348]	Crystalline size of 4.42 nm		~ 30% removal after 180 min
Cobalt-TiO$_2$ nanotubes/ anodization [349]	Inner diameter of 90–100 nm, wall thickness of 20-25 nm	Methylene blue (2 ppm)/ visible	~ 60% degradation after 60 min
WO$_3$-TiO$_2$ nanotubes/anodization [349]	Particles size of Co 20-50 nm		~ 70% degradation after 60 min

27

Table 2.3 (Continued)

			~ 97% degradation after 60 min
Cobalt –tungsten oxide- TiO₂ nanotubes/anodizing [349]			
Silver -TiO₂ nanoparticle/sol-gel [350]	Absorption wavelength around 400 nm	Rhodamine B/ visible	Complete remediation after 10 min
Silver/silver chloride-TiO₂ nanotubes/ anodization [351]	Inner diameter of 120 nm and length of 550nm	Methyl orange (10^{-5} M)/ visible	Complete remediation after 60 min
Vanadium-TiO₂/sol-gel [352]	Particle size of 6 to 8 nm	Methylene blue (2.8×10^{-5}M)/ visible	Reaction rate of 3.87×10^{-7}mol/lh
Cerium-TiO₂ nanoparticle /sol-gel [353]	Average size approx.10.3 nm	Nitrobenzene (50 ppm)/ visible	5% conversion within 4 h
N-cerium-TiO₂ nanoparticle/sol-gel [353]			52% conversion within 4 h
Cerium -TiO₂ hollow sphere/hydrothermal [354]	Crystalline size of 8.3 nm	Reactive brilliant red X-3B (25 ppm)/ visible	Degradation around 92.3% after 80 min
Nitrogen -Fluorine -TiO₂ nanotubes/ anodization [355]	Amorphous structure	Methylene blue (2 ppm)/ visible	80% remediated after 2 h
Carbon-TiO₂ /hydrothermal [356]	Pore diameter – 8nm	Rhodamine B /visible	59% degradation after 5 h
Carbon nanotube-TiO₂ /hydrothermal [357]	Crystalline size of TiO₂ is 6.4 nm	Methyl orange (20 ppm)/ visible	95% reduction in 240 min
Graphene-TiO₂ nanoparticle/ hydrothermal [340]	30-50 nm in size	Methylene blue (2 ppm)/ solar light	100 % degradation in less than 40 min
Graphene doped TiO₂ nanowire/hydrothermal [340]	Width 20-200 nm, length upto several μm		100 % degradation in less than 20 min

ZnO is one of the most highly used materials in solar cell applications. It faces the same major drawback of faster electron-hole recombination time [186, 187] as TiO₂. It has been observed that photocatalytic activity of ZnO is greatly affected by morphologies, size and dopants. Figure 2.19 [358] shows the effect of particle size on photocatalytic performance of

28

ZnO for oxidation for $n-C_7H_{16}$. It is clear from the figure that reduction of the nanoparticle size showed increases in the photocatalytic activity.
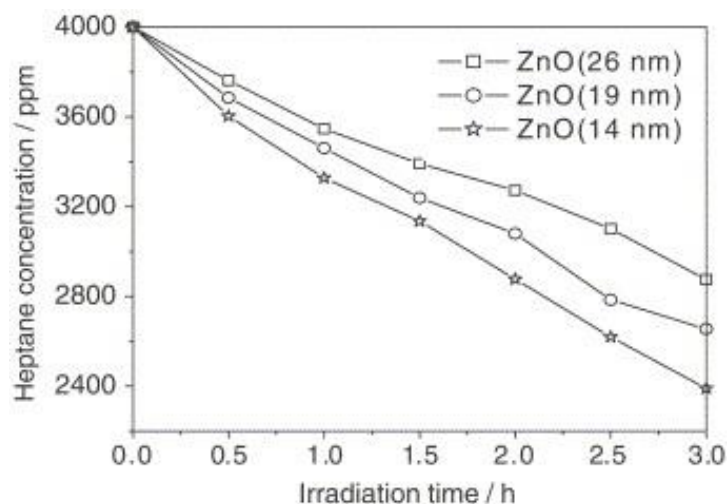
Figure 2.19 Photocatalytic remediation of $n-C_7H_{16}$ using ZnO nanoparticles. Reprinted with permission from "Relationships of surface oxygen vacancies with photoluminescence and photocatalytic performance of ZnO nanoparticles" [358] by Jing et al. © (2005) Springer.

Table 2.4 shows the photocatalytic properties under the visible light spectrum (wavelength > 400nm) for ZnO nanostructured materials with and without doping. The dopant in ZnO does not necessarily increase the photocatalytic activity as shown in Table 2.4. The enhanced photocatalytic activity is shown by comparing the nanowire to the nanoparticle structures of ZnO [359]. The metal dopants create intermittent band gaps rather than narrowing band gap of ZnO nanostructures.

Table 2.4 ZnO nanostructured materials, with and without doping, for visible light photocatalytic remediation.

Material/ Synthesis method	Properties of materials	Pollutant/ light source	Results
ZnO nanoparticle/ thermal plasma [359]	Granular structure	Methylene blue $(10^{-5}$ M)/ visible	80% decomposition after 30 h
ZnO tetrapod/ thermal plasma [359]	30 nm diameter and 100-200 nm in length		90% decomposition after 30 h

29

Table 2.4 (Continued)

ZnO nanorods/ thermal plasma [359]	30-50 nm diameter, 200-300 nm length		95% decomposition after 30 h
ZnO nanofiber/ electrospinning [360]	Mean diameter of 78 nm	Rhodamine B/ visible	90% degraded after 19 h
Cobalt - ZnO nanorods/ hydrothermal [361]	Diameter 50-80 nm & lengths of 0.2-1.5 μm	Alizarin red dye (20 ppm)/ visible	93% decomposed after 60 min.
Nitrogen-ZnO nanopowders/ spray pyrolysis [362]	Crystalline size 25.2 nm	Acetaldehyde gas phase/ visible	Roughly 10 times faster than ZnO nanoparticles
Manganese -ZnO/ wet chemical [363]	Average particle size-73nm	Methylene blue 10^{-5} M in 20 ml ethanol/ visible	50 % decoloration in 5 min, 50 times faster than undoped ZnO particles
Carbon - ZnO nanosheet flowers/ pyrolysis [364]	9 μm particle size, 10 nm thickness	Rhodamine B (10^{-5} M)/ visible	Almost disappears after 80 min.
Nickel - ZnO nanosheets/ sol gel [365]	Width 0.5–1μm, length ~5 μm	Malachite green/ visible	Decreases photocatalytic activity compared to ZnO nanosheets
Sodium - ZnO nanowire/ thermal decomposition [366]	Average diameter 40 nm	Orange G (0.02 nM)/ visible	Complete degradation after 120 min
Silver nanospheres on ZnO nanorods/ microwave reactor [367]	ZnO – 10-20 nm diameter Ag- 60 nm average	Methylene blue (5 ppm)/ visible	85% degradation after 120 min
Cobalt - ZnO nanowires/ solvothermal [368]	Diameter 25-200 nm, length up to 3 μm	Methylene orange (10 ppm)/ visible	90% remediated with 5 h

WO$_3$ has a lower band gap (2.4 – 2.8 eV) compared to TiO$_2$ and ZnO materials. The structure, morphology and doping in WO$_3$ is varied to enhance photocatalytic activity. Figure 2.20 [369] shows CO$_2$ conversion efficiency of Pt and N-doped WO$_3$ compared to TiO$_2$ based

30

nanostructures in visible light radiation. It is clear from the Figure 2.20, that doping has enhanced the photocatalytic activity of WO_3.
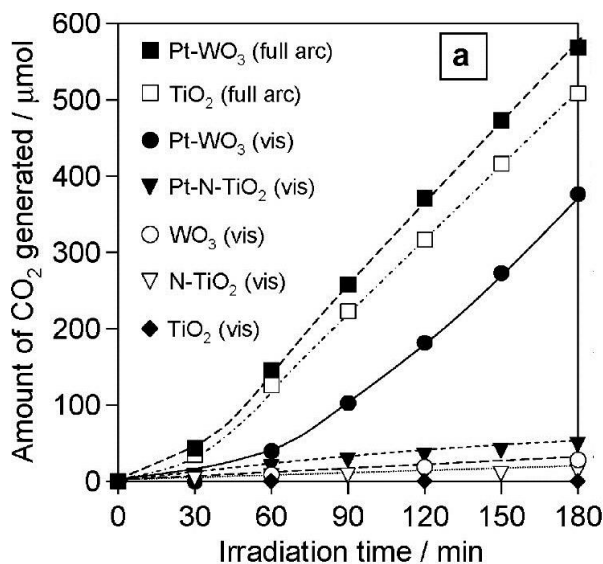
Figure 2.20 The photocatalytic activity for WO_3 and TiO_2 with Pt and N dopants. Reprinted with permission from "Pristine Simple Oxides as Visible Light Driven Photocatalysts: Highly Efficient Decomposition of Organic Compounds over Platinum Loaded Tungsten Oxide" [369] by Abe et al. © (2008) American Chemical Society.

Table 2.5 shows the WO_3/W_xO_y nanostructured materials, with and without doping, for photocatalytic properties under visible light. Table 2.5 shows photocatalytic studies of different WO_3 structures with and without dopants. The nano cubic/wire structures of WO_3 exhibit higher photocatalytic properties when compared to the nanoparticle based structures. It also shows that doping WO_3 increases photocatalytic properties[337].

Table 2.5 Tungsten oxide nanostructured material, with and without doping, for visible light photocatalytic remediation.

Material/ Synthesis method	Properties of materials	Pollutant/ light source	Results
WO_3 nanoparticle commercial[370]	-	Methyl orange (20 ppm)/ visible	20% degradation in 300 min
TiO_2 – WO_3 nanocomposites/ hydrothermal [370]	Particle size – 16 nm		85% degradation in 300 min

31

Table 2.5 (Continued)

WO_3 spherical flower/ hydrothermal[371]	Size 2 -4 μm	Rhodamine B $(10^{-5}$ M)/ visible	60% degradation within 5 h
Pt doped WO_3 nanoparticle - commercial[215]	Average diameters of 2- 4nm	Acetaldehyde (500ppm)/ visible	90% conversion to CO_2 after 4 h
Pt doped WO_3 nanotubes/ solvothermal[371]	Outer diameter 300-1000nm & lengths 2-20μm		100 conversions to CO_2 after 4 h.
$W_{18}O_{49}$ nanowire/ hydrothermal[371]	10-20 nm diameter with lengths 1-2 μm	Methylene orange (50 ppm)/ visible light	68% degradation in 25 min
$W_{18}O_{49}$- RGO/ hydrothermal [371]			Complete remediation within 25 min
$KTi_{0.5}W_{1.5}O_6$/ sol-gel[372]	-	Methylene blue (10 ppm)/ visible	66% degradation after 180 min
N doped $KTi_{0.5}W_{1.5}O_6$/ annealing[372]	0.23% nitrogen by weight		83% degradation after 180 min
Tin-$KTi_{0.5}W_{1.5}O_6$/ ion exchange method[372]	7.93% tin by weight		94% degradation after 180 min
Na^+ -WO_3 nanowire/ in situ doping (bulk) [373]	Diameter-100nm/single crystal	Methylene blue (25 ppm)/ visible	90% degradation for bulk doped 60% degradation for surface doped
Palladium - WO_3 nanoparticle/ photo deposition[374]	Pd addition ratio – 0.5 wt. %	Methylene blue (10 ppm)/ visible	27 times faster than pure WO_3
CuO-WO_3 nanoparticle/ flame spray[375]	Average diameter 20 nm	Methylene blue (50 ppm)	27% degradation after 6 h
Iron-WO_3 hollow spheres/ template [376]	Grain size – 10 nm	Rhodamine B (20 ppm)/ visible	95% degradation within 120 min
Cerium - $W_{18}O_{49}$/ solvothermal[377]	Average diameter of tens of nm and lengths - 200 nm to μm	Methylene orange (10 ppm)/ visible	89% reduction after 30 min

2.5 Literature Review Summary

Photocatalytic remediation has significant advantages over other methods (mechanical, chemical, and biological), since it uses naturally available energy (UV light & visible light) to

32

remediate organic pollutants into harmless by-products to carbon dioxide (CO_2) and water (H_2O).Photocatalysts for wastewater treatment and drinking water applications have been increasing over the last decade along with water splitting applications for the production of hydrogen. Photocatalytic process is environmentally sustainable method to remediate the hazardous organic waste compounds, and recently attention has been shifted towards the oxidation/reduction of both volatile organic and inorganic compounds existing in the ground water for effective treatment process.

Photocatalysts faces a major challenge due to faster electron-hole recombination time, which makes it difficult in organic remediation applications where there is insoluble organic compounds. In this investigation the issue by changing the interfacial charge though a doping process, and modification of surface properties/morphologies such as nanowires /nanotubes / nanoparticles and application of surfactant to enhance the contact of insoluble pollutant with the photocatalyst have been undertaken. It is known that photocatalyst destroys any organic matrix which encounters, so investigation of a new binder material has been undertaken which would not only react with photocatalyst, but also enhances its photocatalytic performance.

Beside these limitations, photocatalysts have a major edge over other procedures because it is only green-assisted procedure over chemical, mechanical and biological techniques. The decontamination through photocatalysts is considered a 100 % oxidation/reduction or mineralization of pollutant compounds similar to biological treatment which is highly economical treatment and highly compatible with the environment. The solar light can be employed for green technological applications and biological treatment can be replaced by heterogeneous photocatalysts for pollutant removal.

33

CHAPTER 3: TITANIUM OXIDE BASED NANOSTRUCTURE MATERIALS FOR WATER REMEDIATION[2, 3]

3.1 Introduction

Titanium oxide (TiO_2) nanostructure has been most studied metal oxide photocatalyst material. It has a large bandgap of 3.2 eV which makes it suitable for UV spectrum of light (wavelength $\lambda < 400$ nm) but not suitable for visible light photocatalysis ($\lambda > 400$nm). When doping materials such as platinum (Pt), silver (Ag), molybdenum (Mo), boron nitride (BN), and boric acid etc., have been introduced, it is observed the band gap of TiO_2 photocatalyst is narrowed towards visible light radiation. Dopants like Ag and Pt are expensive and cannot be used in mass conditions. To test the effect of doping material on photocatalytic performance of TiO_2, various dopants have been considered like boron nitride (BN), boric acid, molybdenum disulfide (MoS_2), Ag along with graphene (G) as G being a unique material with exceptional electrical and quantum properties. The samples of TiO_2 nanowires were prepared using standard hydrothermal methods along with different dopants and photocatalytic performance have been measured using methyl orange as organic pollutant in water. Further photocatalytic performance of TiO_2 is compared in nanoparticle and nanowire structure with and without 'G' as doping material.

---

[2] Srikanth Gunti, Ashok Kumar, Manoj K. Ram, "Comparative Organics Remediation Properties of Nanostructured Graphene Doped Titanium Oxide and Graphene Doped Zinc Oxide Photocatalysts", published 30 July 2015, American Journal of Analytical Chemistry, 2015, 6, 708-717

[3] Srikanth Gunti, Michael McCrory, Ashok Kumar, Manoj K. Ram, "Enhanced Photocatalytic Remediation Using Graphene (G)-Titanium Oxide (TiO_2) Nanocomposite Material in Visible Light Radiation", published 21 July 2016, American Journal of Analytical Chemistry, 2016, 7, 576-587

Appendix A for copyright permission

TiO$_2$ nanostructures have been synthesized through various techniques like sol-gel, sol, hydrothermal and solvothermal. For simplicity and homogeneity of nanostructures obtained through sol-gel (nanoparticle) and hydrothermal (nanowire), these two methods have been employed in synthesis of nanoparticle and nanowire structures of TiO$_2$. The chemicals such as hydrochloric acid (HCl), propanol, titanium (IV) isopropoxide, sodium hydroxide (NaOH), methyl orange (MO) and other reagents were used for the preparation of nanostructured materials and the chemicals were procured from Sigma-Aldrich (USA). The commercial TiO$_2$/P25 was also obtained from Sigma Aldrich (USA) for comparative remediation studies. The graphene (G) platelets of size < 20 nm in thickness were acquired from Angstron Materials, a commercial company in USA.

3.1.1 Synthesis Procedure

The nanowire structure of TiO$_2$ was synthesized using hydrothermal technique with initial precursors of titanium oxide (TiO$_2$) nanoparticles in aqueous solution of sodium hydroxide (NaOH). The synthesis was initiated by addition of 6 g TiO$_2$ (P25) to 70 ml of 10 M NaOH solution with resulting solution stirred for 30 min and, 20 ml of the solution was transferred to Teflon coated autoclave and kept at a constant temperature of 150 ℃ for 48h. The precipitate was washed using 0.1 M HCl solution for multiple times with an observation that the precipitate showed pH of below 7. The precipitate was centrifuged, and dried at 100 ℃ for 24 h and further annealed at 300 ℃ for 4 h to obtain pristine TiO$_2$ nanowire structures. Various doping materials of 100mg each as G, MoS$_2$, AgNO$_3$, BN, Boric acid have been added to initial precursors of TiO$_2$ nanoparticles and NaOH to obtain doped TiO$_2$ nanowires with no alteration of procedure.

TiO$_2$ nanoparticles were synthesized by using sol-gel technique with initial precursors of titanium (IV) isopropoxide in propanol solution. Initially, 20 ml propanol is mixed with slow

35

addition of 4 ml of titanium (IV) isopropoxide in round bottom flask. The mixture was stirred for 30 min, and later, HCl solution was added drop wise, and allowed the solution to stir for another 24 h at room temperature. The precipitate was washed using deionized water (DI) for removing the unreacted organic residues, later it was centrifuged and dried at 100℃. For synthesizing G doped TiO_2 nanoparticles, 0.193 g of G was mixed with initial precursor of 20 ml propanol with no alteration of procedure.

3.1.2 Sample Preparation and Decontamination Setup

In the process, 0.2 g of photocatalytic material were coated onto a petri dish with the use of acetic acid and dried at room temperature. Later, it was heated at 200°C for 30 min. 20 ppm of 40 ml MO was added to petri dishes, and illuminated by light of 30-watt with light intensity of 800 W/m^2. The decontamination setup on petri dish can be seen in Figure 3.1. The remediated samples were collected from the main remediating sample in an interval scale of hours. Attempts were also taken to vary the time interval in some cases in collecting the remediating sample. JASCO V-530 UV-Visible spectrometer was used to measure the absorbance of MO. Initial concentration of MO was taken as C_o at 0 hours. The percentage of concentration ratio was calculated by using C_n/C_o with respect to time in hours.

$$\% \, Concentration \, Ratio \; = \; 100 * \frac{Concentration \, at \, time \, interval \, (Cn)}{Initial \, concentration \, (Co)}$$
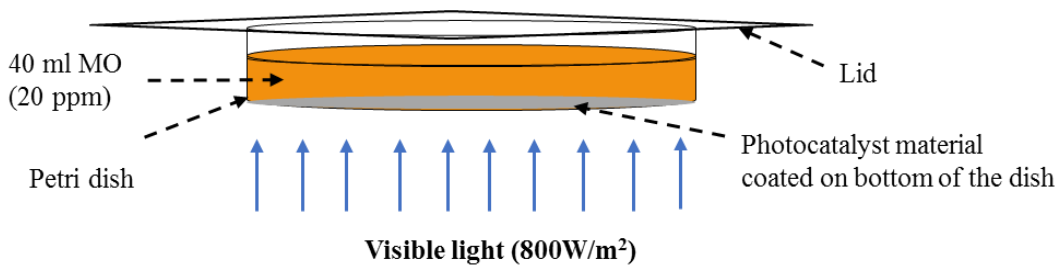
Figure 3.1 Decontamination setup.

3.2 Photocatalytic Performance of Various Dopants onto TiO₂ Nanowire

3.2.1 Scanning Electron Microscopy (SEM)

Figure 3.2 (a, b, c, d, e & f) shows the nanowire structures of TiO₂ synthesized using various dopants. Figure 3.2 a shows the pristine TiO₂ nanowire (TiO₂ NW) structure synthesized through hydrothermal method. It can be observed that the nanowires are around 50-500 nm in diameter and 500nm to 3000 nm in length.
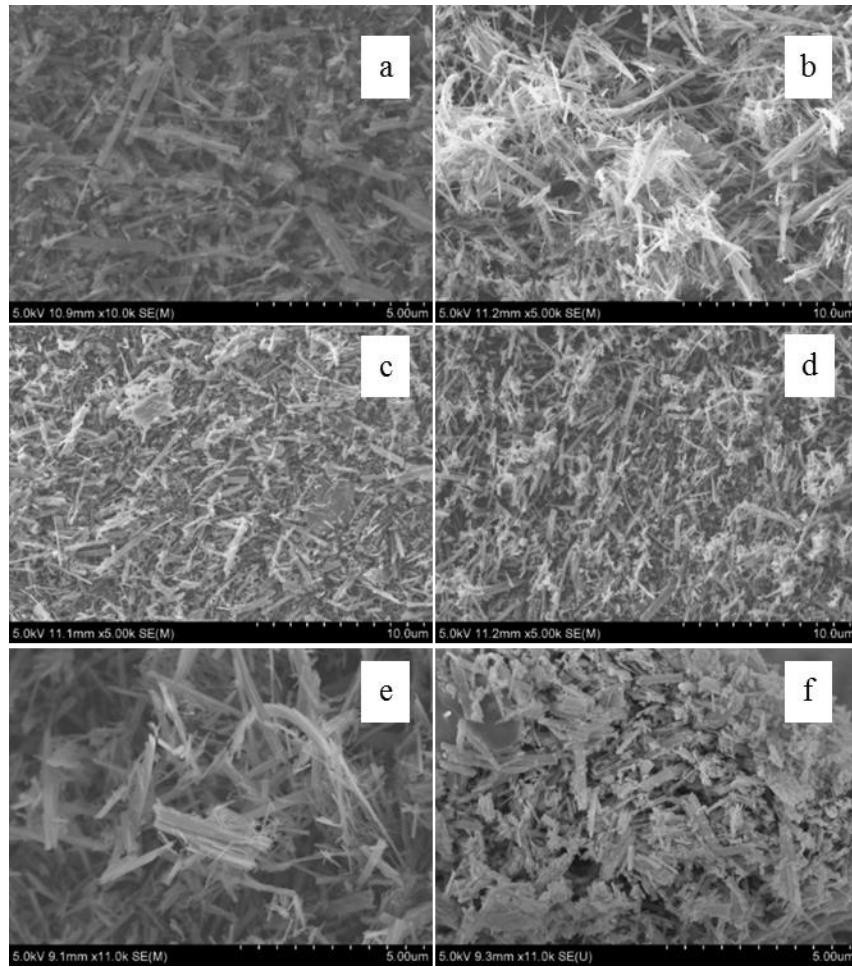
Figure 3.2 SEM images of (a) TiO₂ NW (b) G-TiO₂ NW (c) MoS₂- TiO₂ NW (d) Ag- TiO₂ NW (e) BN-TiO₂ NW (f) Boric acid -TiO₂ NW at various magnifications.

To confirm whether agglomeration of nanowires occurred, transmission electron microscopy (TEM) for the pristine TiO₂ NW have been shown in Figure 3.3. It has been

37

observed form Figure 3.3 that the nanowires of TiO_2 have indeed agglomerated together during synthesis procedures and the size of nanowires was observed to be in-between 30-100 nm in diameter and lengths up to 100-3000 nm. In Figure 3.2 b, shows the SEM image of G –TiO_2 NW distribution in which graphene flakes have been distributed onto TiO_2 NW. Figures 3.2 (c, d, e & f) shows the SEM images of MoS_2- TiO_2 NW, Ag- TiO_2 NW, BN-TiO_2 NW, boric acid -TiO_2 NW, respectively. It can be observed that nanowires obtained through various doping materials are also within 50-500 nm in diameter and 500-3000 nm in length due to agglomeration during process.
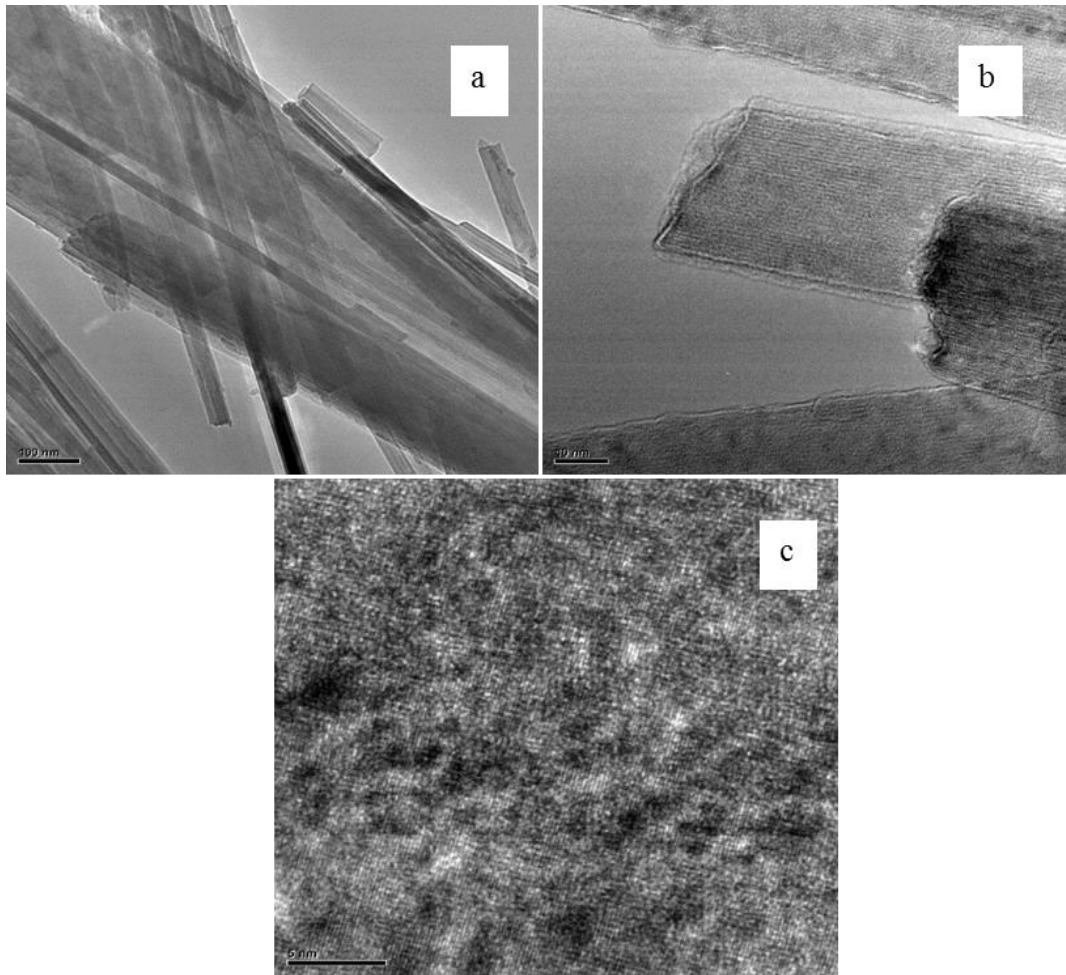
Figure 3.3 (a, b, c) TEM images of TiO_2 nanowire at various magnifications.

3.2.2 X-ray Diffraction (XRD)
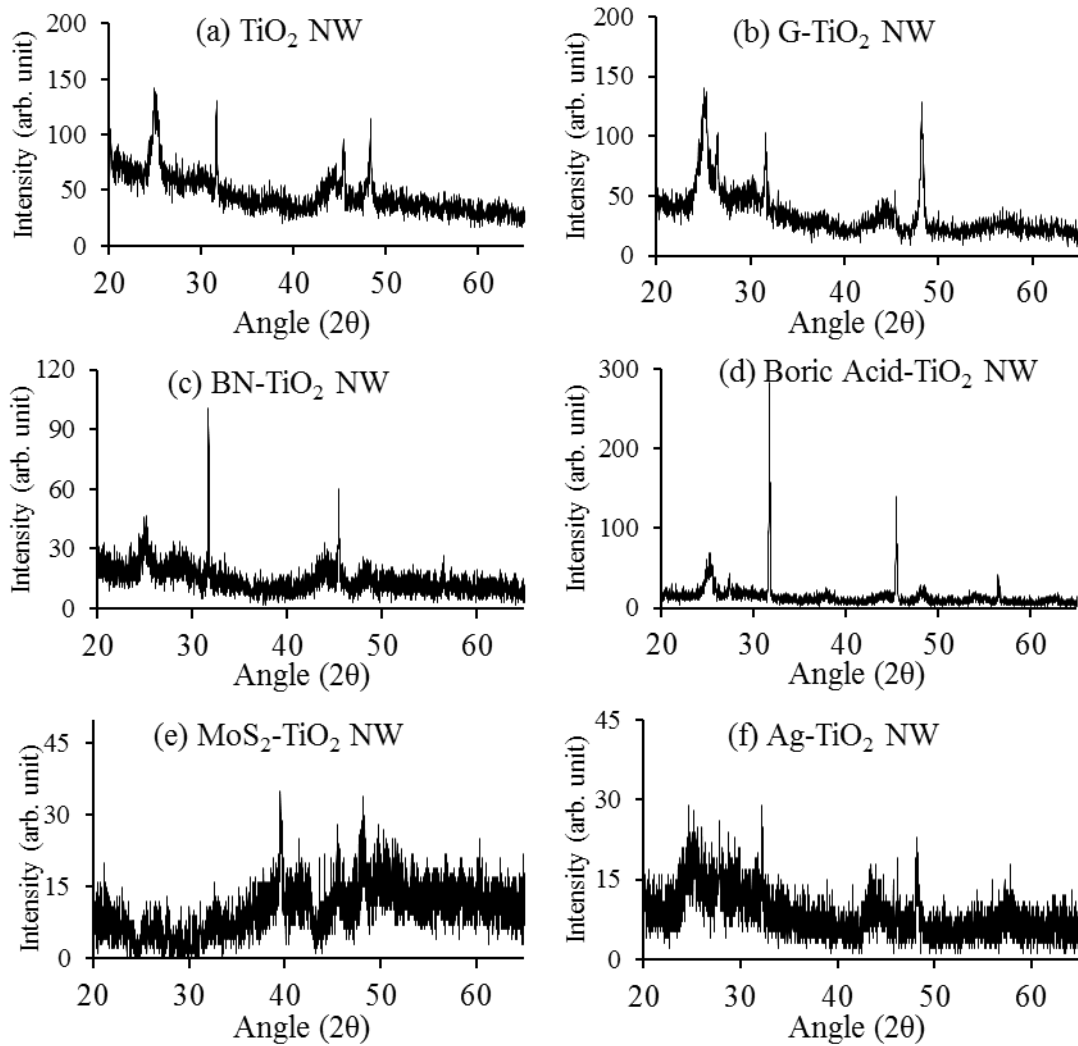
Figure 3.4 XRD pattern of (a) TiO₂ NW (b) G-TiO₂ NW (c) BN-TiO₂ NW (d) Boric acid -TiO₂ NW (e) MoS₂- TiO₂ NW (f) Ag- TiO₂ NW.

XRD images of TiO₂ NW with various doping's have been shown in Figure 3.4. The presence of peaks at 25.27, 37.85, 47.83, 54.55, 63.59 degrees are due to TiO₂ anatase phase. In Figure 3.4 b, shows the presence of the peak at 26.5 degrees is due to the presence of graphene (002) plane [378]. In Figure 3.4 c shows the hexagonal BN (002) peak at 25 degrees coinciding with peak of anatase TiO₂ around 24.27 degrees. In Figure 3.4 d, the peak 32 degrees is due to the presence of boric acid which has an angle shift when doped onto TiO₂ NW [379]. In Figure

3.4 (e & f), shows doping with MoS_2 and Ag decreased the overall crystallinity of the NW of TiO_2 with no characteristic peaks for MoS_2, Ag.

3.2.3 Photocatalytic Activity

Figure 3.5 shows the photocatalytic performance of TiO_2 NW in comparison with doped TiO_2 NW for remediation of 20 ppm of 40 ml methyl orange (MO). It can be observed that G doped TiO_2 nanowires have the best photocatalytic performance over other doped TiO_2 nanowires. It can be understood that, due to graphene unique electrical properties, high photocatalytic performance has been observed for G-TiO_2 NW. It can also be seen that MoS_2 doped TiO_2 NW has very low photocatalytic performance as compared to pristine TiO_2 NW which is due to the fact that not all doping materials will enhance the performance of TiO_2 photocatalyst. Based on the results obtained for remediation of MO with different doping materials in TiO_2 NW, G have been chosen as primary doping material for further studies.
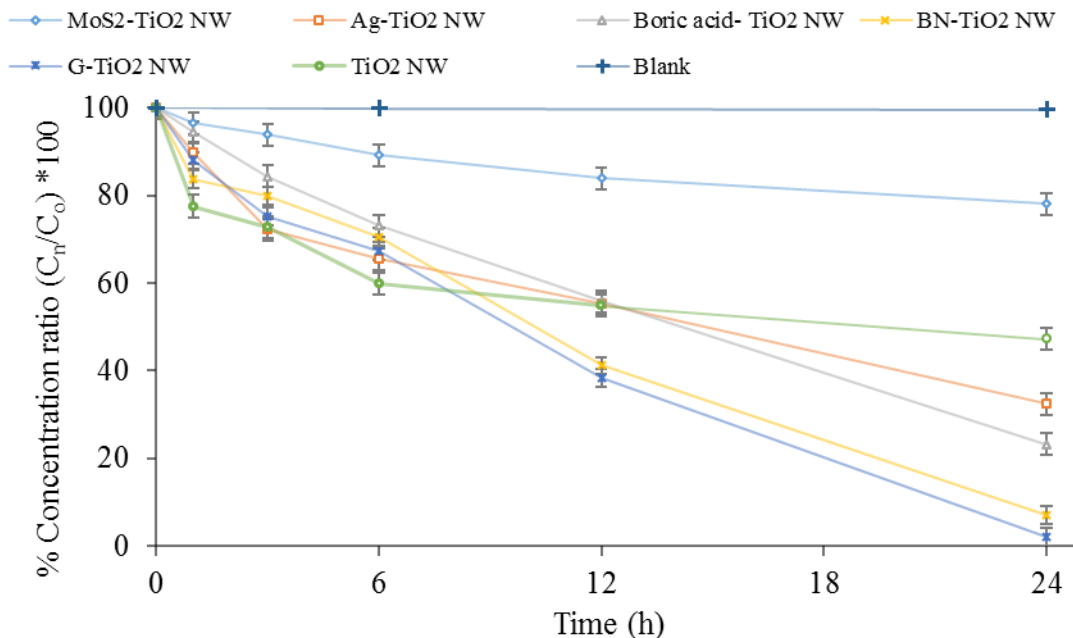
Figure 3.5 Photocatalytic performance of TiO_2 NW in comparison with G-TiO_2 NW, MoS_2-TiO_2 NW, Ag- TiO_2 NW, BN-TiO_2 NW and Boric acid -TiO_2 NW.

40

3.3 Photocatalytic Performance of Nanowire vs Nanoparticle Structures of TiO$_2$

3.3.1 Scanning Electron Microscopy (SEM)
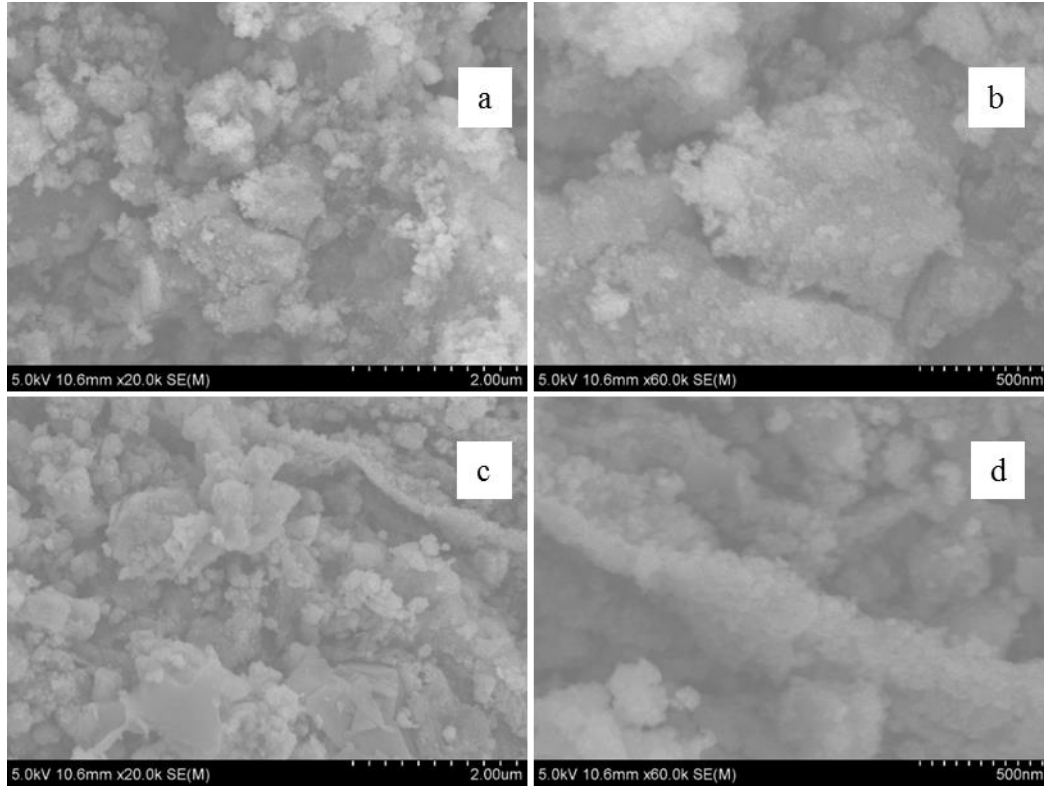
Figure 3.6 SEM images of (a, b) TiO$_2$ nanoparticles, (c, d) G-TiO$_2$ nanoparticles at various magnifications.

Figure 3.6 shows the SEM image of TiO$_2$ nanoparticle (TiO$_2$ NP) and G doped TiO$_2$ nanoparticle (G-TiO$_2$ NP). Figure 3.6 c observes the surface morphology of G-TiO$_2$ NP, which reveals the compact particles distribution of photocatalytic material. A potential explanation for formation for compact particle structure in G-TiO$_2$ NP is due to dispersion of TiO$_2$ particles on graphene sheets. The Figure 3.6 d, shows the SEM image of G-TiO$_2$ NP at 500 nm magnification. The typical graphene structure is covered by TiO$_2$ NP, which range in between 20-50 nm. The size of nanoparticles of G-TiO$_2$ is observed in transmission electron microscopy (TEM) study, which can be witnessed in Figure 3.7. Indeed, shows the well-defined graphene coated TiO$_2$ nanoparticles. Figure 3.7 b reveals d-spacing with inter-planar structure of G-TiO$_2$

41

nanoparticles. The Y-axis shows d spacing of different crystalline planes presented in the G-TiO$_2$ nanomaterial. The x-axis in Figure 3.7 b is the characteristics ring used for calculation of inter-planar place of G-TiO$_2$ based polycrystalline nanomaterial. The error bar is calculated using 10 different measurements per crystalline structure which confirms the polycrystalline structure in G-TiO$_2$ nanocomposite.
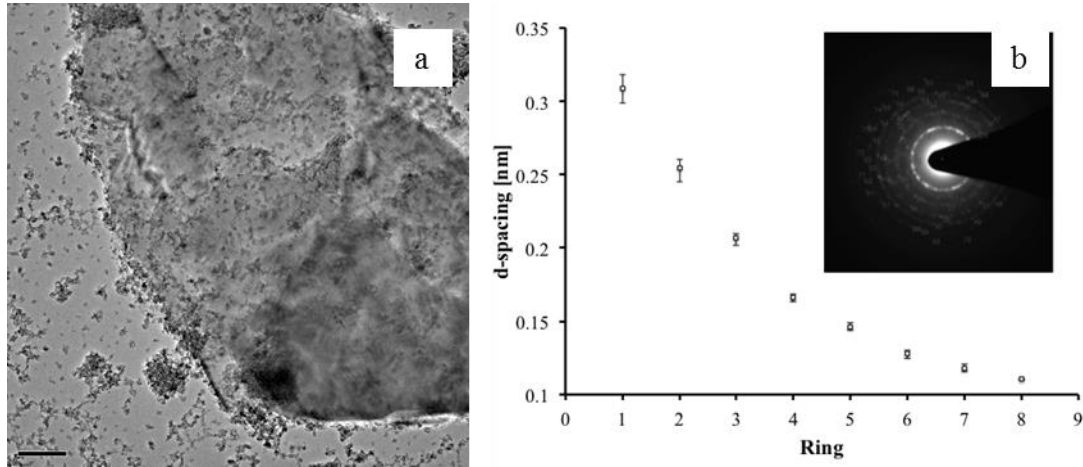
Figure 3.7 TEM image of G-TiO$_2$ nanoparticles.

3.3.2 X ray Diffraction (XRD)
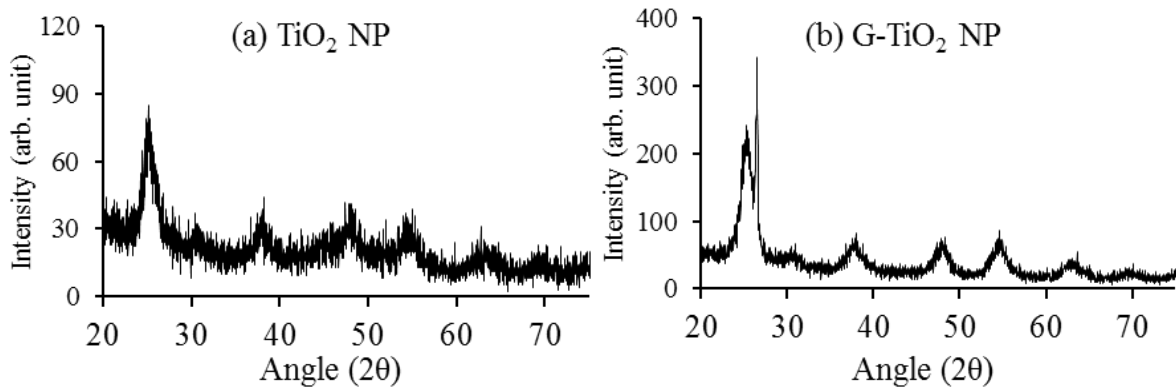
Figure 3.8 XRD pattern of (a) TiO$_2$ NP, (b) G-TiO$_2$ NP.

Figure 3.8 shows the XRD pattern of TiO$_2$ NP and G-TiO$_2$ NP. The strong diffraction peak at 26.51 degrees [378] is indicative of presence of graphene (002) plane in G-TiO$_2$ structure in Figure 3.8 b. The presence of peaks at 25.27, 37.85, 47.83, 54.55, 63.59, 70.15 degrees are due

42

to the anatase TiO$_2$ phase present in TiO$_2$ NP and G-TiO$_2$ NP which correspond to (101), (004), (200), (105), (204), (220) planes of anatase TiO$_2$ respectively [380]. The structure indicates the forms of crystallinity TiO$_2$ and G-TiO$_2$ nanomaterials.

3.3.3 UV–visible Spectroscopy
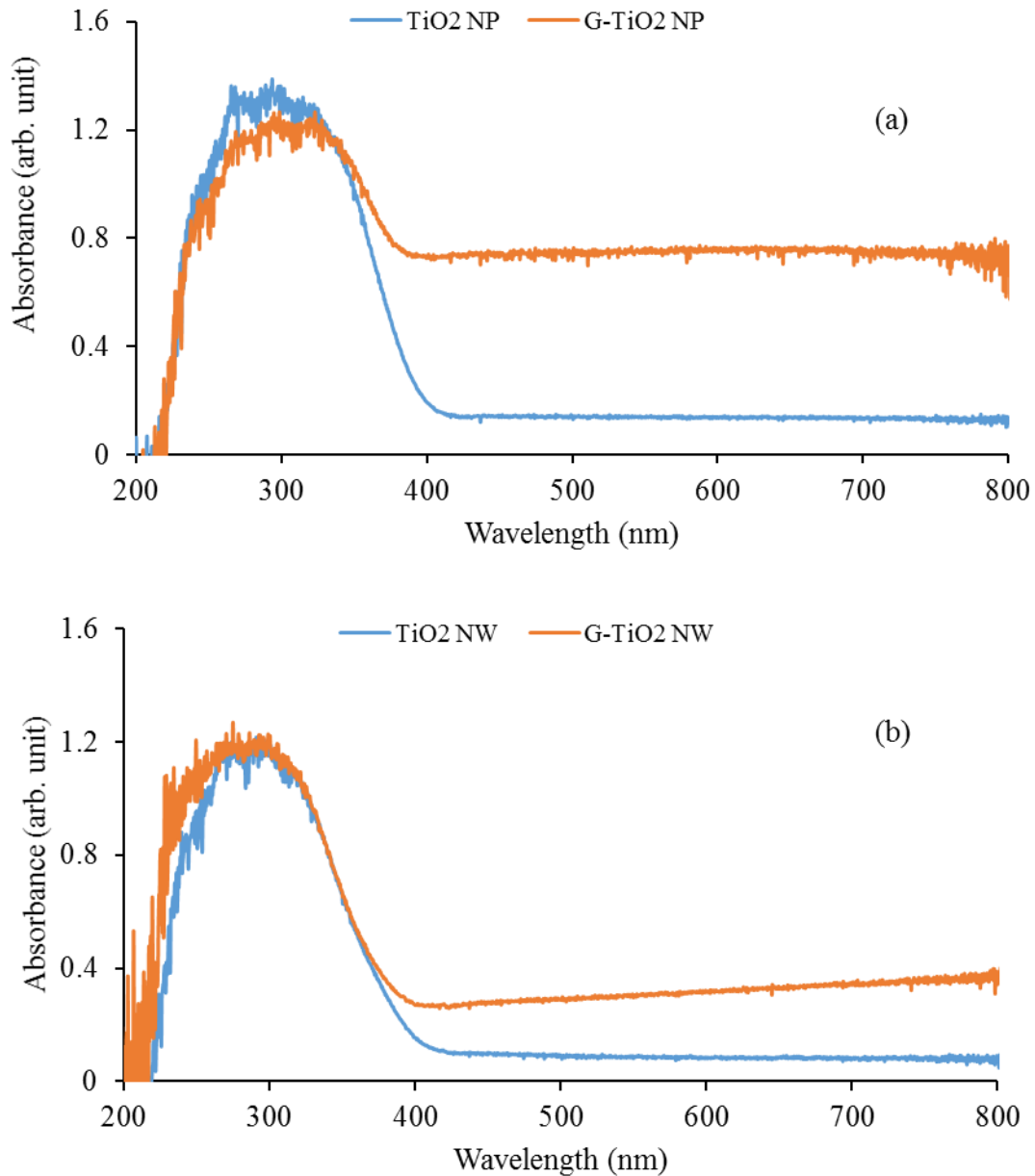
Figure 3.9 UV-visible spectra of (a) TiO$_2$ NP and G-TiO$_2$ NP (b) TiO$_2$ NW and G-TiO$_2$ NW.

Figure 3.9 shows the UV-visible spectra of (a) TiO_2 NP, G-TiO_2 NP and (b) TiO_2 NW, G-TiO_2 NW, respectively. It can be observed that the effect of graphene doping increases absorption of the nanomaterial under visible light region ($\lambda > 400nm$). This suggests that graphene doping can affect the bandgap due to temporary holding of electrons onto the graphene surface allowing the oxidative and reduction reactions of pollutant. Table 3.1 shows the bandgaps calculated by plotting $(\alpha.h\nu)^2$ vs photon energy($h\nu$). The band gap of nanoparticle structure of TiO_2 has been considerably reduced from 3.28 eV to 3.11 eV. In case of TiO_2 NW, graphene doping does not affect the bandgap as it reduced slightly from 3.40 eV to 3.39 eV , but showing an increase in absorbance in visible light radiation ($\lambda >400nm$).

Table 3.1 Bandgap of TiO_2 nanostructures calculated by plotting $(\alpha.h\nu)^2$ vs photon energy ($h\nu$).

Material	Band gap (eV)
TiO_2 NW	3.40
G-TiO_2 NW	3.39
TiO_2 NP	3.28
G-TiO_2 NP	3.11

3.3.4 Fourier Transform Infrared Spectroscopy (FTIR)

Figure 3.10 (a, b, c & d) shows the FTIR spectrum of TiO_2 NP, G-TiO_2 NP, TiO_2 NW, G-TiO_2 NW, respectively. Figure 3.10 (a, b, c & d), reveals the IR band from 400-900 cm^{-1} is due to skeletal vibration of Ti-O-Ti. The IR band at 3100-4000 cm^{-1} is primarily due to the presence of atmospheric water content i.e., OH bond stretching [381, 382]. The skeletal vibration of graphene is at 1600 cm^{-1}, but it cannot be distinguished due to the presence of organic impurities in the nanomaterials which have an IR band for C-C at 1500 to 1650 cm^{-1}, but the presence of graphene can be observed in XRD pattern from Figure 3.8.

44
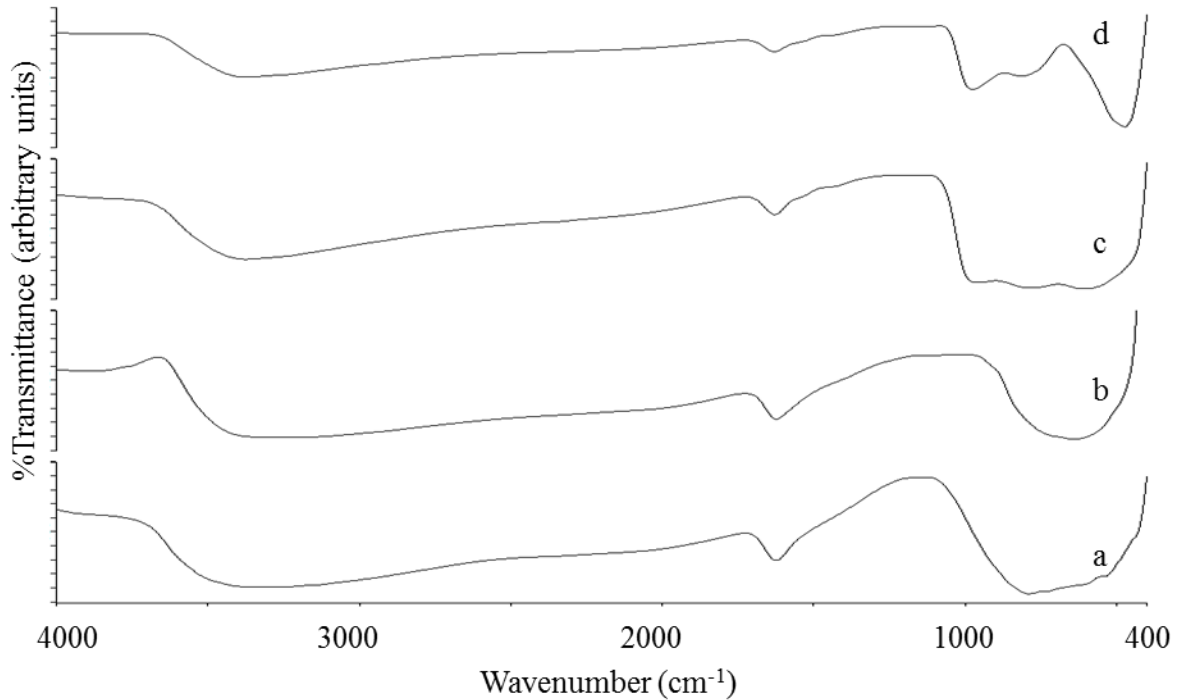
Figure 3.10 FTIR spectrum of (a) TiO_2 NP, (b) G-TiO_2 NP, (c) TiO_2 NW (d) G-TiO_2 NW.

3.3.5 Particle Analyzer
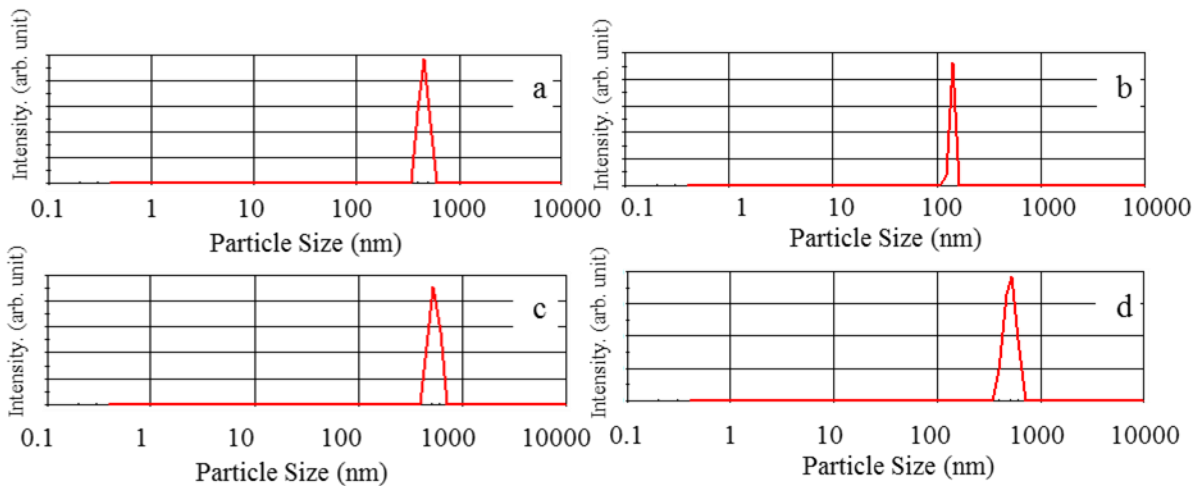
Figure 3.11 Particle size data for (a) TiO_2 NP (b) G-TiO_2 NP (c) TiO_2 NW (d) G-TiO_2 NW.

Figure 3.11 (a, b, c & d) shows the images for average particle sizes in water obtained through particle analyzer for TiO_2 NP, G-TiO_2 NP, TiO_2 NW, G-TiO_2 NW, respectively. It is important to understand the particle distribution of photocatalyst in water. Figure 3.11a, shows

45

www.manaraa.com

the agglomeration of particles with size from 150-300 nm for TiO_2 NP, similarly agglomeration

of particles in G-TiO_2 NP with particle size in between 100 nm-200 nm is also observed. Figure

3.11 (c & d) shows particle sizes ranging from 300 to 800 nm for TiO_2 NW and G-TiO_2 NW

corresponding to the SEM images found for the same suggesting agglomeration of

nanocomposite in water medium.

3.3.6 Comparison of Photocatalytic Activity
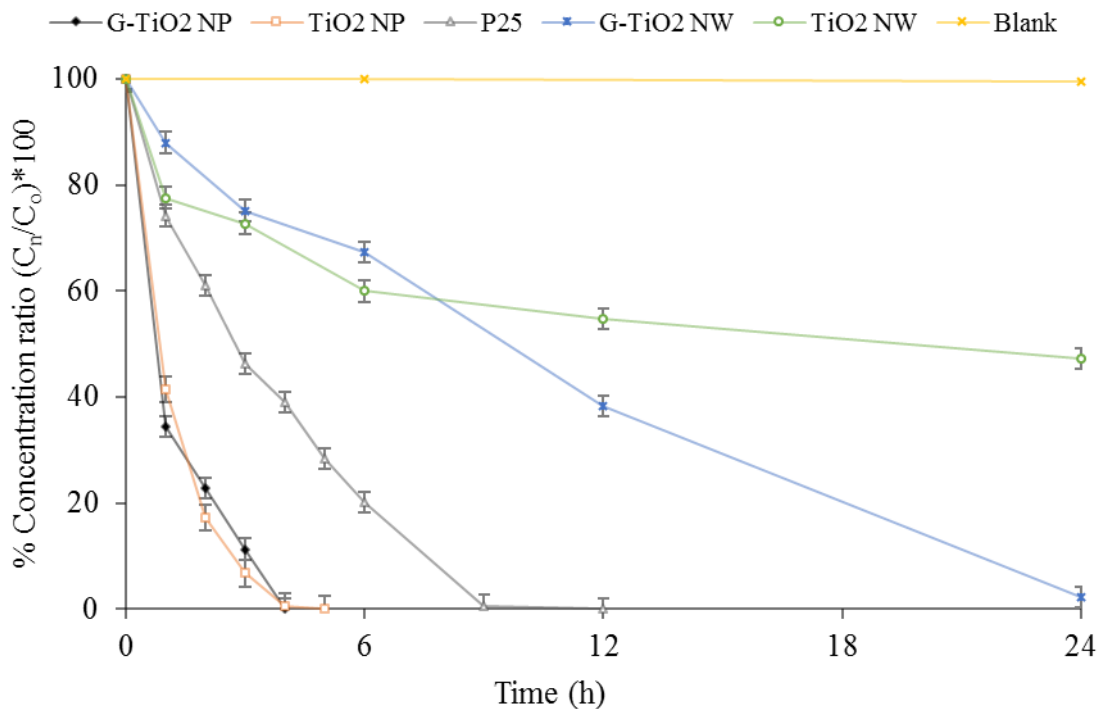
Figure 3.12 Photocatalytic remediation MO (pollutant) TiO_2 NP, G-TiO_2 NP, P25 (Degussa), TiO_2 NW and G-TiO_2 NW.

Figure 3.12 shows the photocatalytic performance of TiO_2 NP, G-TiO_2 NP, TiO_2 NW and

G-TiO_2 NW along with commercial TiO_2/P25 nanoparticles with 20 ppm (40ml) MO as organic

pollutant. Light intensity of 800 W/m^2 has been irradiated with 0.2 g of photocatalytic material

coated on the petri dish using acetic acid with sample collection in a time interval of hours. The

G-TiO_2 NP shows fastest total remediation of MO in 4 hours followed by TiO_2 NP in 5 hours.

46

Commercial P25 (TiO$_2$) takes around 12 hours to remediate complete organic pollutant. TiO$_2$ NW with and without graphene do not effectively remediate the MO completely even after 24 hours of exposure to light. This reveals that the nanoparticle form of TiO$_2$ with graphene doping has the optimum photocatalytic performance over TiO$_2$ nanowire in both doped and undoped states. For further study, G-TiO$_2$ NP has been employed based on the results from Figure 3.12.
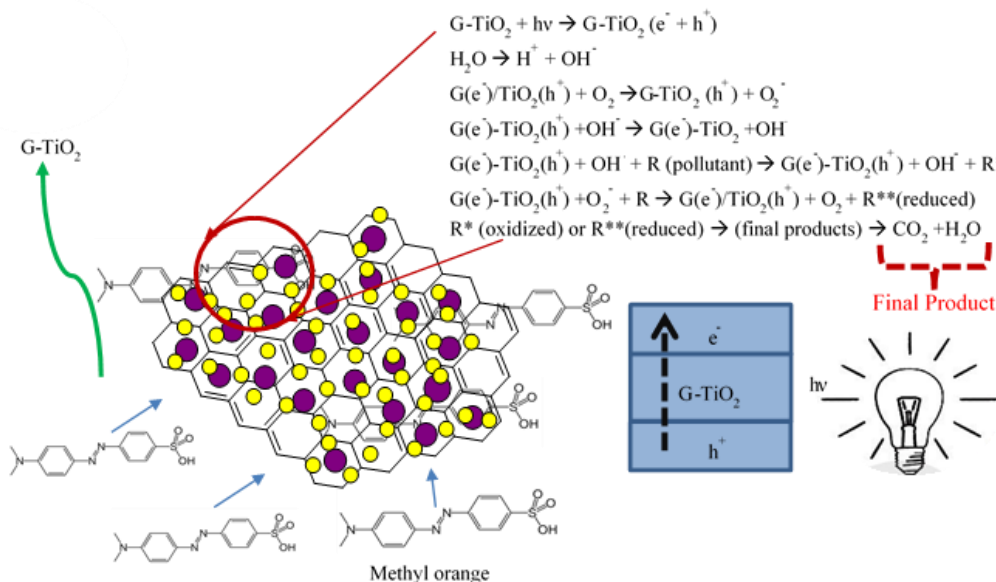
Figure 3.13 Schematic of remediation of methyl orange using G-TiO$_2$ nanomaterial.

The schematic of MO remediation is shown in Figure 3.13 using G-TiO$_2$ nanostructured material. The schematic has revealed how G-TiO$_2$ produces radical with the use of water molecule and oxygen. The free radicals OH$^.$ and O$_2^-$ were created when light interacted with G-TiO$_2$ nanomaterials. The pollutants were oxidized and finally broke into CO$_2$ and H$_2$O molecules. The stepwise remediation of pollutant is given in equation 1-7. Further, Figure 3.13 shows schematic of reaction of G-TiO$_2$ for remediation of MO.

$$G\text{-}TiO_2 + h\nu \rightarrow G\text{-}TiO_2\ (e^- + h^+) \tag{1}$$

$$H_2O \rightarrow H^+ + OH^- \tag{2}$$

$$G(e^-)\text{-}TiO_2(h^+) + O_2 \rightarrow G\text{-}TiO_2\ (h^+) + O_2^- \tag{3}$$

47

$$G(e^-)\text{-}TiO_2(h^+) + OH^- \rightarrow G(e^-)\text{-}TiO_2 + OH^. \tag{4}$$

$$G(e^-)\text{-}TiO_2(h^+) + OH^. + R \text{ (pollutant)} \rightarrow G(e^-)\text{-}TiO_2(h^+) + OH^- + R^* \text{ (oxidized)} \tag{5}$$

$$G(e^-)\text{-}TiO_2(h^+) + O_2\text{-} + R \rightarrow G(e^-)/TiO_2(h^+) + O_2 + R^{**} \text{(reduced)} \tag{6}$$

$$R^* \text{ (oxidized) or } R^{**} \text{(reduced)} \rightarrow \text{ (final products)} \rightarrow CO_2 + H_2O \tag{7}$$
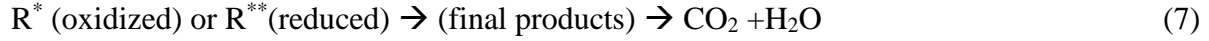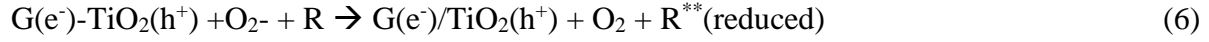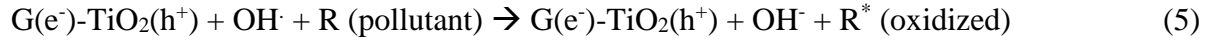
3.4 Conclusion

Pristine TiO_2 nanowires were synthesized using hydrothermal technique, where size of TiO_2 nanowires are ~50-500 nm in diameters and ~500 nm -3000nm in length measured from SEM studies. G doped TiO_2 NW has shown highest photocatalytic activity over other doped TiO_2 NW for remediation of MO from water under visible light radiation. This increase in photocatalytic activity is due to increase in visible light absorbance and decrease in bandgap due to graphene doping. Sol gel G-TiO_2 nanoparticles are superior photocatalytic properties than G-TiO_2 NW (hydrothermal), TiO_2 NW (hydrothermal) and TiO_2 NP (sol-gel) and commercially available P25 under visible light. The photocatalytic remediation of MO were completed in less than 4h using G-TiO_2 NP.

48

CHAPTER 4: ZINC OXIDE AND OTHER PHOTOCATALYSTS NANOSTRUCTURES FOR WATER REMEDIATION[4]

4.1 Introduction

The challenge to synthesize both nanowire and nanoparticle structures of ZnO along with G doping is carried out by simple and cost effective hydrothermal [319] & precipitation by super saturation [316] techniques. In a typical hydrothermal method ZnO nanowires were synthesized by using zinc nitrate, hexamethylenetetramine with ZnO nanoparticle as seeding layer with subsequent washing and drying processes. In typical synthesis of ZnO nanoparticles using precipitation method was performed by dissolving zinc chloride in deionized (DI) water with drop wise addition of sodium hydroxide with subsequent washing and drying.

ZnO nanoparticles (ZnO NP), G doped ZnO nanoparticles (G-ZnO NP), ZnO nanowires (ZnO NW), G doped ZnO nanowires (G-ZnO NW), TiO_2 seeded ZnO nanowires (TiO_2 seeded ZnO NW) and G doped TiO_2 seeded ZnO nanowires (G-TiO_2 seeded ZnO NW) were synthesized using precipitation and hydrothermal methods. ZnO nanostructures were characterized using scanning electron microscopy (SEM), Transmission electron microscopy (TEM), Raman spectroscopy, X-ray diffraction (XRD), UV-visible spectroscopy, Fourier transform infrared spectroscopy (FTIR) and particle analyser. Standard methyl orange (MO) was

---

[4] Portion of these results have been communicated with Journal- Colloid and Interface Science Communications, Elsevier publications with title "Effective Visible Light Based Photocatalytic Remediation of Organics Using Different Zinc Oxide Nanostructures" with Ref: CIS 2017 _152, which is currently under review.
Appendix A for copyright permission

employed as organic pollutant in the water and remediation was made using synthesized ZnO nanostructured materials under visible light radiation.

Chemicals and solvents such as ZnO nanoparticles, commercial TiO_2/P25, zinc nitrate hexahydrate ($Zn(NO_3)_2 \cdot 6H_2O$), hexamethylenetetramine (HMTA), zinc chloride ($ZnCl_2$) anhydrous, ethanol, sodium hydroxide (NaOH), MO which were used for the synthesis and decontamination using synthesized nanostructured materials were obtained from Sigma-Aldrich Chemicals company (USA). The G platelets of average thickness < 20 nm were procured from Angstron Materials (USA)

4.1.1 Synthesis Procedure

ZnO nanowires were synthesized by employing simple hydrothermal method with initial precursors $Zn(NO_3)_2 \cdot 6H_2O$ and surfactant 'hexamethylenetetramine (HMTA)'. Initially, 250 ml deionized water (DI) was maintained at 80˚C with addition of precursors $Zn(NO_3)_2 \cdot 6H_2O$ and HMTA with concentration of 25 mM/l. As seeding particles for the growth of nanowires, ZnO nanoparticles (avg 50 nm) were sonicated and added as nucleation sites. The solution was maintained for 4 h at 80˚C followed by washing and centrifugation with DI water & ethanol. The samples were dried to remove water content at 100˚C for 24 h. For obtaining G doped ZnO nanowires, 0.1 g of G was added to the solution along with initial precursors of $Zn(NO_3)_2 \cdot 6H_2O$ and HMTA without alteration of the optimized procedure.

TiO_2 seeded ZnO nanowires were synthesized by employing simple hydrothermal method with initial precursors $Zn(NO_3)_2 \cdot 6H_2O$ and surfactant (HMTA). Initially, 250 ml deionized water (DI) was maintained at 80˚C with addition of precursors $Zn(NO_3)_2 \cdot 6H_2O$ and HMTA with concentration of 25 mM/l. As seeding particles for the growth of nanowires, TiO_2 nanoparticles (avg 21 nm) were sonicated and added as nucleation sites. The solution was

50

maintained for 4 h at 80˚C followed by washing and centrifugation with DI water & ethanol. The samples were dried to remove water content at 100˚C for 24 h. For obtaining G doped TiO_2 seeded ZnO nanowires, 0.1 g of G was added to the solution along with initial precursors of $Zn(NO_3)_2 \cdot 6H_2O$ and HMTA without alteration of the optimized procedure.

ZnO nanoparticles were synthesized by dissolving 5.5 g of zinc chloride ($ZnCl_2$) in 200 ml of DI with stirring at 90ºC followed by drop wise addition of 5 M (16 ml) sodium hydroxide (NaOH) aqueous solution. The particles were separated by sedimentation process from the supernatant dispersion. The suspension was washed by DI water & ethanol using centrifugation. The washed samples were collected from centrifuge and dried at 250 ºC for 5 h. The G doped ZnO nanoparticles was synthesized using 0.15 g of G with precursor $ZnCl_2$ without alterations to the procedure.

4.1.2 Sample Preparation and Decontamination Setup

The photocatalytic activity of synthesized ZnO NP, G-ZnO NP, ZnO NW, G-ZnO NW, TiO_2 seeded ZnO NW, G-TiO_2 seeded ZnO NW were studied to remediate MO as a pollutant. The decontamination setup is shown in Figure 3.1 from Chapter 3 without any alteration to the procedure. In typical process, 0.2 g of synthesized photocatalytic material were coated using acetic acid onto a petri dish and dried at 200˚C for 30 min. MO (pollutant) with initial concentration of 20 ppm (40 ml) was added to petri dish, and illuminated with a 30-watt bulb to irradiate with light intensity of 800 W/m^2. With time interval scale in hours, samples were collected from the main remediating sample and analysed for absorbance of MO using JASCO V-530 UV-visible spectrometer. At 0 hours, initial MO concentration was taken as C_o. The percentage of remediation was calculated by using concentration ratio of C_n/C_o with respect to time in hours.

51

4.2 Results and Discussion

4.2.1 Scanning Electron Microscopy (SEM)

Figure 4.1 SEM images of (a) ZnO nanoparticle (b) G-ZnO nanoparticle (c) ZnO nanowire (d) G-ZnO nanowire (e) TiO$_2$ seeded ZnO nanowires (f) G-TiO$_2$ seeded ZnO nanowire at various magnifications.

The surface morphology of ZnO nanoparticle & G-ZnO nanoparticle can be observed in Figure 4.1 (a, b) respectively, which reveals the size of ZnO NP ranging from 40-60 nm in both undoped and doped (G) condition. In Figure 4.1 b, the G sheets have been dispersed around ZnO NP. Figure 4.1 (c, d) shows the nanowire structures of ZnO & G-ZnO grown through hydrothermal method by using ZnO nanoparticles as seeding material. The ZnO NW & G-ZnO NW sizes vary 50-150 nm in diameter and 800-900 nm in length. Figure 4.1 (e, f) shows the

52

nanowires structure of TiO$_2$ seeding ZnO nanowire and G-TiO$_2$ seeded ZnO nanowire. The formation of thinner ZnO nanowire with TiO$_2$ as seeding layer with diameters in-between 40-100 nm and length 400-500 nm are observed. The formation of smaller size nanowires in Figure 4.1(e, f) is credited due to smaller size (<21 nm) of TiO$_2$ nanoparticles as seeding layer for the synthesis of ZnO nanowires.
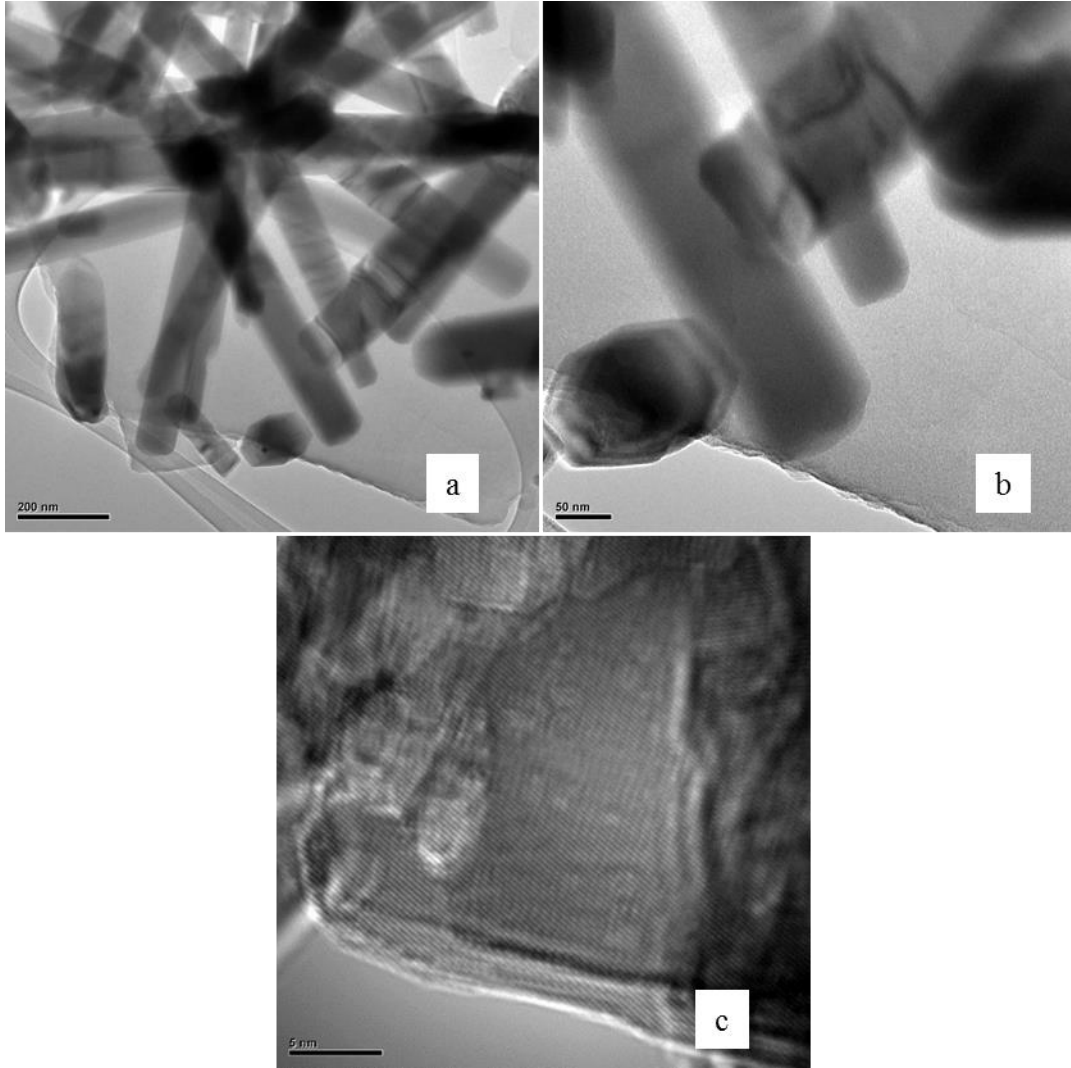
Figure 4.2 TEM image of G-ZnO NW at various magnifications.

Above Figure 4.2, TEM images of G doped ZnO nanowire (G-ZnO NW) is shown. G-ZnO NW obtained from Figure 4.2 (a & b), has a size of around 50-150 nm in diameter which is

in correlation with SEM image of G-ZnO NW in Figure 4.1 d. ZnO nanowires are dispersed on G sheets in Figure 4.2 (a & b), which show the presence of few layers of G doped on to ZnO NW. In TEM image of Figure 4.2c, the d-spacing of planes of ZnO NW and an average d-spacing value of 0.25 nm can be observed. This value of d-spacing corresponds to (101) plane of ZnO which has a peak at 36.2º in XRD pattern in Figure 4.3d.

4.2.2 X-ray Diffraction (XRD)
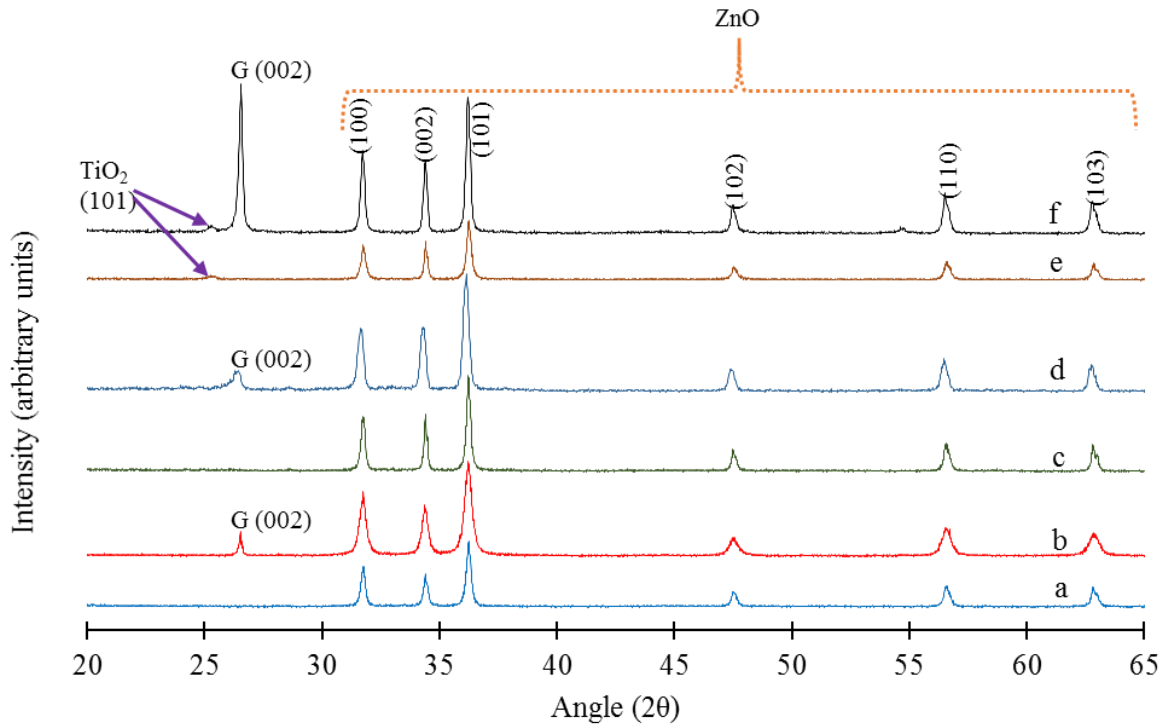
Figure 4.3 XRD pattern of (a) ZnO nanoparticle (b) G-ZnO nanoparticle (c) ZnO nanowire (d) G-ZnO nanowire (e) TiO$_2$ seeded ZnO nanowire (f) G -TiO$_2$ seeded ZnO nanowire.

The XRD patterns of ZnO NP and NW structures with and without G doping are shown in Figure 4.3. The diffraction peaks are obtained at 31.7º, 34.4º, 36.2º, 47.5º, 56.6º, 62.8º which correspond to hexagonal ZnO structure with crystallographic (100), (002), (101), (102), (110) and (103) directions in Figure 4.3 (a, b, c, d, e & f) [319, 383]. However, the diffraction peak at 26.5º shows the presence of G (002) in doped ZnO nanostructures as shown in figure 4.3 (b, d &

54

www.manaraa.com

f) [378]. Further, the diffraction peak at 25.3º shows the presence of TiO$_2$ in ZnO nanostructures in Figure 4.3 (e & f), which is used as seeding layer for synthesis of ZnO nanostructures.

4.2.3 UV-visible Spectroscopy
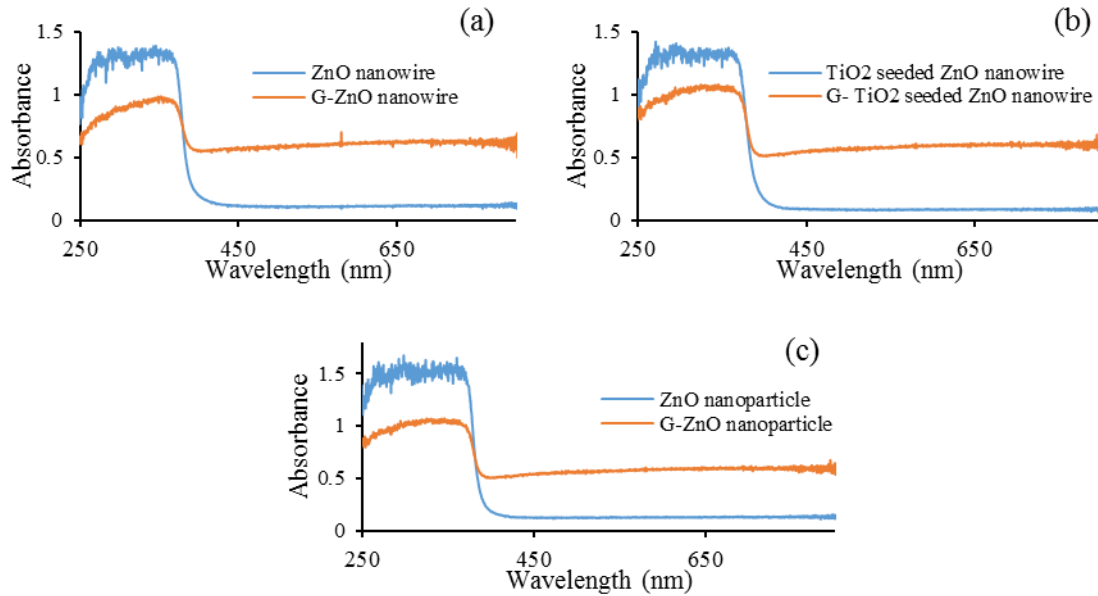
Figure 4.4 UV-visible absorbance spectra of (a) ZnO & G-ZnO nanowire (b) TiO$_2$ seeded ZnO & G-TiO$_2$ seeded ZnO nanowire (c) ZnO & G-ZnO nanoparticle.

Table 4.1 Band gap of ZnO nanostructures calculated by plotting $(\alpha.h\nu)^2$ vs photon energy (hν).

Material	Band gap (eV)
ZnO NW	3.22
G-ZnO NW	3.15
TiO$_2$ seeded ZnO NW	3.23
G-TiO$_2$ seeded ZnO NW	3.19
ZnO NP	3.24
G-ZnO NP	3.18

Figure 4.4 shows the UV-visible spectra of ZnO nanostructures with and without G doping. The ZnO nanowire (Figure 4.4a), TiO$_2$ seeded ZnO nanowire (Figure 4.4b) and ZnO nanoparticle (Figure 4.4c) display absorption below 400nm whereas G doping reveals an

increase in the absorption in visible > 400nm in addition to decrease in absorptivity in < 400 nm. The graphene doping shows the reduction in bandgap of ZnO nanostructures. Table 4.1 shows the estimated band gap of various ZnO nanostructures. The band gap of nanostructures of ZnO have been calculated using the empirical relationship of $(\alpha.h\nu)^2$ vs photon energy [384].

4.2.4 Fourier Transform Infrared Spectroscopy (FTIR)

Figure 4.5 (a, b, c, d, e, f) shows the FTIR spectra of various ZnO nanostructured materials. Figure 4.5(a, b, c, d, e, and f) shows the characteristic absorption band due to transverse optical stretching of ZnO between 420 cm^{-1} to 520 cm^{-1} [385] and the peak at 3450 cm^{-1} correlates to OH presence due to atmospheric moisture absorbed onto surface of ZnO nanostructures[386]. The skeletal absorption of G is observed at 1600 cm^{-1} [387] in Figure 4.5 (b, d and f) in addition G peak, the organic impurities in ZnO at 1590 cm^{-1} & 1410 cm^{-1} are found. It is hard to differentiate the G peak in Figure 4.5 (b, d and f), however the presence of G is confirmed through X-ray diffraction measurements as shown in Figure 4.3.
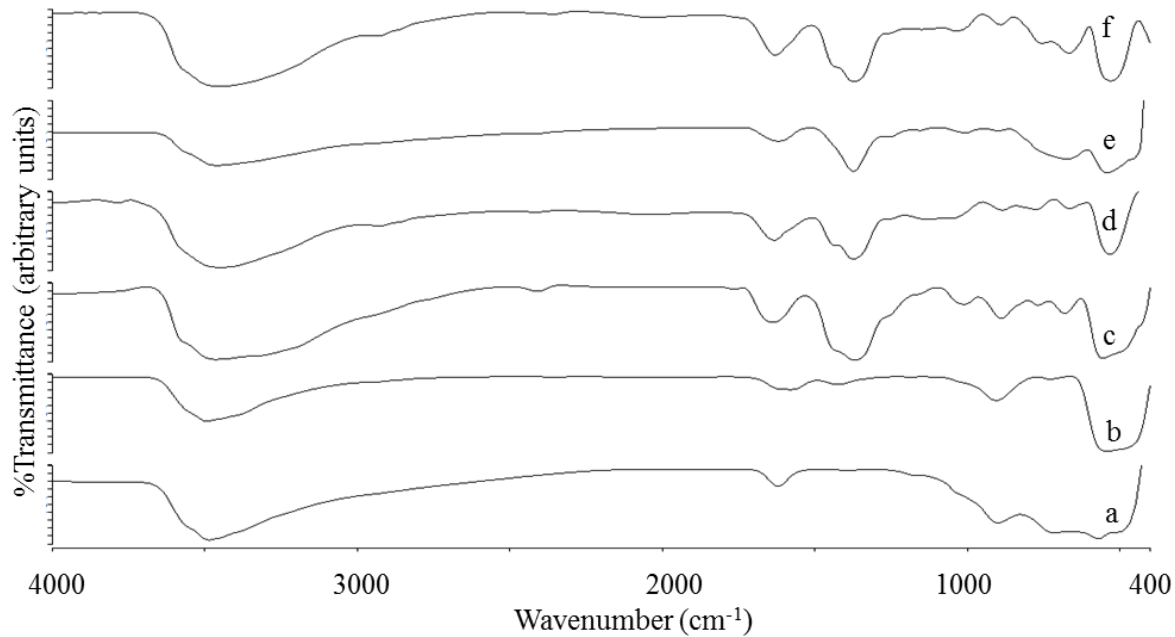
Figure 4.5 FTIR images of (a) ZnO nanoparticle (b) G-ZnO nanoparticle (c) ZnO nanowire (d) G-ZnO nanowire (e) TiO$_2$ seeded ZnO nanowire (f) G-TiO$_2$ seeded ZnO nanowire.

56

4.2.5 Particle Analyzer
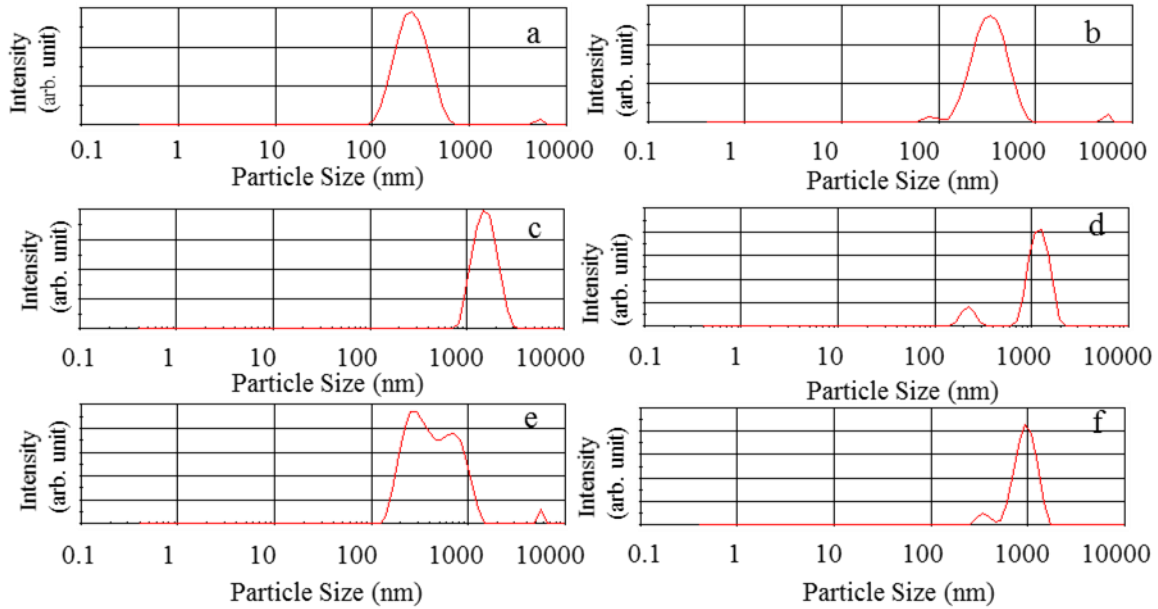
Figure 4.6 Particle size distribution of (a) ZnO nanoparticle (b) G-ZnO nanoparticle (c) ZnO nanowire (d) G-ZnO nanowire (e) TiO$_2$ seeded ZnO nanowire (f) G -TiO$_2$ seeded ZnO nanowire.

Figure 4.6 shows the particle size distribution of ZnO nanostructures measured in aqueous medium. The Figure 4.6 (a, b) shows the particle size distribution of ZnO NP and G-ZnO NP materials in water. The particle size distribution is observed in-between 100 to 1000 nm, which is correlated to SEM images where the size of particles is observed between 40 to 60 nm. Similarly in Figure 4.6(c, d), the size around 800-2000 nm corresponding to ZnO NW and G-ZnO NW nanowire has been observed. The SEM image of similar sample in powder form shows the particle diameter size around 100-150 and length in 800-900 nm. Similarly, Figure 4.6 (e, f) shows the particle sizes around 200-1000nm which corresponds to TiO$_2$ seeded ZnO NW and G- TiO$_2$ seeded ZnO NW, SEM images of ZnO NW and G-TiO$_2$ seeded ZnO NW has been measured as diameters in between 40-100 nm and length to 400-500 nm. The larger distribution size observed in particle analyser is pertaining to agglomeration of ZnO nanostructures in aqueous medium. This study is important to understand the behaviour of the photocatalytic

57

particles in aqueous media. The hydrophilicity of ZnO shows the aggregation in the colloidal state. Such information is important to understand the effective remediation due to size of the photocatalytic material in water.

4.2.6 Decontamination Study
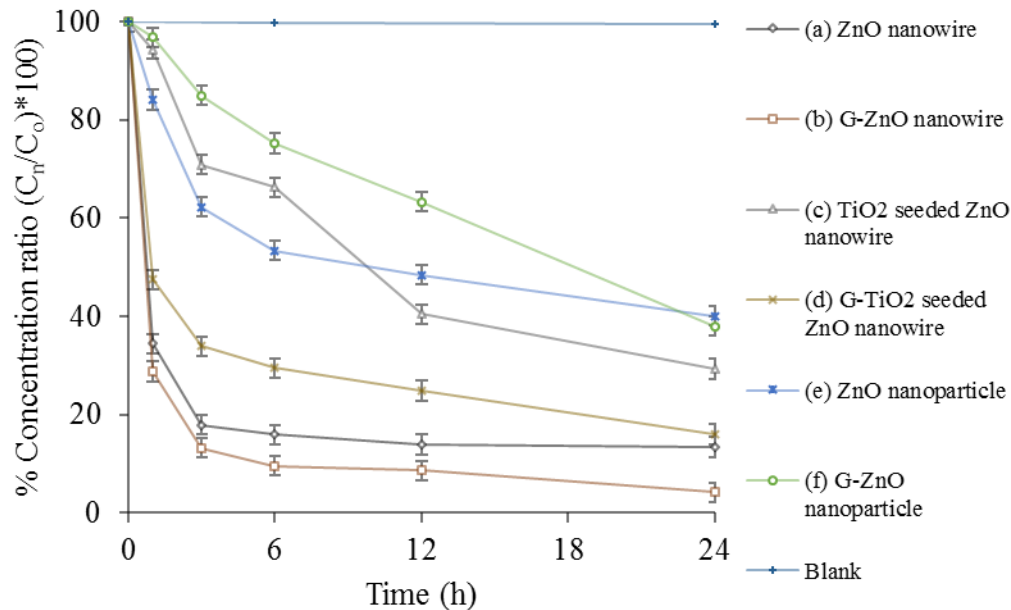
Figure 4.7 Decontamination of MO under visible light radiation using (a) ZnO nanowire (b) G-ZnO nanowire (c) TiO$_2$ seeded ZnO nanowire (d) G-TiO$_2$ seeded ZnO nanowire (e) ZnO nanoparticle (f) G-ZnO nanoparticle.

The nanostructures of ZnO (ZnO NP, G-ZnO NP, ZnO NW, G-ZnO NW, TiO$_2$ seeded ZnO NW & G-TiO$_2$ seeded ZnO NW) have been tested for photocatalytic activity with the use of MO. 0.2 g of photocatalytic material were coated onto a petri dish and 20 ppm of 40 ml MO solution was used to understand the photocatalytic remediation. A 30-watt lamp with intensity of 800 W/m^2 was used to understand the visible light remediation for MO as pollutant in water. The MO remediated samples with continuous irradiation of light was collected in an interval of an hour. Figure 4.7 shows the photocatalytic activity of ZnO nanostructures. It can be clearly realized that G doped ZnO NW (G-ZnO NW) shows the best photocatalytic performance than all

58

other structured ZnO nanomaterials. The enhancement photocatalytic activity of G-ZnO NW over ZnO NW is primarily due to G doping. Doping with G enhanced the photocatalytic activity due to slight decrease in bandgap energy of the nanostructured material and increase in absorbance of photocatalyst under visible spectrum of light, which has been observed in Figure 4.4 and estimated bandgap values in Table 4.1.

Further, attempts haven been made to understand the reaction rate of ZnO nanostructures using pseudo first order kinetic reaction as shown in Figure 4.8. Figure 4.8, shows the plot of ln (C_o/C_n) vs time (hour) to obtain reaction rate k_a.

$$ln\left(\frac{C_o}{C_n}\right) = k_a t$$

The C_o is initial concentration at t = 0 and C_n at time t, k_a is the reaction rate constant.

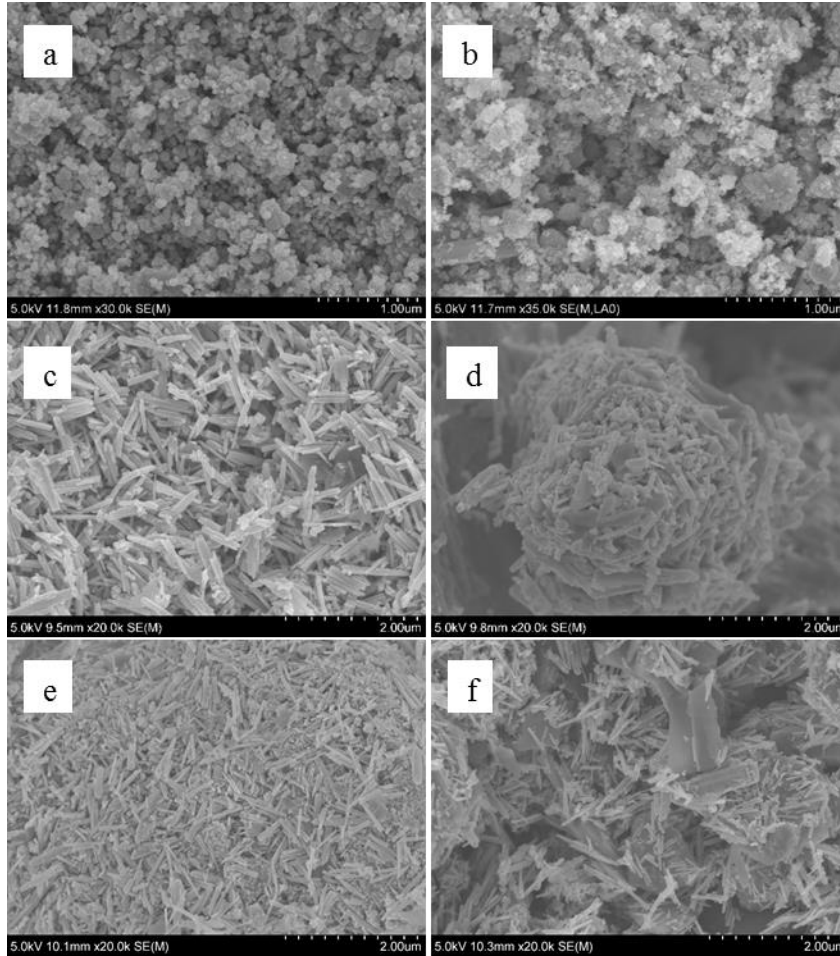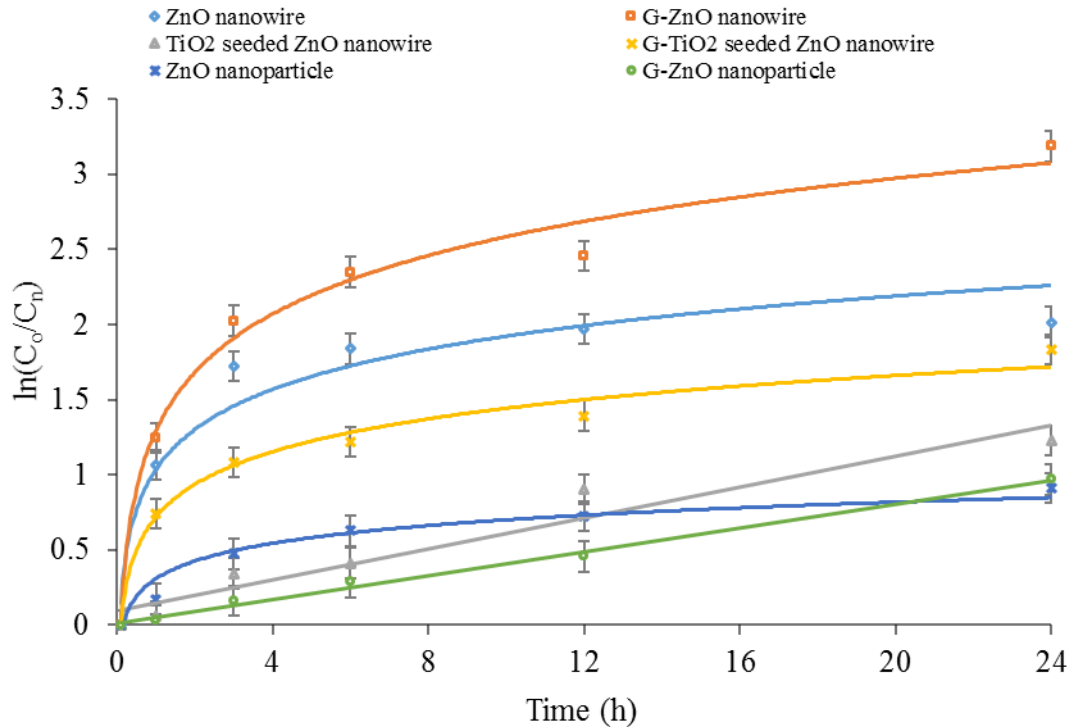Figure 4.8 Reaction rate of ZnO nanostructures using pseudo first order kinetic reaction (a) ZnO nanoparticle (b) G-ZnO nanoparticle (c) ZnO nanowire (d) G-ZnO nanowire (e) TiO₂ seeded ZnO nanowire (f) G - TiO₂ seeded ZnO nanowire.

59

Table 4.2 Reaction rate equation's obtained through plotting ln (C_o/C_n) vs time (h).

Photocatalyst	Reaction rate equation
ZnO NP	$y = 0.1702\ln(x) + 0.3078$, $R^2 = 0.9488$
G-ZnO NP	$y = 0.0396\,x + 0.0128$, $R^2 = 0.9941$
TiO$_2$ seeded ZnO NW	$y = 0.0516\,x + 0.0941$, $R^2 = 0.9364$
G-TiO$_2$ seeded ZnO NW	$y = 0.3149\ln(x) + 0.7177$, $R^2 = 0.9848$
ZnO NW	$y = 0.3859\ln(x) + 1.0339$, $R^2 = 0.9463$
G-ZnO NW	$y = 0.5612\ln(x) + 1.2926$, $R^2 = 0.9865$

Figure 4.8 shows the non–liner trend of reaction rates obtained for ZnO nanostructures with reaction rates shown in Table 4.2. In fact, the rate of reaction for ZnO photocatalysts follows Langmuir – Hinshelwood first order kinetics due to lower initial concentration of MO (20ppm). So, it is understood that reaction rate is based on pseudo first order kinetics [388]. The rate of decrease in photocatalytic activity of all ZnO nanostructures due to unavailability of electron acceptors like O_2. The available O_2 has been consumed during initial photonic excitation of ZnO nanostructures, and later the remediation of ZnO is solely done by relative efficiency of surface ZnO as h^+ groups [89, 389-391]. The underlying cause for the non-linear pattern of photocatalytic reaction rate is the experiment setup is based on slurry form with no circulation of pollutant or supply of external O_2 through the process. This setup is ideal to conditions where the supply of external sources (air, agitation etc.) or cannot be given into the contaminated water.

The G-ZnO NW has shown excellent remediation of MO as compared to other synthesized nanostructured ZnO based materials as shown in Figure 4.7, schematic representation of G-ZnO NW is shown in Figure 4.9(a & b). Band gap of ZnO is around 3.2-2.37 eV for which valance band (VB) is at-7.25 eV with vacuum and conduction band (CB) is at -4.05 eV with vacuum, which corresponds to work function of -4.05 eV for ZnO structures.
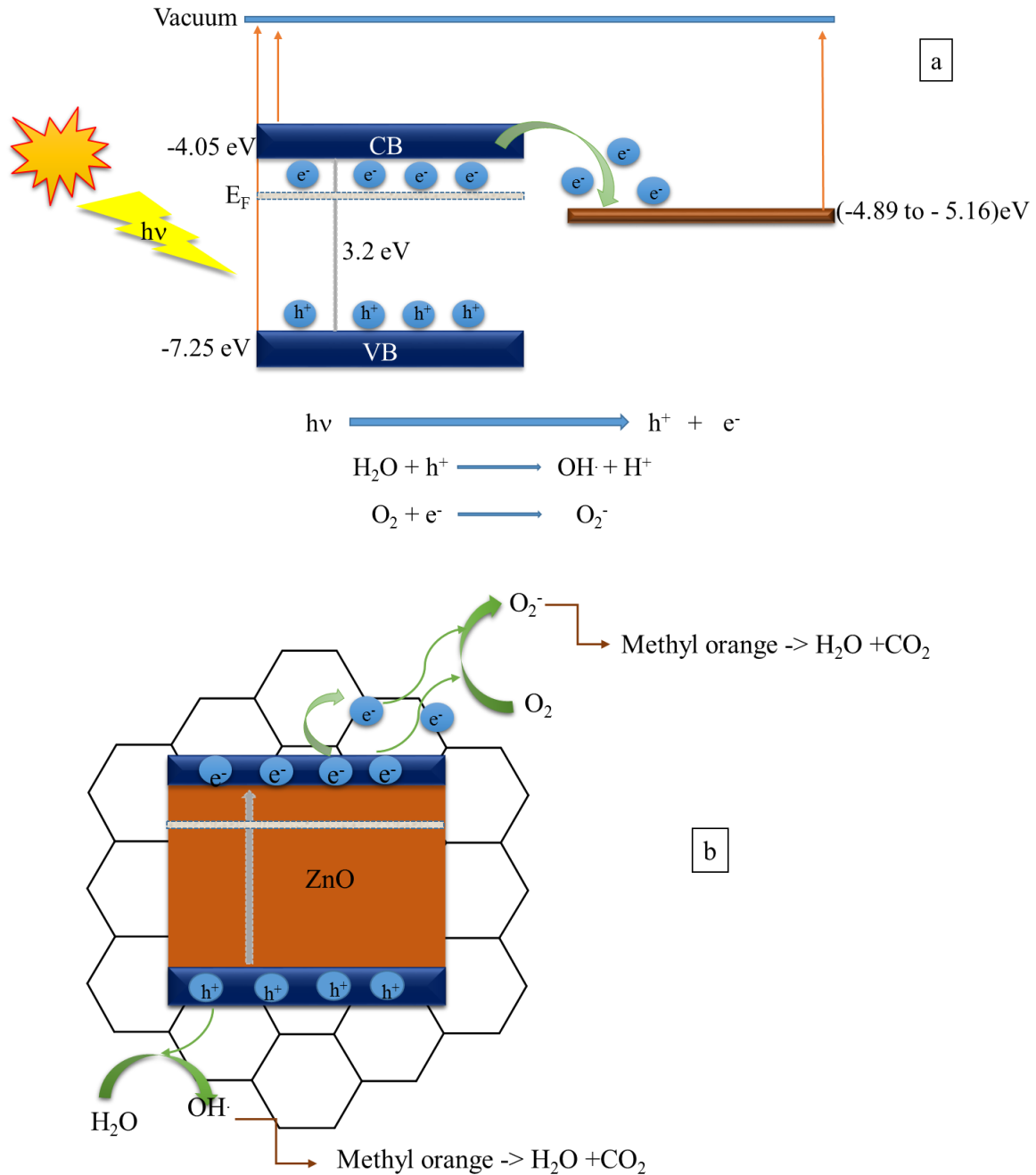
Figure 4.9 (a, b) Schematic of ZnO nanostructured photocatalysts for remediation of MO under visible light radiation.

Once photon energy of greater than or equal to band gap of ZnO illuminates the surface, electron hole pair is created. Without any doping, the photocorrosion is high i.e., electron and hole recombination is very fast there by allowing lower oxidative and reduction reactions around

ZnO. When graphene is used as dopant which has a work function of -4.89 to -5.16 eV which falls in between the VB and CB of ZnO, the electrons are transferred onto G there by allowing oxidative and reduction reactions around ZnO to continue longer there by degrading pollutant, which has been shown in Figure 4.9a. Figure 4.9b shows the mechanism of graphene doped ZnO for remediation of methyl orange. The excellent remediation obtained for G-ZnO NW demonstrates the visible light remediation of wastewater as well as drinking water for practical applications.

4.3 Other Photocatalysts (WO$_3$ and α-Fe$_2$O$_3$)

4.3.1 Chemicals and Reagents

Chemical like sodium sulfate (Na$_2$SO$_4$), lithium sulfate (Li$_2$SO$_4$), ferrous sulfate (FeSO$_4$), oxalic acid (H$_2$C$_2$O$_4$), and sodium tungstate (Na$_2$WO$_4$), acetic acid (CH$_3$COOH) and hydrochloric acid (HCl), iron chloride (FeCl$_3$), sodium hydroxide (NaOH) and other reagents were purchased from Sigma Aldrich, a commercial company from USA.

4.3.2 Synthesis Procedure

Tungsten oxide (WO$_3$) is synthesized through hydrothermal synthesis technique outlined by Xu et al.[337]. Initially, WO$_3$ sol was synthesized by dissolving 4.075g sodium tungstate powder in 100 ml of de-ionised (DI) water. Then Na$_2$WO$_4$ solution was acidified to pH of 1.0–1.2 by HCl (3 mol/L) solution with constant stirring for 30 min. A yellow precipitate was generated to which 3.15g of H$_2$C$_2$O$_4$ was added with further dilution with DI water to 250 ml with constant stirring at room temperature which leads to formation of stable WO$_3$ sol. WO$_3$ sol of 15 ml was taken into a autoclave, and 1 g Na$_2$SO$_4$ was then added to the solution and maintained at constant temperature of 180 °C for 24 h. The precipitate was washed with water and ethanol to remove unreacted organic matter and centrifuged and dried at 100°C. The

62

complete process of synthesizing WO_3 with varying morphologies was easily modified by adding 1g $FeSO_4$ & 1g Li_2SO_4 instead of Na_2SO_4 without altering the procedure. By addition of $FeSO_4$, Na_2SO_4, Li_2SO_4 will lead to the formation of cubic structure of WO_3, nanorods structure of WO_3, toothpick structures of WO_3 toothpicks, respectively.

Hematite (α-Fe_2O_3) or α-iron oxide is synthesized through sol-gel technique. Initially iron chloride of 8.1 g was added to 450 ml of DI water with constant stirring at 60°C for 1 h. 50 ml of 4 M NaOH was slowly added and left for stirring for 24 h and maintained at 90°C. Red sol α-Fe_2O_3 is precipitated, filtered using filter paper, washed with DI water and ethanol to remove unreacted impurities and dried at 70 C for 24 h.

4.3.3 Characterization

Figure 4.10 (a, b, c &d) shows SEM images WO_3 cubic ($FeSO_4$), WO_3 nanorod (Na_2SO_4), WO_3 tooth pick (Li_2SO_4), α-Fe_2O_3, respectively. Figure 4.10a, shows cubic structures of WO_3 with sizes ranging 100 nm to 2 micron. Figures 4.10 (b & c) shows the nanorod and toothpick structures of WO_3 are synthesized with sizes varying from 100-500 nm in diameter with up to few microns in length. The varying structures of WO_3 attributed to SO_4^{2-} which act as structure directing agents along face parallel to WO_3 nanocrystal. Figure 4.10d, shows the nanoparticle structure of hematite (α-Fe_2O_3) with average size around 50-100 nm in size.

Figure 4.11 (a, b, c & d) observes the XRD images of WO_3 (cubic, nanorod, toothpick) and α–Fe_2O_3, respectively. XRD peaks at 23.6, 26.7, 29, 34.2, 42, 50, 57.2 degrees shows the crystalline structures of WO_3. The high crystallinity observed in WO_3 nanostructures is due to the use of sulfates which enabled the crystalline growth of along c –axis. In Figure 4.11d, shows the polycrystalline structure of α–Fe_2O_3.

63
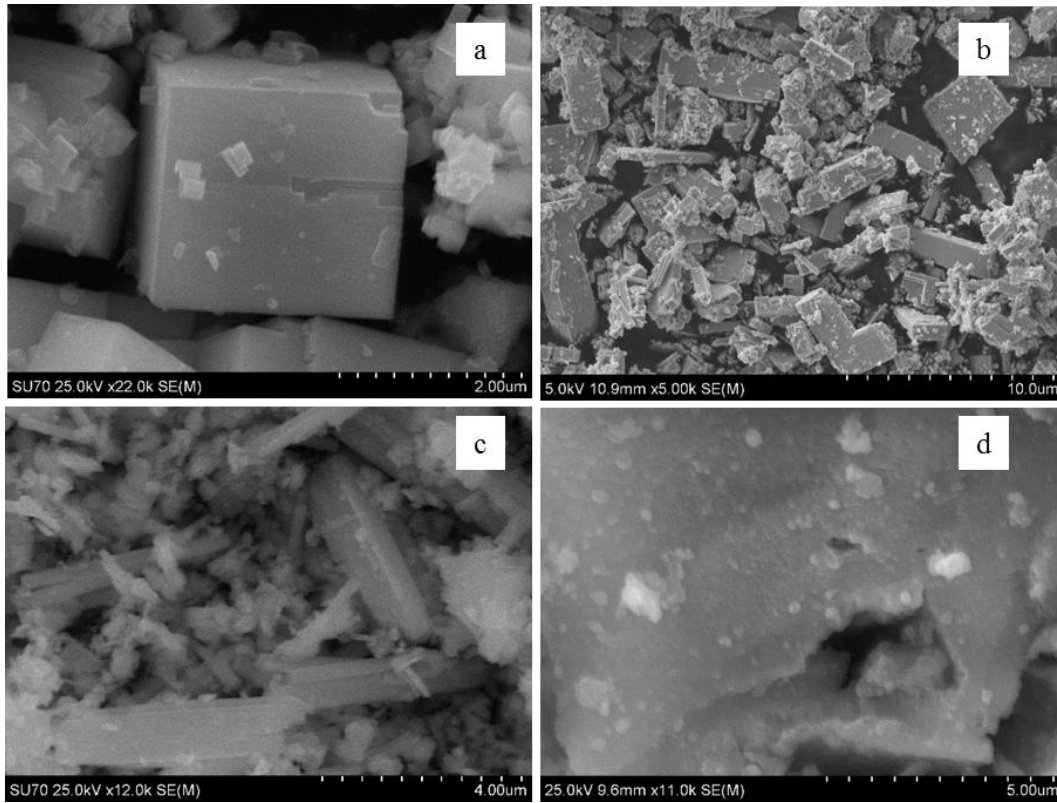
Figure 4.10 SEM images of (a) WO_3 cubic ($FeSO_4$), (b) WO_3 nanorod (Na_2SO_4), (c) WO_3 tooth pick (Li_2SO_4) (d) α–Fe_2O_3(hematite).
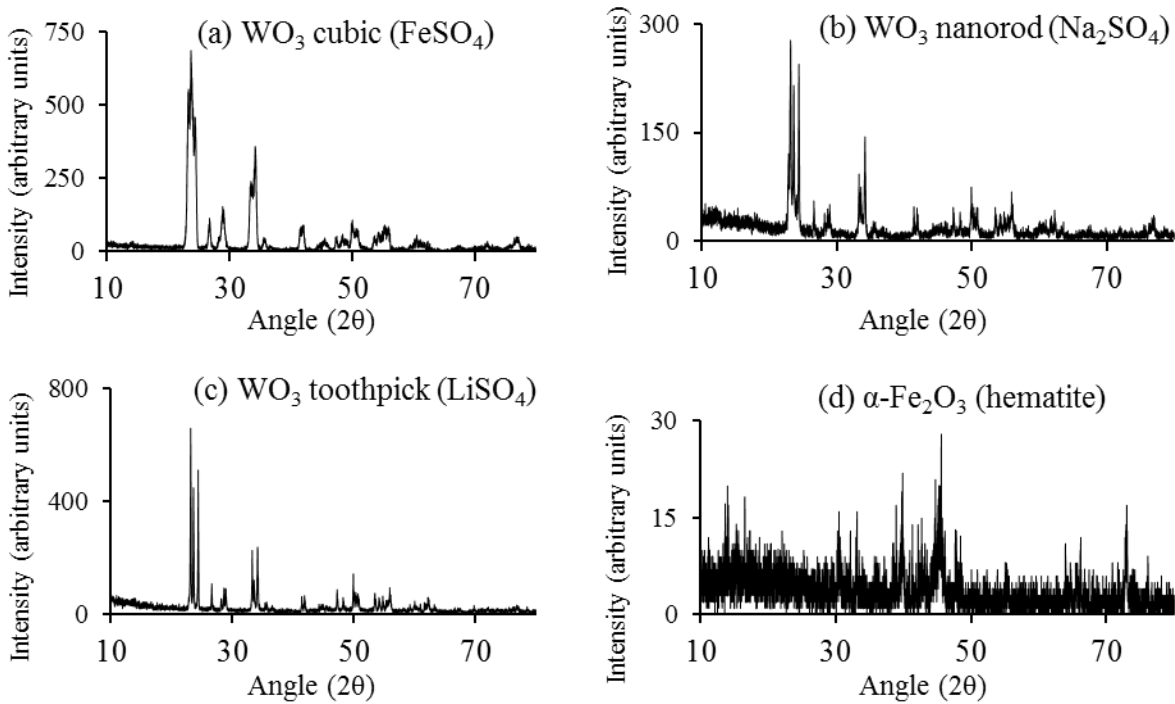
Figure 4.11 XRD pattern of (a) WO_3 cubic ($FeSO_4$), (b) WO_3 nanorod (Na_2SO_4), (c)WO_3 tooth pick (Li_2SO_4) (d) α–Fe_2O_3(hematite).

64

4.3.4 Photocatalytic Comparison

Figure 4.12 shows the decontamination of MO under visible light radiation. 0.2g of photocatalyst is coated onto the petri dish using acetic acid and dried at 200ºC for 30 min. 20 ppm (40ml) MO was used as pollutant with a light intensity of 800 W/m^2 irradiated from below. It can be observed that WO_3 has decontaminated only 18 % of MO under 24 h for cubic samples of WO_3. It can be further understood that WO_3 is not an efficient photocatalytic material but has been used as a passive/secondary photocatalyst [392, 393]. α–Fe_2O_3 has remediated around 50 % of MO under 24 h. When compared to TiO_2 and ZnO nanostructures, WO_3 and α–Fe_2O_3 are not an efficient photocatalytic material for remediation of organics in water.
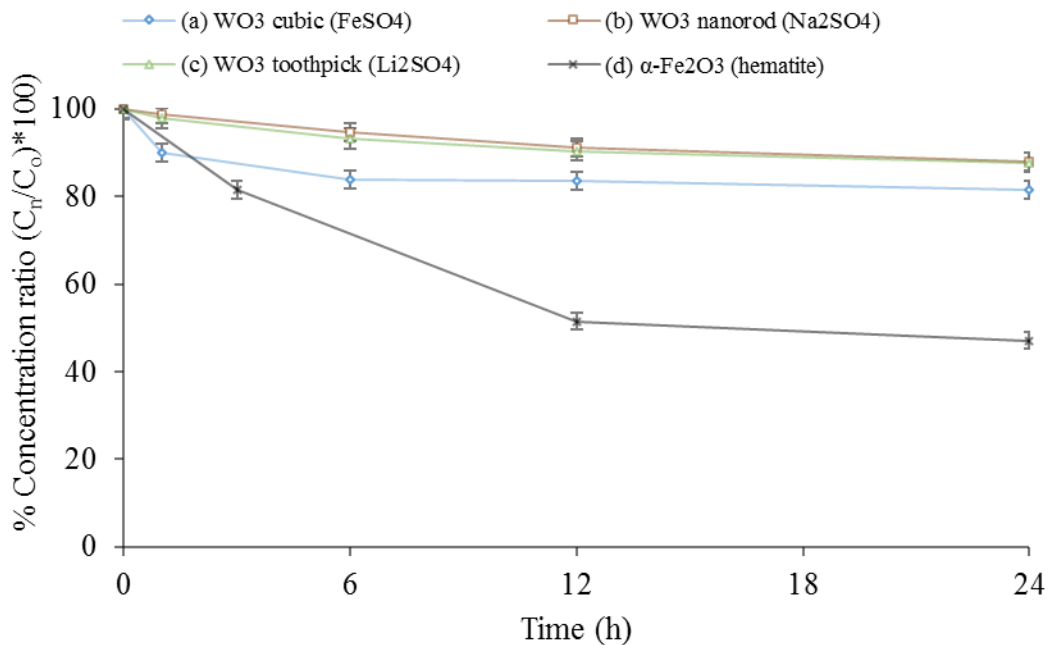
Figure 4.12 Photocatalytic performance of WO_3 (cubic, nanorod, and toothpick) and α–Fe_2O_3 for remediation of MO under visible light radiation.

4.4 Conclusion

Various nanostructures of ZnO were synthesized using precipitation and hydrothermal methods. ZnO NP ranging from 40-60 nm in both undoped and doped (G) condition were

65

synthesized using precipitation method and ZnO NW both undoped and doped (G) condition sizes varied from 50-150 nm in diameter and 800-900 nm in length. The formation of thinner ZnO nanowire with TiO_2 as seeding layer with diameters in-between 40-100 nm and length 400-500 nm are observed. The improved photocatalytic activity of G-ZnO NW is mainly due to G doping which decreases the bandgap energy and reveals an increase in the absorbance under visible spectrum of light. WO_3 and α–Fe_2O_3 have been found an efficient photocatalytic materials for visible light radiation similar to ZnO and G-ZnO based nanowires.

66

CHAPTER 5: EFFECT OF SURFACTANT ON WATER REMEDIATION[5,6]

5.1 Introduction

From Chapter 3 and Chapter 4, it has been established that graphene (G)-titanium oxide (TiO$_2$) nanoparticle (NP) and G-zinc oxide (ZnO) nanowire (NW) are best photocatalytic materials over other nanostructured photocatalysts of TiO$_2$ and ZnO. It is important to understand how photocatalyst material performs for remediation of naphthalene under visible light radiation with light of intensity of 800 W/m^2. Initially tests were done using G-TiO$_2$ NP for remediation of toluene, naphthalene and diesel in water under constant stirring condition. Pollutants like toluene, naphthalene, and diesel do not have a high solubility and therefore tend to stay on the surface of water. This can prevent the pollutants from coming into contact with G-TiO$_2$ nanocomposite. For effective photocatalytic performance, the pollutant should remain in contact with photocatalyst for it to be remediated by visible light radiation.

Organic pollutants like naphthalene, diesel and crude oil have very low solubility and few higher organic molecules have zero solubility in water due to which the insoluble organic pollutant float on the top surface of water. Due to low solubility or zero solubility of these organic compounds, during the photocatalysis process only the soluble content of organic

---

[5] Srikanth Gunti, Ashok Kumar, Manoj K. Ram, "Comparative Organics Remediation Properties of Nanostructured Graphene Doped Titanium Oxide and Graphene Doped Zinc Oxide Photocatalysts", published 30 July 2015, American Journal of Analytical Chemistry, 2015, 6, 708-717

[6] Srikanth Gunti, Michael McCrory, Ashok Kumar, Manoj K. Ram, "Enhanced Photocatalytic Remediation Using Graphene (G)-Titanium Oxide (TiO$_2$) Nanocomposite Material in Visible Light Radiation", published 21 July 2016, American Journal of Analytical Chemistry, 2016, 7, 576-587

Appendix A for copyright permission

material is remediated by oxidative and reduction reactions due electron and hole pair produced by the photocatalyst material. For these oxidative and reduction reactions to transpire for complete remediation of the organic pollutant, the pollutant should come in contact with the photocatalyst. To overcome this major drawback researchers employed the use of photocatalytic reactor, which supplies air & agitation with other physical methods [394, 395]. Using additional methods will increase the cost and energy used in the remediation process for cleaning water.

One simple way to overcome the contact issue is to employ surfactants. Surfactants are generally organic compounds with hydrophobic and hydrophilic group chains in its structure [396] and it is very well known that surfactants are employed to decrease the surface tension of water or an organic solution [397, 398]. Hypothesis for employment of surfactants is that the insoluble organic pollutant will be broken down into much smaller droplets due to hydrophobic chains of surfactant and a homogenous colloidal interface of organic pollutant and water is formed. This enables the smaller droplets of organic pollutant to come in contact with photocatalyst in water for a complete remediation. To enhance the contact of insoluble pollutant, sodium dodecyl sulfonate have been employed as surfactant. For understanding the surfactant affect, G-TiO$_2$ NP was used for naphthalene remediation as G-TiO$_2$ NP had shown fastest time for the complete remediation of MO under 4 h. Further experiments were done for remediation naphthalene with surfactant for G-TiO$_2$ NW, G-ZnO NW & G-TiO$_2$ seeded ZnO NW.

5.2 Experimental Procedure

5.2.1 Materials and Reagents

Toluene, diesel, naphthalene, sodium dodecyl sulfonate and other reagents were purchased from Sigma-Aldrich, a commercial company in USA. Photocatalyst materials G-TiO$_2$

NP, G-TiO$_2$ NW, G-ZnO NW & G-TiO$_2$ seeded ZnO NW were synthesized using sol-gel and hydrothermal techniques using materials outlined in Chapter 3 and Chapter 4.

5.2.2 Sample Preparation and Decontamination Setup

5.2.2.1 Setup without Surfactant

The organic contaminants (toluene, naphthalene and diesel) at different concentrations were used to decontaminate using G-TiO$_2$ nanocomposite photocatalyst. A 100 W lamp was employed to simulate the solar light intensity of 800 W/m^2. The contaminants solution of 1g G-TiO$_2$ were stirred in closed glass container, and kept closed during the completion of the experiment. Samples were collected at regular intervals, and centrifuged to separate composite G-TiO$_2$ particles from measuring solution. The centrifuged sample of 1 µL solution was passed through a gas chromatography (GC).
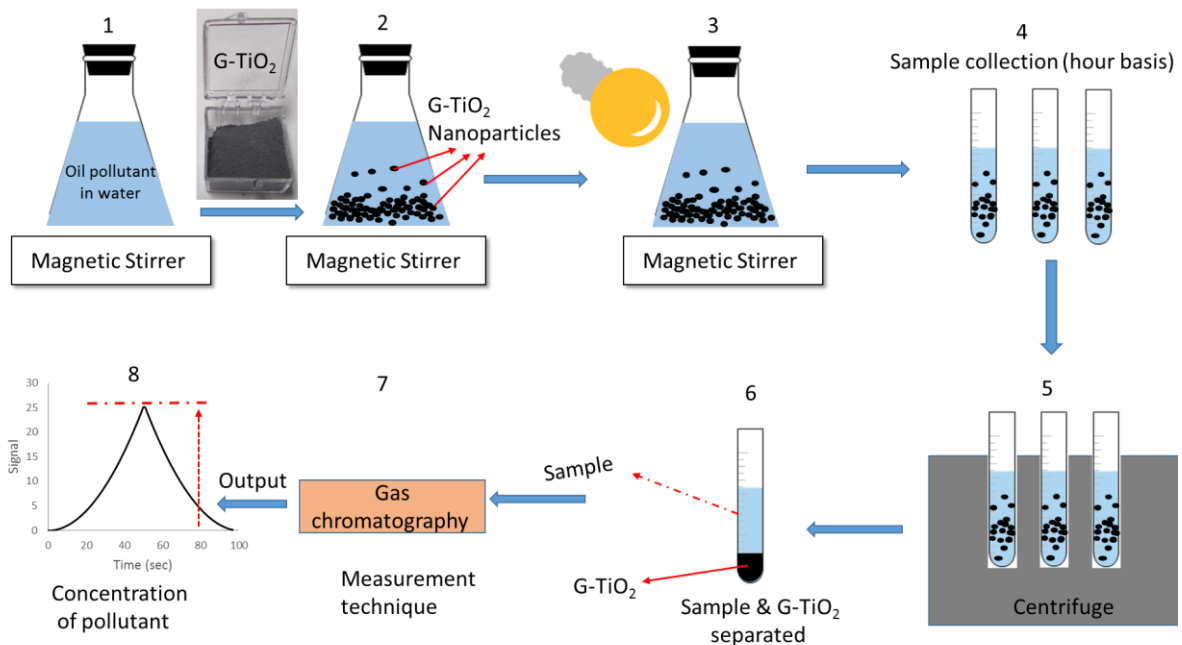
Figure 5.1 Schematic of sample collection and analysis shown in step in step process.

Figure 5.1, shows the schematic of sample collection and analysis shown in step in step process. Diesel, toluene and naphthalene containing water samples have been kept in the

identical conditions, and decontaminated water samples have been collected as a function of time using G-TiO$_2$ photocatalyst. These petroleum molecules may get evaporated especially under stirring and light exposure conditions. It is useful to add a control experiment using the same equipment setup while changing the G-TiO$_2$. The retention time (in min) vs. area under curve was plotted to understand each organic contaminant in the water sample. The ratio of concentrations as C$_o$ (initial concentration) and C$_n$ (concentration of solution at different timed samples with % of sample remained in the solution) were used to understand the change in percentage of concentration with the use of G-TiO$_2$ nanocomposite photocatalyst.

$$\% \, Remediation \; = \; 100 * \frac{Concentration \; at \; time \; interval \; (Cn)}{Initial \; concentration \; (Co)}$$

5.2.2.2 Setup with Surfactant

The performance of 0.2g of photocatalyst (G-TiO$_2$ NP, G-TiO$_2$ NW and G-ZnO NW, G-TiO$_2$ seeded ZnO NW) were used on 30 ppm naphthalene in water using surfactant of sodium dodecyl sulfonate (20ppm) in 100 ml of deionised water. The light intensity of 800 W/m^2 generated by 30 watt bulb was used to remediate naphthalene from water. The samples were analysed using JASCO V-530 UV-visible spectrometer was used to measure the absorbance naphthalene presence in remediated water at 0 and 48 hours similar to one discussed for MO. The naphthalene has UV-visible absorption at 221 nm, 286 nm and 312 nm. The values at these peaks were considered to determine the percentage (%) of naphthalene in the remediated water samples by calculating % concentration ratio (C$_n$/C$_o$)*100. Total organic content is obtained by calculating the average of % concentration ratio for peaks at 221 nm, 286 nm and 312 nm for naphthalene.

70

5.3 Photocatalytic Activity

5.3.1 Remediation of Organics without Surfactant

1 g of G-TiO$_2$ nanoparticle have been used with toluene at 100 ppm (250 ml) under 100 W visible light bulb to simulate the solar light intensity of 800 W/m^2. Figure 5.2, shows ~90% of toluene decontamination in water for exposure of only an hour of visible light. Further, light exposure results in similar values indicating that toluene on surface of water mostly evaporated or there could be continual evaporation of toluene from water surface.
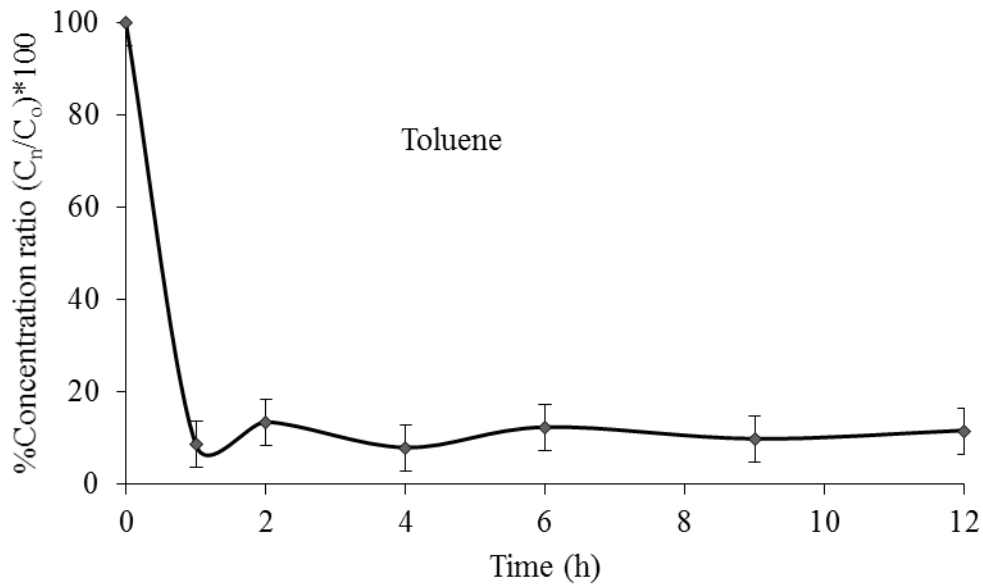
Figure 5.2 The change in the area in toluene measurement as function of hour for toluene decontaminated water in 100 W visible light.

The initial solution of naphthalene solution was 5000 μg/mL in methanol, analytical standard as obtained from Sigma Aldrich. 25 μg/mL naphthalene in DI water (250 mL) was prepared to recognize the effect of decontamination using 1g G-TiO$_2$ nanoparticles under visible light with a 100 W lamp to simulate the solar light intensity of 800 W/m^2. Naphthalene is sparingly soluble in water, so employed methanol naphthalene solution. 25 μg/mL of solution

71

was prepared and decontaminated under visible light radiation. Figure 5.3, shows decontamination of naphthalene under visible light in presence of G-TiO$_2$ nano particles. There was only 50% reduction of naphthalene under visible light over a period of 48 h, measured using GC, which is shown in Figure 5.3.
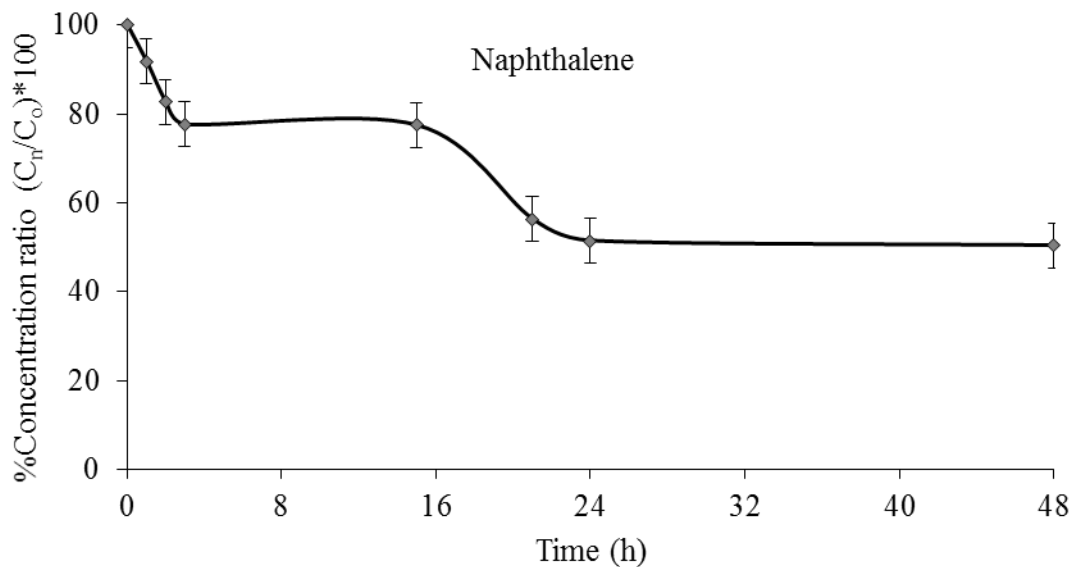
Figure 5.3 The change in the area in naphthalene measurement as function of hour for naphthalene decontaminated water in 100 W visible light.

The composition of diesel in water obtained from Sigma Aldrich contains acetone, methanol and mineral oil type. 25 μg/mL of diesel in DI water (250 mL) was used with 1g G-TiO$_2$ nanoparticle. The methanol is soluble in water whereas acetone and oil are springy soluble in water. It is clear that without organic molecules much in contact with G-TiO$_2$ nanoparticle, it is difficult to decontaminate under visible light. Figure 5.4, shows the change area of diesel measured as a function of time (in hours) under 100 W of visible light lamp. So, organic molecules present in diesel are not in contact with G-TiO$_2$ nanoparticle displaying ∼ 40% reduction of diesel after 48 h of visible light irradiation.

72
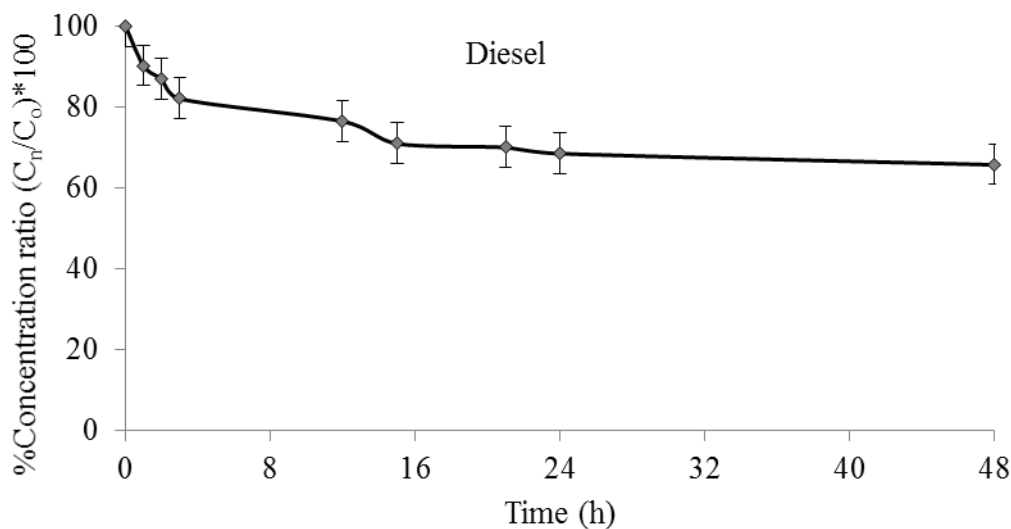
Figure 5.4 The change in the area in diesel measurement as function of hour for diesel decontaminated water in 100 W visible light.

90% of toluene, 50% of naphthalene and 40% of diesel have been remediated using G-TiO$_2$ nanomaterial under visible light as shown in Figures 5.2, 5.3 & 5.4. Figure 5.5 shows the pictorial representation for decontamination mechanism G-TiO$_2$ with petroleum pollutants. The insolubility of petroleum pollutants in water brings contaminant to the surface of water thereby inhibiting photocatalytic effect with G-TiO$_2$ nanoparticles. The contaminants soluble in water remain in contact with G-TiO$_2$ are completely remediated.

The results shown in Table 5.1 reveal that it is easy to remediate toluene than naphthalene or diesel from water. The decontamination depends upon solubility of organics in water or the layer of organics to remain in contact with photocatalysts. Naphthalene as well as diesel are sparingly soluble in water and do not remain in contact with the G-TiO$_2$ nanomaterial whereas toluene remains in contact with photocatalyst. Due to lower density than water both naphthalene and diesel molecules stay on the surface of water. The insolubility in water as well as no contact

73

with G-TiO$_2$ makes diesel and naphthalene to remediate partially up-to 50% and 40% than their initial values.
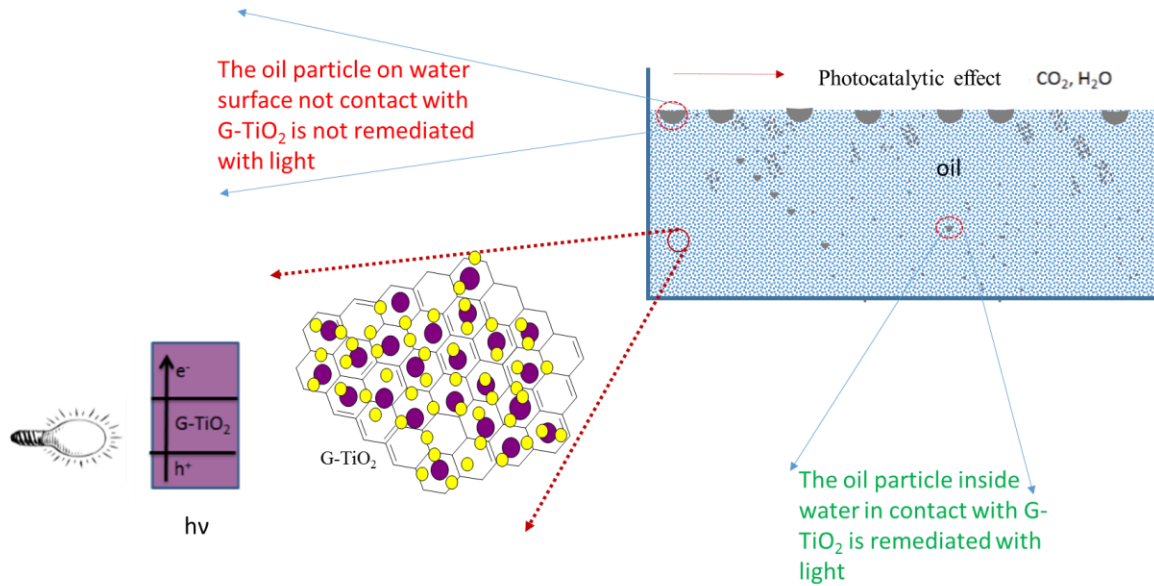
Figure 5.5 Schematic for the remediation of soluble & insoluble organic compounds using G-TiO$_2$.

Table 5.1 Comparative study of petroleum products remediation.

Material/Method	Pollutant/light source	Results	Ref
TiO$_2$ (6nm)/Sol-gel	Toluene (aqueous media)/UV light	Conversion of toluene to CO$_2$ was achieved upto 55%	[399]
TiO$_2$-ZnO /Sol gel Annealed at 380 C	Toluene (aqueous media)/Visible light	45.7% after 2 h of light irradiation	[400]
TiO$_2$-ZnO /Sol gel Annealed at 500 C		39.5% after 2 h of light irradiation	
N doped TiO$_2$-ZnO /Sol-gel Annealed at 380 C		28.6% after 2 h of light irradiation	
N-TiO$_2$/ZnO /Sol gel Annealed at 500 C		12.9% after 2 h of light irradiation	

Table 5.1 (Continued)

Without catalyst		73.2 % after 2 h of visible light irradiation	[400]
TiO₂ – commercial P25	Toluene (aqueous media)/ UV light	60 h to completely remove toluene from water	[401]
TiO₂ dip coated on Autoclaved aerated white concrete	Toluene (11 ppm)(air purification)/UV light	86% remediated after 20 h	[402]
Rutile and anatase TiO₂/ commercial products	Naphthalene (Acetonitrile/water)/ Visible light	Higher efficiency than anatase TiO₂ particles for converting naphthalene to 2-formylcinnamaldehyde (is about only conversion)	[403]
TiO₂ dispersions-commercial P25	Naphthalene (aqueous media)/Visible light	Feasible and fast within 30 min but for when naphthalene is less than 4 ppm (no details are given).	[404]
TiO₂-NiO / insitu – modified sol-gel	Naphthalene (aqueous media)/Visible light & UV light	1.5 to 2.5 faster than TiO₂ (sol-gel) material for less than 20 ppm of naphthalene for time of more than 100 h	[405]
G-TiO₂ /sol-gel	Toluene (aqueous media)/ only Visible light	90% in one h	this investigation
G-TiO₂ /sol-gel	Naphthalene/(aqueous media)/ only Visible light	50% in 48 h	
G-TiO₂ /sol-gel	Diesel	40% in 48 h	

5.3.2 Remediation of Organics with Surfactant

The performance of 0.2g of photocatalyst (G-TiO₂ NP, G-TiO₂ NW and G-ZnO NW, G-TiO₂ seeded ZnO NW) were used on 30 ppm naphthalene in water using surfactant of sodium dodecyl sulfonate (20ppm) in 100 ml of deionised water. The light intensity of 800 W/m² generated by 30 watt bulb was used to remediate naphthalene from water. Figures 5.6(a, b) and

75

5.7 (a, b) show disappearance of UV-visible absorption peaks at 221, 286 and 321 nm from remediated samples.
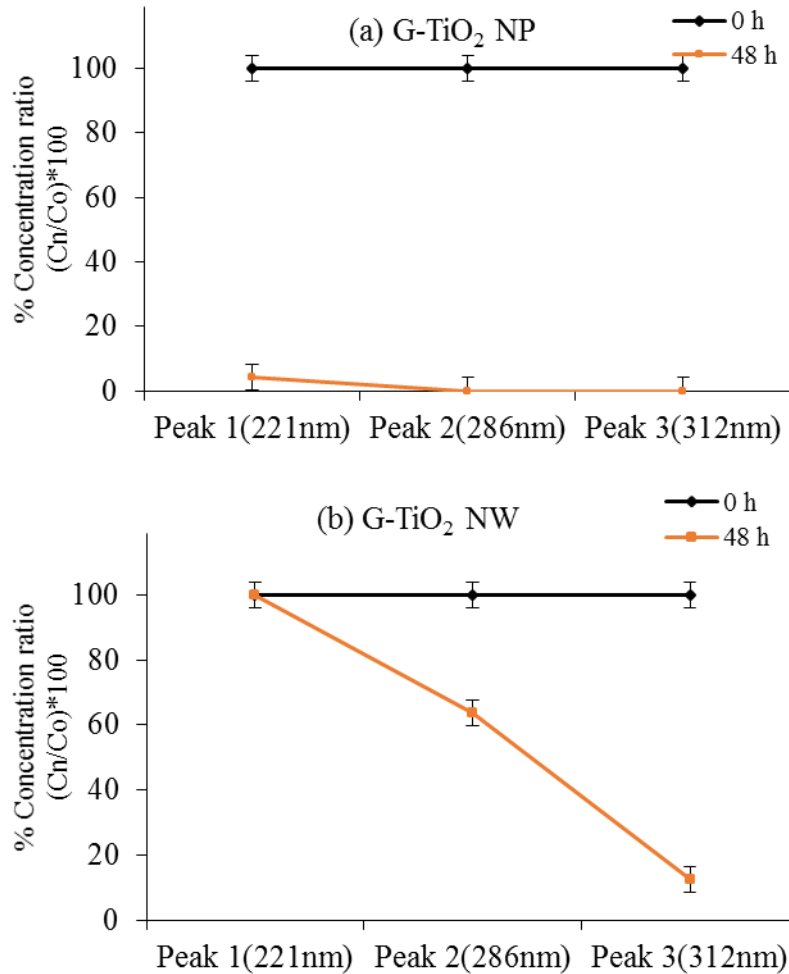
Figure 5.6 (a, b) Comparative graph of $\%C_n/C_o$ vs time duration (h) for G-TiO$_2$ nanoparticles, G-TiO$_2$ nanowire for naphthalene respectively.

From Figures 5.6 (a, b) and Figures 5.7 (a, b), the total % of naphthalene remediated with surfactant have been calculated by the averaging the % of concentration ratio for 3 peaks of naphthalene (221, 286 and 321 nm) is found to be 98.62 % for G-TiO$_2$ NP, 41.26 % for G-TiO$_2$ NW, 12.73 % for G-ZnO NW and 0 % for G-TiO$_2$ seeded ZnO NW after 48 hours. The G-TiO$_2$ nanoparticles have been found to perform better than the G-TiO$_2$ nanowires, G-ZnO nanowires

76

and G-TiO$_2$ seeded ZnO nanowires for the decontamination of naphthalene which shows potential for practical applications.
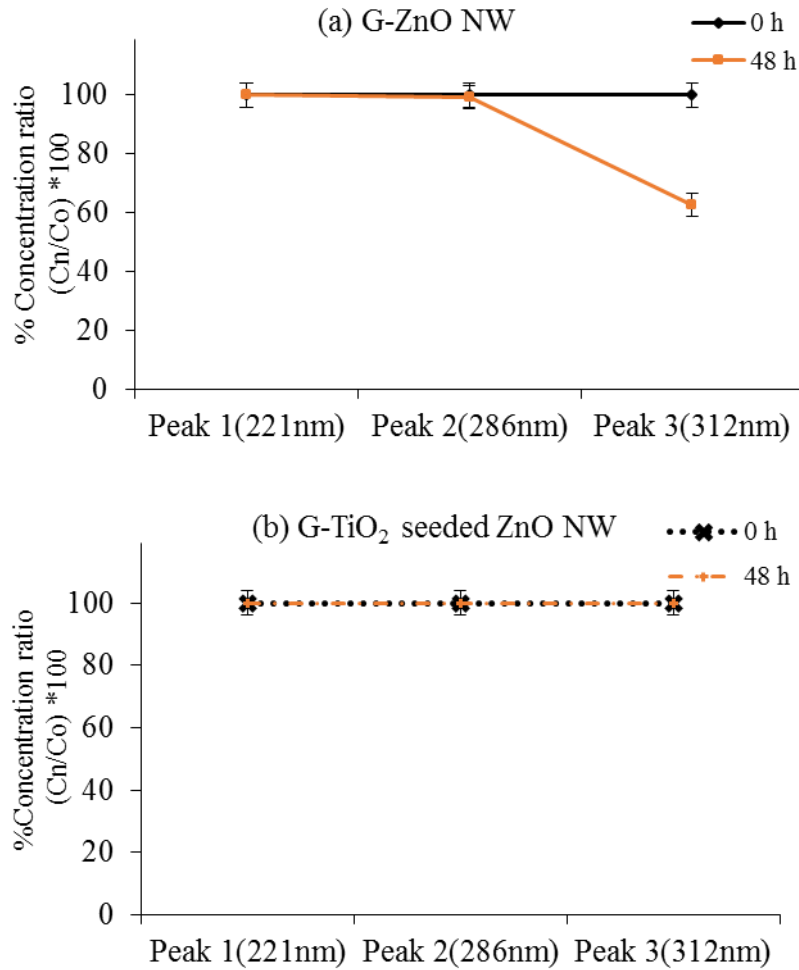
Figure 5.7 (a, b) Comparative graph of %C$_n$/C$_o$ vs time duration (h) for G-ZnO nanowire, G-TiO$_2$ seeded ZnO nanowire for naphthalene respectively.

5.3.3 Comparison of Photocatalytic Activity with and without Surfactant

By calculating the percentage of total organic content of naphthalene from Figure 5.6 (a, b) and Figure 5.7 (a &b) it can be observed that the despite employing lower weight of photocatalyst 0.2 g G-TiO$_2$ NP for 100 ml of polluted water with surfactant as compared to 1 g of G-TiO$_2$ NP for 250 ml of polluted water without surfactant, the % of naphthalene remediated with surfactant is 98.62 % as compared to 50 % remediated without surfactant for G-TiO$_2$

77

nanoparticles. Surfactant (sodium dodecyl sulfonate) have been employed for increasing the solubility of petroleum contaminants, which helps contaminant to remain in contact with the photocatalyst. Table 5.2 shows the results produced for naphthalene decontamination with surfactant with G-TiO$_2$, suggesting importance of oil pollutant to come in contact with photocatalyst for complete remediation

Table 5.2 Results of visible light photocatalytic remediation of organic pollutants with and without the use of a surfactant.

Material	Pollutant	% remediation
G-TiO$_2$ nanoparticles	Toluene (100 µg/mL)	90% in one h
	Naphthalene (25 µg/mL)	50% in 48 h
	Diesel (25 µg/mL)	40% in 48 h
G-TiO$_2$ nanoparticles	Naphthalene (30 µg/mL) with sodium dodecyl sulfonate as surfactant	98.62% remediation after 48 h
G-TiO$_2$ nanowires		41.26% remediation after 48 h
G-ZnO nanowires		12.73% remediation after 48 h
G-TiO$_2$ seeded ZnO nanowires		0% remediation after 48 h

5.4 Conclusion

The G-TiO$_2$ nanoparticles were synthesized using sol-gel synthesis process and characterized for mass production. G-TiO$_2$ was able to decontaminate 90% of toluene whereas with naphthalene revealed only 50% of reduction and diesel revealed only 40% of reduction from water solution. Naphthalene and diesel insolubility are reason behind the ineffective photocatalytic effect using G-TiO$_2$ nanomaterial. The decontamination depends upon solubility of organics in water or the layer of organics to remain in contact with photocatalysts. Naphthalene as well as diesel are sparingly soluble in water and do not remain in contact with the G-TiO$_2$ nanomaterials whereas toluene remains in contact with photocatalyst. The

78

insolubility in water as well as no contact with G-TiO$_2$ makes diesel and naphthalene to remediate partially up-to 50% and 40% than their initial values.

Based on understanding for the importance of pollutant to remain in contact with photocatalyst material for complete remediation, surfactant has been employed with G-TiO$_2$ nanoparticles to effectively remediate pollutant from water. It can be observed that despite employing lower weight of photocatalyst 0.2 g G-TiO$_2$ NP for 100 ml of polluted water with surfactant as compared to 1 g of G-TiO$_2$ NP for 250 ml of polluted water without surfactant, the % of naphthalene remediated with surfactant is 98.62 % as compared to 50 % remediated without surfactant for G-TiO$_2$ nanoparticles.

CHAPTER 6: INVESTIGATION OF CONDUCTING POLYMER AS A NANOSTRUCTURED/POLYMER PHOTOCATALYST FOR WATER REMEDIATION[7]

6.1 Introduction

The TiO_2 and ZnO photocatalytic nanomaterials have been extensively studied and used for remediation of organics under UV-radiation (200nm <wavelength (λ) < 400nm) [406-411], however each one have drawbacks in terms of photocorrosion and poor efficiency in generating electron-hole pairs under visible radiation of light (400 nm < λ <700 nm) [61, 412-414]. The nitrogen, silver, magnesium, aluminium, gold, platinum etc., are doped in both TiO_2 and ZnO to overcome the photocorrosion and photocatalytic efficiency [133, 167, 345, 361, 415-419]. The graphene (G) doping has shown an increase in the photocatalytic behaviour and a decrease in photocorrosion under visible light [420, 421]. Recently, Gunti et al., have shown G doped TiO_2 and G doped ZnO are highly efficient photocatalytic materials for organic remediation in water [420, 421]. Further, Gunti et al. have revealed a high photocatalytic efficiency of both G doped TiO_2 nanoparticles (G-TiO_2 NP) and G doped ZnO nanowires (G-ZnO NW), due to their lower band gap and an increase in light absorption over other nanostructured TiO_2 and ZnO materials [420, 421]. G-TiO_2 NP and G-ZnO NW have been found to be highly suitable materials to

---

[7] Portion of these results have been communicated with Journal of Environmental Chemical Engineering, Elsevier publications with title "The Use of Conducting Polymer to Stabilize the Nanostructured Photocatalyst for Water Remediation", which is currently under review.
Appendix A for copyright permission

remediate methyl orange (MO) in water as shown by Gunti et al. & Yangyang et al. [82, 143, 157, 420-423].

In general, G doped photocatalysts have difficulties in adhering on glass substrate due to their strong hydrophobic nature [424-426]. To overcome this drawback, vacuum deposition technique is employed to deposit G-TiO_2 as well as G-ZnO, on glass substrates, which are quite expensive to synthesize and low-yield making it less practical for mass applications [427-429]. Several organic materials (polyethylene, polyvinylchloride, weak acids like acetic acid, citric acid etc.) are used as binders [430-436]. It has been shown that when acetic acid used as binder for photocatalysts to coat onto the substrates, it peels off under wet conditions in a few hours [420, 421]. One major technical issue of an organic acidic binder is the degradation due to photocatalytic activity along with pollutant from water.

The polyaniline (PANI) as a binder material, has been introduced for G-TiO_2 NP and G-ZnO NW, which allowed to remediate the organics in water under visible light as well as to employ photoelectrochemical catalytic application. PANI is most studied conducting polymer, due to its electrochemical, electrical, optical, and processable properties [437-439]. The processed PANI has absorption characteristics, thereby producing an electron-hole pair similar to a photocatalytic material, and it enables photocurrent generation in the undoped form [440, 441]. Besides, the composite TiO_2-conducting polymer nanocomposite materials has been recently studied [442-444]. PANI can be employed as a binder to coat G-TiO_2 NP and G-ZnO NW on substrates. PANI does not only act as binder but also enhances the photocatalytic performance of G-TiO_2 NP and G-ZnO NW nanomaterials.

PANI was synthesized by oxidative polymerization technique [445]. Initially, emeraldine salt state I was synthesized, then emeraldine base was formed by undoping in sodium hydroxide

81

solution. Undoped PANI (emeraldine base) was made soluble in N-Methyl-2-pyrrolidone, and can be coated on any substrate. Emeraldine base in its undoped state, can be changed to emeraldine salt state II by doping in a protonic acid. Due to the adhesion and electrochemical properties of PANI in PANI:G-TiO$_2$ NP and PANI:G-ZnO NW, now it can be used for photoelectrochemical catalytic applications. The PANI:photocatalyst (PC) is used generally to understand the PANI:G-TiO$_2$ NP and PANI:G-ZnO NW.

The PANI, (1:1, 1:2, 2:1) PANI:G-TiO$_2$ NP and 1:1 PANI:G-ZnO NW were synthesized and characterized using SEM, XRD, UV-vis and FTIR techniques. The photocatalytic as well as photoelectrochemical catalytic analysis on methyl orange (pollutant) in water was made using PANI:G-TiO$_2$ NP and 1:1 PANI:G-ZnO NW nanomaterials. The ease in coating of PANI:G-TiO$_2$ NP and PANI:G-ZnO NW on various substrates and visible light remediation permits the use of such materials for remediation of organics from water and processes for practical applications.

6.2 Experiment

6.2.1 Reagents and Materials

The chemicals such as hydrochloric acid (HCl), propanol, titanium (IV) isopropoxide, sodium hydroxide (NaOH), zinc oxide (ZnO) particles, zinc nitrate hexahydrate (Zn(NO$_3$)$_2$·6H$_2$O), hexamethylenetetramine (HMTA), methyl orange (MO), aniline, ammonium persulfate (APS), acetone, methanol, N-Methyl-2-pyrrolidone (NMP) and other reagents were procured from Sigma-Aldrich (USA). The graphene (G) platelets of size < 20 nm in thickness were acquired from Angstron Materials, a commercial company in USA. All materials and reagents which were employed as procured without any modification or further purification unless specified.

82

6.2.2 Synthesis of Photocatalyst (PC) and PANI:PC

G-TiO$_2$ NP was synthesized using sol-gel method. Initially, G was mixed in propanol followed by addition of titanium (IV) isopropoxide with slow addition of HCl at room temperature. The precipitate was washed, centrifuged and dried at 100 ^{o}C to obtain G-TiO$_2$ NP [421]. G-ZnO NW was synthesized by using a hydrothermal method using precursors of Zn(NO$_3$)$_2$·6H$_2$O, HMTA and G. Initially Zn(NO$_3$)$_2$·6H$_2$O and HMTA were dissolved in deionized water (DI) with an addition of G, and maintained at 80 ^{o}C. ZnO nanoparticles (average particle size of 50 nm) were added as nucleation sites for the growth of nanowires. The solution was washed, centrifuged, and dried at 100 ^{o}C to obtain G-ZnO NW [420].

Table 6.1 Composition of aniline and photocatalyst (PC) in synthesis of PANI:photocatalyst (PC).

PANI : PC	Aniline	PC (photocatalyst)
1:1 PANI:G-TiO$_2$ NP	0.9515 ml (1M/100 ml)	0.931 g of G-TiO$_2$ NP
1:2 PANI:G-TiO$_2$ NP	0.9515 ml (1M/100 ml)	1.862 g of G-TiO$_2$ NP
2:1 PANI:G-TiO$_2$ NP	0.9515 ml (1M/100 ml)	0.4655 g of G-TiO$_2$ NP
1:1 PANI:G-TiO$_2$ NP	0.9515 ml (1M/100 ml)	0.931 g of G-ZnO NW
PANI	0.9515 ml (1M/100 ml)	-

PANI:PC was synthesized by a chemical oxidative polymerization technique using aniline and ammonium persulfate (APS) in HCl under controlled conditions [445, 446]. Ratios of PANI:PC were obtained by maintaining the ratios of aniline:PC as stated in Table 6.1 for 100 ml of solution. Initially, 0.9515 ml of aniline was added to 50 ml of 1M HCl along with the PC mentioned in the Table 6.1, which was cooled at 4 ^{o}C under controlled stirring. APS (1.14g) was added to 50ml of 1M HCl, which was then added drop wise to the aniline:PC solution and maintained at 4°C for 12 hours. A dark green PANI:PC precipitate was obtained and separated

by vacuum filtration. The precipitate was washed with DI water, methanol and acetone to remove unreacted oligomers and lower molecular weight polymers, and then dried at 100 $^{\circ}$C. the dried PANI:PC was emeraldine salt state 1 which was then undoped by treating with a 1M NaOH solution and conversion into emeraldine base. The emeraldine base of PANI:PC was dissolved in NMP, and coated onto a petri dish or ITO glass and dried at 70 $^{\circ}$C. The obtained PANI:PC emeraldine base films on the petri dish or ITO glass were then dedoped by 1M HCl to make PANI:PC films in emeraldine salt state II. Pristine PANI was synthesized with similar procedure without addition of any photocatalyst in the synthesis process. Table 6.1 shows various ratios of synthesized and studied (1:1, 1:2, 2:1) PANI:G-TiO$_2$ NP , 1:1 PANI:G-ZnO NW and PANI materials for photocatalytic performance and compared with G-TiO$_2$ NP and G-ZnO NW.

6.2.3 Sample Preparation and Decontamination Setup

The photocatalytic performance was measured using 0.2 g of PANI:PC (Table 6.1) coated as a thin film onto a petri dish using NMP and later, dedoped using 1M HCl. In comparison, 0.2g of G-TiO$_2$ NP & G-ZnO NW were coated onto a petri dish using acetic acid and dried at 200 $^{\circ}$C. The photocatalytic decontamination setup consists of PANI:PC coated petri dish, a 30-watt light bulb with a light intensity of 800 W/m^2, and 20 ppm (40 ml) MO used as an organic pollutant. The samples were collected from the remediating MO in intervals of one hour. A JASCO V-530 UV-visible spectrometer was used to measure the absorbance of MO in the remediated sample.

The photoelectrochemical catalytic performance was measured using 0.04 g of synthesized samples of 1:1 PANI:G-TiO$_2$ NP, 1:1 PANI:G-ZnO NW and PANI coated on ITO glass substrates. The coated samples were dedoped using 1M HCl. 20 ppm of MO (40 ml) and

84

0.01M HCl were used as pollutant and electrolyte, respectively. The decontamination setup for the photoelectrochemical catalytic application is shown in Figure 6.1 b. Steel mesh was used as counter electrode and 1:1 PANI:G-TiO$_2$ NP, 1:1 PANI:G-ZnO NW and PANI coated ITO glass plates as the working electrode. Current (I)-voltage (V) characteristics were measured at applied voltage of 1V for 4 hours with and without visible light radiation. The initial concentration of MO in water was taken as C$_o$ at 0 hours. The percentage of concentration ratio was calculated by using C$_n$/C$_o$ with respect to time in hours.
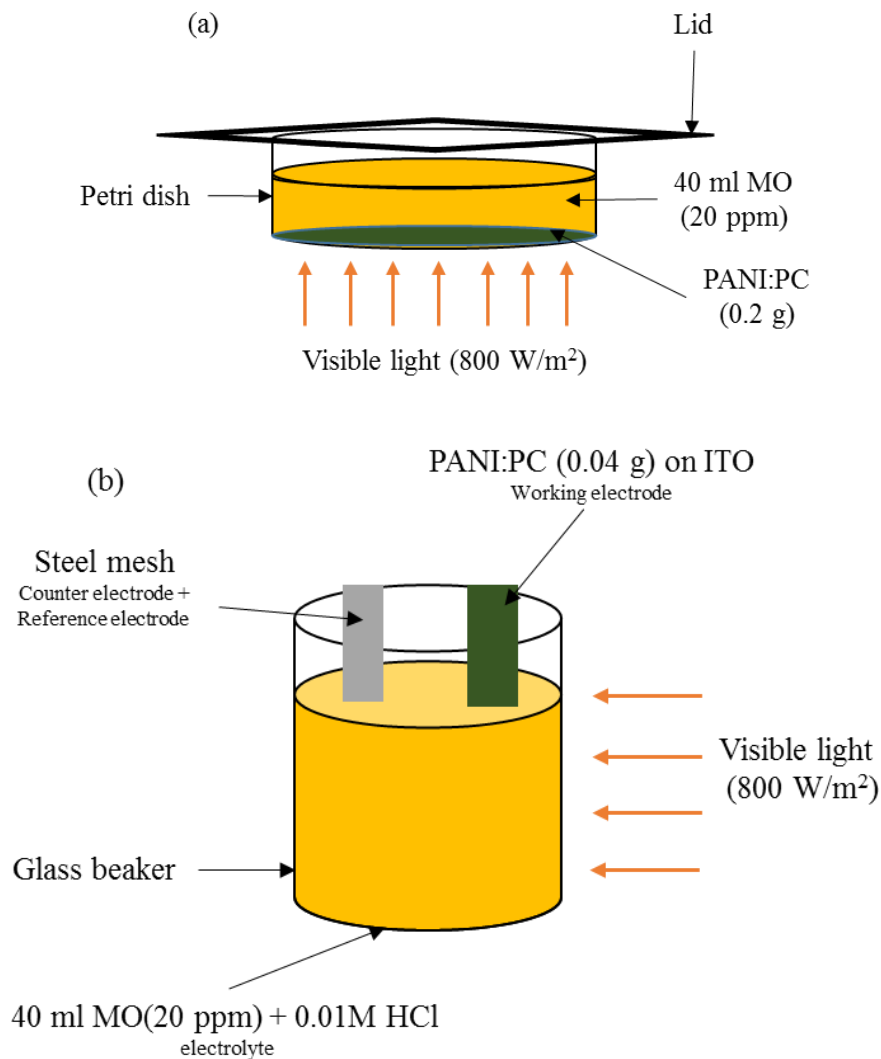
Figure 6.1 (a & b) Decontamination setup for photocatalytic and photoelectrochemical catalytic performance.

6.3 Results and Discussion

6.3.1 Scanning Electron Microscopy (SEM)
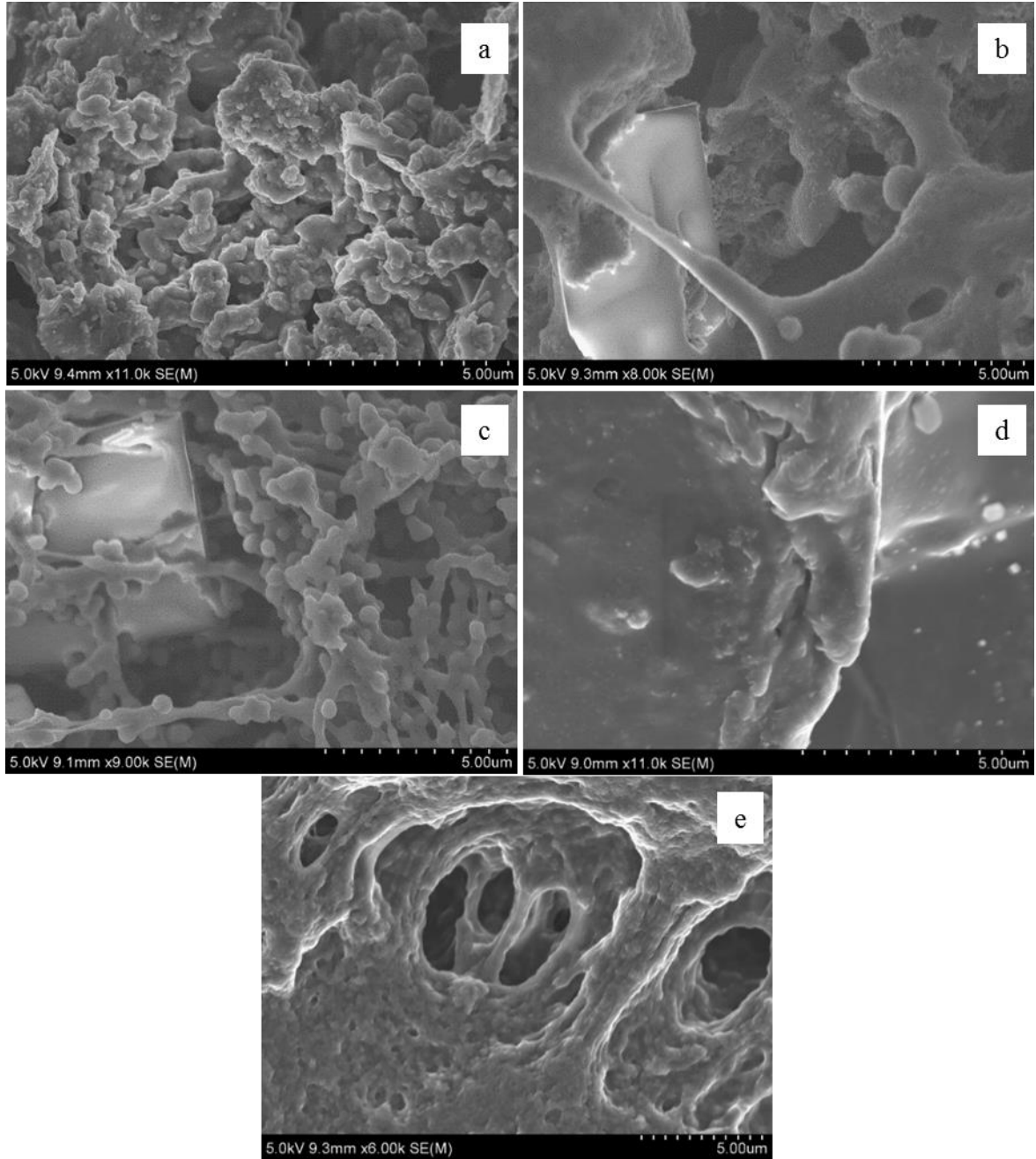
Figure 6.2 SEM image of (a) 1:1 PANI:G-TiO$_2$ NP (b) 2:1 PANI:G-TiO$_2$ NP (c) 1:2 PANI:G-TiO$_2$ NP (d) 1:1 PANI:G-ZnO NW (e) PANI at 5 micron magnification.

Figure 6.2 (a, b, c, d & e) shows SEM images of 1:1 PANI:G-TiO$_2$ NP, 2:1 PANI:G-TiO$_2$

NP, 1:2 PANI:G-TiO$_2$ NP ,1:1 PANI:G-ZnO NW and PANI, respectively. In Figure 6.2 (a, b &

86

c), nanoparticles are observed for G-TiO₂ in composite with PANI (polymeric structure). Figure 6.2d observes the wrapping of nanomaterials by PANI structure. However, it appears that the G-ZnO NW is within the PANI structure. Figure 6.2e, shows polymeric structure at 5µm magnification of PANI. Figure 6.2 (a, d, c& d) shows that the NP and NW are present within PANI's structure. The G-TiO₂ NP and G-ZnO NW have nanoparticle and nanowire structure respectively, which have been observed by Gunti et al. [420, 421].

The EDS images of 1:1 PANI:G-TiO₂ NP and 1:1 PANI:G-ZnO NW undoped form are shown in Figure 6.3 (a & b). The presence of Ti, O, C is observed in Figure 6.3a, revealing the presence of TiO₂, carbons in PANI & G, Na (undoped with NaOH) and Cl (initial 1M HCl in synthesized PANI:PC structure). Figure 6.3 b shows the presence of Zn, C, O elements due to presence of ZnO, G & carbon in PANI.
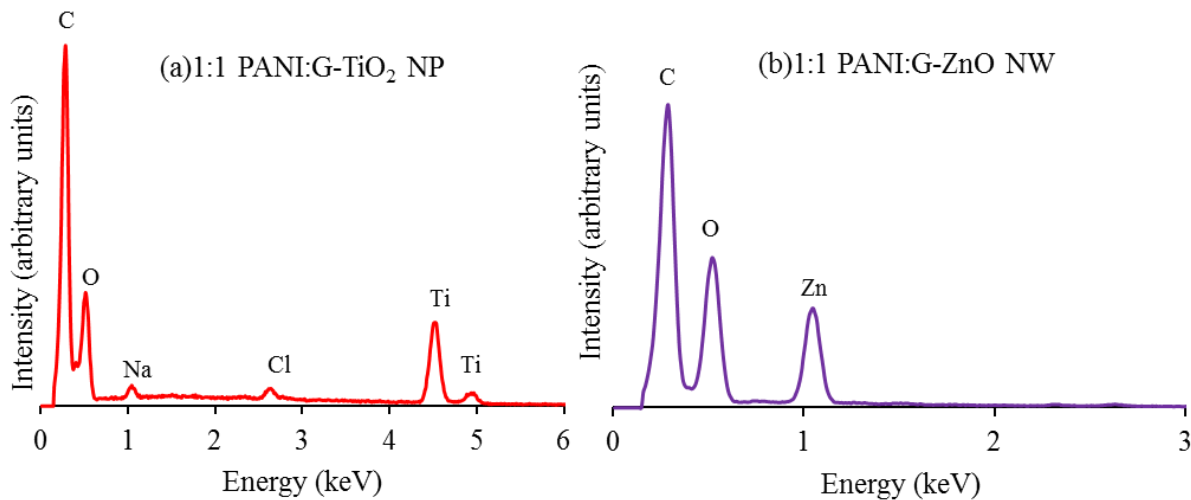
Figure 6.3 (a & b) EDS images of undoped (a) 1:1 PANI:G-TiO₂ NP (b) 1:1 PANI:G-ZnO NW.

6.3.2 X-ray Diffraction (XRD)

Figure 6.4 (a, b & c) observes the XRD spectra of 1:1 PANI:G-TiO₂ NP , 1:1 PANI:G-ZnO NW and PANI. Figure 6.4 a, shows angle (2θ) at 42.9, 54.2, 55.0 degrees for 1:1 PANI:G-

TiO$_2$ NP which corresponds to anatase phase of TiO$_2$. Similarly, Figure 6.4b shows the XRD spectra of 1:1 PANI:G-ZnO NW. No characteristic diffraction angle for G or ZnO are observed as wrapped in of PANI structure. The XRD spectra of PANI shows quasi-crystallinity at 25.8^o in Figure 6.4c. The absence of crystallinity for PANI- G-TiO$_2$ NP and PANI-G-ZnO NW are due to wrapping in PANI, so no crystalline structure is shown in Figure 6.4.
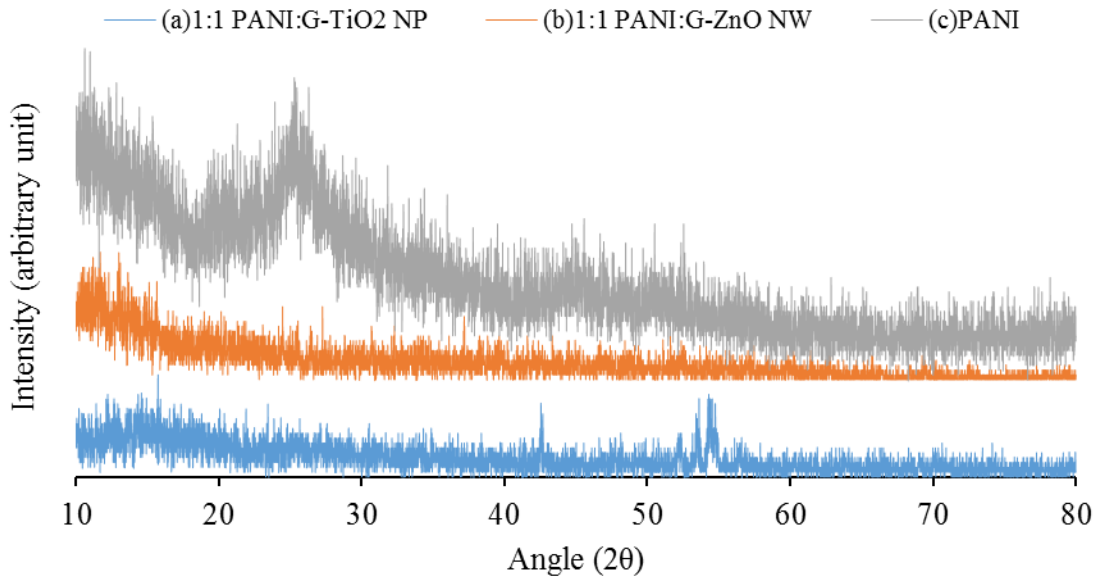
Figure 6.4 XRD pattern of (a) 1:1 PANI:G-TiO$_2$ NP , (b) 1:1 PANI:G-ZnO NW (c) PANI.

6.3.3 UV-visible Spectroscopy

Figure 6.5a shows UV-visible spectra of PANI and PANI:G-TiO$_2$ NP at different molar ratios of PANI with G-TiO$_2$ NP. The increase in absorbance of PANI-G-TiO$_2$ NP in visible light region (λ >400 nm) is due to presence of PANI in G-TiO$_2$ NP. The 1:1 and 2:1 ratio of PANI:G-TiO$_2$ NP reveal larger absorption in visible wavelength compared to 1:2 ratio of PANI:G-TiO$_2$ NP. The PANI with higher molar ratio than G-TiO$_2$ NP shows better visible absorption magnitude. Figure 6.5b shows UV-visible spectra of 1:1 PANI:G-ZnO NW to G-ZnO NW similar to Figure 6.5a. There is an increase in optical absorption in visible wavelength and a

decrease in UV wavelength between 200 to 400 nm has been observed. Figure 6.5 (a & b) observes optical absorption spectra of PANI compared to G-TiO$_2$ NP or G-ZnO NW films. The increase in visible wavelength (λ >400 nm) absorbance magnitude in PANI:G-TiO$_2$ NP and PANI:G-ZnO NW suggests enhanced photocatalytic activity compared to G-TiO$_2$ NP and G-ZnO NW.
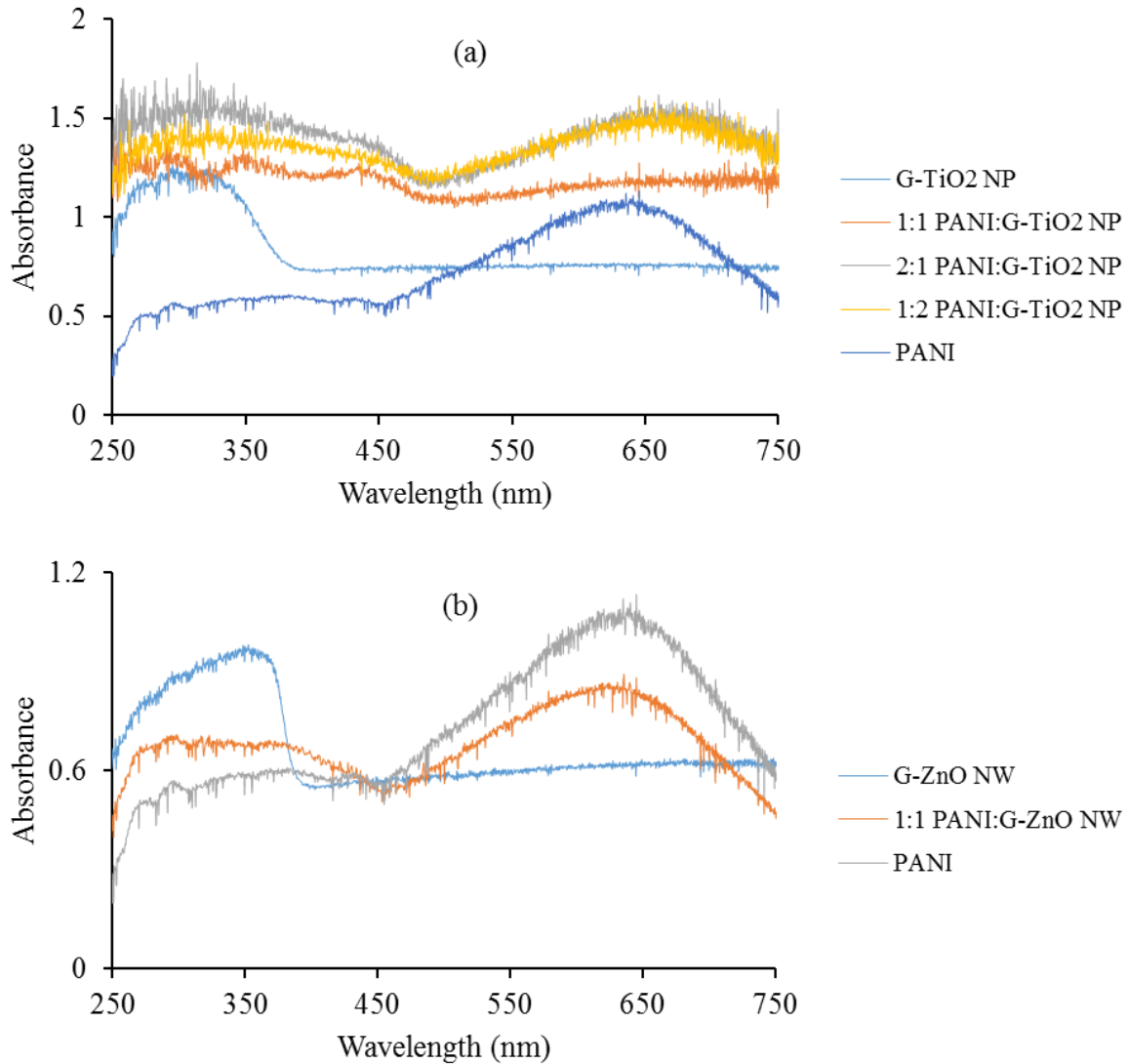
Figure 6.5 (a & b) UV-visible spectra for 1:1 PANI:G-TiO$_2$ NP, 2:1 PANI:G-TiO$_2$ NP, 1:2 PANI:G-TiO$_2$ NP, G-TiO$_2$ NP, 1:1 PANI:G-ZnO NW, G-ZnO NW and PANI.

89

6.3.4 Fourier Transform Infrared Spectroscopy (FTIR)
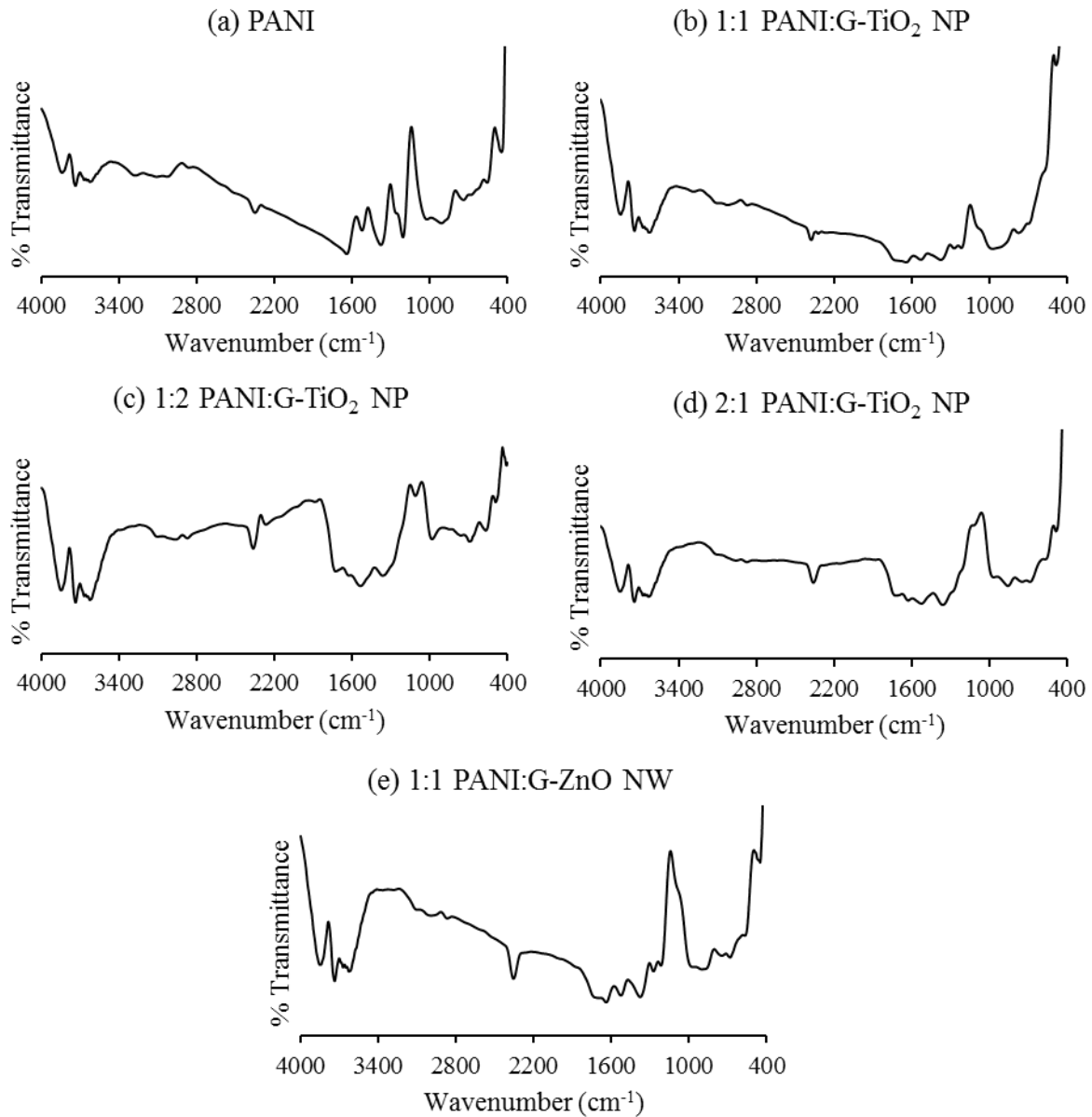
Figure 6.6 FTIR spectrum of (a) PANI (b) 1:1 PANI:G-TiO$_2$ NP (c) 1:2 PANI:G-TiO$_2$ NP (d) 2:1 PANI:G-TiO$_2$ NP (e)1:1 PANI:G-ZnO NW.

Figure 6.6 (a, b, c, d & e) shows FTIR spectra of dedoped PANI:PC nanocomposite photocatalysts. Figure 6.6 a reveals IR bands at 1258, 1374, 1523, 1635, 3125, 3259, 3622 cm^{-1} due to presence of PANI. The IR bands at 1258 and 1374 cm^{-1} are linked to stretching of radical cation (-CN$^{+}\cdot$). The IR band observed at 1523 cm^{-1} is due to stretching of C-C in quinoid ring,

90

and band at 1635 cm^{-1} is due to C-C bond stretching in benzoid ring. The peaks observed at 3125 and 3259 cm^{-1} are due to N-H bond stretching and the peak at 3622 cm^{-1} is due to O-H stretch for the presence of water content. There shift in the wavenumber is also observed for at different ratios of photocatalyst (G-TiO$_2$ NP & G-ZnO NW) in Figures 6.6 (b, c, d & e). In Figures 6.6 (b, c & d) shows peaks at 400-800 cm^{-1} due to skeletal vibration of Ti-O-Ti. Figure 6.6 e, shows the peak at 420-520 cm^{-1} due to transverse optical stretching of ZnO bond. The characteristics IR peak for G which is at 1600 cm^{-1} is not observed due to presence of PANI which has C-C bond stretching at around 1635 cm^{-1}.

6.3.5 Decontamination Study
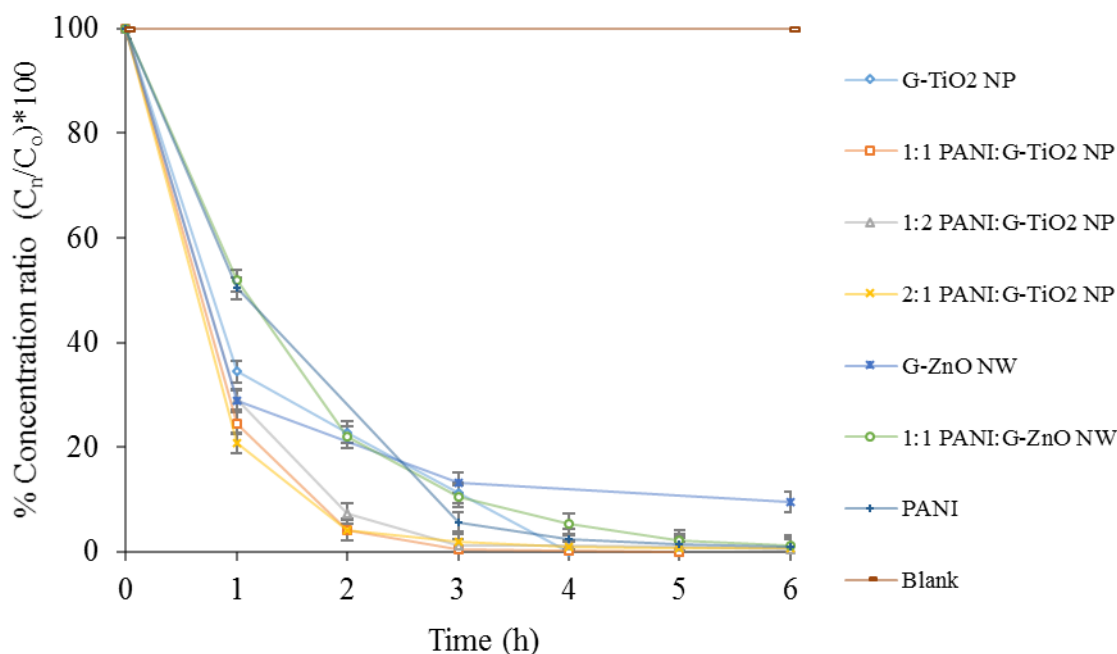
Figure 6.7 Remediation of methyl orange using PANI: PC under visible light irradiation.

PANI:PC (Table 6.1), G-TiO$_2$ NP , G-ZnO NW and PANI were employed to remediate MO under visible light with intensity of 800W/m^2. Initially, 0.2 g of composite material was coated on petri dish and 20 ppm (40 ml) of MO was added. G-TiO$_2$ NP remediates the MO in water in less than 4 hours [420]. The adhesion problem of G-TiO$_2$ NP and G-ZnO NW on petri

dish has caused the loss of photocatalytic material and photocatalytic activity. Whereas, PANI:PC and 1:1 PANI:G-TiO$_2$ NP show faster MO remediation within 3 hours and complete remediation in 5 hours as shown in Figure 6.7. The enhanced photocatalytic activity is due to the presence of PANI in PANI:G-TiO$_2$ NP.

Table 6.2 % Remediation of MO using synthesized materials under visible light.

Material	G-TiO$_2$ NP	1:1 PANI:G-TiO$_2$ NP	1:2 PANI:G-TiO$_2$ NP	2:1 PANI:G-TiO$_2$ NP	G-ZnO NW	1:1 PANI:G-ZnO NW	PANI
% remediation in hours	100 % in 4 h	100 % in 5 h	99.43 % in 6 h	99.43 % in 6 h	90.45 % in 6 h	98.84 % in 6 h	98.98 % in 6 h
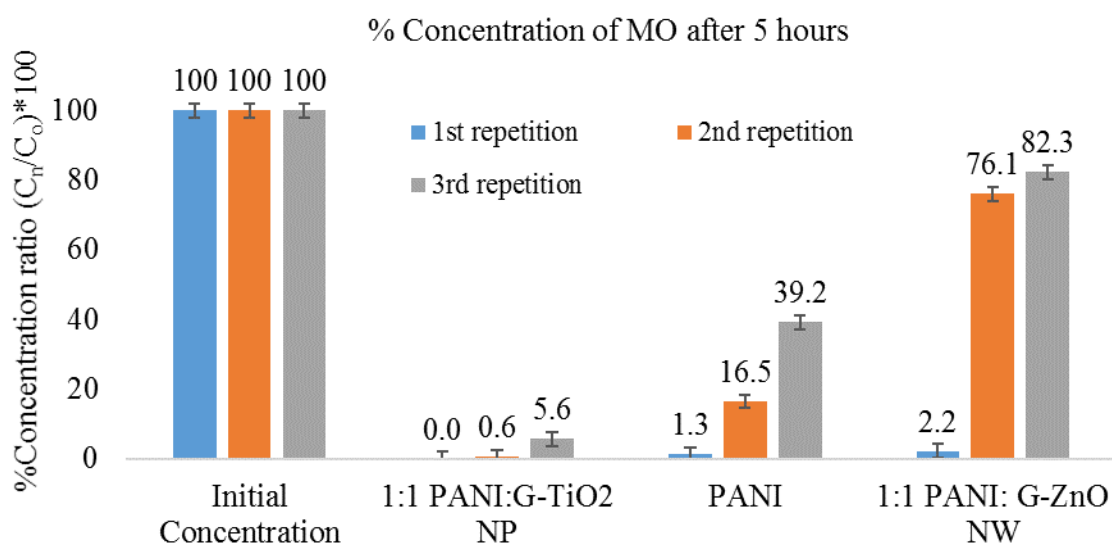
Figure 6.8 Repetitive MO remediation using (a) 1:1 PANI:G-TiO$_2$ NP (b) PANI (c) 1:1 PANI:G-ZnO NW.

Table 6.2 shows percentage of MO remediation under visible light, which has been correlated to Figure 6.7. The remediation of MO for 1:1 PANI:G-TiO$_2$ NP material is well compared with PANI and 1:1 PANI:G-ZnO NW for photoelectrochemical catalytic study. Figure 6.8 shows the plots of % concentration ratio for MO in water to understand the efficiency

92

and the recyclability of 1:1 PANI:G-TiO$_2$ NP, PANI and 1:1 PANI:G-ZnO NW. The 1:1 PANI:G-TiO$_2$ NP displays higher efficiency than 1:1 PANI:G-ZnO NW and PANI. These results are correlated with Figure 6.5 (a & b) where 1:1 PANI:G-TiO$_2$ NP reveals higher absorption in visible spectrum of light compared to 1:1 PANI:G-ZnO NW and PANI.

6.4 Photoelectrochemical Catalytic Study
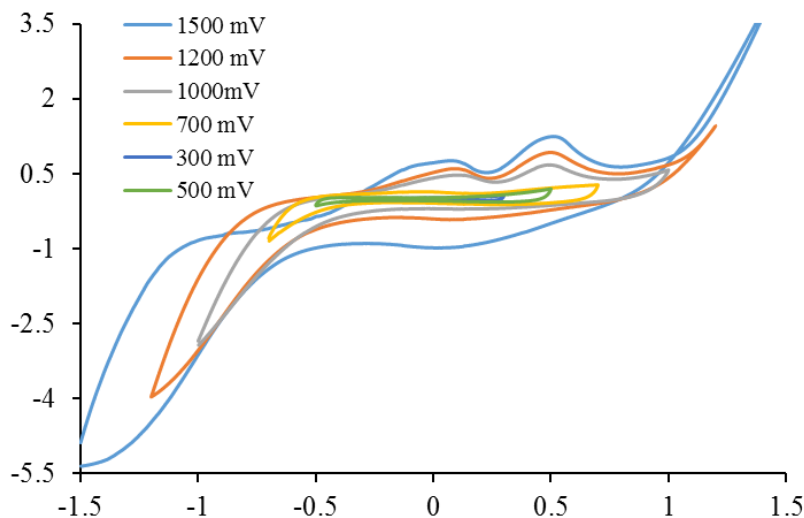
Figure 6.9 Cyclic voltammetry of 1:1 PANI:G-TiO$_2$ NP with 0.01 M HCl as electrolyte.

The photoelectrochemical catalytic performance, for 1:1 PANI:G-TiO$_2$ NP was analysed by coating 0.04g onto indium tin oxide (ITO) and dedoped in 1 M HCl. The 1:1 PANI:G-TiO$_2$ NP coated on ITO acted as working electrode and steel mesh counter electrode in two electrode configuration cell. The cyclic voltammetry (CV) measurements were made at various potential windows to understand the photoelectrochemical catalytic performance of 1:1 PANI:G-TiO$_2$ NP film. Figure 6.9 shows CV study of 1:1 PANI:G-TiO$_2$ NP in the potential range between ±300 mV to ±1500 mV at scan rate of 100 mV/sec. The potential greater than +1000 mV shows polarization effect as shown Figure 6.9. There is insignificant increase in current density after radiating the visible light as shown in Figure 6.10 at potential window ±1000 mV. The photoelectrochemical catalysis has been performed under chronoamperometry test (current vs

93

www.manaraa.com

time at constant voltage application) for an hour in for potential application between +1000 mV to -1000 mV under with and without light.
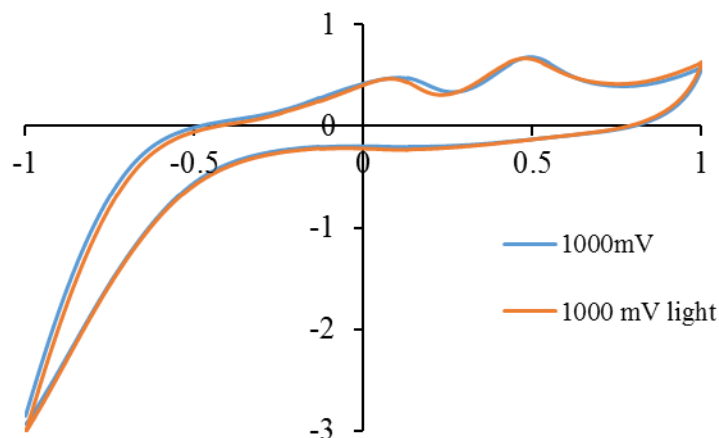
Figure 6.10 Cyclic voltammetry of 1:1 PANI:G-TiO$_2$ NP with 0.01 M HCl as electrolyte with and without shining light.

20 ppm (40ml) of MO in 0.01M HCl was used as pollutant for remediation purpose. Table 6.3 shows the % concentration ratio related to MO remaining in an hour under with and without visible light irradiation at potential between -1000 and +1000 mV. The higher percentage of MO has been remediated under applied potential at +1000mV. So for further study, +1000 mV is applied to correlate with the results of chronoamperometric measurement based on results from table 6.3.

Table 6.3 % Concentration ratio of MO under constant voltage with and without application of light for 1:1 PANI:G-TiO$_2$ NP.

Time (hour)	1000 mV	1000 mV light	- 1000 mV	-1000 mV light
0	100.00	100.00	100.00	100.00
1	91.23	83.55	90.59	84.41

The photoelectrochemical catalytic performance of 1:1 PANI:G-TiO$_2$ NP is studied to compare PANI and 1:1 PANI:G-ZnO NW under with and without light. 0.04 g of nanocomposite photocatalyst were similarly coated onto an ITO substrate, and 20 ppm (40ml) of

94

MO in 0.01M HCl was used as electrolyte in electrochemical studies. Figure 6.11 observes the maximum photoelectrochemical catalytic performance for 1:1 PANI:G-TiO$_2$ NP which shows similar result studied in petri-dish for Figures 6.7 & 6.8. Electrode coated with 1:1 PANI:G-TiO$_2$ NP pertains 31% added remediation effect at +1000 mV with irradiation under visible light. Figure 6.12 shows chronoamperometric data for (a) PANI (b) 1:1 PANI:G-ZnO NW (c) 1:1 PANI:G-TiO$_2$ NP with 20 ppm (40ml) MO in 0.01M HCl. The current density for 1:1 PANI:G-TiO$_2$ NP has been found twice in magnitude after irradiation of light which correlates with the amount of remediated MO in Figure 6.11.
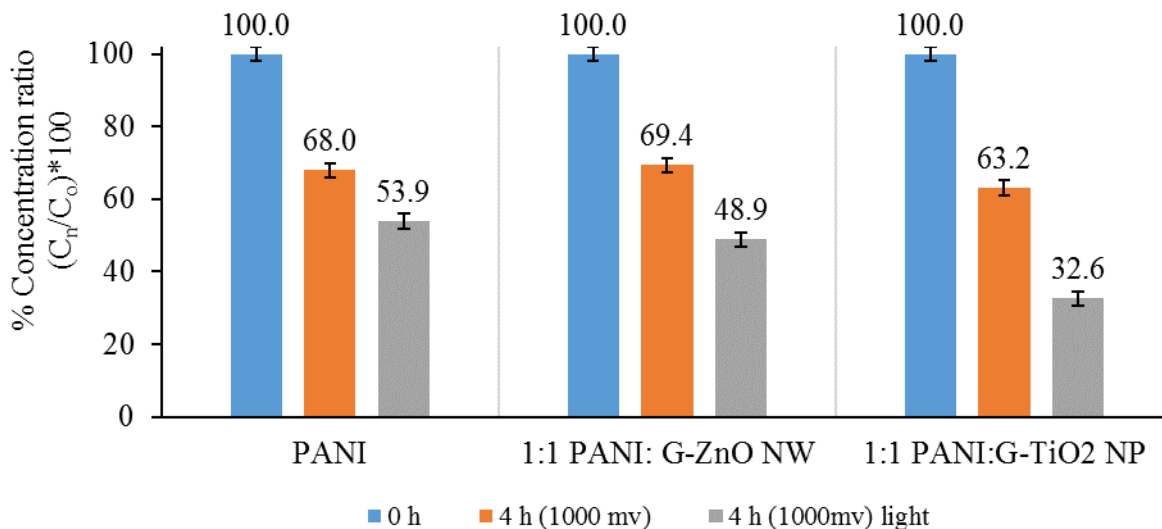
Figure 6.11 Photoelectrochemical catalytic performance of PANI, 1:1 PANI:G-ZnO NW and 1:1 PANI:G-TiO$_2$ NP, with and without light at +1000 mV.

The pH of the electrolyte used in for photoelectrochemical catalytic applications with MO is 2 (0.01M HCl). For practical applications, pH of natural sources i.e., Oceans, rivers and ponds are generally in-between 6.5-8.5 [447, 448]. If natural water sources are contaminated with organic materials, to apply photoelectrochemical catalysis it is important to understand the performance of PANI:PC material performance at pH in-between 6.5-8.5. Three electrolytes with

www.manaraa.com

concentration of pollutant MO at 20 ppm at pH 6.5, pH 7.5, pH 8.5, have been made with $3*10^{-7}$ M of HCl, $3*10^{-7}$ M NaOH, $3*10^{-6}$ M NaOH respectively.
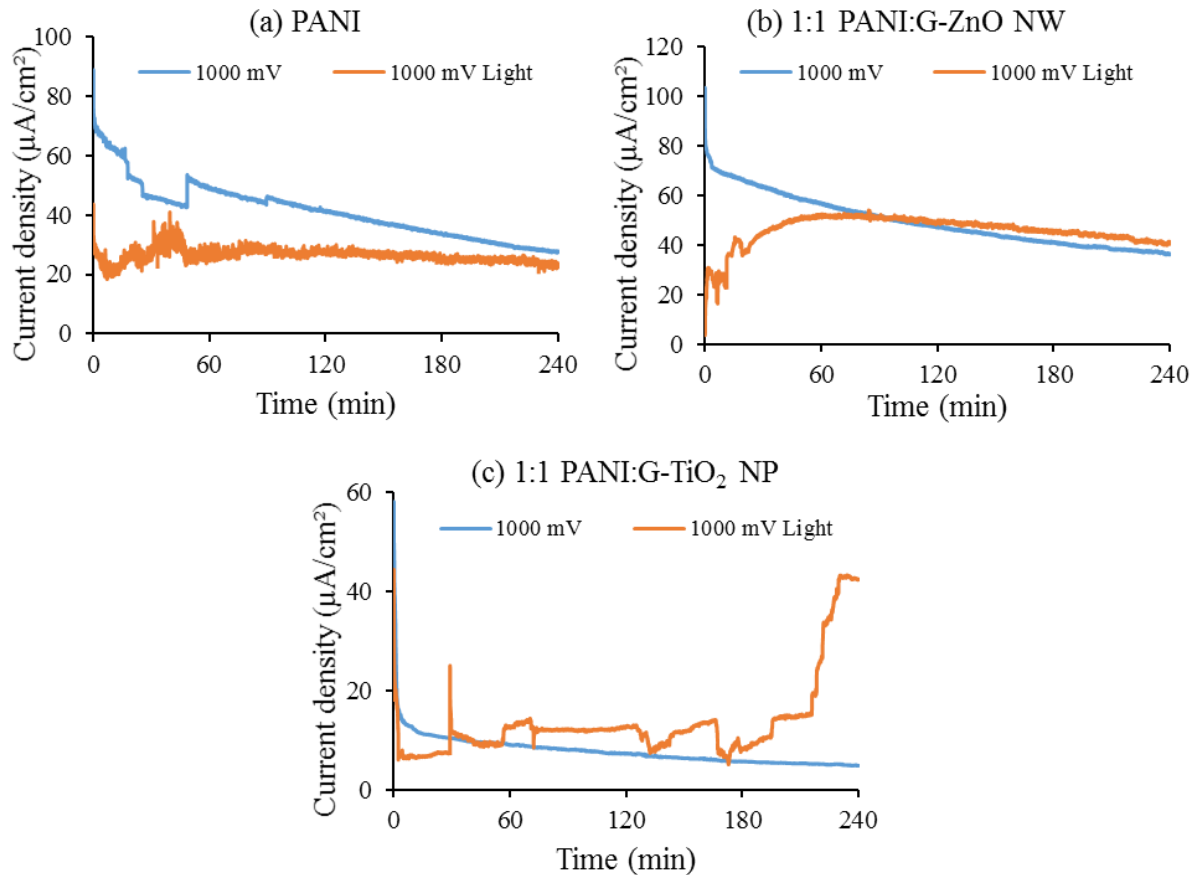
Figure 6.12 Chronoamperometric data (current density vs time) under 1000 mV constant voltage application for 4h for (a) PANI (b) 1:1 PANI:G-ZnO NW (c) 1:1 PANI:G-TiO$_2$ NP.

The photoelectrochemical catalytic performance of 1:1 PANI:G-TiO$_2$ NP is studied to with and without visible light radiation at pH 6.5, pH 7.5, pH 8.5. 0.04 g of nanocomposite photocatalyst were similarly coated onto an ITO substrate, and 20 ppm (40ml) of MO in pH 6.5, pH 7.5, pH 8.5 was used as electrolyte in electrochemical study. Figure 6.13 observes the photoelectrochemical catalytic performance for 1:1 PANI:G-TiO$_2$ NP which shows lower % of remediation of MO at pH 6.5 & pH 7.5 for application of +1000 mV for 4 hours which is due to inefficient electrolyte concentration. At pH 8.5, due to higher concentration of electrolyte there

has been higher % of MO remediation with application of +1000 mV for 4 hours. At all different pH (6.5, 7.5 & 8.5) in Figure 6.13 shows application of light at constant voltage of +1000 mV and higher % of remediated MO. This reveals that 1:1 PANI:G-TiO$_2$ NP can be used as photocatalyst material when the pH is closer to neutral and photoelectrochemical catalytic application when the polluted water has acidic or basic pH.
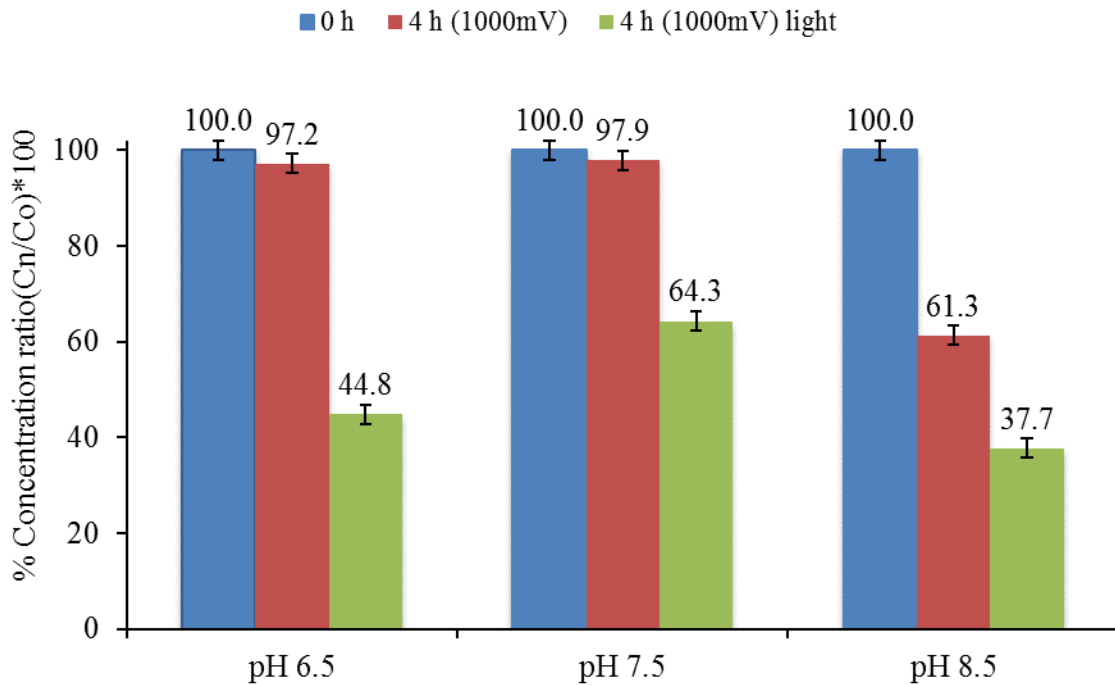
Figure 6.13 Photoelectrochemical catalytic performance of 1:1 PANI:G-TiO$_2$ NP, with and without light at +1000 mV for 20 ppm (40ml) MO in pH 6.5, pH 7.5, pH 8.5.

6.4.1 Reaction Mechanism

The visible light photocatalytic mechanism of PANI:G-TiO$_2$ NP composite is shown in Figure 6.14. Under visible light irradiation in PANI:G-TiO$_2$ NP structure, the presence of PANI shows absorption in the visible light resulting into the electron- hole pair generation due to π (HOMO)-π*(LUMO) transition. The conduction band of G-TiO$_2$ and LUMO orbital in PANI allow the excited electrons from π* (LUMO) orbital which transit into the conduction band of G-TiO$_2$ NP. Further, it reacts with oxygen to yield O$_2^-$ radical which degrades MO. The hole

generated at π (HOMO) orbital in PANI as well as valance band in G-TiO$_2$ NP reacts with water leading to the formation of radical OH$^{.}$, which degrades MO into carbon dioxide (CO$_2$) and water (H$_2$O). The enhancement of photocatalytic of PANI:G-TiO$_2$ NP can be mainly attributes to rapid migration of charge carriers due to the presence of interface between PANI and G-TiO$_2$.
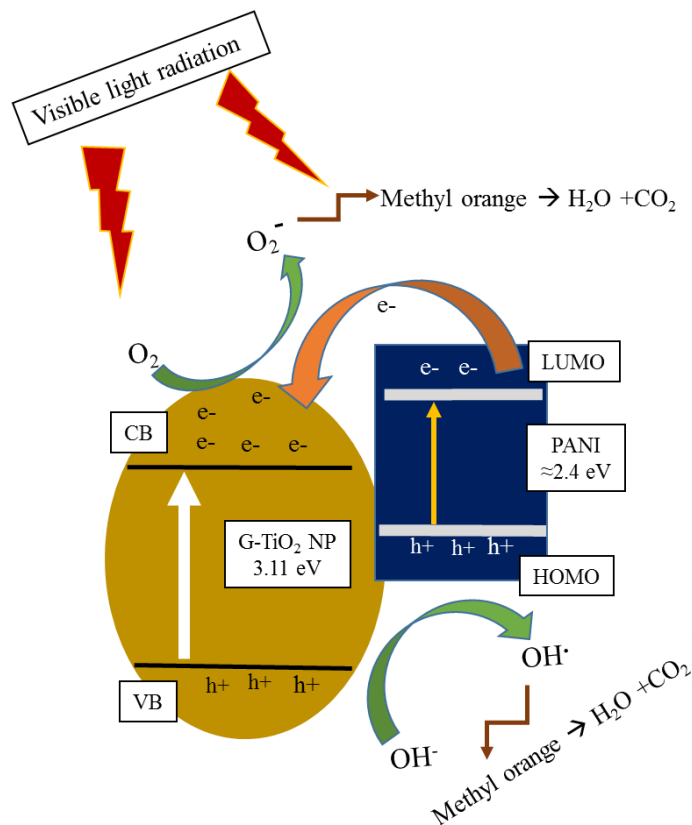
Figure 6.14 Visible light photocatalytic mechanism of PANI:G-TiO$_2$ NP for remediation of methyl orange.

Figure 6.15 shows the schematic of photoelectrochemical catalysis process using PANI:G-TiO$_2$ NP for remediation of MO in acidic or basic medium. ITO glass coated with PANI:G-TiO$_2$ NP when applied with external potential along with irradiation of visible light could observe oxidative and reduction (redox) reactions transpiring into the degradation of MO due to the visible light photonic excitations, but also due to the applied potential, there will be the reduction reactions over counter electrode . If applied potential is greater than 1.2 V, there

will be formation of H_2 near counter electrode or if applied potential is <1.2 V, there will be reduction of oxygen into O_2^- radical, in both cases there is further enhancement of degradation of pollutant as this decreases the photocorrosion in the PANI:G-TiO$_2$ NP nanomaterial.
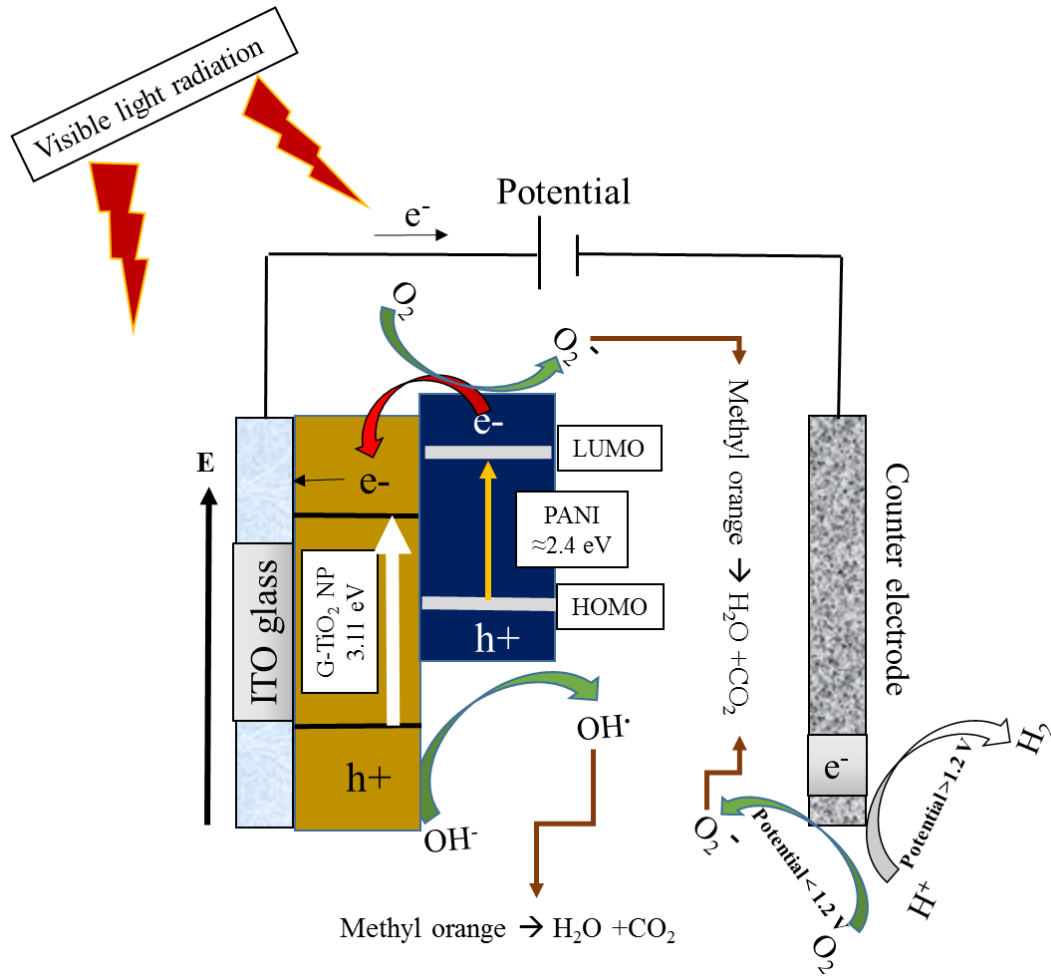
Figure 6.15 Schematic of photoelectrochemical catalysis process using PANI:G-TiO$_2$ NP/ITO glass electrode for remediation of methyl orange.

6.5 Conclusion

The PANI:photocatalyst (PC) nanomaterial was synthesized by oxidative polymerization technique and undoped PANI:PC in NMP solvent was coated on various substrates (ITO coated glass or petri dish). The PANI:PC nanomaterial was used to remediate MO in water. PANI composite with PC (G-TiO$_2$ or G-ZnO) has revealed enhanced photocatalytic performance under

99

visible light. 1:1 PANI:G-TiO$_2$ NP shows improved photocatalytic performance by remediating 100% of MO in nearly 5 h under visible light. The stability of PANI:PC films over petri dich has enabled to use the material for photoelectrochemical catalytic application. 1:1 PANI:G-TiO$_2$ NP shows added 31% remediation of MO in water at potential of +1000 mV. The PANI:PC material could be used for remediation of organics through photoelectrochemical catalytic process which could drastically reduce the cost by not employing a separate photocatalytic reactor setup for house hold as well as industrial applications.

CHAPTER 7: CONCLUSION

The main goals of this dissertation are (1) to enhance the photoactivity of photocatalytic materials under visible spectrum of light, thus enabling it to use natural available energy (solar light) saving huge amount of resources (2) enabling the use of surfactants along with new photocatalyst to further increase the rate of decontamination of organic pollutant (3) to overcome the issues of binder material by introducing conducting polymer into the photocatalyst thus further enabling the material to be used not only for just photocatalytic activity but also for photoelectrochemical catalytic applications in visible spectrum of light have been achieved.

Pristine TiO_2 nanowires have been synthesized through simple hydrothermal technique, where size of TiO_2 nanowires are around 50-500 nm in diameters and 500 nm -3000nm in length which were observed in through SEM. Several doping materials (BN, boric acid, MoS_2, Ag and G) have been introduced onto TiO_2 NW and photocatalytic performance have been observed. G doped TiO_2 NW shows highest photocatalytic activity over other doped TiO_2 NW for remediation of MO from water under visible light radiation. Sol-gel synthesis have been employed to obtain nanoparticle structures of TiO_2 with graphene doping, typically graphene structure is covered by TiO_2 NP with size of nanoparticles observed in-between 20-50 nm. Sol gel G-TiO_2 nanoparticles have superior photocatalytic properties than G-TiO_2 NW (hydrothermal), TiO_2 NW (hydrothermal) and TiO_2 NP (sol-gel) and commercially available P25 under visible light. The photocatalytic remediation of MO has been completed in less than 4 h for G-TiO_2 NP.

101

Various nanostructures of ZnO were synthesized using precipitation and hydrothermal methods. ZnO NP ranging from 40-60 nm in both undoped and doped (G) condition were synthesized using precipitation method where particle size measurement correlates to the size of particles. The use of surfactant 'HMTA' allows to synthesize controlled size ZnO NW based structures for ZnO NW & G-ZnO NW where sizes varied from 50-150 nm in diameter and 800-900 nm in length. The formation of thinner ZnO nanowire with TiO_2 as seeding layer with diameters in-between 40-100 nm and length 400-500 nm are observed. The peaks obtained through XRD correspond to hexagonal ZnO structure with crystallographic (100), (002), (101), (102), (110) and (103) directions. The diffraction peak of G at 26.5^o has been clearly identified for G in the hexagonal ZnO structures, and further confirmed the presence of G using FTIR measurement. The improved photocatalytic activity of G-ZnO NW is mainly due to G doping which decreases the bandgap energy and reveals an increase in the absorbance under visible spectrum of light. The MO remediation in water using G-ZnO NW is understood through band diagram, which divulges the visible light remediation of organic in water.

The G-TiO_2 nanoparticles have been synthesized using sol-gel synthesis process and characterized for mass production. The particle distribution has been studied in water, which shows the agglomeration from 100 nm to 1 µm size particle. G-TiO_2 was able to decontaminate 90% of toluene whereas with naphthalene shows only 50% of reduction and diesel reveals only 40% of reduction from water solution. Naphthalene and diesel insolubility is reason behind the ineffective photocatalytic effect using G-TiO_2 nanomaterial. The mechanism of petroleum-based contaminant has been understood using G-TiO_2 nanocomposite material. Comparison have been made for toluene and naphthalene remediation using different types of TiO_2 synthesized photocatalyst material with G-TiO_2 nanoparticle material. The decontamination depends upon

102

solubility of organics in water or the layer of organics to remain in contact with photocatalysts. Naphthalene as well as diesel are springily soluble in water and do not remain in contact with the G-TiO$_2$ nanomaterials whereas toluene remains in contact with photocatalyst. Due to lower density than water both naphthalene and diesel molecules stay on the surface of water. The insolubility in water as well as no contact with G-TiO$_2$ makes diesel and naphthalene to remediate partially up-to 50% and 40% than their initial values.

Based on understanding the importance of pollutant to remain in contact with photocatalyst material for complete remediation, surfactant (sodium dodecyl sulphonate) has been employed with G-TiO$_2$ nanoparticles to effectively remediate pollutant from water. It can be observed that the despite employing lower weight of 0.2 g G-TiO$_2$ NP for 100 ml of polluted water with surfactant as compared to 1 g of G-TiO$_2$ NP for 250 ml of polluted water without surfactant, the % of naphthalene remediated with surfactant is 98.62 % as compared to 50 % remediated without surfactant for G-TiO$_2$ nanoparticles.

The PANI:photocatalyst (PC) nanomaterial was synthesized by oxidative polymerization technique and undoped PANI:PC in NMP solvent was coated on various substrates (ITO coated glass or petri dish). The PANI:PC nanomaterial was used to remediate MO in water. PANI composite with PC (G-TiO$_2$ or G-ZnO) has shown enhanced photocatalytic performance under visible light. 1:1 PANI:G-TiO$_2$ NP shows improved photocatalytic performance by remediating 100% of MO in nearly 5 h under visible light. Besides, PANI has enabled the photo-catalytic properties due to generation of electron- hole pair under visible light. The stability of PANI:PC films over petri dich has enabled to use the material for photoelectrochemical catalytic application. 1:1 PANI:G-TiO$_2$ NP shows added 31% remediation of MO in water at potential of +1000 mV. The PANI:PC material can be used to remediate organics through

103

photoelectrochemical catalytic process which could drastically reduce the cost by not employing a separate photocatalytic reactor setup for house hold as well as industrial applications.

7.1 Future Work

The photocatalytic study using enhanced photocatalyst (G doped TiO_2 and G doped ZnO) should be employed for air purification application and disinfection of various micro bacterial organisms. Additional study is required for optimization of graphene doping onto metal oxide (TiO_2 and ZnO), surfactant and ratio in-between PANI to metal oxide (TiO_2 and ZnO) employed for remediation of organic pollutants. This optimization process will lead to provide the best experimental conditions. Understanding of colloidal interface science for employment of various organic/bio surfactants and study for investigation of various conducting polymers for photocatalytic and photoelectrochemical catalytic activities for cost effective remediation. Study is needed to perform long-term tests to check reusability and large scale testing using the G doped TiO_2 and G doped ZnO photocatalyst for optimization, scale up and cost effectiveness.

REFERENCES

1. Fujishima, A., *Electrochemical photolysis of water at a semiconductor electrode.* nature, 1972. **238**: p. 37-38.
2. Fujishima, A., K.-i. Honda, and S.-i. Kikuchi, *Photosensitized Electrolytic Oxidation on Semiconducting n-Type TiO₂ Electrode.* The Journal of the Society of Chemical Industry, Japan, 1969. **72**(1): p. 108-113.
3. AGENCY, U.S.E.P., *Municipal Solid Waste*. 2016: EPA Website.
4. Robinson, T., G. McMullan, R. Marchant, and P. Nigam, *Remediation of dyes in textile effluent: a critical review on current treatment technologies with a proposed alternative.* Bioresource Technology, 2001. **77**(3): p. 247-255.
5. Pearce, C.I., J.R. Lloyd, and J.T. Guthrie, *The removal of colour from textile wastewater using whole bacterial cells: a review.* Dyes and Pigments, 2003. **58**(3): p. 179-196.
6. Talarposhti, A.M., T. Donnelly, and G.K. Anderson, *Colour removal from a simulated dye wastewater using a two-phase Anaerobic packed bed reactor.* Water Research, 2001. **35**(2): p. 425-432.
7. Shannon, M.A., P.W. Bohn, M. Elimelech, J.G. Georgiadis, B.J. Mariñas, and A.M. Mayes, *Science and technology for water purification in the coming decades.* nature, 2008. **452**(7185): p. 301-310.
8. Broussard Sr, P.C., *Separation of petroleum oil from contaminated water, trichlorotrifluoroethane absorber.* 1992, Google Patents.
9. *Toxics in the Community, National and Local Perspectives*, in *the 1989 Toxics Release Inventory National Report*, U.S. EPA, Editor. 1991: U.S. Government Printing Office, Washington, DC (1991).
10. Pimentel, D., L. McLaughlin, A. Zepp, B. Lakitan, T. Kraus, P. Kleinman, F. Vancini, W.J. Roach, E. Graap, W.S. Keeton, and G. Selig, *Environmental and Economic Effects of Reducing Pesticide Use.* BioScience, 1991. **41**(6): p. 402-409.
11. Wania, F. and D. MacKay, *Peer Reviewed: Tracking the Distribution of Persistent Organic Pollutants.* Environmental Science & Technology, 1996. **30**(9): p. 390A-396A.
12. Ghoreishi, S.M. and R. Haghighi, *Chemical catalytic reaction and biological oxidation for treatment of non-biodegradable textile effluent.* Chemical Engineering Journal, 2003. **95**(1–3): p. 163-169.
13. Ayed, L., K. Chaieb, A. Cheref, and A. Bakhrouf, *Biodegradation of triphenylmethane dye Malachite Green by Sphingomonas paucimobilis.* World Journal of Microbiology and Biotechnology, 2008. **25**(4): p. 705-711.
14. Andreozzi, R., V. Caprio, A. Insola, and R. Marotta, *Advanced oxidation processes (AOP) for water purification and recovery.* Catalysis Today, 1999. **53**(1): p. 51-59.
15. Cooper, C.M., *Biological Effects of Agriculturally Derived Surface Water Pollutants on Aquatic Systems—A Review.* Journal of Environmental Quality, 1993. **22**(3).

105

16. Davidson, D.A., A.C. Wilkinson, J.M. Blais, L.E. Kimpe, K.M. McDonald, and D.W. Schindler, *Orographic Cold-Trapping of Persistent Organic Pollutants by Vegetation in Mountains of Western Canada.* Environmental Science & Technology, 2003. **37**(2): p. 209-215.

17. Kampa, M. and E. Castanas, *Human health effects of air pollution.* Environmental Pollution, 2008. **151**(2): p. 362-367.

18. Becker, S., S. Mundandhara, R.B. Devlin, and M. Madden, *Regulation of cytokine production in human alveolar macrophages and airway epithelial cells in response to ambient air pollution particles: Further mechanistic studies.* Toxicology and Applied Pharmacology, 2005. **207**(2, Supplement): p. 269-275.

19. Lisk, D.J., *Environmental implications of incineration of municipal solid waste and ash disposal.* Science of the total environment, 1988. **74**: p. 39-66.

20. Giusti, L., *A review of waste management practices and their impact on human health.* Waste Management, 2009. **29**(8): p. 2227-2239.

21. Stoner, G.D., F.B. Daniel, K.M. Schenck, H.A. Schut, P.J. Goldblatt, and D.W. Sandwisch, *Metabolism and DNA binding of benzo [a] pyrene in cultured human bladder and bronchus.* Carcinogenesis, 1982. **3**(2): p. 195-201.

22. Reid, W.D., K.F. Ilett, J.M. Glick, and G. Krishna, *Metabolism and Binding of Aromatic Hydrocarbons in the Lung: Relationship to Experimental Bronchiolar Necrosis 1.* American Review of Respiratory Disease, 1973. **107**(4): p. 539-551.

23. Agency, U.S.E.P., *Table of Regulated Drinking Water Contaminants*, U.S. EPA, Editor.

24. WHO, *WHO guidelines for indoor air quality: selected pollutants*, W.H. Organiazation, Editor. 2010: Europe.

25. EPA, U., *Reducing Risk: Setting Priorities and Strategies for Environmental Protection*, EPA, Editor. 1990, US EPA.

26. Little, J.C., A.T. Hodgson, and A.J. Gadgil, *Modeling emissions of volatile organic compounds from new carpets.* Atmospheric Environment, 1994. **28**(2): p. 227-234.

27. Meininghaus, R., T. Salthammer, and H. Knöppel, *Interaction of volatile organic compounds with indoor materials—a small-scale screening method.* Atmospheric Environment, 1999. **33**(15): p. 2395-2401.

28. Kim, Y.M., S. Harrad, and R.M. Harrison, *Concentrations and sources of VOCs in urban domestic and public microenvironments.* Environmental Science & Technology, 2001. **35**(6): p. 997-1004.

29. Wang, S., H. Ang, and M.O. Tade, *Volatile organic compounds in indoor environment and photocatalytic oxidation: state of the art.* Environment international, 2007. **33**(5): p. 694-705.

30. Auvinen, J. and L. Wirtanen, *The influence of photocatalytic interior paints on indoor air quality.* Atmospheric Environment, 2008. **42**(18): p. 4101-4112.

31. OEHHA. *California's Office of Environmental Health Hazard Assessment*. 2007; Available from: http://www.oehha.ca.gov/air.html.

32. Fisk, W.J. and A.H. Rosenfeld, *Estimates of improved productivity and health from better indoor environments.* Indoor air, 1997. **7**(3): p. 158-172.

33. Khan, F.I. and A.K. Ghoshal, *Removal of volatile organic compounds from polluted air.* Journal of loss prevention in the process industries, 2000. **13**(6): p. 527-545.

34. Khan, F.I. and A. Kr. Ghoshal, *Removal of Volatile Organic Compounds from polluted air.* Journal of loss prevention in the process industries, 2000. **13**(6): p. 527-545.

35. Patkar, A. and J. Laznow, *Hazardous air pollutant control technologies.* Hazmat World, 1992. **2**: p. 78.

36. Laznow, J. and A. Patkar. *The Utilization of Pollution Prevention Programs and Technology for Industrial Growth Environmental Planning Policies in Developing Countries*. in *A AND WMA ANNUAL MEETING*. 1992. AIR & WASTE MANAGEMENT ASSOCIATION.

37. Soccol, C.R., A.L. Woiciechowski, L.P. Vandenberghe, M. Soares, G. Neto, and V. Thomaz-Soccol, *Biofiltration: an emerging technology.* Indian Journal of biotechnology, 2003. **2**(3): p. 396-410.

38. Fulazzaky, M.A., A. Talaiekhozani, M. Ponraj, M. Abd Majid, T. Hadibarata, and A. Goli, *Biofiltration process as an ideal approach to remove pollutants from polluted air.* Desalination and Water Treatment, 2014. **52**(19-21): p. 3600-3615.

39. Majumdar, S., D. Bhaumik, K. Sirkar, and G. Simes, *A pilot-scale demonstration of a membrane-based absorption-stripping process for removal and recovery of volatile organic compounds.* Environmental progress, 2001. **20**(1): p. 27-35.

40. Sacchetti, M., G. Aguzzi, G. Bianchi, and G. Caroprese, *Process for removing and recovering volatile organic substances from industrial waste gases*. 1983, Google Patents.

41. Khaleel, A., P.N. Kapoor, and K.J. Klabunde, *Nanocrystalline metal oxides as new adsorbents for air purification.* Nanostructured Materials, 1999. **11**(4): p. 459-468.

42. Bodzek, M., *Membrane techniques in air cleaning.* Polish Journal of Environmental Studies, 2000. **9**(1): p. 1-12.

43. Freemantle, M., *Membranes for gas separation.* Chem. Eng. News, 2005. **83**(40): p. 3.

44. Greenlee, L.F., D.F. Lawler, B.D. Freeman, B. Marrot, and P. Moulin, *Reverse osmosis desalination: water sources, technology, and today's challenges.* Water Research, 2009. **43**(9): p. 2317-2348.

45. Pérez-González, A., A. Urtiaga, R. Ibáñez, and I. Ortiz, *State of the art and review on the treatment technologies of water reverse osmosis concentrates.* Water Research, 2012. **46**(2): p. 267-283.

46. Fakhru'l-Razi, A., A. Pendashteh, L.C. Abdullah, D.R.A. Biak, S.S. Madaeni, and Z.Z. Abidin, *Review of technologies for oil and gas produced water treatment.* Journal of Hazardous materials, 2009. **170**(2): p. 530-551.

47. Pradeep, T., *Noble metal nanoparticles for water purification: a critical review*. Thin Solid Films, 2009. **517**(24): p. 6441-6478.

48. Dadd, R.C., *Ozone/ultraviolet water purification*. 1980, Google Patents.

49. Leek Jr, K.F., *Domestic grey water purifier using diverter and UV filter treater with preheater*. 1992, Google Patents.

50. Papić, S., N. Koprivanac, A.L. Božić, and A. Meteš, *Removal of some reactive dyes from synthetic wastewater by combined Al (III) coagulation/carbon adsorption process.* Dyes and Pigments, 2004. **62**(3): p. 291-298.

51. Shukla, A., Y.-H. Zhang, P. Dubey, J. Margrave, and S.S. Shukla, *The role of sawdust in the removal of unwanted materials from water.* Journal of Hazardous materials, 2002. **95**(1): p. 137-152.

52. Kurniawan, T.A., G.Y. Chan, W.-H. Lo, and S. Babel, *Physico–chemical treatment techniques for wastewater laden with heavy metals.* Chemical Engineering Journal, 2006. **118**(1): p. 83-98.

107

53. Am Water Works Res, F., B. Langlais, D.A. Reckhow, and D.R. Brink, *Ozone in water treatment: application and engineering*. 1991: CRC press.
54. Glaze, W.H., J.-W. Kang, and D.H. Chapin, *The chemistry of water treatment processes involving ozone, hydrogen peroxide and ultraviolet radiation*. 1987.
55. Gupta, V.K., I. Ali, T.A. Saleh, A. Nayak, and S. Agarwal, *Chemical treatment technologies for waste-water recycling—an overview*. Rsc Advances, 2012. **2**(16): p. 6380-6388.
56. Zularisam, A., A. Ismail, and R. Salim, *Behaviours of natural organic matter in membrane filtration for surface water treatment—a review*. Desalination, 2006. **194**(1): p. 211-231.
57. Hagen, K., *Removal of particles, bacteria and parasites with ultrafiltration for drinking water treatment*. Desalination, 1998. **119**(1): p. 85-91.
58. Simpson, D.R., *Biofilm processes in biologically active carbon water purification*. Water Research, 2008. **42**(12): p. 2839-2848.
59. Wiszniowski, J., D. Robert, J. Surmacz-Gorska, K. Miksch, and J. Weber, *Landfill leachate treatment methods: A review*. Environmental Chemistry Letters, 2006. **4**(1): p. 51-61.
60. Sarria, V., S. Parra, N. Adler, P. Péringer, N. Benitez, and C. Pulgarin, *Recent developments in the coupling of photoassisted and aerobic biological processes for the treatment of biorecalcitrant compounds*. Catalysis Today, 2002. **76**(2): p. 301-315.
61. Carp, O., C.L. Huisman, and A. Reller, *Photoinduced reactivity of titanium dioxide*. Progress in solid state chemistry, 2004. **32**(1): p. 33-177.
62. Schneider, J., M. Matsuoka, M. Takeuchi, J. Zhang, Y. Horiuchi, M. Anpo, and D.W. Bahnemann, *Understanding TiO_2 photocatalysis: mechanisms and materials*. Chemical Reviews, 2014. **114**(19): p. 9919-9986.
63. Hennig, H. and R. Billing, *Advantages and disadvantages of photocatalysis induced by light-sensitive coordination compounds*. Coordination Chemistry Reviews, 1993. **125**(1): p. 89-100.
64. Shon, H., S. Phuntsho, Y. Okour, D. Cho, K. Kim, H. Li, S. Na, J. Kim, and J. Kim, *Visible light responsive titanium dioxide (TiO_2)*. Journal of the Korean Industrial and Engineering Chemistry, 2008.
65. Chong, M.N., B. Jin, C.W. Chow, and C. Saint, *Recent developments in photocatalytic water treatment technology: a review*. Water Research, 2010. **44**(10): p. 2997-3027.
66. Hagfeldt, A. and M. Graetzel, *Light-Induced Redox Reactions in Nanocrystalline Systems*. Chemical Reviews, 1995. **95**(1): p. 49-68.
67. Chatterjee, D. and S. Dasgupta, *Visible light induced photocatalytic degradation of organic pollutants*. Journal of Photochemistry and Photobiology C: Photochemistry Reviews, 2005. **6**(2): p. 186-205.
68. Ibhadon, A.O. and P. Fitzpatrick, *Heterogeneous photocatalysis: recent advances and applications*. Catalysts, 2013. **3**(1): p. 189-218.
69. Doushita, K. and H. Inomata, *Photocatalyst article, anti-fogging, anti-soiling articles, and production method of anti-fogging, anti-soiling articles*. 2003, Google Patents.
70. Erkan, A., U. Bakir, and G. Karakas, *Photocatalytic microbial inactivation over Pd doped SnO_2 and TiO_2 thin films*. Journal of Photochemistry and Photobiology A: Chemistry, 2006. **184**(3): p. 313-321.

71. Bräuer, G. and S. Kondruweit, *Surface and coating technologies*, in *Technology Guide*. 2009, Springer. p. 42-47.

72. Paz, Y., *Application of TiO₂ photocatalysis for air treatment: patents' overview.* Applied Catalysis B: Environmental, 2010. **99**(3): p. 448-460.

73. Kozlova, E.A., P.G. Smirniotis, and A.V. Vorontsov, *Comparative study on photocatalytic oxidation of four organophosphorus simulants of chemical warfare agents in aqueous suspension of titanium dioxide.* Journal of Photochemistry and Photobiology A: Chemistry, 2004. **162**(2): p. 503-511.

74. Kudo, A. and Y. Miseki, *Heterogeneous photocatalyst materials for water splitting.* Chemical Society Reviews, 2009. **38**(1): p. 253-278.

75. Wunderlich, W., T. Oekermann, L. Miao, N. Hue, S. Tanemura, and M. Tanemura, *ELECTRONIC PROPERTIES OF NANO-POROUS TiO₂- AND ZnO THIN FILMS-COMPARISON OF SIMULATIONS AND EXPERIMENTS.* Journal of Ceramic Processing & Research, 2004. **5**(4): p. 343-354.

76. Nolan, N.T., M.K. Seery, and S.C. Pillai, *Spectroscopic Investigation of the Anatase-to-Rutile Transformation of Sol−Gel-Synthesized TiO₂ Photocatalysts.* The Journal of Physical Chemistry C, 2009. **113**(36): p. 16151-16157.

77. Chen, X. and S.S. Mao, *Titanium dioxide nanomaterials: synthesis, properties, modifications, and applications.* Chemical Reviews, 2007. **107**(7): p. 2891-2959.

78. Choi, W., A. Termin, and M.R. Hoffmann, *The role of metal ion dopants in quantum-sized TiO₂: correlation between photoreactivity and charge carrier recombination dynamics.* The Journal of Physical Chemistry, 1994. **98**(51): p. 13669-13679.

79. Liqiang, J., Q. Yichun, W. Baiqi, L. Shudan, J. Baojiang, Y. Libin, F. Wei, F. Honggang, and S. Jiazhong, *Review of photoluminescence performance of nano-sized semiconductor materials and its relationships with photocatalytic activity.* Solar Energy Materials and Solar Cells, 2006. **90**(12): p. 1773-1787.

80. Serpone, N., D. Lawless, R. Khairutdinov, and E. Pelizzetti, *Subnanosecond Relaxation Dynamics in TiO₂ Colloidal Sols (Particle Sizes Rp = 1.0-13.4 nm). Relevance to Heterogeneous Photocatalysis.* The Journal of Physical Chemistry, 1995. **99**(45): p. 16655-16661.

81. Anpo, M. and M. Takeuchi, *The design and development of highly reactive titanium oxide photocatalysts operating under visible light irradiation.* Journal of Catalysis, 2003. **216**(1): p. 505-516.

82. Udom, I., D. Goswami, M. Ram, E. Stefanakos, A. Hepp, M. Kulis, J. McNatt, D. Jaworske, and C. Jones. *Enhanced TiO₂ Photocatalytic Processing of Organic Wastes for Green Space Exploration.* in *51st AIAA Aerospace Sciences Meeting including the New Horizons Forum and Aerospace Exposition*. 2013.

83. Kato, S.-i. and F. Masuo, *Titanium dioxide-photocatalyzed oxidation. I.* Titanium dioxide photocatalyzed liquid phase oxidation of tetralin, Kogyo Kagaku Zasshi, 1964. **67**: p. 1136-1140.

84. McLintock, I.S. and M. Ritchie, *Reactions on titanium dioxide; photo-adsorption and oxidation of ethylene and propylene.* Transactions of the Faraday Society, 1965. **61**: p. 1007-1016.

85. Kamat, P.V., *Photochemistry on nonreactive and reactive (semiconductor) surfaces.* Chemical Reviews, 1993. **93**(1): p. 267-300.

109

86. Mills, A., R.H. Davies, and D. Worsley, *Water purification by semiconductor photocatalysis.* Chem. Soc. Rev., 1993. **22**(6): p. 417-425.
87. Watanabe, T., A. Kitamura, E. Kojima, C. Nakayama, K. Hashimoto, A. Fujishima, D. Ollis, and H. Al-Ekabi, *Photocatalytic purification and treatment of water and air.* Elsevier, Amsterdam, 1993: p. 747.
88. Pichat, P., *Partial or complete heterogeneous photocatalytic oxidation of organic compounds in liquid organic or aqueous phases.* Catalysis Today, 1994. **19**(2): p. 313-333.
89. Hoffmann, M.R., S.T. Martin, W. Choi, and D.W. Bahnemann, *Environmental Applications of Semiconductor Photocatalysis.* Chemical Reviews, 1995. **95**(1): p. 69-96.
90. Mills, A. and S. Le Hunte, *An overview of semiconductor photocatalysis.* Journal of Photochemistry and Photobiology A: Chemistry, 1997. **108**(1): p. 1-35.
91. Sauer, M.L. and D.F. Ollis, *Photocatalyzed oxidation of ethanol and acetaldehyde in humidified air.* Journal of Catalysis, 1996. **158**(2): p. 570-582.
92. Pichat, P., J. Disdier, C. Hoang-Van, D. Mas, G. Goutailler, and C. Gaysse, *Purification/deodorization of indoor air and gaseous effluents by TiO_2 photocatalysis.* Catalysis Today, 2000. **63**(2): p. 363-369.
93. Butterfield, I., P. Christensen, A. Hamnett, K. Shaw, G. Walker, S. Walker, and C. Howarth, *Applied studies on immobilized titanium dioxide films ascatalysts for the photoelectrochemical detoxification of water.* Journal of Applied Electrochemistry, 1997. **27**(4): p. 385-395.
94. Bianco Prevot, A., C. Baiocchi, M.C. Brussino, E. Pramauro, P. Savarino, V. Augugliaro, G. Marci, and L. Palmisano, *Photocatalytic degradation of acid blue 80 in aqueous solutions containing TiO_2 suspensions.* Environmental Science & Technology, 2001. **35**(5): p. 971-976.
95. Comparelli, R., E. Fanizza, M. Curri, P. Cozzoli, G. Mascolo, R. Passino, and A. Agostiano, *Photocatalytic degradation of azo dyes by organic-capped anatase TiO_2 nanocrystals immobilized onto substrates.* Applied Catalysis B: Environmental, 2005. **55**(2): p. 81-91.
96. Wender, H., A.F. Feil, L.B. Diaz, C.S. Ribeiro, G.J. Machado, P. Migowski, D.E. Weibel, J. Dupont, and S.R. Teixeira, *Self-organized TiO_2 nanotube arrays: synthesis by anodization in an ionic liquid and assessment of photocatalytic properties.* ACS applied materials & interfaces, 2011. **3**(4): p. 1359-1365.
97. Mor, G.K., K. Shankar, M. Paulose, O.K. Varghese, and C.A. Grimes, *Use of highly-ordered TiO_2 nanotube arrays in dye-sensitized solar cells.* Nano letters, 2006. **6**(2): p. 215-218.
98. Bach, U., D. Lupo, P. Comte, J. Moser, F. Weissörtel, J. Salbeck, H. Spreitzer, and M. Grätzel, *Solid-state dye-sensitized mesoporous TiO_2 solar cells with high photon-to-electron conversion efficiencies.* nature, 1998. **395**(6702): p. 583-585.
99. O'regan, B. and M. Grfitzeli, *A low-cost, high-efficiency solar cell based on dye-sensitized.* nature, 1991. **353**(6346): p. 737-740.
100. Chiba, Y., A. Islam, Y. Watanabe, R. Komiya, N. Koide, and L. Han, *Dye-sensitized solar cells with conversion efficiency of 11.1%.* Japanese Journal of Applied Physics, 2006. **45**(7L): p. L638.

101. Zhu, Y., J. Shi, Z. Zhang, C. Zhang, and X. Zhang, *Development of a gas sensor utilizing chemiluminescence on nanosized titanium dioxide.* Analytical Chemistry, 2002. **74**(1): p. 120-124.

102. Savage, N., B. Chwieroth, A. Ginwalla, B.R. Patton, S.A. Akbar, and P.K. Dutta, *Composite n–p semiconducting titanium oxides as gas sensors.* Sensors and Actuators B: Chemical, 2001. **79**(1): p. 17-27.

103. Varghese, O.K., D. Gong, M. Paulose, K.G. Ong, and C.A. Grimes, *Hydrogen sensing using titania nanotubes.* Sensors and Actuators B: Chemical, 2003. **93**(1): p. 338-344.

104. Mor, G.K., O.K. Varghese, M. Paulose, K.G. Ong, and C.A. Grimes, *Fabrication of hydrogen sensors with transparent titanium oxide nanotube-array thin films as sensing elements.* Thin Solid Films, 2006. **496**(1): p. 42-48.

105. Khan, S.U., M. Al-Shahry, and W.B. Ingler, *Efficient photochemical water splitting by a chemically modified n-TiO_2.* Science, 2002. **297**(5590): p. 2243-2245.

106. Ni, M., M.K. Leung, D.Y. Leung, and K. Sumathy, *A review and recent developments in photocatalytic water-splitting using TiO_2 for hydrogen production.* Renewable and Sustainable Energy Reviews, 2007. **11**(3): p. 401-425.

107. Anpo, M., H. Yamashita, Y. Ichihashi, and S. Ehara, *Photocatalytic reduction of CO_2 with H_2O on various titanium oxide catalysts.* Journal of Electroanalytical Chemistry, 1995. **396**(1): p. 21-26.

108. Anpo, M. and K. Chiba, *Photocatalytic reduction of CO_2 on anchored titanium oxide catalysts.* Journal of Molecular Catalysis, 1992. **74**(1-3): p. 207-212.

109. Matsunaga, T., R. Tomoda, T. Nakajima, and H. Wake, *Photoelectrochemical sterilization of microbial cells by semiconductor powders.* FEMS Microbiology letters, 1985. **29**(1-2): p. 211-214.

110. Amezaga-Madrid, P., G. Nevarez-Moorillon, E. Orrantia-Borunda, and M. Miki-Yoshida, *Photoinduced bactericidal activity against Pseudomonas aeruginosa by TiO_2 based thin films.* FEMS Microbiology letters, 2002. **211**(2): p. 183-188.

111. Ibáñez, J.A., M.I. Litter, and R.A. Pizarro, *Photocatalytic bactericidal effect of TiO_2 on Enterobacter cloacae: comparative study with other gram (−) bacteria.* Journal of Photochemistry and Photobiology A: Chemistry, 2003. **157**(1): p. 81-85.

112. Melián, J.H., J.D. Rodrıguez, A.V. Suárez, E.T. Rendón, C.V. Do Campo, J. Arana, and J.P. Peña, *The photocatalytic disinfection of urban waste waters.* Chemosphere, 2000. **41**(3): p. 323-327.

113. Kühn, K.P., I.F. Chaberny, K. Massholder, M. Stickler, V.W. Benz, H.-G. Sonntag, and L. Erdinger, *Disinfection of surfaces by photocatalytic oxidation with titanium dioxide and UVA light.* Chemosphere, 2003. **53**(1): p. 71-77.

114. Cornish, B.J., L.A. Lawton, and P.K. Robertson, *Hydrogen peroxide enhanced photocatalytic oxidation of microcystin-LR using titanium dioxide.* Applied Catalysis B: Environmental, 2000. **25**(1): p. 59-67.

115. Weir, A., P. Westerhoff, L. Fabricius, K. Hristovski, and N. von Goetz, *Titanium dioxide nanoparticles in food and personal care products.* Environmental Science & Technology, 2012. **46**(4): p. 2242-2250.

116. Sullivan, W., *Weatherability of titanium-dioxide-containing paints.* Progress in Organic Coatings, 1972. **1**(2): p. 157-203.

117. Matskevich, L. and V. Bazhinov, *Titanium dioxide optical coatings.* Optiko Mekhanicheskaia Promyshlennost, 1977. **44**: p. 41-43.

111

118.   Day, R., *The role of titanium dioxide pigments in the degradation and stabilisation of polymers in the plastics industry.* Polymer Degradation and Stability, 1990. **29**(1): p. 73-92.

119.   Tan, M.H., C.A. Commens, L. Burnett, and P.J. Snitch, *A pilot study on the percutaneous absorption of microfine titanium dioxide from sunscreens.* Australasian Journal of Dermatology, 1996. **37**(4): p. 185-187.

120.   Sadrieh, N., A.M. Wokovich, N.V. Gopee, J. Zheng, D. Haines, D. Parmiter, P.H. Siitonen, C.R. Cozart, A.K. Patri, and S.E. McNeil, *Lack of significant dermal penetration of titanium dioxide (TiO₂) from sunscreen formulations containing nano-and sub-micron-size TiO₂ particles.* Toxicological Sciences, 2010: p. kfq041.

121.   Brunette, D.M., P. Tengvall, M. Textor, and P. Thomsen, *Titanium in medicine: material science, surface science, engineering, biological responses and medical applications*. 2012: Springer Science & Business Media.

122.   Losee, P., F.R. Austin, and B.D. Austin, *Inclusion of tooth whitening oxidation chemistries into a tooth-paste composition*. 1998, Google Patents.

123.   Kamat, P.V., *TiO₂ nanostructures: Recent physical chemistry advances.* The Journal of Physical Chemistry C, 2012. **116**(22): p. 11849-11851.

124.   Mowbray, D., J.I. Martinez, F. Calle-Vallejo, J. Rossmeisl, K.S. Thygesen, K.W. Jacobsen, and J.K. Nørskov, *Trends in metal oxide stability for nanorods, nanotubes, and surfaces.* The Journal of Physical Chemistry C, 2010. **115**(5): p. 2244-2252.

125.   Fang, W.Q., X.-Q. Gong, and H.G. Yang, *On the unusual properties of anatase TiO₂ exposed by highly reactive facets.* The Journal of Physical Chemistry Letters, 2011. **2**(7): p. 725-734.

126.   Yu, J., Y. Hai, and B. Cheng, *Enhanced photocatalytic H₂-production activity of TiO₂ by Ni(OH)₂ cluster modification.* The Journal of Physical Chemistry C, 2011. **115**(11): p. 4953-4958.

127.   Nishijima, Y., K. Ueno, Y. Yokota, K. Murakoshi, and H. Misawa, *Plasmon-assisted photocurrent generation from visible to near-infrared wavelength using a Au-nanorods/TiO₂ electrode.* The Journal of Physical Chemistry Letters, 2010. **1**(13): p. 2031-2036.

128.   Tang, Z.-R., F. Li, Y. Zhang, X. Fu, and Y.-J. Xu, *Composites of titanate nanotube and carbon nanotube as photocatalyst with high mineralization ratio for gas-phase degradation of volatile aromatic pollutant.* The Journal of Physical Chemistry C, 2011. **115**(16): p. 7880-7886.

129.   Ng, Y.H., I.V. Lightcap, K. Goodwin, M. Matsumura, and P.V. Kamat, *To what extent do graphene scaffolds improve the photovoltaic and photocatalytic response of TiO₂ nanostructured films?* The Journal of Physical Chemistry Letters, 2010. **1**(15): p. 2222-2227.

130.   Bell, N.J., Y.H. Ng, A. Du, H. Coster, S.C. Smith, and R. Amal, *Understanding the enhancement in photoelectrochemical properties of photocatalytically prepared TiO₂-reduced graphene oxide composite.* The Journal of Physical Chemistry C, 2011. **115**(13): p. 6004-6009.

131.   Kamat, P.V., *Graphene-based nanoarchitectures. Anchoring semiconductor and metal nanoparticles on a two-dimensional carbon support.* The Journal of Physical Chemistry Letters, 2009. **1**(2): p. 520-527.

132. Asahi, R., T. Morikawa, T. Ohwaki, K. Aoki, and Y. Taga, *Visible-light photocatalysis in nitrogen-doped titanium oxides.* Science, 2001. **293**(5528): p. 269-271.

133. Ihara, T., M. Miyoshi, Y. Iriyama, O. Matsumoto, and S. Sugihara, *Visible-light-active titanium oxide photocatalyst realized by an oxygen-deficient structure and by nitrogen doping.* Applied Catalysis B: Environmental, 2003. **42**(4): p. 403-409.

134. Pillai, S.C., P. Periyat, R. George, D.E. McCormack, M.K. Seery, H. Hayden, J. Colreavy, D. Corr, and S.J. Hinder, *Synthesis of high-temperature stable anatase TiO$_2$ photocatalyst.* The Journal of Physical Chemistry C, 2007. **111**(4): p. 1605-1611.

135. Wang, C.-C. and J.Y. Ying, *Sol-gel synthesis and hydrothermal processing of anatase and rutile titania nanocrystals.* Chemistry of Materials, 1999. **11**(11): p. 3113-3120.

136. Zhao, G., H. Kozuka, and T. Yoko, *Sol—gel preparation and photoelectrochemical properties of TiO$_2$ films containing Au and Ag metal particles.* Thin Solid Films, 1996. **277**(1): p. 147-154.

137. Ansari, S.A., M.M. Khan, M.O. Ansari, and M.H. Cho, *Nitrogen-doped titanium dioxide (N-doped TiO$_2$) for visible light photocatalysis.* New Journal of Chemistry, 2016. **40**(4): p. 3000-3009.

138. Richard, C., F. Bosquet, and J.-F. Pilichowski, *Photocatalytic transformation of aromatic compounds in aqueous zinc oxide suspensions: effect of substrate concentration on the distribution of products.* Journal of Photochemistry and Photobiology A: Chemistry, 1997. **108**(1): p. 45-49.

139. Driessen, M., T. Miller, and V. Grassian, *Photocatalytic oxidation of trichloroethylene on zinc oxide: characterization of surface-bound and gas-phase products and intermediates with FT-IR spectroscopy.* Journal of Molecular Catalysis A: Chemical, 1998. **131**(1): p. 149-156.

140. Villaseñor, J., P. Reyes, and G. Pecchi, *Photodegradation of pentachlorophenol on ZnO.* Journal of chemical technology and biotechnology, 1998. **72**(2): p. 105-110.

141. Yeber, M.C., J. Rodríguez, J. Freer, N. Durán, and H.D. Mansilla, *Photocatalytic degradation of cellulose bleaching effluent by supported TiO$_2$ and ZnO.* Chemosphere, 2000. **41**(8): p. 1193-1197.

142. Yu, J. and X. Yu, *Hydrothermal synthesis and photocatalytic activity of zinc oxide hollow spheres.* Environmental Science & Technology, 2008. **42**(13): p. 4902-4907.

143. Zhang, Y., M.K. Ram, E.K. Stefanakos, and D.Y. Goswami, *Enhanced photocatalytic activity of iron doped zinc oxide nanowires for water decontamination.* Surface and Coatings Technology, 2013. **217**: p. 119-123.

144. Mahato, T., G. Prasad, B. Singh, J. Acharya, A. Srivastava, and R. Vijayaraghavan, *Nanocrystalline zinc oxide for the decontamination of sarin.* Journal of Hazardous materials, 2009. **165**(1): p. 928-932.

145. Sapkota, A., A.J. Anceno, S. Baruah, O.V. Shipin, and J. Dutta, *Zinc oxide nanorod mediated visible light photoinactivation of model microbes in water.* Nanotechnology, 2011. **22**(21): p. 215703.

146. Prasad, G., P. Ramacharyulu, B. Singh, K. Batra, A.R. Srivastava, K. Ganesan, and R. Vijayaraghavan, *Sun light assisted photocatalytic decontamination of sulfur mustard using ZnO nanoparticles.* Journal of Molecular Catalysis A: Chemical, 2011. **349**(1): p. 55-62.

113

147. Abdollahi, Y., A.H. Abdullah, Z. Zainal, and N.A. Yusof, *Photocatalytic degradation of p-Cresol by zinc oxide under UV irradiation.* International journal of molecular sciences, 2011. **13**(1): p. 302-315.

148. Rao, G.D., M. Kaushik, and A. Halve, *An efficient synthesis of naphtha [1, 2-e] oxazinone and 14-substituted-14H-dibenzo [a, j] xanthene derivatives promoted by zinc oxide nanoparticle under thermal and solvent-free conditions.* Tetrahedron Letters, 2012. **53**(22): p. 2741-2744.

149. Lam, S.-M., J.-C. Sin, A.Z. Abdullah, and A.R. Mohamed, *Degradation of wastewaters containing organic dyes photocatalysed by zinc oxide: a review.* Desalination and Water Treatment, 2012. **41**(1-3): p. 131-169.

150. Gaya, U.I., A.H. Abdullah, M.Z. Hussein, and Z. Zainal, *Photocatalytic removal of 2, 4, 6-trichlorophenol from water exploiting commercial ZnO powder.* Desalination, 2010. **263**(1): p. 176-182.

151. Sun, H., X. Feng, S. Wang, H.M. Ang, and M.O. Tadé, *Combination of adsorption, photochemical and photocatalytic degradation of phenol solution over supported zinc oxide: Effects of support and sulphate oxidant.* Chemical Engineering Journal, 2011. **170**(1): p. 270-277.

152. Baruah, S., S. K Pal, and J. Dutta, *Nanostructured zinc oxide for water treatment.* Nanoscience & Nanotechnology-Asia, 2012. **2**(2): p. 90-102.

153. Chan, S.H.S., T. Yeong Wu, J.C. Juan, and C.Y. Teh, *Recent developments of metal oxide semiconductors as photocatalysts in advanced oxidation processes (AOPs) for treatment of dye waste-water.* Journal of chemical technology and biotechnology, 2011. **86**(9): p. 1130-1158.

154. Anju, S., S. Yesodharan, and E. Yesodharan, *Zinc oxide mediated sonophotocatalytic degradation of phenol in water.* Chemical Engineering Journal, 2012. **189**: p. 84-93.

155. Kukreja, L.M., S. Barik, and P. Misra, *Variable band gap ZnO nanostructures grown by pulsed laser deposition.* Journal of Crystal Growth, 2004. **268**(3–4): p. 531-535.

156. Neppolian, B., S. Sakthivel, B. Arabindoo, M. Palanichamy, and V. Murugesan, *Degradation of textile dye by solar light using TiO$_2$ and ZnO photocatalysts.* Journal of Environmental Science & Health Part A, 1999. **34**(9): p. 1829-1838.

157. Zhang, Y., M.K. Ram, E.K. Stefanakos, and D.Y. Goswami, *Synthesis, characterization, and applications of ZnO nanowires.* Journal of Nanomaterials, 2012. **2012**: p. 20.

158. Kansal, S., M. Singh, and D. Sud, *Studies on photodegradation of two commercial dyes in aqueous phase using different photocatalysts.* Journal of Hazardous materials, 2007. **141**(3): p. 581-590.

159. Gouvea, C.A., F. Wypych, S.G. Moraes, N. Duran, N. Nagata, and P. Peralta-Zamora, *Semiconductor-assisted photocatalytic degradation of reactive dyes in aqueous solution.* Chemosphere, 2000. **40**(4): p. 433-440.

160. Khodja, A.A., T. Sehili, J.-F. Pilichowski, and P. Boule, *Photocatalytic degradation of 2-phenylphenol on TiO$_2$ and ZnO in aqueous suspensions.* Journal of Photochemistry and Photobiology A: Chemistry, 2001. **141**(2): p. 231-239.

161. Sakthivel, S., B. Neppolian, M. Shankar, B. Arabindoo, M. Palanichamy, and V. Murugesan, *Solar photocatalytic degradation of azo dye: comparison of photocatalytic efficiency of ZnO and TiO$_2$.* Solar Energy Materials and Solar Cells, 2003. **77**(1): p. 65-82.

114

162. Sobana, N. and M. Swaminathan, *The effect of operational parameters on the photocatalytic degradation of acid red 18 by ZnO.* Separation and Purification Technology, 2007. **56**(1): p. 101-107.

163. Dindar, B. and S. Içli, *Unusual photoreactivity of zinc oxide irradiated by concentrated sunlight.* Journal of Photochemistry and Photobiology A: Chemistry, 2001. **140**(3): p. 263-268.

164. Van Dijken, A., A. Janssen, M. Smitsmans, D. Vanmaekelbergh, and A. Meijerink, *Size-selective photoetching of nanocrystalline semiconductor particles.* Chemistry of Materials, 1998. **10**(11): p. 3513-3522.

165. Yamaguchi, Y., M. Yamazaki, S. Yoshihara, and T. Shirakashi, *Photocatalytic ZnO films prepared by anodizing.* Journal of Electroanalytical Chemistry, 1998. **442**(1): p. 1-3.

166. Wang, T., Z. Jiao, T. Chen, Y. Li, W. Ren, S. Lin, G. Lu, J. Ye, and Y. Bi, *Vertically aligned ZnO nanowire arrays tip-grafted with silver nanoparticles for photoelectrochemical applications.* Nanoscale, 2013. **5**(16): p. 7552-7557.

167. Udom, I., Y. Zhang, M.K. Ram, E.K. Stefanakos, A.F. Hepp, R. Elzein, R. Schlaf, and D.Y. Goswami, *A simple photolytic reactor employing Ag-doped ZnO nanowires for water purification.* Thin Solid Films, 2014. **564**: p. 258-263.

168. Hosono, E., S. Fujihara, I. Honma, and H. Zhou, *The fabrication of an upright-standing zinc oxide nanosheet for use in dye-sensitized solar cells.* Advanced Materials, 2005. **17**(17): p. 2091-2094.

169. Du Pasquier, A., H. Chen, and Y. Lu, *Dye sensitized solar cells using well-aligned zinc oxide nanotip arrays.* Applied physics letters, 2006. **89**(25): p. 253513.

170. Tennakone, K., V. Perera, I. Kottegoda, and G. Kumara, *Dye-sensitized solid state photovoltaic cell based on composite zinc oxide/tin (IV) oxide films.* Journal of Physics D: Applied Physics, 1999. **32**(4): p. 374.

171. Lupan, O., S. Shishiyanu, L. Chow, and T. Shishiyanu, *Nanostructured zinc oxide gas sensors by successive ionic layer adsorption and reaction method and rapid photothermal processing.* Thin Solid Films, 2008. **516**(10): p. 3338-3345.

172. Nanto, H., T. Minami, and S. Takata, *Zinc-oxide thin-film ammonia gas sensors with high sensitivity and excellent selectivity.* Journal of Applied Physics, 1986. **60**(2): p. 482-484.

173. Steinfeld, A., *Solar hydrogen production via a two-step water-splitting thermochemical cycle based on Zn/ZnO redox reactions.* International Journal of Hydrogen Energy, 2002. **27**(6): p. 611-619.

174. Sahoo, S., M. Maiti, A. Ganguly, J. Jacob George, and A.K. Bhowmick, *Effect of zinc oxide nanoparticles as cure activator on the properties of natural rubber and nitrile rubber.* Journal of applied polymer science, 2007. **105**(4): p. 2407-2415.

175. Ibarra, L., A. Marcos-Fernandez, and M. Alzorriz, *Mechanistic approach to the curing of carboxylated nitrile rubber (XNBR) by zinc peroxide/zinc oxide.* Polymer, 2002. **43**(5): p. 1649-1655.

176. Wong, J., *Zinc oxide ceramic*. 1977, Google Patents.

177. Gupta, T.K., *Application of zinc oxide varistors.* Journal of the American Ceramic Society, 1990. **73**(7): p. 1817-1840.

178. Kachynski, A.V., A.N. Kuzmin, M. Nyk, I. Roy, and P.N. Prasad, *Zinc oxide nanocrystals for nonresonant nonlinear optical microscopy in biology and medicine.* The Journal of Physical Chemistry C, 2008. **112**(29): p. 10721-10724.

179.   Kuschner, W.G., A. D'Alessandro, H. Wong, and P.D. Blanc, *Early pulmonary cytokine responses to zinc oxide fume inhalation.* Environmental research, 1997. **75**(1): p. 7-11.
180.   Bates, J.W.W. and I.C.H. Keith, *Tobacco smoke filter*. 1966, Google Patents.
181.   Espitia, P.J.P., N.d.F.F. Soares, J.S. dos Reis Coimbra, N.J. de Andrade, R.S. Cruz, and E.A.A. Medeiros, *Zinc oxide nanoparticles: synthesis, antimicrobial activity and food packaging applications.* Food and Bioprocess Technology, 2012. **5**(5): p. 1447-1464.
182.   Johnson, J.A., J.J. Heidenreich, R.A. Mantz, P.M. Baker, and M.S. Donley, *A multiple-scattering model analysis of zinc oxide pigment for spacecraft thermal control coatings.* Progress in Organic Coatings, 2003. **47**(3): p. 432-442.
183.   Lansdown, A. and A. Taylor, *Zinc and titanium oxides: promising UV‑absorbers but what influence do they have on the intact skin?* International journal of cosmetic science, 1997. **19**(4): p. 167-172.
184.   Jagtap, R., P. Patil, and S. Hassan, *Effect of zinc oxide in combating corrosion in zinc-rich primer.* Progress in Organic Coatings, 2008. **63**(4): p. 389-394.
185.   Wang, Z.L. and J. Song, *Piezoelectric nanogenerators based on zinc oxide nanowire arrays.* Science, 2006. **312**(5771): p. 242-246.
186.   Liqiang, J., W. Dejun, W. Baiqi, L. Shudan, X. Baifu, F. Honggang, and S. Jiazhong, *Effects of noble metal modification on surface oxygen composition, charge separation and photocatalytic activity of ZnO nanoparticles.* Journal of Molecular Catalysis A: Chemical, 2006. **244**(1): p. 193-200.
187.   Stroyuk, A., V. Shvalagin, and S.Y. Kuchmii, *Photochemical synthesis and optical properties of binary and ternary metal–semiconductor composites based on zinc oxide nanoparticles.* Journal of Photochemistry and Photobiology A: Chemistry, 2005. **173**(2): p. 185-194.
188.   Shaporev, A., V. Ivanov, A. Baranchikov, and Y.D. Tret'yakov, *Hydrothermal synthesis and photocatalytic activity of highly dispersed ZnO powders.* Russian journal of inorganic chemistry, 2006. **51**(10): p. 1523-1527.
189.   Xu, F., Z.-Y. Yuan, G.-H. Du, M. Halasa, and B.-L. Su, *High-yield synthesis of single-crystalline ZnO hexagonal nanoplates and accounts of their optical and photocatalytic properties.* Applied Physics A, 2007. **86**(2): p. 181-185.
190.   Akhavan, O., M. Mehrabian, K. Mirabbaszadeh, and R. Azimirad, *Hydrothermal synthesis of ZnO nanorod arrays for photocatalytic inactivation of bacteria.* Journal of Physics D: Applied Physics, 2009. **42**(22): p. 225305.
191.   Zuo, A., P. Hu, L. Bai, and F. Yuan, *Synthesis of tunable 3D ZnO architectures assemblied with nanoplates.* Crystal Research and Technology, 2009. **44**(6): p. 613-618.
192.   Wang, D., Y. Zhao, and C. Song, *Synthesis and properties of cuboid-shaped ZnO hierarchical structures.* Solid State Sciences, 2010. **12**(5): p. 776-782.
193.   Ladanov, M., P. Algarin-Amaris, G. Matthews, M. Ram, S. Thomas, A. Kumar, and J. Wang, *Microfluidic hydrothermal growth of ZnO nanowires over high aspect ratio microstructures.* Nanotechnology, 2013. **24**(37): p. 375301.
194.   Ladanov, M., P.C.A. Amaris, G. Matthews, M.K. Ram, S.W. Thomas, A. Kumar, J. Wang, and A. Takshi, *Microstructured crystalline device in confined space, a dye-sensitized solar cell, and method of preparation thereof.* 2013, Google Patents.
195.   Santato, C., M. Odziemkowski, M. Ulmann, and J. Augustynski, *Crystallographically Oriented Mesoporous WO₃ Films: Synthesis, Characterization, and Applications.* Journal of the American Chemical Society, 2001. **123**(43): p. 10639-10649.

116

196. Granqvist, C.G., *Electrochromic tungsten oxide films: review of progress 1993–1998.* Solar Energy Materials and Solar Cells, 2000. **60**(3): p. 201-262.

197. Baeck, S.H., K.S. Choi, T.F. Jaramillo, G.D. Stucky, and E.W. McFarland, *Enhancement of photocatalytic and electrochromic properties of electrochemically fabricated mesoporous WO₃ thin films.* Advanced Materials, 2003. **15**(15): p. 1269-1273.

198. Solis, J., S. Saukko, L. Kish, C. Granqvist, and V. Lantto, *Semiconductor gas sensors based on nanostructured tungsten oxide.* Thin Solid Films, 2001. **391**(2): p. 255-260.

199. Qu, W. and W. Wlodarski, *A thin-film sensing element for ozone, humidity and temperature.* Sensors and Actuators B: Chemical, 2000. **64**(1): p. 42-48.

200. Li, Y., Y. Bando, and D. Golberg, *Quasi-Aligned Single-Crystalline W₁₈O₄₉ Nanotubes and Nanowires.* Advanced Materials, 2003. **15**(15): p. 1294-1296.

201. Bechinger, C., M. Burdis, and J.-G. Zhang, *Comparison between electrochromic and photochromic coloration efficiency of tungsten oxide thin films.* Solid state communications, 1997. **101**(10): p. 753-756.

202. Svensson, J. and C. Granqvist, *Electrochromic tungsten oxide films for energy efficient windows.* Solar energy materials, 1984. **11**(1): p. 29-34.

203. Avendano, E., L. Berggren, G.A. Niklasson, C.G. Granqvist, and A. Azens, *Electrochromic materials and devices: Brief survey and new data on optical absorption in tungsten oxide and nickel oxide films.* Thin Solid Films, 2006. **496**(1): p. 30-36.

204. Livage, J. and G. Guzman, *Aqueous precursors for electrochromic tungsten oxide hydrates.* Solid State Ionics, 1996. **84**(3): p. 205-211.

205. Subrahmanyam, A. and A. Karuppasamy, *Optical and electrochromic properties of oxygen sputtered tungsten oxide (WO₃) thin films.* Solar Energy Materials and Solar Cells, 2007. **91**(4): p. 266-274.

206. Jelle, B. and G. Hagen, *Transmission spectra of an electrochromic window based on polyaniline, prussian blue and tungsten oxide.* Journal of the Electrochemical Society, 1993. **140**(12): p. 3560-3564.

207. Granqvist, C.G., *Electrochromic materials: Microstructure, electronic bands, and optical properties.* Applied Physics A. **57**(1): p. 3-12.

208. Bamwenda, G.R. and H. Arakawa, *The visible light induced photocatalytic activity of tungsten trioxide powders.* Applied Catalysis A: General, 2001. **210**(1–2): p. 181-191.

209. Le Bellac, D., A. Azens, and C. Granqvist, *Angular selective transmittance through electrochromic tungsten oxide films made by oblique angle sputtering.* Applied physics letters, 1995. **66**(14): p. 1715-1716.

210. Zheng, H., J.Z. Ou, M.S. Strano, R.B. Kaner, A. Mitchell, and K. Kalantar-zadeh, *Nanostructured tungsten oxide–properties, synthesis, and applications.* Advanced Functional Materials, 2011. **21**(12): p. 2175-2196.

211. Tao, C., S. Ruan, G. Xie, X. Kong, L. Shen, F. Meng, C. Liu, X. Zhang, W. Dong, and W. Chen, *Role of tungsten oxide in inverted polymer solar cells.* Applied physics letters, 2009. **94**(4): p. 043311-1-043311-3.

212. Han, S., W.S. Shin, M. Seo, D. Gupta, S.-J. Moon, and S. Yoo, *Improving performance of organic solar cells using amorphous tungsten oxides as an interfacial buffer layer on transparent anodes.* Organic Electronics, 2009. **10**(5): p. 791-797.

213. Lethy, K., D. Beena, V. Mahadevan Pillai, and V. Ganesan, *Bandgap renormalization in titania modified nanostructured tungsten oxide thin films prepared by pulsed laser deposition technique for solar cell applications.* Journal of Applied Physics, 2008. **104**(3): p. 3515.

214. Tan, Z.a., L. Li, C. Cui, Y. Ding, Q. Xu, S. Li, D. Qian, and Y. Li, *Solution-processed tungsten oxide as an effective anode buffer layer for high-performance polymer solar cells.* The Journal of Physical Chemistry C, 2012. **116**(35): p. 18626-18632.

215. Zhao, Z.G. and M. Miyauchi, *Nanoporous-Walled Tungsten Oxide Nanotubes as Highly Active Visible-Light-Driven Photocatalysts.* Angewandte Chemie, 2008. **120**(37): p. 7159-7163.

216. Nemoto, Y., S. Shigeta, and Y. Yokokawa, *Optical recording medium.* 1985, Google Patents.

217. Aoki, T., T. Matsushita, A. Suzuki, K. Tanabe, and M. Okuda, *Write-once optical recording using WO_2 films prepared by pulsed laser deposition.* Thin Solid Films, 2006. **509**(1): p. 107-112.

218. Maekawa, T., J. Tamaki, N. Miura, and N. Yamazoe, *Gold-Loaded Tungsten Oxide Sensor for Detection of Ammonia in Air.* Chemistry Letters, 1992(4): p. 639-642.

219. Polleux, J., A. Gurlo, N. Barsan, U. Weimar, M. Antonietti, and M. Niederberger, *Template-Free Synthesis and Assembly of Single-Crystalline Tungsten Oxide Nanowires and their Gas-Sensing Properties.* Angewandte Chemie, 2006. **118**(2): p. 267-271.

220. Ponzoni, A., E. Comini, G. Sberveglieri, J. Zhou, S.Z. Deng, N.S. Xu, Y. Ding, and Z.L. Wang, *Ultrasensitive and highly selective gas sensors using three-dimensional tungsten oxide nanowire networks.* Applied physics letters, 2006. **88**(20): p. 203101.

221. Kim, Y.S., S.-C. Ha, K. Kim, H. Yang, S.-Y. Choi, Y.T. Kim, J.T. Park, C.H. Lee, J. Choi, and J. Paek, *Room-temperature semiconductor gas sensor based on nonstoichiometric tungsten oxide nanorod film.* Applied physics letters, 2005. **86**(21): p. 3105.

222. Akiyama, M., J. Tamaki, N. Miura, and N. Yamazoe, *Tungsten Oxide-Based Semiconductor Sensor Highly Sensitive to NO and NO_2.* Chemistry Letters, 1991(9): p. 1611-1614.

223. Sekimoto, S., H. Nakagawa, S. Okazaki, K. Fukuda, S. Asakura, T. Shigemori, and S. Takahashi, *A fiber-optic evanescent-wave hydrogen gas sensor using palladium-supported tungsten oxide.* Sensors and Actuators B: Chemical, 2000. **66**(1): p. 142-145.

224. Rout, C.S., M. Hegde, and C. Rao, *H_2S sensors based on tungsten oxide nanostructures.* Sensors and Actuators B: Chemical, 2008. **128**(2): p. 488-493.

225. Tamaki, J., Z. Zhang, K. Fujimori, M. Akiyama, T. Harada, N. Miura, and N. Yamazoe, *Grain-size effects in tungsten oxide-based sensor for nitrogen oxides.* Journal of the Electrochemical Society, 1994. **141**(8): p. 2207-2210.

226. Zhou, J., L. Gong, S.Z. Deng, J. Chen, J.C. She, N.S. Xu, R. Yang, and Z.L. Wang, *Growth and field-emission property of tungsten oxide nanotip arrays.* Applied physics letters, 2005. **87**(22): p. 223108.

227. Liu, J., Z. Zhang, Y. Zhao, X. Su, S. Liu, and E. Wang, *Tuning the Field-Emission Properties of Tungsten Oxide Nanorods.* Small, 2005. **1**(3): p. 310-313.

228. Chang, M.T., L.J. Chou, Y.L. Chueh, Y.C. Lee, C.H. Hsieh, C.D. Chen, Y.W. Lan, and L.J. Chen, *Nitrogen-Doped Tungsten Oxide Nanowires: Low-Temperature Synthesis on Si, and Electrical, Optical, and Field-Emission Properties.* Small, 2007. **3**(4): p. 658-664.

118

229. Seelaboyina, R., J. Huang, J. Park, D.H. Kang, and W.B. Choi, *Multistage field enhancement of tungsten oxide nanowires and its field emission in various vacuum conditions.* Nanotechnology, 2006. **17**(19): p. 4840.

230. Sayama, K., K. Mukasa, R. Abe, Y. Abe, and H. Arakawa, *Stoichiometric water splitting into H_2 and O_2 using a mixture of two different photocatalysts and an $IO_3{-}/I{-}$ shuttle redox mediator under visible light irradiation.* Chemical Communications, 2001(23): p. 2416-2417.

231. Zhang, L., Y. Li, Q. Zhang, and H. Wang, *Hierarchical nanostructure of WO_3 nanorods on TiO_2 nanofibers and the enhanced visible light photocatalytic activity for degradation of organic pollutants.* CrystEngComm, 2013. **15**(30): p. 5986-5993.

232. Hwang, D.W., J. Kim, T.J. Park, and J.S. Lee, *Mg-Doped WO_3 as a Novel Photocatalyst for Visible Light-Induced Water Splitting.* Catalysis Letters. **80**(1): p. 53-57.

233. Hameed, A., M.A. Gondal, and Z.H. Yamani, *Effect of transition metal doping on photocatalytic activity of WO_3 for water splitting under laser illumination: role of 3d-orbitals.* Catalysis Communications, 2004. **5**(11): p. 715-719.

234. Tang, J. and J. Ye, *Correlation of crystal structures and electronic structures and photocatalytic properties of the W-containing oxides.* Journal of Materials Chemistry, 2005. **15**(39): p. 4246-4251.

235. Xiang, Q., G.F. Meng, H.B. Zhao, Y. Zhang, H. Li, W.J. Ma, and J.Q. Xu, *Au Nanoparticle Modified WO_3 Nanorods with Their Enhanced Properties for Photocatalysis and Gas Sensing.* The Journal of Physical Chemistry C, 2010. **114**(5): p. 2049-2055.

236. Bhowmik, R. and A. Saravanan, *Surface magnetism, Morin transition, and magnetic dynamics in antiferromagnetic α-Fe_2O_3 (hematite) nanograins.* Journal of Applied Physics, 2010. **107**(5): p. 053916.

237. Lin, S., *Magnetic properties of hematite single crystals. I. Magnetization isotherms, antiferromagnetic susceptibility, and weak ferromagnetism of a natural crystal.* Physical Review, 1959. **116**(6): p. 1447.

238. Prior, D.J., P.W. Trimby, U.D. Weber, and D.J. Dingley, *Orientation contrast imaging of microstructures in rocks using forescatter detectors in the scanning electron microscope.* Mineralogical Magazine, 1996. **60**(6): p. 859-869.

239. Laurent, S., A.A. Saei, S. Behzadi, A. Panahifar, and M. Mahmoudi, *Superparamagnetic iron oxide nanoparticles for delivery of therapeutic agents: opportunities and challenges.* Expert opinion on drug delivery, 2014. **11**(9): p. 1449-1470.

240. Gou, X., G. Wang, J. Park, H. Liu, and J. Yang, *Monodisperse hematite porous nanospheres: synthesis, characterization, and applications for gas sensors.* Nanotechnology, 2008. **19**(12): p. 125606.

241. Fang, X.-L., C. Chen, M.-S. Jin, Q. Kuang, Z.-X. Xie, S.-Y. Xie, R.-B. Huang, and L.-S. Zheng, *Single-crystal-like hematite colloidal nanocrystal clusters: synthesis and applications in gas sensors, photocatalysis and water treatment.* Journal of Materials Chemistry, 2009. **19**(34): p. 6154-6160.

242. Gou, X., G. Wang, X. Kong, D. Wexler, J. Horvat, J. Yang, and J. Park, *Flutelike Porous Hematite Nanorods and Branched Nanostructures: Synthesis, Characterisation and Application for Gas-Sensing.* Chemistry–A European Journal, 2008. **14**(19): p. 5996-6002.

119

243. Chen, J., L. Xu, W. Li, and X.-l. Gou, *α-Fe₂O₃ nanotubes in gas sensor and lithium-ion battery applications.* Advanced Materials, 2005. **17**(5): p. 582-586.

244. Wu, Z., K. Yu, S. Zhang, and Y. Xie, *Hematite hollow spheres with a mesoporous shell: controlled synthesis and applications in gas sensor and lithium ion batteries.* The Journal of Physical Chemistry C, 2008. **112**(30): p. 11307-11313.

245. Meng, F., J. Li, S.K. Cushing, J. Bright, M. Zhi, J.D. Rowley, Z. Hong, A. Manivannan, A.D. Bristow, and N. Wu, *Photocatalytic water oxidation by hematite/reduced graphene oxide composites.* ACS Catalysis, 2013. **3**(4): p. 746-751.

246. Chen, Y.-H. and F.-A. Li, *Kinetic study on removal of copper (II) using goethite and hematite nano-photocatalysts.* Journal of Colloid and Interface Science, 2010. **347**(2): p. 277-281.

247. Tong, G., J. Guan, and Q. Zhang, *Goethite hierarchical nanostructures: Glucose-assisted synthesis, chemical conversion into hematite with excellent photocatalytic properties.* Materials Chemistry and Physics, 2011. **127**(1): p. 371-378.

248. Young, K.M., B.M. Klahr, O. Zandi, and T.W. Hamann, *Photocatalytic water oxidation with hematite electrodes.* Catalysis Science & Technology, 2013. **3**(7): p. 1660-1671.

249. Batzill, M. and U. Diebold, *The surface and materials science of tin oxide.* Progress in surface science, 2005. **79**(2): p. 47-154.

250. Park, Y., V. Choong, Y. Gao, B.R. Hsieh, and C.W. Tang, *Work function of indium tin oxide transparent conductor measured by photoelectron spectroscopy.* Applied physics letters, 1996. **68**(19): p. 2699-2701.

251. Ishibashi, S., Y. Higuchi, Y. Ota, and K. Nakamura, *Low resistivity indium–tin oxide transparent conductive films. II. Effect of sputtering voltage on electrical property of films.* Journal of Vacuum Science & Technology A, 1990. **8**(3): p. 1403-1406.

252. Ohta, H., M. Orita, M. Hirano, H. Tanji, H. Kawazoe, and H. Hosono, *Highly electrically conductive indium–tin–oxide thin films epitaxially grown on yttria-stabilized zirconia (100) by pulsed-laser deposition.* Applied physics letters, 2000. **76**(19): p. 2740-2742.

253. Jones, C.A., J.J. Leonard, and J.A. Sofranko, *Tin oxide catalyst*. 1984, Google Patents.

254. Jinkawa, T., G. Sakai, J. Tamaki, N. Miura, and N. Yamazoe, *Relationship between ethanol gas sensitivity and surface catalytic property of tin oxide sensors modified with acidic or basic oxides.* Journal of Molecular Catalysis A: Chemical, 2000. **155**(1): p. 193-200.

255. Furuta, S., H. Matsuhashi, and K. Arata, *Catalytic action of sulfated tin oxide for etherification and esterification in comparison with sulfated zirconia.* Applied Catalysis A: General, 2004. **269**(1): p. 187-191.

256. Coles, G.S., G. Williams, and B.M. Smith, *Tin oxide gas sensors*. 1995, Google Patents.

257. Watson, J., *The tin oxide gas sensor and its applications.* Sensors and Actuators, 1984. **5**(1): p. 29-42.

258. Suehle, J.S., R.E. Cavicchi, M. Gaitan, and S. Semancik, *Tin oxide gas sensor fabricated using CMOS micro-hotplates and in-situ processing.* IEEE Electron Device Letters, 1993. **14**(3): p. 118-120.

259. Wlodek, S., K. Colbow, and F. Consadori, *Signal-shape analysis of a thermally cycled tin-oxide gas sensor.* Sensors and Actuators B: Chemical, 1991. **3**(1): p. 63-68.

260. Wang, G., W. Lu, J. Li, J. Choi, Y. Jeong, S.Y. Choi, J.B. Park, M.K. Ryu, and K. Lee, *V-Shaped Tin Oxide Nanostructures Featuring a Broad Photocurrent Signal: An Effective Visible-Light-Driven Photocatalyst.* Small, 2006. **2**(12): p. 1436-1439.

261. Habibi, M.H. and N. Talebian, *Photocatalytic degradation of an azo dye X₆G in water: a comparative study using nanostructured indium tin oxide and titanium oxide thin films.* Dyes and Pigments, 2007. **73**(2): p. 186-194.

262. Dholam, R., N. Patel, A. Santini, and A. Miotello, *Efficient indium tin oxide/Cr-doped-TiO₂ multilayer thin films for H₂ production by photocatalytic water-splitting.* International Journal of Hydrogen Energy, 2010. **35**(18): p. 9581-9590.

263. Dholam, R., N. Patel, and A. Miotello, *Efficient H₂ production by water-splitting using indium–tin-oxide/V-doped TiO₂ multilayer thin film photocatalyst.* International Journal of Hydrogen Energy, 2011. **36**(11): p. 6519-6528.

264. Vinodgopal, K. and P.V. Kamat, *Enhanced rates of photocatalytic degradation of an azo dye using SnO₂/TiO₂ coupled semiconductor thin films.* Environmental Science & Technology, 1995. **29**(3): p. 841-845.

265. Tennakone, K. and J. Bandara, *Photocatalytic activity of dye-sensitized tin (IV) oxide nanocrystalline particles attached to zinc oxide particles: long distance electron transfer via ballistic transport of electrons across nanocrystallites.* Applied Catalysis A: General, 2001. **208**(1): p. 335-341.

266. Lin, J., C.Y. Jimmy, D. Lo, and S. Lam, *Photocatalytic activity of rutile Ti₁₋ₓSnₓO₂ solid solutions.* Journal of Catalysis, 1999. **183**(2): p. 368-372.

267. Pan, R., S. Pan, J. Zhou, and Y. Wu, *Surface-modification of indium tin oxide nanoparticles with titanium dioxide by a nonaqueous process and its photocatalytic properties.* Applied Surface Science, 2009. **255**(6): p. 3642-3647.

268. Bessekhouad, Y., D. Robert, and J.V. Weber, *Synthesis of photocatalytic TiO₂ nanoparticles: optimization of the preparation conditions.* Journal of Photochemistry and Photobiology A: Chemistry, 2003. **157**(1): p. 47-53.

269. Kim, K.D. and H.T. Kim, *Synthesis of titanium dioxide nanoparticles using a continuous reaction method.* Colloids and Surfaces A: Physicochemical and Engineering Aspects, 2002. **207**(1–3): p. 263-269.

270. Kuznetsova, I.N., V. Blaskov, I. Stambolova, L. Znaidi, and A. Kanaev, *TiO₂ pure phase brookite with preferred orientation, synthesized as a spin-coated film.* Materials Letters, 2005. **59**(29–30): p. 3820-3823.

271. Lee, J.H. and Y.S. Yang, *Effect of hydrolysis conditions on morphology and phase content in the crystalline TiO₂ nanoparticles synthesized from aqueous TiCl₄ solution by precipitation.* Materials Chemistry and Physics, 2005. **93**(1): p. 237-242.

272. Manorama, S.V., K. Madhusudan Reddy, C.V. Gopal Reddy, S. Narayanan, P. Rajesh Raja, and P.R. Chatterji, *Photostabilization of dye on anatase titania nanoparticles by polymer capping.* Journal of Physics and Chemistry of Solids, 2002. **63**(1): p. 135-143.

273. Sugimoto, T., K. Okada, and H. Itoh, *Synthetic of Uniform Spindle-Type Titania Particles by the Gel–Sol Method.* Journal of Colloid and Interface Science, 1997. **193**(1): p. 140-143.

274. Sugimoto, T., X. Zhou, and A. Muramatsu, *Synthesis of uniform anatase TiO₂ nanoparticles by gel–sol method: 3. Formation process and size control.* Journal of Colloid and Interface Science, 2003. **259**(1): p. 43-52.

275. Znaidi, L., R. Séraphimova, J.F. Bocquet, C. Colbeau-Justin, and C. Pommier, *A semi-continuous process for the synthesis of nanosize TiO₂ powders and their use as photocatalysts.* Materials Research Bulletin, 2001. **36**(5–6): p. 811-825.

276. Sato, G., Y. Arima, H. Tanaka, and S. Hiraoka, *Titanium oxide sol and process for preparation thereof.* 1995, Google Patents.

277. Niederberger, M., M.H. Bartl, and G.D. Stucky, *Benzyl alcohol and titanium tetrachloride a versatile reaction system for the nonaqueous and low-temperature preparation of crystalline and luminescent titania nanoparticles.* Chemistry of Materials, 2002. **14**(10): p. 4364-4370.

278. Parala, H., A. Devi, R. Bhakta, and R.A. Fischer, *Synthesis of nano-scale TiO₂ particles by a nonhydrolytic approach.* Journal of Materials Chemistry, 2002. **12**(6): p. 1625-1627.

279. Tang, J., F. Redl, Y. Zhu, T. Siegrist, L.E. Brus, and M.L. Steigerwald, *An organometallic synthesis of TiO₂ nanoparticles.* Nano letters, 2005. **5**(3): p. 543-548.

280. Lafond, V., P. Mutin, and A. Vioux, *Control of the texture of titania-silica mixed oxides prepared by nonhydrolytic sol-gel.* Chemistry of Materials, 2004. **16**(25): p. 5380-5386.

281. Trentler, T.J., T.E. Denler, J.F. Bertone, A. Agrawal, and V.L. Colvin, *Synthesis of TiO₂ nanocrystals by nonhydrolytic solution-based reactions.* Journal of the American Chemical Society, 1999. **121**(7): p. 1613-1614.

282. Andersson, M., L. Österlund, S. Ljungstroem, and A. Palmqvist, *Preparation of nanosize anatase and rutile TiO₂ by hydrothermal treatment of microemulsions and their activity for photocatalytic wet oxidation of phenol.* The Journal of Physical Chemistry B, 2002. **106**(41): p. 10674-10679.

283. Yuan, Z.-Y. and B.-L. Su, *Titanium oxide nanotubes, nanofibers and nanowires.* Colloids and Surfaces A: Physicochemical and Engineering Aspects, 2004. **241**(1): p. 173-183.

284. Barbe, C.J., F. Arendse, P. Comte, M. Jirousek, F. Lenzmann, V. Shklover, and M. Grätzel, *Nanocrystalline titanium oxide electrodes for photovoltaic applications.* Journal of the American Ceramic Society, 1997. **80**(12): p. 3157-3171.

285. Sterte, J., *Synthesis and properties of titanium oxide cross-linked montmorillonite.* Clays and Clay Minerals, 1986. **34**(6): p. 658-664.

286. Chae, S.Y., M.K. Park, S.K. Lee, T.Y. Kim, S.K. Kim, and W.I. Lee, *Preparation of size-controlled TiO₂ nanoparticles and derivation of optically transparent photocatalytic films.* Chemistry of Materials, 2003. **15**(17): p. 3326-3331.

287. Yang, J., S. Mei, and J.M. Ferreira, *Hydrothermal synthesis of nanosized titania powders: influence of peptization and peptizing agents on the crystalline phases and phase transitions.* Journal of the American Ceramic Society, 2000. **83**(6): p. 1361-1368.

288. Yang, J., S. Mei, and J.M. Ferreira, *In situ preparation of weakly flocculated aqueous anatase suspensions by a hydrothermal technique.* Journal of Colloid and Interface Science, 2003. **260**(1): p. 82-88.

289. Xie, R.-C. and J.K. Shang, *Morphological control in solvothermal synthesis of titanium oxide.* Journal of materials science, 2007. **42**(16): p. 6583-6589.

290. Li, G. and K.A. Gray, *Preparation of mixed-phase titanium dioxide nanocomposites via solvothermal processing.* Chemistry of Materials, 2007. **19**(5): p. 1143-1146.

291. Yang, H.G., G. Liu, S.Z. Qiao, C.H. Sun, Y.G. Jin, S.C. Smith, J. Zou, H.M. Cheng, and G.Q. Lu, *Solvothermal synthesis and photoreactivity of anatase TiO2 nanosheets with dominant {001} facets.* Journal of the American Chemical Society, 2009. **131**(11): p. 4078-4083.

292. Kominami, H., Y. Ishii, M. Kohno, S. Konishi, Y. Kera, and B. Ohtani, *Nanocrystalline brookite-type titanium (IV) oxide photocatalysts prepared by a solvothermal method: correlation between their physical properties and photocatalytic activities.* Catalysis Letters, 2003. **91**(1-2): p. 41-47.

293. Choi, H.G., Y.H. Jung, and D.K. Kim, *Solvothermal synthesis of tungsten oxide nanorod/nanowire/nanosheet.* Journal of the American Ceramic Society, 2005. **88**(6): p. 1684-1686.

294. Zhao, L., X. Chen, X. Wang, Y. Zhang, W. Wei, Y. Sun, M. Antonietti, and M.M. Titirici, *One‐Step Solvothermal Synthesis of a Carbon@ TiO₂ Dyade Structure Effectively Promoting Visible‐Light Photocatalysis.* Advanced Materials, 2010. **22**(30): p. 3317-3321.

295. Gaya, U.I. and A.H. Abdullah, *Heterogeneous photocatalytic degradation of organic contaminants over titanium dioxide: a review of fundamentals, progress and problems.* Journal of Photochemistry and Photobiology C: Photochemistry Reviews, 2008. **9**(1): p. 1-12.

296. Su, C., B.-Y. Hong, and C.-M. Tseng, *Sol–gel preparation and photocatalysis of titanium dioxide.* Catalysis Today, 2004. **96**(3): p. 119-126.

297. Sanchez, C., B. Lebeau, F. Chaput, and J.P. Boilot, *Optical properties of functional hybrid organic–inorganic nanocomposites.* Advanced Materials, 2003. **15**(23): p. 1969-1994.

298. Su, C., B.Y. Hong, and C.M. Tseng, *Sol–gel preparation and photocatalysis of titanium dioxide.* Catalysis Today, 2004. **96**(3): p. 119-126.

299. Banfield, J., *Thermodynamic analysis of phase stability of nanocrystalline titania.* Journal of Materials Chemistry, 1998. **8**(9): p. 2073-2076.

300. Zhang, H. and J.F. Banfield, *Size dependence of the kinetic rate constant for phase transformation in TiO₂ nanoparticles.* Chemistry of Materials, 2005. **17**(13): p. 3421-3425.

301. Zhang, H., M. Finnegan, and J.F. Banfield, *Preparing single-phase nanocrystalline anatase from amorphous titania with particle sizes tailored by temperature.* Nano letters, 2001. **1**(2): p. 81-85.

302. Spanhel, L. and M.A. Anderson, *Semiconductor clusters in the sol-gel process: quantized aggregation, gelation, and crystal growth in concentrated zinc oxide colloids.* Journal of the American Chemical Society, 1991. **113**(8): p. 2826-2833.

303. Tang, W. and D. Cameron, *Aluminum-doped zinc oxide transparent conductors deposited by the sol-gel process.* Thin Solid Films, 1994. **238**(1): p. 83-87.

304. Asakuma, N., H. Hirashima, H. Imai, T. Fukui, and M. Toki, *Crystallization and reduction of sol-gel-derived zinc oxide films by irradiation with ultraviolet lamp.* Journal of Sol-Gel Science and Technology, 2003. **26**(1-3): p. 181-184.

305. Natsume, Y. and H. Sakata, *Zinc oxide films prepared by sol-gel spin-coating.* Thin Solid Films, 2000. **372**(1): p. 30-36.

306. Lauf, R.J. and W. Bond, *Fabrication of high-field zinc oxide varistors by sol-gel processing.* Am. Ceram. Soc. Bull.;(United States), 1984. **63**(2).

307. Li, H., J. Wang, H. Liu, C. Yang, H. Xu, X. Li, and H. Cui, *Sol–gel preparation of transparent zinc oxide films with highly preferential crystal orientation.* Vacuum, 2004. **77**(1): p. 57-62.

123

308. Sinha, R., M. Ganesana, S. Andreescu, and L. Stanciu, *AChE biosensor based on zinc oxide sol–gel for the detection of pesticides.* Analytica chimica acta, 2010. **661**(2): p. 195-199.

309. Ladanov, M., P.A. Amaris, P. Villalba, G. Matthews, M. Ram, J. Wang, and A. Kumar. *ZnO Nanowires Grown on ZnO Thin Film Deposited by Atomic Layer Deposition*. in *AIP Conference Proceedings*. 2012. American Institute of Physics, Ste. 1 NO 1 Melville NY 11747-4502 United States.

310. Laudise, R. and A. Ballman, *HYDROTHERMAL SYNTHESIS OF ZINC OXIDE AND ZINC SULFIDE1.* The Journal of Physical Chemistry, 1960. **64**(5): p. 688-691.

311. Laudise, R., E. Kolb, and A. Caporaso, *Hydrothermal growth of large sound crystals of zinc oxide.* Journal of the American Ceramic Society, 1964. **47**(1): p. 9-12.

312. Xu, H., H. Wang, Y. Zhang, W. He, M. Zhu, B. Wang, and H. Yan, *Hydrothermal synthesis of zinc oxide powders with controllable morphology.* Ceramics International, 2004. **30**(1): p. 93-97.

313. Joo, J., B.Y. Chow, M. Prakash, E.S. Boyden, and J.M. Jacobson, *Face-selective electrostatic control of hydrothermal zinc oxide nanowire synthesis.* Nature materials, 2011. **10**(8): p. 596-601.

314. Dem'Yanets, L., L. Li, and T. Uvarova, *Zinc oxide: hydrothermal growth of nano-and bulk crystals and their luminescent properties.* Journal of materials science, 2006. **41**(5): p. 1439-1444.

315. Ladanov, M., P. Algarin-Amaris, P. Villalba, Y. Emirov, G. Matthews, S. Thomas, M.K. Ram, A. Kumar, and J. Wang, *Effects of the physical properties of atomic layer deposition grown seeding layers on the preparation of ZnO nanowires.* Journal of Physics and Chemistry of Solids, 2013. **74**(11): p. 1578-1588.

316. Becheri, A., M. Dürr, P.L. Nostro, and P. Baglioni, *Synthesis and characterization of zinc oxide nanoparticles: application to textiles as UV-absorbers.* Journal of Nanoparticle Research, 2008. **10**(4): p. 679-689.

317. Sugunan, A., H.C. Warad, M. Boman, and J. Dutta, *Zinc oxide nanowires in chemical bath on seeded substrates: role of hexamine.* Journal of Sol-Gel Science and Technology, 2006. **39**(1): p. 49-56.

318. Ladanov, M., M.K. Ram, G. Matthews, and A. Kumar, *Structure and Opto-electrochemical Properties of ZnO Nanowires Grown on n-Si Substrate.* Langmuir, 2011. **27**(14): p. 9012-9017.

319. Ladanov, M., M. Ram, A. Kumar, and G. Matthews. *Novel Aster-like ZnO Nanowire Clusters for Nanocomposites*. in *MRS Proceedings*. 2011. Cambridge Univ Press.

320. Sivakumar, R., M. Jayachandran, and C. Sanjeeviraja, *Studies on the effect of substrate temperature on (VI–VI) textured tungsten oxide (WO_3) thin films on glass, SnO_2: F substrates by PVD: EBE technique for electrochromic devices.* Materials Chemistry and Physics, 2004. **87**(2): p. 439-445.

321. Miller, E.L., B. Marsen, B. Cole, and M. Lum, *Low-temperature reactively sputtered tungsten oxide films for solar-powered water splitting applications.* Electrochemical and Solid-State Letters, 2006. **9**(7): p. G248-G250.

322. Baek, Y. and K. Yong, *Controlled growth and characterization of tungsten oxide nanowires using thermal evaporation of WO_3 powder.* The Journal of Physical Chemistry C, 2007. **111**(3): p. 1213-1218.

323. Hong, K., M. Xie, R. Hu, and H. Wu, *Synthesizing tungsten oxide nanowires by a thermal evaporation.* Applied physics letters, 2007. **90**(17): p. 173121.

324. Senthil, K. and K. Yong, *Growth and characterization of stoichiometric tungsten oxide nanorods by thermal evaporation and subsequent annealing.* Nanotechnology, 2007. **18**(39): p. 395604.

325. Breedon, M., P. Spizzirri, M. Taylor, J. du Plessis, D. McCulloch, J. Zhu, L. Yu, Z. Hu, C. Rix, and W. Wlodarski, *Synthesis of nanostructured tungsten oxide thin films: A simple, controllable, inexpensive, aqueous sol− gel method.* Crystal Growth & Design, 2009. **10**(1): p. 430-439.

326. Takase, A. and K. Miyakawa, *Raman study on sol-gel derived tungsten oxides from tungsten ethoxide.* Japanese Journal of Applied Physics, 1991. **30**(8B): p. L1508.

327. Özer, N., *Optical and electrochemical characteristics of sol-gel deposited tungsten oxide films: a comparison.* Thin Solid Films, 1997. **304**(1): p. 310-314.

328. Nishide, T. and F. Mizukami, *Crystal structures and optical properties of tungsten oxide films prepared by a complexing-agent-assisted sol-gel process.* Thin Solid Films, 1995. **259**(2): p. 212-217.

329. Deepa, M., P. Singh, S. Sharma, and S. Agnihotry, *Effect of humidity on structure and electrochromic properties of sol–gel-derived tungsten oxide films.* Solar Energy Materials and Solar Cells, 2006. **90**(16): p. 2665-2682.

330. Song, X., Y. Zhao, and Y. Zheng, *Hydrothermal synthesis of tungsten oxide nanobelts.* Materials Letters, 2006. **60**(28): p. 3405-3408.

331. You, L., Y. Sun, J. Ma, Y. Guan, J. Sun, Y. Du, and G. Lu, *Highly sensitive NO_2 sensor based on square-like tungsten oxide prepared with hydrothermal treatment.* Sensors and Actuators B: Chemical, 2011. **157**(2): p. 401-407.

332. Li, Y., X. Su, J. Jian, and J. Wang, *Ethanol sensing properties of tungsten oxide nanorods prepared by microwave hydrothermal method.* Ceramics International, 2010. **36**(6): p. 1917-1920.

333. Mukherjee, N., M. Paulose, O.K. Varghese, G. Mor, and C.A. Grimes, *Fabrication of nanoporous tungsten oxide by galvanostatic anodization.* Journal of materials research, 2003. **18**(10): p. 2296-2299.

334. Di Paola, A., F. Di Quarto, and C. Sunseri, *Electrochromism in anodically formed tungsten oxide films.* Journal of the Electrochemical Society, 1978. **125**(8): p. 1344-1347.

335. Di Paola, A., F. Di Quarto, and C. Sunseri, *Anodic oxide films on tungsten—I. The influence of anodizing parameters on charging curves and film composition.* Corrosion Science, 1980. **20**(8): p. 1067-1078.

336. Supothina, S., P. Seeharaj, S. Yoriya, and M. Sriyudthsak, *Synthesis of tungsten oxide nanoparticles by acid precipitation method.* Ceramics International, 2007. **33**(6): p. 931-936.

337. Xu, Z., I. Tabata, K. Hirogaki, K. Hisada, T. Wang, S. Wang, and T. Hori, *Preparation of platinum-loaded cubic tungsten oxide: A highly efficient visible light-driven photocatalyst.* Materials Letters, 2011. **65**(9): p. 1252-1256.

338. Yu, J., H. Yu, B. Cheng, M. Zhou, and X. Zhao, *Enhanced photocatalytic activity of TiO_2 powder (P25) by hydrothermal treatment.* Journal of Molecular Catalysis A: Chemical, 2006. **253**(1–2): p. 112-118.

339. Yu, J.C., J. Lin, D. Lo, and S. Lam, *Influence of thermal treatment on the adsorption of oxygen and photocatalytic activity of TiO_2.* Langmuir, 2000. **16**(18): p. 7304-7308.

125

340. Pan, X., Y. Zhao, S. Liu, C.L. Korzeniewski, S. Wang, and Z. Fan, *Comparing graphene-TiO₂ nanowire and graphene-TiO₂ nanoparticle composite photocatalysts.* ACS applied materials & interfaces, 2012. **4**(8): p. 3944-3950.

341. Yang, G., Z. Jiang, H. Shi, T. Xiao, and Z. Yan, *Preparation of highly visible-light active N-doped TiO₂ photocatalyst.* Journal of Materials Chemistry, 2010. **20**(25): p. 5301-5309.

342. Wang, J., D.N. Tafen, J.P. Lewis, Z. Hong, A. Manivannan, M. Zhi, M. Li, and N. Wu, *Origin of photocatalytic activity of nitrogen-doped TiO₂ nanobelts.* Journal of the American Chemical Society, 2009. **131**(34): p. 12290-12297.

343. Lai, Y.-K., J.-Y. Huang, H.-F. Zhang, V.-P. Subramaniam, Y.-X. Tang, D.-G. Gong, L. Sundar, L. Sun, Z. Chen, and C.-J. Lin, *Nitrogen-doped TiO₂ nanotube array films with enhanced photocatalytic activity under various light sources.* Journal of Hazardous materials, 2010. **184**(1): p. 855-863.

344. He, Z., L. Zhan, F. Hong, S. Song, Z. Lin, J. Chen, and M. Jin, *A visible light-responsive iodine-doped titanium dioxide nanosphere.* Journal of Environmental Sciences, 2011. **23**(1): p. 166-170.

345. Hong, X., Z. Wang, W. Cai, F. Lu, J. Zhang, Y. Yang, N. Ma, and Y. Liu, *Visible-light-activated nanoparticle photocatalyst of iodine-doped titanium dioxide.* Chemistry of Materials, 2005. **17**(6): p. 1548-1552.

346. Song, S., J. Tu, Z. He, F. Hong, W. Liu, and J. Chen, *Visible light-driven iodine-doped titanium dioxide nanotubes prepared by hydrothermal process and post-calcination.* Applied Catalysis A: General, 2010. **378**(2): p. 169-174.

347. Song, S., F. Hong, Z. He, H. Wang, X. Xu, and J. Chen, *Influence of zirconium doping on the activities of zirconium and iodine co-doped titanium dioxide in the decolorization of methyl orange under visible light irradiation.* Applied Surface Science, 2011. **257**(23): p. 10101-10108.

348. He, Z., X. Xu, S. Song, L. Xie, J. Tu, J. Chen, and B. Yan, *A visible light-driven titanium dioxide photocatalyst codoped with lanthanum and iodine: an application in the degradation of oxalic acid.* The Journal of Physical Chemistry C, 2008. **112**(42): p. 16431-16437.

349. Momeni, M.M. and Y. Ghayeb, *Preparation of cobalt coated TiO₂ and WO₃–TiO₂ nanotube films via photo-assisted deposition with enhanced photocatalytic activity under visible light illumination.* Ceramics International, 2016. **42**(6): p. 7014-7022.

350. Seery, M.K., R. George, P. Floris, and S.C. Pillai, *Silver doped titanium dioxide nanomaterials for enhanced visible light photocatalysis.* Journal of Photochemistry and Photobiology A: Chemistry, 2007. **189**(2–3): p. 258-263.

351. Yu, J., G. Dai, and B. Huang, *Fabrication and Characterization of Visible-Light-Driven Plasmonic Photocatalyst Ag/AgCl/TiO₂ Nanotube Arrays.* The Journal of Physical Chemistry C, 2009. **113**(37): p. 16394-16401.

352. Wu, J.C.-S. and C.-H. Chen, *A visible-light response vanadium-doped titania nanocatalyst by sol–gel method.* Journal of Photochemistry and Photobiology A: Chemistry, 2004. **163**(3): p. 509-515.

353. Shen, X.-Z., Z.-C. Liu, S.-M. Xie, and J. Guo, *Degradation of nitrobenzene using titania photocatalyst co-doped with nitrogen and cerium under visible light illumination.* Journal of Hazardous materials, 2009. **162**(2–3): p. 1193-1198.

126

354. Wang, C., Y. Ao, P. Wang, J. Hou, J. Qian, and S. Zhang, *Preparation, characterization, photocatalytic properties of titania hollow sphere doped with cerium.* Journal of Hazardous materials, 2010. **178**(1–3): p. 517-521.

355. Li, Q. and J.K. Shang, *Self-organized nitrogen and fluorine co-doped titanium oxide nanotube arrays with enhanced visible light photocatalytic performance.* Environmental Science & Technology, 2009. **43**(23): p. 8923-8929.

356. Ren, W., Z. Ai, F. Jia, L. Zhang, X. Fan, and Z. Zou, *Low temperature preparation and visible light photocatalytic activity of mesoporous carbon-doped crystalline TiO_2.* Applied Catalysis B: Environmental, 2007. **69**(3–4): p. 138-144.

357. Wang, S. and S. Zhou, *Photodegradation of methyl orange by photocatalyst of CNTs/P-TiO_2 under UV and visible-light irradiation.* Journal of Hazardous materials, 2011. **185**(1): p. 77-85.

358. Jing, L., F. Yuan, H. Hou, B. Xin, W. Cai, and H. Fu, *Relationships of surface oxygen vacancies with photoluminescence and photocatalytic performance of ZnO nanoparticles.* Science in China Series B: Chemistry. **48**(1): p. 25-30.

359. Lin, H.-F., S.-C. Liao, and S.-W. Hung, *The dc thermal plasma synthesis of ZnO nanoparticles for visible-light photocatalyst.* Journal of Photochemistry and Photobiology A: Chemistry, 2005. **174**(1): p. 82-87.

360. Liu, H., J. Yang, J. Liang, Y. Huang, and C. Tang, *ZnO nanofiber and nanoparticle synthesized through electrospinning and their photocatalytic activity under visible light.* Journal of the American Ceramic Society, 2008. **91**(4): p. 1287-1291.

361. Lu, Y., Y. Lin, D. Wang, L. Wang, T. Xie, and T. Jiang, *A high performance cobalt-doped ZnO visible light photocatalyst and its photogenerated charge transfer properties.* Nano Research, 2011. **4**(11): p. 1144-1152.

362. Li, D. and H. Haneda, *Synthesis of nitrogen-containing ZnO powders by spray pyrolysis and their visible-light photocatalysis in gas-phase acetaldehyde decomposition.* Journal of Photochemistry and Photobiology A: Chemistry, 2003. **155**(1–3): p. 171-178.

363. Ullah, R. and J. Dutta, *Photocatalytic degradation of organic dyes with manganese-doped ZnO nanoparticles.* Journal of Hazardous materials, 2008. **156**(1–3): p. 194-200.

364. Liu, S., C. Li, J. Yu, and Q. Xiang, *Improved visible-light photocatalytic activity of porous carbon self-doped ZnO nanosheet-assembled flowers.* CrystEngComm, 2011. **13**(7): p. 2533-2541.

365. Kaneva, N.V., D.T. Dimitrov, and C.D. Dushkin, *Effect of nickel doping on the photocatalytic activity of ZnO thin films under UV and visible light.* Applied Surface Science, 2011. **257**(18): p. 8113-8120.

366. Wu, C. and Q. Huang, *Synthesis of Na-doped ZnO nanowires and their photocatalytic properties.* Journal of Luminescence, 2010. **130**(11): p. 2136-2141.

367. Saoud, K., R. Alsoubaihi, N. Bensalah, T. Bora, M. Bertino, and J. Dutta, *Synthesis of supported silver nano-spheres on zinc oxide nanorods for visible light photocatalytic applications.* Materials Research Bulletin, 2015. **63**: p. 134-140.

368. Šutka, A., T. Käämbre, R. Pärna, I. Juhnevica, M. Maiorov, U. Joost, and V. Kisand, *Co doped ZnO nanowires as visible light photocatalysts.* Solid State Sciences, 2016. **56**: p. 54-62.

369. Abe, R., H. Takami, N. Murakami, and B. Ohtani, *Pristine simple oxides as visible light driven photocatalysts: highly efficient decomposition of organic compounds over platinum-loaded tungsten oxide.* Journal of the American Chemical Society, 2008. **130**(25): p. 7780-7781.

370. Leghari, S.A.K., S. Sajjad, F. Chen, and J. Zhang, *WO₃/TiO₂ composite with morphology change via hydrothermal template-free route as an efficient visible light photocatalyst.* Chemical Engineering Journal, 2011. **166**(3): p. 906-915.

371. Yu, J. and L. Qi, *Template-free fabrication of hierarchically flower-like tungsten trioxide assemblies with enhanced visible-light-driven photocatalytic activity.* Journal of Hazardous materials, 2009. **169**(1–3): p. 221-227.

372. Jitta, R.R., R. Guje, N.K. Veldurthi, S. Prathapuram, R. Velchuri, and V. Muga, *Preparation, characterization and photocatalytic studies of N, Sn-doped defect pyrochlore oxide KTi₀.₅W₁.₅O₆.* Journal of Alloys and Compounds, 2015. **618**: p. 815-823.

373. Wang, X., L. Pang, X. Hu, and N. Han, *Fabrication of ion doped WO₃ photocatalysts through bulk and surface doping.* Journal of Environmental Sciences, 2015. **35**: p. 76-82.

374. Sakai, Y., A. Shimanaka, M. Shioi, S. Kato, S. Satokawa, T. Kojima, and A. Yamasaki, *Fabrication of high-sensitivity palladium loaded tungsten trioxide photocatalyst by photodeposite method.* Catalysis Today, 2015. **241, Part A**: p. 2-7.

375. Lee, J. and P.I. Gouma, *Flame-Spray-Processed CuO-WO₃ Nanopowders as Photocatalysts.* Journal of the American Ceramic Society, 2014. **97**(12): p. 3719-3720.

376. Song, H., Y. Li, Z. Lou, M. Xiao, L. Hu, Z. Ye, and L. Zhu, *Synthesis of Fe-doped WO₃ nanostructures with high visible-light-driven photocatalytic activities.* Applied Catalysis B: Environmental, 2015. **166–167**: p. 112-120.

377. Chang, X., S. Sun, Y. Zhou, L. Dong, and Y. Yin, *Solvothermal synthesis of Ce-doped tungsten oxide nanostructures as visible-light-driven photocatalysts.* Nanotechnology, 2011. **22**(26): p. 265603.

378. Wang, G., J. Yang, J. Park, X. Gou, B. Wang, H. Liu, and J. Yao, *Facile synthesis and characterization of graphene nanosheets.* The Journal of Physical Chemistry C, 2008. **112**(22): p. 8192-8195.

379. Atasoy, A., *The aluminothermic reduction of boric acid.* International Journal of Refractory Metals and Hard Materials, 2010. **28**(5): p. 616-622.

380. Ingale, S.V., P.B. Wagh, A.K. Tripathi, R.S. Srivastav, I.K. Singh, R.C. Bindal, and S.C. Gupta, *TiO₂-Polysulfone Beads for Use in Photo Oxidation of Rhodamine B.* 2012.

381. Kumar, P.M., S. Badrinarayanan, and M. Sastry, *Nanocrystalline TiO₂ studied by optical, FTIR and X-ray photoelectron spectroscopy: correlation to presence of surface states.* Thin Solid Films, 2000. **358**(1): p. 122-130.

382. Kiwi, J. and V. Nadtochenko, *Evidence for the mechanism of photocatalytic degradation of the bacterial wall membrane at the TiO₂ interface by ATR-FTIR and laser kinetic spectroscopy.* Langmuir, 2005. **21**(10): p. 4631-4641.

383. Huang, M.H., Y. Wu, H. Feick, N. Tran, E. Weber, and P. Yang, *Catalytic growth of zinc oxide nanowires by vapor transport.* Advanced Materials, 2001. **13**(2): p. 113-116.

384. Misra, S., M. Ram, S. Pandey, B. Malhotra, and S. Chandra, *Vacuum‑deposited metal/polyaniline Schottky device.* Applied physics letters, 1992. **61**(10): p. 1219-1221.

385. Hayashi, S., N. Nakamori, and H. Kanamori, *Generalized theory of average dielectric constant and its application to infrared absorption by ZnO small particles.* Journal of the Physical Society of Japan, 1979. **46**(1): p. 176-183.

386. Anžlovar, A., Z.C. Orel, K. Kogej, and M. Žigon, *Polyol-mediated synthesis of zinc oxide nanorods and nanocomposites with poly (methyl methacrylate).* Journal of Nanomaterials, 2012. **2012**: p. 31.

387. Zhang, H., X. Lv, Y. Li, Y. Wang, and J. Li, *P25-Graphene Composite as a High Performance Photocatalyst.* ACS nano, 2010. **4**(1): p. 380-386.

388. Nasr, M., S. Balme, C. Eid, R. Habchi, P. Miele, and M. Bechelany, *Enhanced Visible-Light Photocatalytic Performance of Electrospun rGO/TiO₂ Composite Nanofibers.* The Journal of Physical Chemistry C, 2016.

389. Kormann, C., D. Bahnemann, and M. Hoffmann, *Photolysis of chloroform and other organic molecules in aqueous TiO₂ suspensions.* Environ. Sci. Technol, 1991. **25**(3): p. 494-500.

390. Hoffman, A.J., E.R. Carraway, and M.R. Hoffmann, *Photocatalytic production of H₂O₂ and organic peroxides on quantum-sized semiconductor colloids.* Environmental Science & Technology, 1994. **28**(5): p. 776-785.

391. Kormann, C., D.W. Bahnemann, and M.R. Hoffmann, *Photocatalytic production of H₂O₂ and organic peroxides in aqueous suspensions of TiO₂, ZnO, and desert sand.* Environ. Sci. Technol, 1988. **22**(7): p. 798-806.

392. Chen, Y.-L., S.-L. Lo, H.-L. Chang, H.-M. Yeh, L. Sun, and C. Oiu, *Photocatalytic hydrogen production of the CdS/TiO₂-WO₃ ternary hybrid under visible light irradiation.* Water science and technology, 2016. **73**(7): p. 1667-1672.

393. Akurati, K.K., A. Vital, J.-P. Dellemann, K. Michalow, T. Graule, D. Ferri, and A. Baiker, *Flame-made WO₃/TiO₂ nanoparticles: relation between surface acidity, structure and photocatalytic activity.* Applied Catalysis B: Environmental, 2008. **79**(1): p. 53-62.

394. Shephard, G.S., S. Stockenström, D. de Villiers, W.J. Engelbrecht, and G.F. Wessels, *Degradation of microcystin toxins in a falling film photocatalytic reactor with immobilized titanium dioxide catalyst.* Water Research, 2002. **36**(1): p. 140-146.

395. Sreethawong, T., Y. Suzuki, and S. Yoshikawa, *Synthesis, characterization, and photocatalytic activity for hydrogen evolution of nanocrystalline mesoporous titania prepared by surfactant-assisted templating sol–gel process.* Journal of Solid State Chemistry, 2005. **178**(1): p. 329-338.

396. Rosen, M.J. and J.T. Kunjappu, *Surfactants and interfacial phenomena.* 2012: John Wiley & Sons.

397. Lu, J.R., A. Marrocco, T.J. Su, R.K. Thomas, and J. Penfold, *Adsorption of dodecyl sulfate surfactants with monovalent metal counterions at the air-water interface studied by neutron reflection and surface tension.* Journal of Colloid and Interface Science, 1993. **158**(2): p. 303-316.

398. Funasaki, N. and S. Hada, *Surface tension of aqueous solutions of surfactant mixtures. The composition of mixed micelles.* Journal of Physical Chemistry, 1979. **83**(19): p. 2471-2475.

399. Maira, A., K.L. Yeung, J. Soria, J. Coronado, C. Belver, C. Lee, and V. Augugliaro, *Gas-phase photo-oxidation of toluene using nanometer-size TiO₂ catalysts.* Applied Catalysis B: Environmental, 2001. **29**(4): p. 327-336.

400. Ferrari-Lima, A.M., R.P. de Souza, S.S. Mendes, R.G. Marques, M.L. Gimenes, and N.R.C. Fernandes-Machado, *Photodegradation of benzene, toluene and xylenes under visible light applying N-doped mixed TiO₂ and ZnO catalysts.* Catalysis Today, 2015. **241, Part A**: p. 40-46.

401.   Lannoy, A., N. Kania, R. Bleta, S. Fourmentin, C. Machut-Binkowski, E. Monflier, and A. Ponchel, *Photocatalysis of Volatile Organic Compounds in water: Towards a deeper understanding of the role of cyclodextrins in the photodegradation of toluene over titanium dioxide.* Journal of Colloid and Interface Science, 2016. **461**: p. 317-325.

402.   Ramirez, A.M., K. Demeestere, N. De Belie, T. Mäntylä, and E. Levänen, *Titanium dioxide coated cementitious materials for air purifying purposes: preparation, characterization and toluene removal potential.* Building and Environment, 2010. **45**(4): p. 832-838.

403.   Ohno, T., K. Tokieda, S. Higashida, and M. Matsumura, *Synergism between rutile and anatase TiO_2 particles in photocatalytic oxidation of naphthalene.* Applied Catalysis A: General, 2003. **244**(2): p. 383-391.

404.   Pramauro, E., A.B. Prevot, M. Vincenti, and R. Gamberini, *Photocatalytic degradation of naphthalene in aqueous TiO_2 dispersions: effect of nonionic surfactants.* Chemosphere, 1998. **36**(7): p. 1523-1542.

405.   Sharma, A. and B.-K. Lee, *Adsorptive/photo-catalytic process for naphthalene removal from aqueous media using in-situ nickel doped titanium nanocomposite.* Journal of Environmental Management, 2015. **155**: p. 114-122.

406.   Shie, J.-L., C.-H. Lee, C.-S. Chiou, C.-T. Chang, C.-C. Chang, and C.-Y. Chang, *Photodegradation kinetics of formaldehyde using light sources of UVA, UVC and UVLED in the presence of composed silver titanium oxide photocatalyst.* Journal of Hazardous materials, 2008. **155**(1): p. 164-172.

407.   Pozzo, R.L., M.A. Baltanas, and A.E. Cassano, *Supported titanium oxide as photocatalyst in water decontamination: state of the art.* Catalysis Today, 1997. **39**(3): p. 219-231.

408.   Li, D. and H. Haneda, *Morphologies of zinc oxide particles and their effects on photocatalysis.* Chemosphere, 2003. **51**(2): p. 129-137.

409.   Wang, Z.L., *Zinc oxide nanostructures: growth, properties and applications.* Journal of Physics: Condensed Matter, 2004. **16**(25): p. R829.

410.   Kajbafvala, A., H. Ghorbani, A. Paravar, J.P. Samberg, E. Kajbafvala, and S. Sadrnezhaad, *Effects of morphology on photocatalytic performance of Zinc oxide nanostructures synthesized by rapid microwave irradiation methods.* Superlattices and Microstructures, 2012. **51**(4): p. 512-522.

411.   Height, M.J., S.E. Pratsinis, O. Mekasuwandumrong, and P. Praserthdam, *Ag-ZnO catalysts for UV-photodegradation of methylene blue.* Applied Catalysis B: Environmental, 2006. **63**(3): p. 305-312.

412.   Shvalagin, V., A. Stroyuk, and S.Y. Kuchmii, *Role of quantum-sized effects on the cathodic photocorrosion of ZnO nanoparticles in ethanol.* Theoretical and Experimental Chemistry, 2004. **40**(6): p. 378-382.

413.   Han, C., M.-Q. Yang, B. Weng, and Y.-J. Xu, *Improving the photocatalytic activity and anti-photocorrosion of semiconductor ZnO by coupling with versatile carbon.* Physical Chemistry Chemical Physics, 2014. **16**(32): p. 16891-16903.

414.   Awazu, K., M. Fujimaki, C. Rockstuhl, J. Tominaga, H. Murakami, Y. Ohki, N. Yoshida, and T. Watanabe, *A plasmonic photocatalyst consisting of silver nanoparticles embedded in titanium dioxide.* Journal of the American Chemical Society, 2008. **130**(5): p. 1676-1680.

415. Sakthivel, S. and H. Kisch, *Daylight photocatalysis by carbon‑modified titanium dioxide.* Angewandte Chemie International Edition, 2003. **42**(40): p. 4908-4911.

416. Dvoranová, D., V. Brezová, M. Mazúr, and M.A. Malati, *Investigations of metal-doped titanium dioxide photocatalysts.* Applied Catalysis B: Environmental, 2002. **37**(2): p. 91-105.

417. Seery, M.K., R. George, P. Floris, and S.C. Pillai, *Silver doped titanium dioxide nanomaterials for enhanced visible light photocatalysis.* Journal of Photochemistry and Photobiology A: Chemistry, 2007. **189**(2): p. 258-263.

418. Ullah, R. and J. Dutta, *Photocatalytic degradation of organic dyes with manganese-doped ZnO nanoparticles.* Journal of Hazardous materials, 2008. **156**(1): p. 194-200.

419. Iwasaki, M., M. Hara, H. Kawada, H. Tada, and S. Ito, *Cobalt ion-doped TiO₂ photocatalyst response to visible light.* Journal of Colloid and Interface Science, 2000. **224**(1): p. 202-204.

420. Gunti, S., A. Kumar, and M.K. Ram, *Comparative Organics Remediation Properties of Nanostructured Graphene Doped Titanium Oxide and Graphene Doped Zinc Oxide Photocatalysts.* American Journal of Analytical Chemistry, 2015. **6**(8): p. 708.

421. Gunti, S., M. McCrory, A. Kumar, and M.K. Ram, *Enhanced Photocatalytic Remediation Using Graphene (G)-Titanium Oxide (TiO₂) Nanocomposite Material in Visible Light Radiation.* American Journal of Analytical Chemistry, 2016. **7**(07): p. 576.

422. Udom, I., M.K. Ram, E.K. Stefanakos, A.F. Hepp, and D.Y. Goswami, *One dimensional-ZnO nanostructures: Synthesis, properties and environmental applications.* Materials Science in Semiconductor Processing, 2013. **16**(6): p. 2070-2083.

423. Udom, I., Y. Zhang, M.K. Ram, E.K. Stefanakos, A.F. Hepp, R. Elzein, R. Schlaf, and D.Y. Goswami, *A simple photolytic reactor employing Ag-doped ZnO nanowires for water purification.* Thin Solid Films, 2014.

424. Stankovich, S., D.A. Dikin, R.D. Piner, K.A. Kohlhaas, A. Kleinhammes, Y. Jia, Y. Wu, S.T. Nguyen, and R.S. Ruoff, *Synthesis of graphene-based nanosheets via chemical reduction of exfoliated graphite oxide.* carbon, 2007. **45**(7): p. 1558-1565.

425. Wang, G., X. Shen, B. Wang, J. Yao, and J. Park, *Synthesis and characterisation of hydrophilic and organophilic graphene nanosheets.* carbon, 2009. **47**(5): p. 1359-1364.

426. Lee, J., H.-R. Chae, Y.J. Won, K. Lee, C.-H. Lee, H.H. Lee, I.-C. Kim, and J.-m. Lee, *Graphene oxide nanoplatelets composite membrane with hydrophilic and antifouling properties for wastewater treatment.* Journal of membrane science, 2013. **448**: p. 223-230.

427. Mattevi, C., H. Kim, and M. Chhowalla, *A review of chemical vapour deposition of graphene on copper.* Journal of Materials Chemistry, 2011. **21**(10): p. 3324-3334.

428. Bunch, J.S. and M.L. Dunn, *Adhesion mechanics of graphene membranes.* Solid state communications, 2012. **152**(15): p. 1359-1364.

429. Yoon, T., W.C. Shin, T.Y. Kim, J.H. Mun, T.-S. Kim, and B.J. Cho, *Direct measurement of adhesion energy of monolayer graphene as-grown on copper and its application to renewable transfer process.* Nano letters, 2012. **12**(3): p. 1448-1452.

430. Heller, A., M.V. Pishko, and E. Heller, *Photocatalyst-binder compositions*. 1997, Google Patents.

431.	Sopyan, I., M. Watanabe, S. Murasawa, K. Hashimoto, and A. Fujishima, *A film-type photocatalyst incorporating highly active TiO$_2$ powder and fluororesin binder: photocatalytic activity and long-term stability.* Journal of Electroanalytical Chemistry, 1996. **415**(1-2): p. 183-186.

432.	Chen, J., S.-c. Kou, and C.-s. Poon, *Photocatalytic cement-based materials: comparison of nitrogen oxides and toluene removal potentials and evaluation of self-cleaning performance.* Building and Environment, 2011. **46**(9): p. 1827-1833.

433.	Dhananjeyan, M., E. Mielczarski, K. Thampi, P. Buffat, M. Bensimon, A. Kulik, J. Mielczarski, and J. Kiwi, *Photodynamics and surface characterization of TiO$_2$ and Fe$_2$O$_3$ photocatalysts immobilized on modified polyethylene films.* The Journal of Physical Chemistry B, 2001. **105**(48): p. 12046-12055.

434.	Wang, D., L. Shi, Q. Luo, X. Li, and J. An, *An efficient visible light photocatalyst prepared from TiO$_2$ and polyvinyl chloride.* Journal of materials science, 2012. **47**(5): p. 2136-2145.

435.	Kwon, C.H., H. Shin, J.H. Kim, W.S. Choi, and K.H. Yoon, *Degradation of methylene blue via photocatalysis of titanium dioxide.* Materials Chemistry and Physics, 2004. **86**(1): p. 78-82.

436.	Liao, S., H. Donggen, D. Yu, Y. Su, and G. Yuan, *Preparation and characterization of ZnO/TiO$_2$, SO$_4^{2-}$/ZnO/TiO$_2$ photocatalyst and their photocatalysis.* Journal of Photochemistry and Photobiology A: Chemistry, 2004. **168**(1): p. 7-13.

437.	Monkman, A. and P. Adams, *Optical and electronic properties of stretch-oriented solution-cast polyaniline films.* Synthetic metals, 1991. **40**(1): p. 87-96.

438.	Su, S.-J. and N. Kuramoto, *Processable polyaniline–titanium dioxide nanocomposites: effect of titanium dioxide on the conductivity.* Synthetic metals, 2000. **114**(2): p. 147-153.

439.	Paul, R.K. and C. Pillai, *Melt/solution processable conducting polyaniline with novel sulfonic acid dopants and its thermoplastic blends.* Synthetic metals, 2000. **114**(1): p. 27-35.

440.	Xiong, P., Q. Chen, M. He, X. Sun, and X. Wang, *Cobalt ferrite–polyaniline heteroarchitecture: a magnetically recyclable photocatalyst with highly enhanced performances.* Journal of Materials Chemistry, 2012. **22**(34): p. 17485-17493.

441.	Annapoorni, S., N. Sundaresan, S. Pandey, and B. Malhotra, *Photocarrier mobility in processable polyaniline.* Journal of applied physics, 1993. **74**(3): p. 2109-2111.

442.	Chowdhury, D., A. Paul, and A. Chattopadhyay, *Photocatalytic Polypyrrole− TiO$_2$− Nanoparticles Composite Thin Film Generated at the Air− Water Interface.* Langmuir, 2005. **21**(9): p. 4123-4128.

443.	Zhao, X., L. Lv, B. Pan, W. Zhang, S. Zhang, and Q. Zhang, *Polymer-supported nanocomposites for environmental application: a review.* Chemical Engineering Journal, 2011. **170**(2): p. 381-394.

444.	Lu, X., W. Zhang, C. Wang, T.-C. Wen, and Y. Wei, *One-dimensional conducting polymer nanocomposites: synthesis, properties and applications.* Progress in Polymer Science, 2011. **36**(5): p. 671-712.

445.	Gomez, H., M.K. Ram, F. Alvi, E. Stefanakos, and A. Kumar, *Novel Synthesis, Characterization, and Corrosion Inhibition Properties of Nanodiamond− Polyaniline Films.* The Journal of Physical Chemistry C, 2010. **114**(44): p. 18797-18804.

446.	Stejskal, J. and R. Gilbert, *Polyaniline. Preparation of a conducting polymer (IUPAC technical report).* Pure and Applied Chemistry, 2002. **74**(5): p. 857-867.

447. Sabine, D.C., *Ocean Acidification: Surface pH*.
https://sos.noaa.gov/Datasets/dataset.php?id=172: NOAA.
448. *Water Quality* NASA: https://www.grc.nasa.gov/www/k-12/fenlewis/Waterquality.html.

www.manaraa.com

APPENDIX A: COPYRIGHT PERMISSIONS FOR MATERIAL USED IN

CHAPTERS 2, 3, 4, 5 AND 6

Below is permission for the use of material in Chapter 2.

Below is permission for the use of material in Chapter 3 & Chapter 5.

USF

Srikanth Gunti <srikanth2@mail.usf.edu>

Permission for my Published Papers(AJAC) to be used in my Dissertation

ajac <ajac@scirp.org>   Sun, May 14, 2017 at 12:06 AM
To: Srikanth Gunti <srikanth2@mail.usf.edu>
Cc: Manoj Ram <mkram@usf.edu>

Dear Colleague,

Thank you for the email.

It is alright to use the material but please add proper citations.

Best Regards,

MA Tingting (Martina)
AJAC Editorial Office
LinkedIn: cn.linkedin.com/pub/martina-ma/28/661/93a

Google Scholar calculated the h5-index for some of SCIRP's Journals. The h5-index for the journal American Journal of Analytical Chemistry is 14 based on the Google Scholar Metrics (June 2016). It is ranked 8th in the publications matching "Analytical Chemistry" based on the Google Scholar Metrics (June 2016).

If you have any complaints or suggestions, please contact feedback@scirp.org.

From: Srikanth Gunti <srikanth2@mail.usf.edu>
Sent: Sunday, May 14, 2017 3:48:01 AM
To: ajac
Cc: Manoj Ram
Subject: Permission for my Published Papers(AJAC) to be used in my Dissertation

Hello,

I am Srikanth Gunti, First author of 2 published articles in AJAC journal. Please find the titles of the publications below.

Article No 1:
"Comparative Organics Remediation Properties of Nanostructured Graphene Doped Titanium Oxide and Graphene Doped Zinc Oxide Photocatalysts". American Journal of Analytical Chemistry Vol.6 No.8, Pub. Date: July30, 2015. **Srikanth Gunti,** Ashok Kumar, Manoj K. Ram

Articles No 2:
"Enhanced Photocatalytic Remediation Using Graphene (G)-Titanium Oxide (TiO2) Nanocomposite Material in Visible Light Radiation". American Journal of Analytical Chemistry Vol.7 No.7, Pub. Date: July 21, 2016. **Srikanth Gunti,** Michael McCrory, Ashok Kumar, Manoj K. Ram

I am planning to re-use both Articles (1 & 2), completely in my PhD dissertation report. (includes Figures, Tables , Text etc.,)

I need Copyright permission from you which i need to include in my appendix of my Dissertation Report for allowing me to use articles material completely.

Looking forward to hear from you.

Regards

--
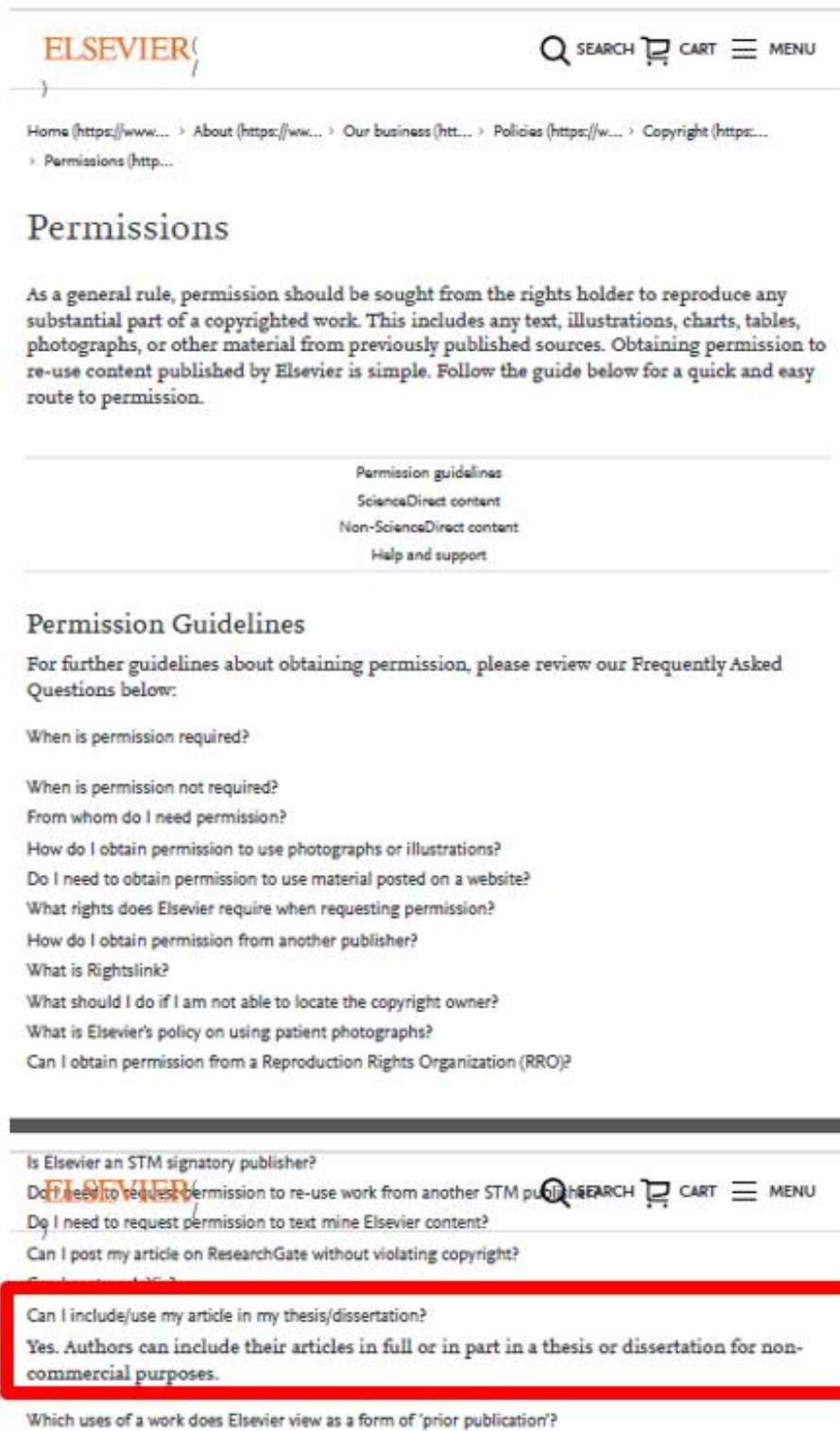
Regards
Srikanth Gunti

Below is permission for the use of material in Chapter 4 & Chapter 6

Permissions

As a general rule, permission should be sought from the rights holder to reproduce any substantial part of a copyrighted work. This includes any text, illustrations, charts, tables, photographs, or other material from previously published sources. Obtaining permission to re-use content published by Elsevier is simple. Follow the guide below for a quick and easy route to permission.

Permission guidelines
ScienceDirect content
Non-ScienceDirect content
Help and support

Permission Guidelines

For further guidelines about obtaining permission, please review our Frequently Asked Questions below:

When is permission required?

When is permission not required?

From whom do I need permission?

How do I obtain permission to use photographs or illustrations?

Do I need to obtain permission to use material posted on a website?

What rights does Elsevier require when requesting permission?

How do I obtain permission from another publisher?

What is Rightslink?

What should I do if I am not able to locate the copyright owner?

What is Elsevier's policy on using patient photographs?

Can I obtain permission from a Reproduction Rights Organization (RRO)?

Is Elsevier an STM signatory publisher?

Do I need to request permission to re-use work from another STM publisher? SEARCH 🛒 CART ≡ MENU

Do I need to request permission to text mine Elsevier content?

Can I post my article on ResearchGate without violating copyright?

Can I include/use my article in my thesis/dissertation?

Yes. Authors can include their articles in full or in part in a thesis or dissertation for non-commercial purposes.

Which uses of a work does Elsevier view as a form of 'prior publication'?
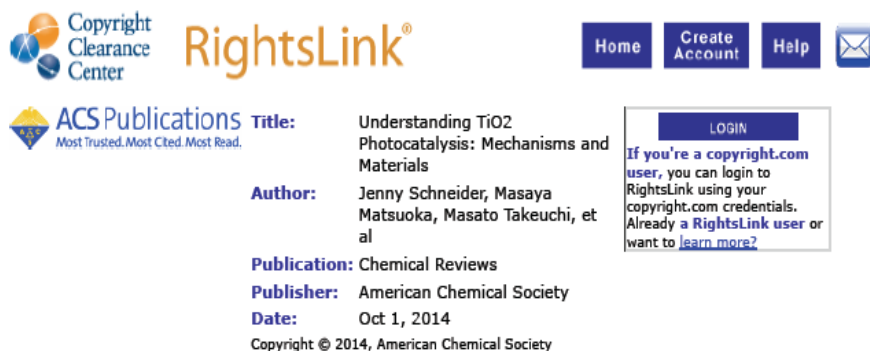
APPENDIX B: COPYRIGHT PERMISSIONS FOR FIGURES

Below is copyright permission for Figure 2.1.

137

Below is copyright permission for Figure 2.2.

138

www.manaraa.com

Below is copyright permission for Figure 2.3.

**ROYAL SOCIETY OF CHEMISTRY LICENSE
TERMS AND CONDITIONS**

May 12, 2017

This Agreement between Srikanth Gunti ("You") and Royal Society of Chemistry ("Royal Society of Chemistry") consists of your license details and the terms and conditions provided by Royal Society of Chemistry and Copyright Clearance Center.

License Number	4106841293149
License date	May 12, 2017
Licensed Content Publisher	Royal Society of Chemistry
Licensed Content Publication	New Journal of Chemistry
Licensed Content Title	Nitrogen-doped titanium dioxide (N-doped TiO2) for visible light photocatalysis
Licensed Content Author	Sajid Ali Ansari,Mohammad Mansoob Khan,Mohd Omaish Ansari,Moo Hwan Cho
Licensed Content Date	Feb 15, 2016
Licensed Content Volume	40
Licensed Content Issue	4
Type of Use	Thesis/Dissertation
Requestor type	academic/educational
Portion	figures/tables/images
Number of figures/tables/images	1
Format	print and electronic
Distribution quantity	1000
Will you be translating?	no
Order reference number	
Title of the thesis/dissertation	Enhanced Visible Light Photocatalytic Remediation of Organics in Water Using Zinc Oxide and Titanium Oxide Nanostructures
Expected completion date	Dec 2017
Estimated size	150
Requestor Location	Srikanth Gunti 4202 E.Fowler Ave Mechanical Engineering
	TAMPA, FL 33620 United States Attn: Srikanth Gunti
Billing Type	Invoice

139

Below is copyright permission for Figure 2.4.

ROYAL SOCIETY OF CHEMISTRY LICENSE
TERMS AND CONDITIONS

May 12, 2017

This Agreement between Srikanth Gunti ("You") and Royal Society of Chemistry ("Royal Society of Chemistry") consists of your license details and the terms and conditions provided by Royal Society of Chemistry and Copyright Clearance Center.

License Number	4106840516442
License date	May 12, 2017
Licensed Content Publisher	Royal Society of Chemistry
Licensed Content Publication	Nanoscale
Licensed Content Title	Vertically aligned ZnO nanowire arrays tip-grafted with silver nanoparticles for photoelectrochemical applications
Licensed Content Author	Teng Wang,Zhengbo Jiao,Tao Chen,Yawen Li,Wei Ren,Shengling Lin,Gongxuan Lu,Jinhua Ye,Yingpu Bi
Licensed Content Date	May 29, 2013
Licensed Content Volume	5
Licensed Content Issue	16
Type of Use	Thesis/Dissertation
Requestor type	academic/educational
Portion	figures/tables/images
Number of figures/tables/images	1
Format	print and electronic
Distribution quantity	1000
Will you be translating?	no
Order reference number	
Title of the thesis/dissertation	Enhanced Visible Light Photocatalytic Remediation of Organics in Water Using Zinc Oxide and Titanium Oxide Nanostructures
Expected completion date	Dec 2017
Estimated size	150
Requestor Location	Srikanth Gunti 4202 E.Fowler Ave Mechanical Engineering TAMPA, FL 33620 United States Attn: Srikanth Gunti
Billing Type	Invoice

140

www.manaraa.com

Below is copyright permission for Figure 2.5.

ROYAL SOCIETY OF CHEMISTRY LICENSE
TERMS AND CONDITIONS

May 12, 2017

This Agreement between Srikanth Gunti ("You") and Royal Society of Chemistry ("Royal Society of Chemistry") consists of your license details and the terms and conditions provided by Royal Society of Chemistry and Copyright Clearance Center.

License Number	4106841453568
License date	May 12, 2017
Licensed Content Publisher	Royal Society of Chemistry
Licensed Content Publication	CrystEngComm
Licensed Content Title	Hierarchical nanostructure of WO3 nanorods on TiO2 nanofibers and the enhanced visible light photocatalytic activity for degradation of organic pollutants
Licensed Content Author	Li Zhang,Yaogang Li,Qinghong Zhang,Hongzhi Wang
Licensed Content Date	May 17, 2013
Licensed Content Volume	15
Licensed Content Issue	30
Type of Use	Thesis/Dissertation
Requestor type	academic/educational
Portion	figures/tables/images
Number of figures/tables/images	1
Format	print and electronic
Distribution quantity	1000
Will you be translating?	no
Order reference number	
Title of the thesis/dissertation	Enhanced Visible Light Photocatalytic Remediation of Organics in Water Using Zinc Oxide and Titanium Oxide Nanostructures
Expected completion date	Dec 2017
Estimated size	150
Requestor Location	Srikanth Gunti
4202 E.Fowler Ave
Mechanical Engineering

TAMPA, FL 33620
United States
Attn: Srikanth Gunti |
| Billing Type | Invoice |

141

Below is copyright permission for Figure 2.6 and Figure 2.7.

ELSEVIER LICENSE
TERMS AND CONDITIONS

May 12, 2017

This Agreement between Srikanth Gunti ("You") and Elsevier ("Elsevier") consists of your license details and the terms and conditions provided by Elsevier and Copyright Clearance Center.

License Number	4106850193046
License date	May 12, 2017
Licensed Content Publisher	Elsevier
Licensed Content Publication	Catalysis Today
Licensed Content Title	Sol–gel preparation and photocatalysis of titanium dioxide
Licensed Content Author	C. Su,B.-Y. Hong,C.-M. Tseng
Licensed Content Date	5 October 2004
Licensed Content Volume	96
Licensed Content Issue	3
Licensed Content Pages	8
Start Page	119
End Page	126
Type of Use	reuse in a thesis/dissertation
Portion	figures/tables/illustrations
Number of figures/tables/illustrations	2
Format	both print and electronic
Are you the author of this Elsevier article?	No
Will you be translating?	No
Order reference number	
Original figure numbers	Figure 5 , Figure 6
Title of your thesis/dissertation	Enhanced Visible Light Photocatalytic Remediation of Organics in Water Using Zinc Oxide and Titanium Oxide Nanostructures
Expected completion date	Dec 2017
Estimated size (number of pages)	150
Elsevier VAT number	GB 494 6272 12
Requestor Location	Srikanth Gunti 4202 E.Fowler Ave

142

Below is copyright permission for Figure 2.8 & Figure 2.9.

ELSEVIER LICENSE
TERMS AND CONDITIONS

May 12, 2017

This Agreement between Srikanth Gunti ("You") and Elsevier ("Elsevier") consists of your license details and the terms and conditions provided by Elsevier and Copyright Clearance Center.

License Number	4106850386589
License date	May 12, 2017
Licensed Content Publisher	Elsevier
Licensed Content Publication	Colloids and Surfaces A: Physicochemical and Engineering Aspects
Licensed Content Title	Titanium oxide nanotubes, nanofibers and nanowires
Licensed Content Author	Zhong-Yong Yuan,Bao-Lian Su
Licensed Content Date	14 July 2004
Licensed Content Volume	241
Licensed Content Issue	1-3
Licensed Content Pages	11
Start Page	173
End Page	183
Type of Use	reuse in a thesis/dissertation
Intended publisher of new work	other
Portion	figures/tables/illustrations
Number of figures/tables/illustrations	2
Format	both print and electronic
Are you the author of this Elsevier article?	No
Will you be translating?	No
Order reference number	
Original figure numbers	Figure 2 & Figure 6
Title of your thesis/dissertation	Enhanced Visible Light Photocatalytic Remediation of Organics in Water Using Zinc Oxide and Titanium Oxide Nanostructures
Expected completion date	Dec 2017
Estimated size (number of pages)	150
Elsevier VAT number	GB 494 6272 12

Below is copyright permission for Figure 2.10 & Figure 2.11.

SPRINGER LICENSE
TERMS AND CONDITIONS

May 14, 2017

This Agreement between Srikanth Gunti ("You") and Springer ("Springer") consists of your license details and the terms and conditions provided by Springer and Copyright Clearance Center.

License Number	4107441048542
License date	May 14, 2017
Licensed Content Publisher	Springer
Licensed Content Publication	Journal of Nanoparticle Research
Licensed Content Title	Synthesis and characterization of zinc oxide nanoparticles: application to textiles as UV-absorbers
Licensed Content Author	Alessio Becheri
Licensed Content Date	Jan 1, 2007
Licensed Content Volume	10
Licensed Content Issue	4
Type of Use	Thesis/Dissertation
Portion	Figures/tables/illustrations
Number of figures/tables/illustrations	2
Author of this Springer article	No
Order reference number	
Original figure numbers	Figure 2 & Figure 4
Title of your thesis / dissertation	Enhanced Visible Light Photocatalytic Remediation of Organics in Water Using Zinc Oxide and Titanium Oxide Nanostructures
Expected completion date	Dec 2017
Estimated size(pages)	150
Requestor Location	Srikanth Gunti 4202 E.Fowler Ave Mechanical Engineering TAMPA, FL 33620 United States Attn: Srikanth Gunti
Billing Type	Invoice
Billing Address	Srikanth Gunti 4202 E.Fowler Ave Mechanical Engineering TAMPA, FL 33620 United States Attn: Srikanth Gunti
Total	0.00 USD
Terms and Conditions	

144

Below is copyright permission for Figure 2.12 & Figure 2.13.

145

www.manaraa.com

Below is copyright permission for Figure 2.14 & Figure 2.15.

ELSEVIER LICENSE
TERMS AND CONDITIONS

May 13, 2017

This Agreement between Srikanth Gunti ("You") and Elsevier ("Elsevier") consists of your license details and the terms and conditions provided by Elsevier and Copyright Clearance Center.

License Number	4106851355128
License date	May 13, 2017
Licensed Content Publisher	Elsevier
Licensed Content Publication	Ceramics International
Licensed Content Title	Synthesis of tungsten oxide nanoparticles by acid precipitation method
Licensed Content Author	Sitthisuntorn Supothina,Panpailin Seeharaj,Sorachon Yoriya,Mana Sriyudthsak
Licensed Content Date	August 2007
Licensed Content Volume	33
Licensed Content Issue	6
Licensed Content Pages	6
Start Page	931
End Page	936
Type of Use	reuse in a thesis/dissertation
Intended publisher of new work	other
Portion	figures/tables/illustrations
Number of figures/tables/illustrations	2
Format	both print and electronic
Are you the author of this Elsevier article?	No
Will you be translating?	No
Order reference number	
Original figure numbers	Figure 3 & Figure 4
Title of your thesis/dissertation	Enhanced Visible Light Photocatalytic Remediation of Organics in Water Using Zinc Oxide and Titanium Oxide Nanostructures
Expected completion date	Dec 2017
Estimated size (number of pages)	150

146

Below is copyright permission for Figure 2.16 & Figure 2.17.

**ELSEVIER LICENSE
TERMS AND CONDITIONS**

May 13, 2017

This Agreement between Srikanth Gunti ("You") and Elsevier ("Elsevier") consists of your license details and the terms and conditions provided by Elsevier and Copyright Clearance Center.

License Number	4106860043745
License date	May 13, 2017
Licensed Content Publisher	Elsevier
Licensed Content Publication	Materials Letters
Licensed Content Title	Preparation of platinum-loaded cubic tungsten oxide: A highly efficient visible light-driven photocatalyst
Licensed Content Author	Zhanglian Xu,Isao Tabata,Kazumasa Hirogaki,Kenji Hisada,Tao Wang,Sheng Wang,Teruo Hori
Licensed Content Date	15 May 2011
Licensed Content Volume	65
Licensed Content Issue	9
Licensed Content Pages	5
Start Page	1252
End Page	1256
Type of Use	reuse in a thesis/dissertation
Intended publisher of new work	other
Portion	figures/tables/illustrations
Number of figures/tables/illustrations	2
Format	both print and electronic
Are you the author of this Elsevier article?	No
Will you be translating?	No
Order reference number	
Original figure numbers	Figure 1 & Figure 2
Title of your thesis/dissertation	Enhanced Visible Light Photocatalytic Remediation of Organics in Water Using Zinc Oxide and Titanium Oxide Nanostructures
Expected completion date	Dec 2017
Estimated size (number of pages)	150

147

Below is copyright permission for Figure 2.18.

ELSEVIER LICENSE
TERMS AND CONDITIONS

May 13, 2017

This Agreement between Srikanth Gunti ("You") and Elsevier ("Elsevier") consists of your license details and the terms and conditions provided by Elsevier and Copyright Clearance Center.

License Number	4106860227228
License date	May 13, 2017
Licensed Content Publisher	Elsevier
Licensed Content Publication	Journal of Molecular Catalysis A: Chemical
Licensed Content Title	Enhanced photocatalytic activity of TiO2 powder (P25) by hydrothermal treatment
Licensed Content Author	Jiaguo Yu,Huogen Yu,Bei Cheng,Minghua Zhou,Xiujian Zhao
Licensed Content Date	1 July 2006
Licensed Content Volume	253
Licensed Content Issue	1-2
Licensed Content Pages	7
Start Page	112
End Page	118
Type of Use	reuse in a thesis/dissertation
Intended publisher of new work	other
Portion	figures/tables/illustrations
Number of figures/tables/illustrations	1
Format	both print and electronic
Are you the author of this Elsevier article?	No
Will you be translating?	No
Order reference number	
Original figure numbers	Figure 4
Title of your thesis/dissertation	Enhanced Visible Light Photocatalytic Remediation of Organics in Water Using Zinc Oxide and Titanium Oxide Nanostructures
Expected completion date	Dec 2017
Estimated size (number of pages)	150

Below is copyright permission for Figure 2.19.

SPRINGER LICENSE
TERMS AND CONDITIONS

May 14, 2017

This Agreement between Srikanth Gunti ("You") and Springer ("Springer") consists of your license details and the terms and conditions provided by Springer and Copyright Clearance Center.

License Number	4107441264625
License date	May 14, 2017
Licensed Content Publisher	Springer
Licensed Content Publication	Science in China Series B: Chemistry
Licensed Content Title	Relationships of surface oxygen vacancies with photoluminescence and photocatalytic performance of ZnO nanoparticles
Licensed Content Author	Liqiang Jing
Licensed Content Date	Jan 1, 2005
Licensed Content Volume	48
Licensed Content Issue	1
Type of Use	Thesis/Dissertation
Portion	Figures/tables/illustrations
Number of figures/tables/illustrations	1
Author of this Springer article	No
Country of republication	other
Order reference number	
Original figure numbers	Figure 6
Title of your thesis / dissertation	Enhanced Visible Light Photocatalytic Remediation of Organics in Water Using Zinc Oxide and Titanium Oxide Nanostructures
Expected completion date	Dec 2017
Estimated size(pages)	150
Requestor Location	Srikanth Gunti 4202 E.Fowler Ave Mechanical Engineering TAMPA, FL 33620 United States Attn: Srikanth Gunti
Billing Type	Invoice
Billing Address	Srikanth Gunti 4202 E.Fowler Ave Mechanical Engineering TAMPA, FL 33620 United States Attn: Srikanth Gunti
Total	0.00 USD

Terms and Conditions

https://s100.copyright.com/AppDispatchServlet

149

Below is copyright permission for Figure 2.20.

150

ABOUT THE AUTHOR

Srikanth Gunti received his B.E. in Mechanical Engineering from University College of Engineering, Osmania University, India in 2010. He has prior work experience as an Assistant Manager (2010-2012) in Body in White (BIW), Design & Development Research group at Maruti Suzuki India ltd, India. He started his graduate studies at the University of South Florida, Tampa-Florida, in 2012 and obtained his Ph.D. candidacy in 2015. Srikanth continued his doctoral research in Nanomaterial Research group and started working on Photocatalytic materials for Organic Remediation application. During the summer of 2015 and 2016, he joined the Shell Technology Research Center at Houston-Texas as a graduate student intern position to work on surfactant chemistry in Lubricant oil.